EUROPEAN ORGANIZATION FOR NUCLEAR RESEARCH

CERN-PH-EP/2004-024
June 8, 2004

Studies of Hadronic Event Structure in e^+e^- Annihilation from 30 GeV to 209 GeV with the L3 Detector

The L3 Collaboration

Abstract

In this Report, QCD results obtained from a study of hadronic event structure in high energy e^+e^- interactions with the L3 detector are presented. The operation of the LEP collider at many different collision energies from 91 GeV to 209 GeV offers a unique opportunity to test QCD by measuring the energy dependence of different observables. The main results concern the measurement of the strong coupling constant, α_s, from hadronic event shapes and the study of effects of soft gluon coherence in charged particle multiplicity and momentum distributions.

Submitted to *Physics Reports*

Contents

1 Introduction **1**

2 QCD and the Process $e^+e^- \rightarrow$ hadrons **2**
2.1 Theoretical Framework 2
2.2 Experimental Framework 3
2.3 Monte Carlo Programs 3

3 Hadronic Events in L3 **7**
3.1 Calorimeter Energy Measurement 7
3.2 Energy and Angular Resolutions of Jets 8
3.3 Selection of Hadronic Events 9
3.4 Flavour Tagging 10

4 Event-Shape Variables **11**
4.1 Choice of Variables 11
4.2 Measurements 13
4.3 Systematic Uncertainties 14
4.4 Tuning of Monte Carlo Parameters 15

5 Event-Shape Distributions and α_s **16**
5.1 Jet Fractions 17
5.2 Comparison of Event Shapes with Monte Carlo Models 18
5.3 Power Law Correction Analysis 18
5.4 Determination of α_s from event-shape variables 20

6 Soft Gluon Coherence **23**
6.1 Charged Particle Multiplicity 24
6.2 Inclusive Particle Spectrum 25

7 Summary **26**

1 Introduction

Hadronic events produced in e^+e^- annihilation offer a good environment to test the predictions of Quantum Chromodynamics (QCD) [1–9]. The high energy phase of the LEP collider has given a unique opportunity to measure QCD observables over a wide energy range and perform precise tests of the energy dependence of the strong interaction. In addition, it allows to check the validity of the QCD models very often used for background modelling in other studies such as electro-weak studies and new particle searches.

From 1989 to 1995 LEP operated in the region of the Z pole, *i.e.*, at centre-of-mass energies, $\sqrt{s}$, around 91.2 GeV. During this period, known as LEP1, each of the four LEP experiments (ALEPH, DELPHI, L3, and OPAL) collected about 4 million hadronic events. This high statistics, combined with very low background, made it possible to perform many detailed QCD studies and precise measurements of the hadronic event structure. Further, events with an observed high energy photon, which have a lower effective hadronic centre-of-mass energy, $\sqrt{s'} < \sqrt{s}$ due to initial- (ISR) or final-state radiation (FSR), enable studies of energy dependence.

In 1995 LEP entered a new phase, known as LEP2, of steadily increasing energy. Data were taken at a number of centre-of-mass energies, listed in Table 1, between 130 and 209 GeV. While the total integrated luminosity collected by L3 at these high energies (more than $600\,\mathrm{pb}^{-1}$) is much larger than for the Z-pole region (about $140\,\mathrm{pb}^{-1}$), the number of hadronic events is much less. This is due in first instance to the much lower hadronic cross section, *e.g.*, about 20 pb at $\sqrt{s} = 200$ GeV, which is roughly 200 times smaller than at the Z pole. Secondly, at high energies a large fraction of the events correspond to hard initial state radiation (ISR) bringing down the effective hadronic centre-of-mass energy, $\sqrt{s'}$, to the Z pole. When these events with hard ISR are rejected the data samples have typically a few hundred to a few thousand hadronic events per energy point. Another experimental challenge at these high energies is the treatment of the dominant background, which, above the W-pair production threshold ($\sqrt{s} > 161$ GeV), comes from W pairs decaying into four quarks. Part of this background can be rejected using topological identification, but the remaining contamination must be subtracted according to model predictions. Nevertheless, the availability of a large range of energies is very important for testing QCD, since the theory predicts, essentially, the energy variation of observables rather than their absolute values. In addition, it is important that the QCD measurements be performed at each energy using the same experimental technique and the same theoretical calculation. The experimental and theoretical uncertainties on the measurement of an observable are then highly correlated between energies. The measurement of the energy dependence of the observable is then insensitive to these uncertainties. We note that the flavour composition changes with the energy away from the Z pole. For example, when there is no ISR, the fraction of $\mathrm{b\bar{b}}$ drops from about 22% at the Z pole to about 16% at $\sqrt{s} \approx 209$ GeV. This must be taken into account when measuring the energy dependence of observables which depend on the quark-flavour composition of the events.

The work presented in this report concerns mainly the variation of hadronic event shapes with centre-of-mass energy and the study of soft gluon coherence through charged particle multiplicity and momentum distributions. The measurements of the event shapes are used to determine the strong coupling constant, α_s.

Six event-shape distributions are measured, as well as the charged particle multiplicity and momentum distributions, using the data collected with the L3 detector [10–16] at various energies. At the Z pole they are measured for b and lighter (udsc) flavours as well as for all flavours. The measured distributions are compared with predictions from event generators

based on an improved leading logarithmic approximation (Parton Shower models including QCD coherence effects). These Monte Carlo programs use different approaches to describe both the perturbative parton shower evolution and non-perturbative hadronisation processes. They are tuned to reproduce the global event-shape distributions and the charged particle multiplicity distribution measured at 91.2 GeV.

Moments of the event-shape variables are measured between 41.4 GeV and 206.2 GeV. Perturbative and non-perturbative QCD contributions are obtained from a fit using a power correction ansatz [17–21].

The strong coupling constant is also determined at each of these centre-of-mass energies by comparing the measured event-shape distributions with predictions of second order QCD calculations [22,23] supplemented by resummed leading and next-to-leading order terms [24–29].

The mean charged particle multiplicity and the peak position, $\xi^\star$, of the distribution of $\xi = -\ln x$, where x is the charged particle momentum scaled by the beam energy, are measured at different centre-of-mass energies. The energy dependence of these two observables is compared with QCD predictions including soft gluon coherence. A study of the differences between udsc-quark, b-quark and all flavours is also presented for the Z-pole data.

The results presented here update and complete previously published L3 results on QCD obtained from various e^+e^- energy studies. The first one was a study of hadronic event structure at the Z pole [30–32]. This study was extended subsequently to high energies [33–37]. The energy range was also extended to as low as 30 GeV by exploiting hadronic events from Z decays with isolated high energy photons, which gives reduced hadronic centre-of-mass energies [38]. In these events the high energy photons are radiated through initial state radiation or through bremsstrahlung from quarks.

2 QCD and the Process $e^+e^- \rightarrow$ hadrons

2.1 Theoretical Framework

QCD [1–9] is the gauge theory proposed for the strong interaction. It describes the interactions between the quarks and the neutral vector gauge bosons mediating the strong interactions, the gluons. Quarks and gluons carry a quantum number, called colour, which allows the existence of a coupling between gluons as well as between quarks and gluons. This gluon self interaction leads to a fundamental property of QCD, called asymptotic freedom, predicting the decrease of the strong coupling constant, α_s, with energy scale.

From the theoretical point of view, the process of hadron production from a quark-antiquark pair in e^+e^- annihilations may be seen as composed of two different regimes governed by the strong interactions and referred to as the perturbative and non-perturbative phases. Asymptotic freedom guarantees that calculational techniques based on perturbation theory may be applied to describe quark and gluon production with high momentum transfers. This defines the first regime corresponding to a parton cascade where primary quarks split into further partons down to an energy scale of about 1 GeV, where perturbative techniques cease to be valid. The main perturbative calculations available to describe the hadronic event structure at the parton level are:

- $\mathcal{O}(\alpha_s^2)$ calculations of event-shape variables [22, 23];
- improved calculations, incorporating the resummation of leading and next-to-leading logarithmic terms [24–29] matched to $\mathcal{O}(\alpha_s^2)$ results, for several event shape variables;

- $\mathcal{O}(\alpha_s^3)$ calculation (full 1-loop) of 4-parton states [39, 40];
- analytical calculations based on several leading logarithmic approximations [41–52].

In order to relate the parton-level calculations to final state hadrons, one approach is to use phenomenological models describing the non-perturbative transition phase. These models are included in the commonly used QCD Monte Carlo programs. Another, more recent, approach consists of describing the non-perturbative effects analytically by means of power corrections. These corrections have been calculated for low-order moments and differential distributions of some e^+e^- event-shape observables [53].

Finally, in the case of analytical calculations of inclusive quantities (*e.g.*, charged particle mean multiplicity or momentum distributions) the hypothesis of Local Parton Hadron Duality [54, 55] is usually invoked. It suggests that the calculated parton distributions are related to the measured hadron distributions by a simple normalization constant. This hypothesis is used here for the study of the energy dependence of charged particle distributions.

2.2 Experimental Framework

In the last 25 years the study of hadronic events produced in e^+e^- annihilation has made a major contribution to demonstrating the validity of QCD. This is largely due to the fact that e^+e^- interactions offer a very clean environment to study basic QCD processes. QCD affects only the final state; there is no contamination from beam remnants; and, apart from initial and final state electromagnetic radiation, the hadronic centre-of-mass energy is well defined. The observed hadronic event structure is directly related to the gluon radiation pattern produced in the parton (quark and gluon) QCD processes.

Direct evidence for the existence of the quark was given by the observation of two-jet structure in hadronic events produced in e^+e^- collisions at SPEAR [56], and analysis of the jet angular distributions established that their spin is 1/2. The observation of the first three-jet events at PETRA gave the first evidence for the existence of the gluon [57–60] and its coupling to quarks. Subsequently, particle production in the region between a quark and anti-quark was found to be suppressed compared to that between a quark and gluon, the so-called string effect [61, 62]. The existence of the triple gluon vertex coupling was confirmed in a study of jet angular distributions in 4-jet events measured at TRISTAN [63].

Many quantitative tests of QCD have been performed at various e^+e^- colliders. Some detailed reviews of these studies can be found, *e.g.*, in References 64–69.

The LEP experiments have been very active since 1989 in performing quantitative tests of QCD [65–69]. Due to its large hadronic branching ratio, negligible background from other processes, and a strong suppression of initial state radiation, the Z resonance has offered unique conditions for detailed QCD studies. In addition, the precise micro-vertex detectors of the tracking systems of the LEP experiments have allowed flavour-dependent QCD studies to be performed with the high statistics Z-pole data. The higher centre-of-mass energies of LEP2 have allowed studies of the energy-scale dependence of QCD predictions over a wider range. The energy-scale dependence has also been observed in ep deep inelastic scattering at HERA [70, 71] and in $p\overline{p}$ interactions at TEVATRON [72].

2.3 Monte Carlo Programs

Monte Carlo programs simulate the process $e^+e^- \rightarrow$ hadrons by factorizing it into four different phases:

1. production of $q\bar{q}(\gamma)$ (electroweak),

2. gluon radiation (perturbative QCD),

3. hadronisation of quarks and gluons (non-perturbative QCD),

4. decays of unstable particles.

Two approaches to the modelling of perturbative QCD exist [73]. One is the matrix element method, in which Feynman diagrams are calculated exactly, order by order. Because of the technical difficulties of the calculation, matrix elements are only available for a maximum of four partons in the final state.

The other approach is the parton shower method, which is based on an approximation of the full matrix element expression. Each parton produced in the initial hard process may split into two partons, as may successive partons. This results in a description of multi-jet events, with no explicit upper limit on the number of partons involved. The parton shower picture is derived within the framework of the Leading Logarithmic Approximation (LLA) [41–45], in which only the leading terms in the perturbative expansion are kept, or within the framework of the Modified Leading Logarithmic Approximation (MLLA) [50–52], in which some interference effects [74–76] found in the Next-to-Leading Logarithmic Approximation (NLLA) [46–49] are also included. In the branching the energy fractions are distributed according to the leading-order DGLAP splitting functions [77–80]. There are many ambiguities in the LLA description, especially in the renormalisation scheme. Therefore, the parton shower scale parameters extracted from the LLA models through comparisons with data do not correspond to the QCD scale parameter $\Lambda_{\overline{\rm MS}}$. Note, however, that the parton shower programs impose energy-momentum conservation at each splitting, a feature which goes beyond these approximation schemes.

Because perturbative QCD calculations are not valid at low energy scales, the fragmentation of coloured quarks and gluons into colourless hadrons cannot be calculated by perturbative QCD. One needs to rely on phenomenological models. The separation between the perturbative and fragmentation phases is generally characterised by an energy scale (Q_0) with a typical value of a 1–2 GeV. Three different fragmentation models [73] have been developed: independent [81–88], string [89–92], and cluster [93, 94].

The independent fragmentation model assumes that partons fragment in isolation from each other. In this scheme, high momentum quarks evolve separately, splitting into colourless particles and other quarks. It has been shown that the independent fragmentation model fails to describe some experimental data [61, 62].

The string model is derived from the QCD inspired idea that a colour flux tube (string) is stretched between quark and anti-quark pairs, with gluons corresponding to kinks in the string. Hadrons are generated in the formalism of string breaking.

In the cluster model, gluons from the perturbative phase are first split into quark and anti-quark pairs. The quark and anti-quark pairs then form colourless clusters which, depending on their masses, decay either into lower mass clusters or directly into particles.

These different perturbative QCD approaches and fragmentation models have been incorporated into several Monte Carlo programs [73]. In this Report we compare results with the predictions of the following set of programs: Jetset 7.4 PS [95], Ariadne 4.06 [96], Jetset 7.4 ME [95], Herwig 5.9 [99], and Cojets 6.23 [100]. This set of Monte Carlo programs reflects wide differences in the application of perturbative QCD approaches and fragmentation processes.

JETSET PS The JETSET parton shower Monte Carlo program [95] and its successor PYTHIA [95, 103] simulate e^+e^- annihilation into partons and the subsequent quark and gluon branchings. The parton shower is based on the leading logarithmic approximation using as the evolution variable the mass squared of the branching parton. Angular ordering, which is a consequence of gluon interference in the next-to-leading logarithmic approximation, as well as nearest-neighbour intrajet spin correlations, are incorporated in an *ad hoc* manner. The distribution of the first gluon is modified to match the $\mathcal{O}(\alpha_s)$ matrix element distribution. Initial state radiation is included in JETSET using the lowest order calculation, following the approach presented in References 104 and 105. In PYTHIA an 'initial-state shower' is used to simulate ISR. The programs contain both string and independent fragmentation options. Here we only study string fragmentation. Various fragmentation functions are available. They provide the distribution of the fraction, z, of the light-cone fraction, $E + p_L$, carried by the resulting hadron,

$$z = \frac{(E + p_L)^{had}}{(E + p_L)^{par}} . \tag{1}$$

Here E and p_L are the energy and longitudinal momentum relative to the primary parton direction, and the superscripts (had) and (par) refer, respectively, to the hadron after its creation and the parton before creation of the hadron. For c- and b-quarks, we use the Peterson fragmentation function [106]

$$f(z) \propto \frac{1}{z\left(1 - \frac{1}{z} - \frac{\epsilon}{1-z}\right)^2} \tag{2}$$

where ϵ is a fragmentation parameter depending on the flavour of the quark. The light quarks are fragmented according to the Lund symmetric function [107]

$$f(z) \propto \frac{1}{z}(1-z)^a \exp\left(-\frac{bm_T^2}{z}\right) , \tag{3}$$

where $m_T = \sqrt{E^2 - p_L^2} = \sqrt{m^2 + p_T^2}$ is the transverse mass of the system, and a and b are fragmentation parameters. The spectrum of the transverse momentum, p_T, of the hadron is described by the Gaussian function

$$f(p_T) \propto \exp\left(-\frac{p_T^2}{2\sigma_q^2}\right) \tag{4}$$

with σ_q a parameter. The parameters that affect hadronic event structure most are the parton shower scale Λ_{LL}, the parton shower cut-off parameter Q_0, and the fragmentation parameters a, b, and σ_q.

ARIADNE The ARIADNE program [96] also uses a parton shower algorithm. The perturbative QCD cascade in ARIADNE is formulated in terms of two-parton systems, which form colour dipoles. When a gluon is radiated from a dipole, the dipole is then converted into two independent dipoles. This formulation is equivalent, to MLLA accuracy, to a parton shower with angular ordering automatically incorporated [108]. The evolution variable is $Q^2 = p_t^2$, where p_t is the transverse momentum of the radiated gluon. ARIADNE itself does not provide functions for fragmentation and decay processes. Instead, it is

interfaced to the JETSET or PYTHIA fragmentation and decay routines. In addition, ARIADNE uses JETSET or PYTHIA routines to generate the initial $q\bar{q}$ system and ISR. Only the string fragmentation is used here. In the ARIADNE perturbative phase, there are two main parameters that affect the parton configuration most: the parton shower scale parameter Λ_{AR} and the parton shower cut-off parameter $p_{\mathrm{t}}^{\mathrm{min}}$. The relevant fragmentation parameters are the same as those in the JETSET PS model.

JETSET ME Besides the parton shower option, JETSET also provides for a full $\mathcal{O}(\alpha_{\mathrm{s}}^2)$ matrix element [23] treatment of perturbative QCD. In our application, we use 'optimised perturbation theory' [109, 110] with the renormalisation scale, f, set to 0.003 and the minimum scaled invariant mass squared of any two partons in 3- or 4-jet events, y_{min}, set to 0.01. The scale f is chosen so that Q^2 is above the b-quark mass while y_{min} is close to the minimum allowed value that still gives a positive 2-jet production cross section. It has been shown that a small scale f gives significantly improved agreement with the data [111]. In addition, we apply the parameterisation given in Reference 112 for the second order corrections to the 3-jet rate. The generated partons are subsequently fragmented using the string fragmentation model. As for JETSET PS, we use the Peterson function for heavy quark fragmentation and the Lund symmetric function for light quark fragmentation. The relevant parameters for our study are the QCD scale parameter Λ_{ME} and the fragmentation parameters σ_q, a and b of the string model.

HERWIG The HERWIG Monte Carlo program [97–99] is based on parton shower simulation using a coherent branching algorithm. While the energy fractions are distributed according to the LLA, phase space is restricted to an angular-ordered region. The choice of evolution variable is $\approx E^2(1-\cos\theta)$, where E is the energy of the branching parton and θ is the angle between the two resulting partons. This facilitates the inclusion of interference phenomena [74–76] in the treatment of parton shower development. The description of hard gluon emission is improved by matching the parton shower calculation to an $\mathcal{O}(\alpha_{\mathrm{s}})$ matrix element calculation. Fragmentation is performed by a cluster model, which incorporates the preconfinement property of perturbative QCD [54, 93, 94, 108, 113]. The event-shape variables are most sensitive to the parton shower scale parameter, Λ_{MLLA}, the effective gluon mass, M_{g}, and two parameters which control the splitting of clusters: the maximum cluster mass, CLMAX, and the power of the mass, CLPOW, in the expression for the cluster splitting criterion.

COJETS The Monte Carlo program COJETS [100–102] simulates the multiple gluon radiation in the LLA. Like JETSET PS it uses the mass squared of the branching parton as evolution variable, but with incoherent branching. The parton shower algorithm is corrected for single hard gluon emission using an $\mathcal{O}(\alpha_{\mathrm{s}})$ calculation. This simulation is integrated with the independent jet fragmentation according to a modified version of the Field-Feynman model [85]. COJETS has four free parameters in its longitudinal fragmentation function and one free parameter to control the transverse momentum spectra in the fragmentation cascade. Since quarks and gluons fragment independently, these parameters can have different values for quark and gluon jets. As in other parton shower programs, there are also parameters for the parton shower scale, Λ_{LL}, and the parton shower cut-off, Q_0.

3 Hadronic Events in L3

3.1 Calorimeter Energy Measurement

The selection of hadronic events is based on the energy measured in the electromagnetic and hadron calorimeters. Two algorithms are developed to estimate the energy of an event from the raw energy deposits. In its LEP2 configuration, the L3 detector is divided into eleven broad regions, nine of which are calorimeters (regions 1–4 and 6–10, region 5 being no longer present for LEP2). The other two are the central tracker (region 12) and the muon chambers (region 11). A particle can deposit its energy in more than one region. The definition of the regions changed with time depending on the exact detector configuration. The regions as defined during the LEP2 runs are shown in Figure 1. The main changes with respect to LEP1 are the addition of forward/backward muon chambers [15] and calorimeters (SPACAL), constructed using lead and scintillating fibres between the barrel and endcap electromagnetic calorimeters [16].

In one of the approaches (linear algorithm), the energy of a particle, detected as the smallest resolvable calorimeter cluster (SRC), is expressed as a linear sum of energy deposits in the calorimeter, E_i^{c}:

$$E^{\mathrm{c}} = \sum_{i=1}^{10} G_i^{\mathrm{L}} \cdot E_i^{\mathrm{c}} \tag{5}$$

The weighting factors, G_i^{L}, are called G-factors. They compensate for the different calorimeter response to different particle types. The energy of the event is obtained by adding the energy, E^{c}, of all the SRC's in the event and the momenta of the muons. Since the noise levels in different parts of the detectors can have a wide variation, the energy thresholds for different types of SRC's are handled separately.

In the second approach (non-linear algorithm), the clusters are redefined to include tracks in the energy measurement. The new objects, called super-clusters (ECLU), are built by associating the different components of a cluster with charged tracks and muon candidates using angular proximity. The association is carried out as a four step algorithm:

1. All possible pairs of constituents, whose angular separation is smaller than a given cut, are combined to form seeds.

2. If the angular separation between a constituent and the ones which form a seed is smaller than a given cut, it is added to the super-cluster associated to the seed. Each constituent can, in principle, be included in several super-clusters.

3. The ambiguities are then solved by assigning each constituent to its closest super-cluster.

4. The energy of each super-cluster is then calculated.

The energy of the super-cluster is given by

$$\widetilde{E}_\ell^{\mathrm{sc}} = \sum_{i=1}^{12} \widetilde{G}_i^{\mathrm{NL}} \cdot E_i + \sum_{j,k=1}^{12} \widetilde{A}_{jk}^{\mathrm{NL}} \cdot C_\ell(E_j, E_k) \ , \tag{6}$$

where E_i is the uncorrected energy measured in region i. For the calorimeter regions, $E_i = E_i^{\mathrm{c}}$; for tracks E_i is the momentum of the track. The correlation function C_ℓ introduces a non-linear term in the energy measurement. Two parametrisations are tried:

$$C_1(E_j, E_k) = E_j \cdot E_k \qquad \text{and} \qquad C_2(E_j, E_k) = \frac{E_j \cdot E_k}{E_j + E_k} \ . \tag{7}$$

The first parametrisation leads to a better energy resolution while the second provides a smaller non-linearity in the energy measurement. The non-linearity is reduced by scaling the super-cluster energy to obtain

$$E_\ell^{\rm sc} = \frac{E_{\rm tot}}{\sum \widetilde{E}_\ell^{\rm sc}} \cdot \widetilde{E}_\ell^{\rm sc} \ . \tag{8}$$

The total energy, $E_\ell^{\rm tot}$, is given by

$$E_\ell^{\rm tot} = \sum_{i=1}^{12} G_i^{\rm NL} \cdot E_i^{\rm T} + \sum_{j,k=1}^{12} A_{jk}^{\rm NL} \cdot C_\ell(E_j^{\rm T}, E_k^{\rm T}) \ , \tag{9}$$

an expression analogous to that for a super-cluster. Here, $E_i^{\rm T}$ is the sum of the uncorrected energies of all constituents of the entire event in detector region i. The factors $\widetilde{A}_{jk}^{\rm NL}$ and $A_{jk}^{\rm NL}$ have non-vanishing values only for connected neighbouring detector regions.

Energies of electrons, photons and muons are accurately measured in the L3 detector. To benefit from this, with both algorithms, active particle identification has been used to identify electrons, photons and muons. The corresponding clusters, tracks and muon candidates are removed from the list considered in finding the clusters. The identified electromagnetic clusters and muons are then added with their energy measurements from the electromagnetic calorimeter or muon chamber to the list of reconstructed clusters.

For both algorithms, the numerical values of the various coefficients (G-factors), $G^{\rm L}$, $\widetilde{G}^{\rm NL}$, $\widetilde{A}^{\rm NL}$, $G^{\rm NL}$ and $A^{\rm NL}$, are determined by minimising the total energy resolution on hadronic events while constraining the mean visible energy to the centre-of-mass energy. This procedure is performed only after precise absolute calibration of each detector component. The coefficients are re-determined whenever the detector configuration is modified or the beam energy of LEP is significantly changed. This is to overcome a certain amount of non-linearity still left in these energy measurements. This is more pronounced in the non-linear G-factors, but is somewhat reduced by a proper choice of the correlation function C_ℓ and a better identification algorithm for the final state particles.

The non-linear G-factors are only appropriate for events with small missing energy. The linear G-factors are found to be independent of time variation of detector responses and are nearly energy independent. The linear algorithm is well suited to comparison of physics measurements over several centre-of-mass energies. We have therefore used the linear G-factors for all our subsequent analyses and used the non-linear G-factors for systematic checks.

3.2 Energy and Angular Resolutions of Jets

We use energy clusters in the calorimeters with a minimum energy of 100 MeV. Figure 2 shows the scaled visible energy ($E_{\rm vis}/\sqrt{s}$) distribution at centre-of-mass energies of 91.2 and 188.6 GeV for the two different algorithms. The smooth curves shown on the plot are the results of fits of a sum of two Gaussians to the observed distributions. Table 2 summarises the results of the fit as well as the RMS values from the data at $\sqrt{s} = 91.2$ and 188.6 GeV. The energy resolution improves substantially with the ECLU algorithm.

Jet angular resolutions obtained with both the linear and the non-linear G-factors are shown in Figure 3 for polar angle θ and azimuthal angle ϕ. They are computed from the angle between the jets in selected 2-jet events at $\sqrt{s} = 91.2$ GeV and 188.6 GeV. The curves correspond to fits with a sum of two Gaussians for each distribution. The fit results are summarised in Table 2 where the Gaussian widths are denoted σ_i. The RMS values of the distributions are

also given. Table 2 also summarises the resolutions obtained using linear G-factors. There is a slight improvement in ϕ resolution with the ECLU algorithm while the θ resolution is the same. This difference in improvement is due to a better L3 track resolution in ϕ than in θ.

3.3 Selection of Hadronic Events

The principal variables used to distinguish hadronic events from backgrounds are the cluster multiplicity and the energy imbalances. We use energy clusters in the calorimeters to measure the total visible energy, $E_{\rm vis}$, and the energy imbalances parallel and perpendicular to the beam direction: $E_{\parallel} = |\sum E \cos\theta|$ and $E_{\perp} = \sqrt{(\sum E \sin\theta \sin\phi)^2 + (\sum E \sin\theta \cos\phi)^2}$, respectively, where E is the energy of a cluster and θ and ϕ are its polar and azimuthal angles with respect to the beam direction. Backgrounds are different for hadronic Z decays, hadronic events at reduced centre-of-mass energies and at high energies. This results in different selection cuts for these three types of event.

The efficiency of the selection criteria and purity of the data sample are estimated using Monte Carlo events. For the process $e^+e^- \to q\bar{q}(\gamma)$ Monte Carlo events are generated by the programs JETSET 7.3 at the Z pole, PYTHIA 5.7 for higher energies up to 189 GeV and KK2f [114,115], which uses PYTHIA for hadronisation, for the highest energies. The generated events are passed through the L3 detector simulation, which is based on GEANT [116] using the GHEISHA program [117] to simulate hadronic interactions. Background events are simulated with appropriate event generators: PYTHIA and PHOJET [118, 119] for hadron production in two-photon interactions, KORALZ [120] for the $\tau^+\tau^-(\gamma)$ process, BHAGENE [121, 122] and BHWIDE [123] for Bhabha events, KORALW [124, 125] for W-pair production and PYTHIA for Z-pair production.

Hadronic Z decays are selected [30] by imposing simple cuts on visible energy, $0.6 < E_{\rm vis}/\sqrt{s} < 1.4$, relative energy imbalances, $E_{\parallel}/E_{\rm vis} < 0.4$ and $E_{\perp}/E_{\rm vis} < 0.4$, and number of clusters > 12. The event-shape distributions for all flavours have been previously published [30] and are not updated here. They are based on $8.3\,{\rm pb}^{-1}$ of integrated luminosity, rather than the full luminosity available ($142.4\,{\rm pb}^{-1}$). This is sufficient to provide an experimental error on $\alpha_{\rm s}$, which is smaller by a factor 3 than theoretical uncertainties.

Events at reduced centre-of-mass energies are obtained from the entire data collected at the Z pole. Hadronic events are initially selected with the same criteria as described above. In this event sample, isolated photons are selected with energy $E_\gamma > 5$ GeV. The lateral shower profile of the candidate is required to be consistent with an electromagnetic shower and no other cluster with energy above 250 MeV may lie within 10° around the candidate. With these criteria, $1.3 \cdot 10^5$ events are selected. The centre-of-mass energy of the remaining hadronic system is given by

$$\sqrt{s'} = \sqrt{s\left(1 - \frac{2E_\gamma}{\sqrt{s}}\right)} \quad . \tag{10}$$

Six intervals of $\sqrt{s'}$ are chosen such that each interval has reasonable statistics. We have studied whether $\sqrt{s'}$ is the correct scale of hadron production by comparing Monte Carlo hadronic Z decay events containing isolated final-state photons with Monte Carlo e^+e^- events generated without ISR or FSR at $\sqrt{s} \approx \sqrt{s'}$. The distributions of event-shape variables are similar, suggesting that $\sqrt{s'}$ can be used as the QCD scale.

The background for the direct photons is dominated by unresolved π^0 and η decays. To reduce this background, we require that the shower be isolated and that its shape be compatible

with the electromagnetic shower of a single photon. We use a shower-shape discriminator based on an artificial neural network to distinguish multi-photon showers from those of a single photon. The cut values are tuned separately for photon candidates in each of the six different energy ranges by optimising the efficiency and purity at each energy. Details of this selection are given in Reference 38.

At $\sqrt{s} > 130$ GeV, the main background comes from so-called radiative return events, where ISR results in a mass of the hadronic system close to that of the Z boson, m_{Z}. Events are selected by requiring $E_{\mathrm{vis}}/\sqrt{s} > 0.7$, $E_{\perp}/E_{\mathrm{vis}} < 0.4$, number of clusters > 12, and at least one well measured charged track. The distributions of $E_{\mathrm{vis}}/\sqrt{s}$ and the number of clusters are shown, for representative energies, in Figure 4. These cuts eliminate a large fraction of the radiative return events as well as two-photon interactions and other backgrounds. To further reduce the radiative return background, events are rejected if they have a high-energy photon candidate, defined as a cluster in the electromagnetic calorimeter with at least 85% of its energy within a 15° cone and a total energy greater than 15 GeV at $\sqrt{s} = 130.1$ and 136.1 GeV and greater than $0.18\sqrt{s}$ at higher $\sqrt{s}$. The distribution of the energy of the most energetic photon candidate is shown in Figure 5a. Since the ISR photon is often produced at too low an angle to enter the detector, a cut in the two dimensional plane of $E_{\parallel}/E_{\mathrm{vis}}$ and $E_{\mathrm{vis}}/\sqrt{s}$ is also applied, requiring $E_{\mathrm{vis}}/\sqrt{s} > kE_{\parallel}/E_{\mathrm{vis}} + 0.5$ where k is 2.5 at $\sqrt{s} = 130.1$ and 136.1 GeV, 1.5 at $\sqrt{s} = 161.3$ GeV, and 2.0 for $\sqrt{s} \geq 172.3$ GeV. This cut is illustrated in Figure 5b.

Data at $\sqrt{s} = 130.1$ and 136.1 GeV were collected in two separate runs during 1995 [33] and 1997. In the current analysis, data sets from the two years are combined.

For the data at $\sqrt{s} \geq 161.3$ GeV, additional backgrounds arise from W-pair and Z-pair production. A substantial fraction ($\sim 80\%$) of these events are removed by specific selections [34–37]. To reject events where a W or Z decays into leptons we remove events having an electron or muon with energy greater than 40 GeV. Fully hadronic decays are rejected by

- forcing the event to a 4-jet topology using the Durham algorithm [126–129],
- performing a kinematic fit imposing the constraints of energy-momentum conservation,
- making cuts on the energies of the most- and the least-energetic jets and on y_{34}^{D}, the value of the jet resolution parameter at which the event classification changes from 3-jet to 4-jet. Events are rejected if the energy of the most energetic jet is less than $0.4\sqrt{s}$ (see Figure 6a), the ratio of the energy of the most energetic jet to that of the least energetic jet is smaller than 5 (see Figure 6b), $y_{34}^{\mathrm{D}} > 0.007$ (see Figure 6c), there are more than 40 clusters and more than 15 charged tracks, and $E_{\parallel} < 0.2E_{\mathrm{vis}}$ after the kinematic fit.

These cuts remove between 3.6% of signal events at the W-pair threshold and 10.6% at the highest centre-of-mass energy. The data collected at high energy are combined into several energy bins. The integrated luminosity, selection efficiency, purity and number of selected events for each of the energy points are summarised in Table 1.

3.4 Flavour Tagging

Events with b-quarks can be separated from events with other flavours at the Z pole using the characteristic decay properties of the b-hadrons. As the first step, the interaction vertex is estimated by iteratively fitting all of the good tracks measured in the detector in each beam-storage period. Measurements of the decay lengths of all n tracks in the event contribute to a probability, $P^{[n]}$, which would be flat for zero lifetime but otherwise peak at zero. Figure 7

shows the distribution of a weighted discriminant $B_n = -\log\{P^{[n]} \sum_{j=0}^{n-1} \left(-\ln P^{[n]}\right)^j / j!\}$ where $P^{[n]} = \prod_{j=1}^{n} P_j$ and P_j is the probability that track j originates at the primary vertex [130].

A cut on this discriminant is made to distinguish udsc- from b-quark events. The udsc-flavour events are selected using $0.3 < B_n < 1.0$ with an efficiency of 39.2% and a purity of 91.0%. The b-quark contamination amounts to 8.8% of the selected events. The b-flavour events are selected with a cut on $B_n > 3.4$ yielding $6.3 \cdot 10^4$ b-enriched events with efficiency of 36.2% and purity of 92.9%. The contamination due to udsc-flavour events in the sample is 7.0%. Measurement of flavour-tagged quantities uses only data taken after installation and commissioning of the silicon micro-vertex detector [14].

4 Event-Shape Variables

4.1 Choice of Variables

Event-shape variables, constructed from linear sums of measured particle momenta, are sensitive to the amount of hard gluon radiation and offer one of the most direct ways to measure α_s in e^+e^- annihilation. They are insensitive to soft and collinear radiation ('infra-red safe') and so can be reliably calculated in perturbative QCD. We measure six global event-shape variables for which improved analytical QCD calculations [24–29] are available. These are thrust (T), scaled heavy jet mass (ρ_H), total (B_T) and wide (B_W) jet broadening variables and the C- and D-parameters.

Thrust: The global event-shape variable thrust, T, [131, 132] is defined as

$$T = \frac{\sum |\vec{p}_i \cdot \vec{n}_T|}{\sum |\vec{p}_i|} , \tag{11}$$

where $\vec{p}_i$ is the momentum vector of particle i. The thrust axis, $\vec{n}_T$, is the unit vector which maximises the above expression. The value of the thrust can vary from 0.5 for spherical events to 1.0 for narrow 2-jet events.

The plane normal to $\vec{n}_T$ divides space into two hemispheres, $S_\pm$, which are used in the following definitions.

Scaled heavy jet mass: The heavy jet mass, M_H, is defined [133–135] as

$$M_H = \max\left[M_+(\vec{n}_T), M_-(\vec{n}_T)\right] , \tag{12}$$

where $M_\pm$ are the masses of the system of particles in the two hemispheres,

$$M_\pm^2 = \left[\sum_{i \in S_\pm} p_i\right]^2 , \tag{13}$$

where p_i is the four-momentum of particle i. The scaled heavy jet mass, ρ_H, is defined as

$$\rho_H = M_H^2 / E_{vis}^2 . \tag{14}$$

Jet broadening variables: These variables are defined [26, 27] by computing in each hemisphere the quantity

$$B_{\pm} = \frac{\sum_{i \in S_{\pm}} |\vec{p}_i \times \vec{n}_{\mathrm{T}}|}{2 \sum_i |\vec{p}_i|} \ , \tag{15}$$

in terms of which the total jet broadening, B_{T}, and the wide jet broadening, B_{W}, are defined as

$$B_{\mathrm{T}} = B_+ + B_- \quad \text{and} \quad B_{\mathrm{W}} = \max(B_+, B_-) \ . \tag{16}$$

***C*- and *D*-parameters:** The C- and D-parameters are derived from the eigenvalues of the linearised momentum tensor [136, 137]:

$$\Theta^{ij} = \sum_a \frac{p_a^i p_a^j}{|\vec{p}_a|} \Bigg/ \sum_a |\vec{p}_a| \quad i, j = 1, 2, 3, \tag{17}$$

where p_a^i is the i^{th} component of the momentum vector, $\vec{p}_a$, of particle a. With λ_1, λ_2, and λ_3 the eigenvalues of Θ, the C- and D-parameters are defined as

$$C = 3(\lambda_1\lambda_2 + \lambda_2\lambda_3 + \lambda_3\lambda_1) \tag{18}$$

$$D = 27\lambda_1\lambda_2\lambda_3 \ . \tag{19}$$

A few other global event-shape variables are also measured for comparison with the predictions of Monte Carlo models. These variables have linear or quadratic dependence on particle momenta. Some of these parameters are particularly sensitive to the details of fragmentation and hence are used to tune and test Monte Carlo models.

Major, minor: Major (T_{major}) [57] is defined in the same way as thrust but is maximised in the plane perpendicular to the thrust axis. The resulting direction is called the major axis, $\vec{n}_{\mathrm{major}}$. The minor axis, $\vec{n}_{\mathrm{minor}} = \vec{n}_{\mathrm{major}} \times \vec{n}_{\mathrm{T}}$, is defined to give an orthonormal system. Minor (T_{minor}) is the normalised sum of momenta projected onto $\vec{n}_{\mathrm{minor}}$.

Oblateness: Oblateness (O) [57] is the difference of the major and minor values:

$$O = T_{\mathrm{major}} - T_{\mathrm{minor}} \ . \tag{20}$$

Minor of the narrow side: After dividing an event into two hemispheres by the plane perpendicular to the thrust axis, the transverse momentum fraction

$$f_{\mathrm{t}} = \frac{\sum_i |\vec{p}_i \times \vec{n}_{\mathrm{T}}|}{\sum_i |\vec{p}_i|} \tag{21}$$

is calculated for each hemisphere. The hemisphere with the smaller f_{t} is called the narrow side. The minor calculated using only the particles in this hemisphere is defined as the minor of the narrow side, $T_{\mathrm{minor}}^{\mathrm{NS}}$, [138].

Scaled light jet mass: This quantity is defined analogously to the scaled heavy jet mass:

$$\rho_{\mathrm{L}} = M_{\mathrm{L}}^2 / E_{\mathrm{vis}}^2 \ , \quad M_{\mathrm{L}} = \min\left[M_+(\vec{n}_{\mathrm{T}}), M_-(\vec{n}_{\mathrm{T}})\right] \ . \tag{22}$$

Jet resolution parameters: Jets are reconstructed using an invariant mass (JADE [139,140]) or scaled transverse momentum ($k_{\rm t}$ or Durham [126–129]) jet algorithm. The value of the jet resolution parameter, y_{ij}, at which the classification of an event changes from 2-jet to 3-jet is called the 3-jet resolution parameter, $y_{23}^{\rm J}$ and $y_{23}^{\rm D}$ for the JADE and Durham algorithms, respectively.

Fox-Wolfram Moments: The Fox-Wolfram moments [141–143] are given by

$$H_\ell = \sum_{i,j} \frac{|\vec{p}_i|\,|\vec{p}_j|}{s} P_\ell(\cos\alpha_{ij}) \tag{23}$$

where $\vec{p}_i$ and $\vec{p}_j$ are the momenta of particles i and j, respectively, α_{ij} is the angle between these two particles, and P_ℓ is the Legendre polynomial of order ℓ. The sums run over all particles in the events.

Sphericity, aplanarity: Sphericity, S, and aplanarity, A, are defined using the eigenvalues of the sphericity tensor [144],

$$s^{ij} = \frac{\sum_a p_a^i p_a^j}{\sum_a p_a^2} \quad i,j = 1,2,3, \tag{24}$$

where p_a^i is the $i^{\rm th}$ component of the momentum vector $\vec{p}_a$. From the eigenvalues of s^{ij}, $Q_1 \leq Q_2 \leq Q_3$, the sphericity and aplanarity are defined as

$$S = \frac{3}{2}(Q_1 + Q_2)\ ; \qquad A = \frac{3}{2} Q_1\ . \tag{25}$$

Spherocity: The global event-shape variable, spherocity (S') [145, 146] is defined as

$$S' = \frac{4}{\pi} \cdot \frac{\sum |\vec{p}_i \times \vec{n}_{\rm S}|}{\sum |\vec{p}_i|}\ , \tag{26}$$

where $\vec{n}_{\rm S}$, called the spherocity axis, is the unit vector which minimises the above expression.

4.2 Measurements

The distributions of the event-shape variables are measured over the full energy range, 30–209 GeV, which includes the three types of event: reduced-energy, Z-pole and high-energy. For the Z-pole data, they are also measured for b- and udsc-quark samples separately using an integrated luminosity of $26.3\,{\rm pb}^{-1}$

The data distributions are compared to a combination of the signal and the different background Monte Carlo distributions obtained using the same selection procedure and normalised to the integrated luminosity. Figures 8–10 show uncorrected thrust distributions measured in the six energy bins of the reduced centre-of-mass energy, flavour-tagged Z-pole, and high-energy samples, respectively, compared to Monte Carlo predictions. The contributions of the shaded areas indicate the various backgrounds. For the reduced-energy events (Figure 8 the backgrounds considered are unresolved π^0's and η's in the hadronic sample, as well as τ-pair and 2-photon processes. The prediction of JETSET has been scaled to account for the lack of isolated energetic π^0's in the string fragmentation process [147]. At the Z pole, background in

the flavour tagged samples is dominated by hadronic events of the other flavour class, but is negligible for the full sample (Figure 9). At high energies (Figure 10) the main backgrounds are radiative events, W-pair production and 2-photon processes. The Monte Carlo distributions agree with the data reasonably well at all centre-of-mass energies.

The global event-shape variables are calculated before, 'particle level', and after, 'detector level', detector simulation. The calculation before detector simulation takes into account all stable charged and neutral particles. The measured distributions at detector level differ from those at particle level because of detector effects, limited acceptance and resolution. The resolution for the thrust varies from about 0.02 at high values to 0.05 at low values. The resolution is similar for the other shape variables. After subtracting the background obtained from simulations, the measured distributions are corrected for detector effects, acceptance and resolution on a bin-by-bin basis by comparing the detector level results with the particle level results. The level of migration is kept at an acceptable level by using a bin size approximately equal to or greater than the experimental resolution. We also correct the data for initial and final state photon radiation bin-by-bin using Monte Carlo distributions at particle level with and without radiation.

4.3 Systematic Uncertainties

The systematic uncertainties in the distributions of event-shape variables arise mainly from uncertainties in the estimation of detector corrections and background. The uncertainty in the detector correction is estimated by several independent checks:

- The definition of reconstructed objects used to calculate the observables is changed. Instead of using only SRC calorimetric clusters, the analysis is repeated using the ECLU objects defined in Section 3.1.

- The effect of different particle densities in correcting the measured distribution is estimated by using a different signal Monte Carlo program, HERWIG instead of JETSET PS or PYTHIA.

- The acceptance is reduced by restricting the events to the more precise central part of the detector, $|\cos(\theta_{\mathrm{T}})| < 0.7$, where θ_{T} is the polar angle of the thrust axis relative to the beam direction.

The uncertainty on the background composition of the selected event sample is estimated differently at different centre-of-mass energies. The systematic uncertainty in the Z-pole flavour-tagged samples is estimated by varying the background from mis-tagged events by $\pm 10\%$. In addition, the background in the udsc sample from 2-photon processes is varied by $\pm 30\%$.

At reduced energies, the systematic uncertainties are estimated by varying:

- the amount of background from misidentified hadrons or non-direct photon production by the uncertainty of its estimation from data [147];

- the selection cuts used to select direct photons: jet and local isolation angles, energy in the local isolation cone, and the neural network probability.

The uncertainty at high energies is estimated by repeating the analysis with:

- an alternative criterion to reject the hard initial state photon events based on a cut on the kinematically reconstructed effective centre-of-mass energy;

- a variation of the estimated two-photon interaction background by ± 30% and by using the program PHOJET instead of PYTHIA to estimate this background;

- a variation of the background estimate by changing the W-pair rejection criteria. As an extreme variation, no 4-jet events are rejected from the data sample and the number of W-pair events is estimated from KORALW Monte Carlo and subtracted from the data.

At high energies, uncertainties due to ISR and W-pair background are the most important. They are roughly equal and are 2–3 times larger than the uncertainties due to the detector correction.

The systematic uncertainties obtained from different sources are combined in quadrature. Statistical fluctuations are not negligible in the estimation of systematic effects. The statistical component of the systematic uncertainty is determined by splitting the overall Monte Carlo sample into luminosity weighted sub-samples and treating each of these sub-samples as data. The statistical component of the systematic uncertainty is estimated from the differences in these sub-samples. This component is subtracted in quadrature from the original estimate.

4.4 Tuning of Monte Carlo Parameters

The Monte Carlo models involve several parameters. Particular shape-variable distributions are especially sensitive to certain parameters and these distributions are used to tune their values. To match Monte Carlo with data we proceed as follows. First, a few event-shape variables with special sensitivity to certain parameters are chosen to be tuning variables for the comparison of data and Monte Carlo:

- the jet resolution parameter in the JADE algorithm which corresponds to the transition from 2 to 3 jets (y_{23}^{J}). This variable is sensitive primarily to the 3-jet rate.

- the fourth Fox-Wolfram moment (H_4), which is sensitive to the angles between jets.

- the minor of the narrow side ($T_{\mathrm{minor}}^{\mathrm{NS}}$). This variable is sensitive to the lateral size of the quark jet.

- the charged particle multiplicity (N_{ch}).

If a model to describe Bose-Einstein correlations is tuned, the distributions of the four-momentum difference for like- and unlike-sign charged particle pairs are also used.

For a set of values of the parameters, $\vec{\alpha}$, to be tuned, the Monte Carlo distributions of the tuning variables are compared to the data distributions. This is quantified by

$$\chi^2(\vec{\alpha}) = \sum_{i=\text{tun. var}} \sum_{j=\text{bins}} \frac{[\mathrm{Data}(i,j) - \mathrm{MC}(i,j,\vec{\alpha})]^2}{[\sigma_{\mathrm{Data}}^{\mathrm{stat}}(i,j)]^2 + [\sigma_{\mathrm{Data}}^{\mathrm{syst}}(i,j)]^2 + [\sigma_{\mathrm{MC}}^{\mathrm{stat}}(i,j,\vec{\alpha})]^2} \tag{27}$$

where the individual contributions to χ^2 are summed over all bins (j) of the distributions of the chosen tuning variables (i). The optimal parameter set is taken to be the one that minimises the above χ^2 function, and is found using the CERN program package MINUIT [148]. Bins with insignificant statistics are ignored in the fit.

The parameters of a model to be tuned span a continuous multi-dimensional space, and thus the χ^2 function is a continuous function of the tuning variables. However, in any realistic tuning procedure, one starts off with a finite set of guesses for the optimal parameter set, and

generates Monte Carlo distributions for the event-shape variables only at these discrete points in the parameter space.

More than 10^5 events are generated for several points on a grid in the parameter space. For a grid with k-parameters and n_p different values for parameter p, one needs to generate events at $\prod_{p=1}^{k} n_p$ points. In the subsequent minimisation procedure, χ^2 values at points between the grid points are found by a local multidimensional interpolation, either linear or non-linear. The Monte Carlo distribution corresponding to the $j^{\rm th}$ bin for the $i^{\rm th}$ tuning variable, MC(i,j), for points in parameter space inside the grid using a polynomial of given degree is given by

$$\mathrm{MC}(i,j,\vec{\alpha}_0+\delta\vec{\alpha}) = a_0(i,j) + \sum_{m=1}^{k} a_1(i,j)_m \delta\alpha_m + \sum_{m,n=1}^{k} a_2(i,j)_{mn}\delta\alpha_m\delta\alpha_n + \cdots \qquad (28)$$

These fits are repeated by varying the fit range of the tuning variables, the degree of the polynomial in the interpolation, and also by changing the choice of grid points. Each of these systematic variations yields possible sets of optimal values for the tuning parameters. To decide among them, a new χ^2 is calculated using additional global event-shape variables: T, $\rho_{\rm H}$, $\rho_{\rm L}$, $B_{\rm T}$, $y_{23}^{\rm D}$, S, A, S', C, D, $T_{\rm major}$, $T_{\rm minor}$, O and H_3. For the tuning of ARIADNE 4.12, PYTHIA 6.2 and HERWIG 6.2 [149] the sums of the components of momentum in and perpendicular to the event plane, as well as ξ were also used. The set with the smallest value of this χ^2 is taken as the tuned parameter set for the Monte Carlo model. The systematic uncertainties on the parameters are obtained by varying the fit ranges and degree of polynomials in the interpolation function.

Tuning is carried out with event-shape distributions obtained at the Z pole. Separate tunings were done for all quark flavours and for udsc flavours. The results of the tuning are summarised in Table 3 for the models which are compared to data in this Report, except for COJETS, which was previously tuned [30]. The cut-off parameter Q_0 and the fragmentation parameter a in the JETSET 7.4 PS model are fixed at $Q_0 = 1$ GeV and $a = 0.5$. The parameter of the Peterson fragmentation function parameters for charm and bottom quarks are fixed at $\epsilon_{\rm c} = 0.03$ and $\epsilon_{\rm b} = 0.0035$, respectively, which are chosen to reproduce the mean energies of c and b hadrons [150]. For the JETSET 7.4 ME model the parameters kept fixed are: $a = 0.5$, $\epsilon_{\rm c} = 0.10$ and $\epsilon_{\rm b} = 0.004$ in order to obtain the same mean energies for c and b hadrons as for the PS model.

The udsc flavour-tagged data are also used to tune models for precision studies of W-boson processes. The results of tuning the PYTHIA 6.2 parton shower program are summarised in Table 4. These results refer to the cut-off parameter value $Q_0 = 1$ GeV and the fragmentation parameter values $a = 0.5$, $\epsilon_{\rm c} = 0.03$ and $\epsilon_{\rm b} = 0.002$. The results of tuning the ARIADNE 4.12 and HERWIG 6.2 models are summarised in Tables 5 and 6, respectively. The HERWIG program is adapted to use the particle decay and Bose-Einstein routines [151, 152] of PYTHIA 6.2.

5 Event-Shape Distributions and $\alpha_{\rm s}$

Since the probability of hard gluon radiation is directly determined by $\alpha_{\rm s}$, a direct measurement of $\alpha_{\rm s}$ is provided by the fraction of events having a specified number of jets. These so-called jet fractions are measured and their behaviour as a function of centre-of-mass energy investigated in Section 5.1. To determine $\alpha_{\rm s}$, we use the event-shape variables. Their distributions are measured and compared to Monte Carlo models in Section 5.2. The applicability of power law corrections is investigated in Section 5.3, and $\alpha_{\rm s}$ is extracted in Section 5.4.

5.1 Jet Fractions

Jets are constructed using the JADE algorithm [139,140]. The following expression is evaluated for each pair of particles i and j:

$$y_{ij}^{\mathrm{J}} = \frac{2E_iE_j}{s}\,(1-\cos\theta_{ij}) \tag{29}$$

where E_i and E_j are their energies and θ_{ij} is the angle between them. The pair for which y_{ij}^{J} is the smallest is replaced by a pseudo-particle l with four-momentum

$$p_l = p_i + p_j\ . \tag{30}$$

This procedure is repeated until all the y_{ij}^{J}, calculated using the remaining particles and pseudo-particles, exceed the jet resolution parameter $y_{\mathrm{cut}}^{\mathrm{J}}$. These remaining particles and pseudo-particles are called jets. The jet fraction f_i is the fraction of all hadronic events containing i jets

$$f_i = \frac{N_{i\,\mathrm{jets}}}{N_{\mathrm{tot}}}\ . \tag{31}$$

The observed jet fractions are corrected, on a bin-by-bin basis, for the effects of remaining background, detector resolution and acceptance using Monte Carlo events for signal and background processes as described in the treatment of event-shape variables in section 4.2.

The corrected fractions for 2-, 3-, 4- and 5-jet production at the different centre-of-mass energies are summarised in Tables 7–15. These fractions are plotted as a function of the jet resolution parameter $y_{\mathrm{cut}}^{\mathrm{J}}$ in Figure 11 at mean centre-of-mass energies of 130.1, 182.8, 200.2 and 206.2 GeV. The data are compared with predictions of various parton shower models, which are found to describe the data rather well.

Similarly, Tables 16–24 show the corrected jet fractions as a function of $y_{\mathrm{cut}}^{\mathrm{D}}$ for 2-, 3-, 4- and 5-jets at different centre-of-mass energies where the jets are reconstructed using the k_{t} or Durham algorithm [126–129]. This algorithm differs from the JADE algorithm in the definition of the jet resolution parameter y_{ij} between two particles in order to better treat the summing up of soft gluon emission:

$$y_{ij}^{\mathrm{D}} = \frac{2\min(E_i^2,E_j^2)}{s}\,(1-\cos\theta_{ij}) \tag{32}$$

The data are compared with different parton shower models in Figure 12 at mean centre-of-mass energies of 130.1, 182.8, 200.2 and 206.2 GeV. Again the data are well described by the different parton shower models.

In the Cambridge algorithm [153] the ordering parameter for combining particles into pseudo-particles is separated from the jet resolution parameter and a concept called 'soft freezing' is introduced. In this algorithm, the ordering parameter v_{ij} is chosen to be

$$v_{ij} = (1-\cos\theta_{ij})\ . \tag{33}$$

At each step, the pair having the smallest value of v_{ij} is examined. If $y_{ij}^{\mathrm{D}} < y_{\mathrm{cut}}^{\mathrm{D}}$, particles i and j are combined to form a pseudo-particle l as in the previous two algorithms, but if y_{ij}^{D} is larger than $y_{\mathrm{cut}}^{\mathrm{D}}$, the smaller energy object (between i and j) is frozen as a jet and is not considered further. Jet fractions are measured at $\sqrt{s} = 200.2$ and 206.2 GeV using this algorithm and are tabulated in Tables 25 and 26. Figure 13 shows the corrected jet fractions for the Cambridge algorithm as a function of $y_{\mathrm{cut}}^{\mathrm{D}}$ for 2-, 3-, 4- and 5-jets at centre-of-mass energies of 200.2 and 206.2 GeV, respectively. The different QCD models are in good agreement with the data.

Figure 14 shows the energy evolution of the 3-jet fraction using the JADE algorithm at a fixed $y_{\rm cut}^{\rm J}$ of 0.08. The plot shows measurements from the L3 experiment together with similar measurements done at lower energies [63, 139, 140, 154–156]. The data clearly demonstrate a decrease of 3-jet fraction with increasing centre-of-mass energy. This result is in agreement with the running of $\alpha_{\rm s}$ with the energy scale as expected in QCD, which is also shown. The curve corresponds to $\mathcal{O}(\alpha_{\rm s}^2)$ QCD calculations with $\alpha_{\rm s}(m_{\rm Z}) = 0.120$.

5.2 Comparison of Event Shapes with Monte Carlo Models

The corrected distributions of the shape variables $1 - T$, $\rho_{\rm H}$, $B_{\rm T}$, and $B_{\rm W}$ at the different centre-of-mass energies below [38] and above $m_{\rm Z}$ are presented in Tables 27–31, 32–36, 37–41, and 42–46, respectively. Those of C and D at centre-of-mass energies above $m_{\rm Z}$ are shown in Tables 47–49 and 50–52, respectively. Tables for the distributions at the Z pole can be found in Reference 30.

At the Z pole the distributions of the six event-shape variables T, $\rho_{\rm H}$, $B_{\rm T}$, $B_{\rm W}$, C and D are also measured for b and udsc flavours separately. These distributions, corrected for purity by Monte Carlo, are summarised in Tables 53–58 and compared with the JETSET PS, HERWIG and ARIADNE QCD models in Figures 15–20. The figures also contain the distributions for all flavours. The Monte Carlo models provide a reasonable description of the data. Significant flavour-dependent differences exist, particularly for the jet broadenings and the C- and D-parameters. These differences are reasonably described by the models, with the exception of the JETSET ME model.

The distributions for high energy are shown in Figures 21–26. The agreement is satisfactory, with the exception of the JETSET ME comparisons for the jet broadenings and the C- and D-parameters at high energy.

An important test of QCD models is a comparison of the energy evolution of the event-shape variables. The energy dependence of the mean event-shape variables arises mainly from two sources: the logarithmic energy scale dependence of $\alpha_{\rm s}$ and the power law behaviour of non-perturbative effects. The first moments of the six event-shape variables are shown in Figure 27 and are also given in Tables 27–58 along with the differential distributions. Also shown are the energy dependences of these quantities as predicted by JETSET PS, HERWIG, ARIADNE, COJETS and JETSET ME. All models give a good description of the data with the exception of JETSET ME, which decreases too rapidly with $\sqrt{s}$ for the jet broadenings and the C- and D-parameters.

5.3 Power Law Correction Analysis

Rather than the phenomenological fragmentation models of the Monte Carlo programs, the non-perturbative contribution to event-shape distributions can be described using a so-called power correction ansatz. In this approach, the energy dependence of moments of the event-shape variables are described [17–21] as a sum of the perturbative contribution and a power law dependence due to non-perturbative contributions. The first moment of an event-shape variable, y, is written as

$$\langle y \rangle = \langle y_{\rm pert} \rangle \; + \; \langle y_{\rm pow} \rangle \; , \tag{34}$$

where the perturbative contribution $\langle y_{\rm pert} \rangle$ has been calculated [22] to $\mathcal{O}(\alpha_{\rm s}^2)$:

$$\langle y_{\rm pert} \rangle = A_y \frac{\alpha_{\rm s}(\mu)}{2\pi} + \left(A_y \frac{\beta_0}{2} \log \frac{\mu^2}{s} + B_y \right) \left(\frac{\alpha_{\rm s}(\mu)}{2\pi} \right)^2 \; , \tag{35}$$

where A_y and B_y are coefficients depending on the event-shape variable, y, which are obtained by integrating [157] the $\mathcal{O}(\alpha_s^2)$ matrix elements [23], μ is the renormalisation scale (taken equal to $\sqrt{s}$), and $\beta_0 = (11N_c - 2N_f)/3$, with $N_c = 3$ the number of colours and N_f the number of active flavours. The power correction term, for $1-T$, ρ_H, and C, is given by

$$\langle y_{\rm pow} \rangle = c_y F_y \mathcal{P} \ , \tag{36}$$

where the factors c_y and F_y depend on the shape variable y, and $\mathcal{P}$ is supposed to have the universal form [17–21]:

$$\mathcal{P} = \frac{4C_F}{\pi^2}\mathcal{M}\frac{\mu_I}{\sqrt{s}}\left[\alpha_0(\mu_I) - \alpha_s(\mu) - \beta_0\frac{\alpha_s^2(\mu)}{2\pi}\left(\ln\frac{\mu}{\mu_I} + \frac{K}{\beta_0} + 1\right)\right] \tag{37}$$

The parameter α_0 is the average value of α_s in the non-perturbative region below an infrared matching scale μ_I (= 2 GeV); $K = (67/18 - \pi^2/6)C_A - 5N_f/9$; and C_F, C_A are the SU(3) colour factors. The so-called Milan factor, $\mathcal{M}$, is 1.49 for $N_f = 3$ [21]. The shape-variable dependent coefficients, A_y, B_y and c_y are given in Table 59. For $1-T$, ρ_H, C and D, $F_y = 1$, while for the jet broadening variables it is [17–21]

$$F_y = \frac{\pi\sqrt{c_y}}{2\sqrt{C_F\alpha_s\left(1 + K\frac{\alpha_s}{2\pi}\right)}} + \frac{3}{4} - \frac{\beta_0 c_y}{6C_F} - 0.61371 \tag{38}$$

Recently, the power law correction term has been calculated for the D-parameter [158]. Since $A_D = 0$, the leading-order term is second order. To obtain NLO accuracy, $\langle y_{\rm pert} \rangle$ must be computed to third order. This results in an additional term in Equation (35): $+2450\,(\alpha_s/(2\pi))^3$.

We have carried out fits to the first moments of the six event-shape variables separately with $\alpha_s(m_Z)$ and α_0 as free parameters. The diagonal terms of the covariance matrix between the different energy points are constructed by summing in quadrature the systematic and statistical uncertainties. The off-diagonal terms are obtained from the common systematic uncertainties. The results of the fits are summarised in Table 60 and shown in Figures 28 and 29.

The six values of α_0 obtained from the event-shape variables do not agree well. The confidence level for the hypothesis that α_0 is the same for all quantities is only about 3% when the systematic uncertainties are treated as uncorrelated, 1% if only statistical uncertainties are used. In particular, the values of α_0 for D and B_W differ by about 40% and 30% in opposite directions from the unweighted average of the six estimates of α_0:

$$\alpha_0 = 0.478 \ \pm \ 0.054 \ \pm \ 0.024 \ .$$

On the other hand, the six estimates of α_s are consistent with each other, yielding an unweighted average:

$$\alpha_s(m_Z) = 0.1126 \ \pm \ 0.0045 \ \pm \ 0.0039 \ .$$

The first uncertainty is the average of the statistical uncertainties of the measurements. To estimate theoretical uncertainties the renormalisation scale μ is varied between $0.5\sqrt{s}$ and $2.0\sqrt{s}$ resulting in average variations of ± 0.024 and ± 0.0039 for α_0 and $\alpha_s(m_Z)$, respectively. A variation of μ_I in the range 1–3 GeV gives an additional uncertainty on both α_0 and $\alpha_s(m_Z)$ of ± 0.0010. These two estimates of theoretical uncertainty are combined in quadrature and quoted as the second uncertainty.

We have also measured the second moments of these shape variables which are also given in Tables 27–58. The energy dependence of these moments has been analysed in terms of power law corrections. It is expected [159–161] that

$$\langle y^2 \rangle = \langle y^2_{\rm pert} \rangle + 2 \langle y_{\rm pert} \rangle c_y F_y \mathcal{P} + \mathcal{O}\left(\frac{1}{s}\right) \ . \tag{39}$$

The $\mathcal{O}(\frac{1}{s})$ term is expected to be small for $1-T$, $\rho_{\rm H}$, C and D. This assumes that the non-perturbative correction to the distributions causes only a shift in the distributions. Fits are performed to the second moments. In the fits, the $\mathcal{O}(\frac{1}{s})$ term is parametrised as A_2/s, and both α_0 and $\alpha_{\rm s}$ are fixed to the values obtained from the corresponding fits to the first moments. Figure 30 shows the second moments compared to these fits. The contributions of the power term and the $\mathcal{O}(\frac{1}{s})$ term are shown separately. The results of the fits are also given in Table 61. The contribution of the $\mathcal{O}(\frac{1}{s})$ term is not negligible for $1-T$ and C, contrary to the expectation. It is negative for $\rho_{\rm H}$ and $B_{\rm W}$. Further, the shape of the fitted curve is unphysical for $B_{\rm W}$, and the χ^2 of the $B_{\rm T}$ fit is unacceptably low.

Given the mildly discrepant values of α_0 and these problems with the fits to the second moments, one can conclude that the power correction ansatz gives a good qualitative description, but that additional terms will be needed to achieve a good quantitative description.

5.4 Determination of $\alpha_{\rm s}$ from event-shape variables

The presently available QCD predictions in fixed-order perturbation theory do not take into account the effect of emission of more than two gluons. For variables like $1-T$, $B_{\rm T}$, $B_{\rm W}$, $\rho_{\rm H}$ and C this leads to a poor description of the distributions in kinematic regions where multi-gluon emission becomes dominant. It is possible to isolate the leading terms in every order of perturbation theory and to sum them up in the form of an exponential series. These calculations have been carried out for the above variables [24–29] to next-to-leading log order.

For all these variables, denoted by y, the cumulative cross section can be written in the form

$$\begin{aligned}
R(y,\alpha_{\rm s}) \equiv \int_0^y \frac{1}{\sigma}\frac{{\rm d}\sigma}{{\rm d}y} &= C(\alpha_{\rm s})\Sigma(y,\alpha_{\rm s}) + D(\alpha_{\rm s},y) && (40)\\
\text{with } C(\alpha_{\rm s}) &= 1 + \sum_{n=1}^{\infty} C_n \overline{\alpha}_{\rm s}^n && (41)\\
D(\alpha_{\rm s},y) &= \sum_{n=1}^{\infty} D_n(y) \overline{\alpha}_{\rm s}^n && (42)\\
\Sigma(y,\alpha_{\rm s}) &= \exp\left[\sum_{n=1}^{\infty}\sum_{m=1}^{n+1} G_{nm}\overline{\alpha}_{\rm s}^n L^m\right] && (43)\\
&\equiv \exp\left[L g_1(\overline{\alpha}_{\rm s}L) + g_2(\overline{\alpha}_{\rm s}L) + \alpha_{\rm s}\ g_3(\overline{\alpha}_{\rm s}L) + \cdots\right] && (44)\\
\overline{\alpha}_{\rm s} &\equiv \frac{\alpha_{\rm s}}{2\pi} && (45)\\
L &\equiv \ln\left(\frac{1}{y}\right) \ . && (46)
\end{aligned}$$

In the 2-jet region, y is small. Therefore, L and the corrections due to large powers of L are large.

In the fixed-order calculations [22, 23], one can write

$$R(y, \alpha_s) = \alpha_s A(y) + \alpha_s^2 B(y) + \mathcal{O}\left(\alpha_s^3\right) \ . \tag{47}$$

Note that A_y and B_y of Equation (35) are related to $A(y)$ and $B(y)$.

The two approaches are summarised in Table 62. The first two rows have been completely computed in the fixed-order calculations and the first two columns are known to all orders in the recent resummed calculations. In order to describe the data over a wide kinematic region, it is desirable to combine the two sets of calculations, avoiding double-counting of the common parts. This leads to a number of matching schemes [28]. The simplest one matches the two calculations at a given value of y and uses a suitable damping function so that the resummed calculations contribute to the 2-jet region and the fixed-order calculations dominate in the multi-jet region. A preferable approach would be to combine the two calculations and subtract the common terms of the two calculations. This is done by taking the logarithm of the fixed-order calculations and expanding it as a power series. Then the matching can be done in $\ln R(y)$ (called the '$\ln R$ matching' scheme). Alternatively, a similar procedure can be performed in the function $R(y)$ rather than in $\ln R(y)$. This procedure is called the 'R-matching' scheme. In a variation of this scheme, the term $G_{21}\overline{\alpha}_s^2 L$ is included in the term of the exponential and subtracted after exponentiation. This method is called the 'modified R-matching' scheme.

One has to take care of the additional constraint coming from kinematics, namely that the cross sections vanish beyond the kinematic limit

$$R(y = y_{\max}) = 1 \tag{48}$$

$$\frac{\mathrm{d}R}{\mathrm{d}y}(y = y_{\max}) = 0 \ . \tag{49}$$

These constraints are strictly obeyed in the fixed-order calculations but they are not valid for the resummed expansion. The first constraint can be imposed by replacing $R(y)$ by $R(y) - R(y_{\max})$ for the resummed calculations. Alternatively, L can be replaced in the resummed term by $L' = \ln\left(y^{-1} - y_{\max}^{-1} + 1\right)$ in the $\ln R$ matching scheme to fulfil both conditions. This possibility is referred to as the 'modified $\ln R$' matching scheme.

An important improvement of the new QCD calculations with respect to the second-order formulae is their ability to describe also the low-y region. One should note that the sub-leading terms not included beyond next-to-leading logarithmic order are expected to be relatively small at low y.

The calculations for the distributions of the five variables are given in the form of analytical functions

$$f^{\text{pert}}(y; s, \alpha_s(\mu), \mu) \ . \tag{50}$$

The fixed-order calculations include quark masses, while the resummed calculations assume massless partons. To compare the analytical calculations with the experimental distributions, the effect of hadronisation and decays must be taken into account using Monte Carlo programs. We use the parton shower programs JETSET, ARIADNE and HERWIG with the tuned parameter values of Section 4.4. The perturbative calculations for a variable y are convoluted with the probability $p^{\text{non-pert}}(y; y')$ to obtain the value y, after fragmentation and decays, for a parton level value y':

$$f(y) = \int f^{\text{pert}}(y') \cdot p^{\text{non-pert}}(y; y') \ \mathrm{d}y' \ . \tag{51}$$

The resulting differential cross section $f(y)$ is compared to the measurements. The correction for hadronisation and decays changes the perturbative prediction by less than 5% for the event-shape variables over a large kinematic range. However, the corrections increase to as much as 20% in the extreme 2-jet region.

To determine α_s at each energy point, the measured distributions are fitted in the ranges given in Table 63 to the analytical predictions, using the modified $\ln R$ matching scheme after corrections for hadronisation effects. Figure 31 shows the experimental data together with the result of the QCD fits for the five variables at $\langle\sqrt{s}\,\rangle = 200.2$ GeV. Reasonable fits are obtained at all these energy points; the χ^2 per degree of freedom are given in Table 63.

The α_s measurements for the 16 energy points are summarised in Table 64 together with their experimental and theoretical uncertainties. The former includes the statistical and the experimental systematic uncertainties discussed above. The latter is obtained from estimates of the hadronisation uncertainty and of the uncalculated higher orders in the QCD predictions.

The hadronisation uncertainty is obtained from the variation in the fitted value of α_s due to hadronisation corrections determined by comparing JETSET with HERWIG and ARIADNE and by changing the JETSET fragmentation parameters, b, σ_q and $\Lambda_{\rm LLA}$ within their uncertainties, listed in Table 3, as well as by turning off Bose-Einstein correlations. By far the largest uncertainty is that of the fragmentation model, which is therefore taken as the estimate of the overall hadronisation uncertainty. It is evaluated as half of the largest difference in α_s obtained with different models.

The uncertainty coming from uncalculated higher orders in the QCD predictions is estimated in two independent ways: by varying the renormalisation scale, μ, and by changing the matching scheme. The scale uncertainty is obtained by repeating the fit for different values of the renormalisation scale in the interval $0.5\sqrt{s} \leq \mu \leq 2\sqrt{s}$. The matching scheme uncertainty is obtained from half of the maximum spread given by the different matching schemes. The largest of these uncertainties is assigned as the theoretical uncertainty due to uncalculated higher orders.

To obtain a combined value for the strong coupling constant, we take the unweighted average of the five α_s values. The overall theoretical uncertainty is obtained from the average hadronisation uncertainty added in quadrature to the average higher-order uncertainty. A cross-check of this theoretical uncertainty is obtained from a comparison of α_s measurements from the various event-shape variables which are expected to be differently affected by higher order corrections and hadronisation effects. Half of the maximum spread in the five α_s values is found to be consistent with the estimated theoretical uncertainty.

The mean α_s values from the five event-shape distributions are given in Table 65 together with the experimental and theoretical uncertainties. Figure 32a compares the energy dependence of the measured α_s values with the prediction from QCD. The theoretical uncertainties are strongly correlated between these measurements. Hence, the energy dependence of α_s is investigated using only experimental uncertainties. The experimental systematic uncertainties on α_s are partially correlated. The background uncertainties are correlated between data points in the same energy range but not between the low-energy, Z pole and high-energy data sets. The 16 measurements in Figure 32a are shown with experimental uncertainties only, together with a fit to the QCD evolution equation [162] with $\alpha_s(m_Z)$ as a free parameter, assuming 5 active flavours. The covariance matrix used in the fit is obtained assuming that the experimental systematic uncertainties are uncorrelated between the three data sets and that they have a minimum overlap correlation between different energies within the same data set. This definition consists of assigning to the covariance matrix element the smallest of the two squared

uncertainties, *i.e.*, $\sigma^2_{ij} = \min(\sigma^2_{ii}, \sigma^2_{jj})$

The fit, having a χ^2 of 17.9 for 15 degrees of freedom corresponding to a confidence level of 27%, yields a value of α_s:

$$\alpha_s(m_Z) = 0.1227 \ \pm \ 0.0012 \ \pm \ 0.0058 \ .$$

The first uncertainty is experimental and the second theoretical. The latter is obtained from the result of a fit which includes the theoretical uncertainties and their correlations. There are two types of theoretical uncertainties: those associated with the hadronisation corrections, and those due to uncalculated higher order terms. For each type, the correlations are determined assuming minimum overlap. The hadronisation uncertainty is estimated by using different Monte Carlo programs. Its contribution to the total theoretical uncertainty is ± 0.0026. The uncertainty due to uncalculated higher order terms is estimated by varying the renormalisation scale by a factor 2 and by using different matching schemes. This is the largest uncertainty, ± 0.0052. This value of α_s is consistent with the values measured by other experiments at m_Z using event shapes [163–173].

A fit with constant α_s gives a χ^2 of 51.7 for 15 degrees of freedom, corresponding to a confidence level of 6×10^{-6}. These measurements support the energy evolution of the strong coupling constant predicted by QCD.

The energy evolution of α_s depends on the number of active flavours. A fit with N_f, as well as α_s, as free parameters yields:

$$\begin{aligned} N_f &= 6.9 \ \pm \ 1.3 \\ \alpha_s(m_Z) &= 0.1219 \pm 0.0013 \ , \end{aligned}$$

where the uncertainty is only experimental. This result agrees with the expected $N_f = 5$, and the α_s value is compatible with that from the fit with N_f fixed to 5.

Figure 32b summarises the α_s values determined by L3 from the measurement of the τ branching fractions into leptons [174], the Z line shape [175] and event-shape distributions at various energies, together with the QCD prediction obtained from the fit to the event-shape measurements only. The width of the band corresponds to the evolved uncertainty on $\alpha_s(m_Z)$. All the measurements are consistent with the energy evolution of the strong coupling constant predicted by QCD. The uncertainties on these measurements are dominated by the theoretical uncertainty coming from the unknown higher order contributions in the calculations. An improved determination of α_s from these measurements thus awaits improved theoretical calculations of these corrections.

6 Soft Gluon Coherence

The phenomenon of colour coherence in QCD implies destructive interference in soft gluon emission. With the assumption of Local Parton Hadron Duality (LPHD) [54, 55], colour coherence can be studied in charged particle distributions, in particular in the multiplicity distribution and in the charged particle momentum spectrum of the variable $\xi = \ln(1/x)$, where x is the momentum scaled by the beam energy.

To study these distributions, events are selected using cuts very similar to those of Section 3. Well measured charged tracks are selected and the event is required to be in the barrel region of the detector by demanding that the thrust axis calculated from calorimeter clusters be more than 42.3° from the beam axis and that calculated from charged tracks more than 45.6°.

6.1 Charged Particle Multiplicity

The dynamics of hadron production can be probed using the charged particle multiplicity distribution which is found to be very sensitive to the parameters of the QCD models.

The measured distributions are corrected for the remaining estimated background using Monte Carlo on a bin-by-bin basis. The distributions are then corrected for resolution and acceptance, using a matrix unfolding method. At the Z pole, the high statistics warrant a more refined method, and the matrix unfolding is iterated in a Bayesian procedure [176, 177]. In this correction procedure, we assume all particles with mean lifetime greater than 3.3×10^{-10} s to be stable.

The systematic uncertainties are determined as for the global event-shape variables with one additional contribution corresponding to a variation of the quality criteria for track selection.

The corrected distributions together with the mean charged particle multiplicities, $\langle N_{\rm ch} \rangle$, at the Z pole and above are summarised in Tables 66–69. Figures 33 and 34 show the measured charged particle multiplicity distributions at centre-of-mass energies of 91.2, 136.1, 182.8, 194.4 and 206.2 GeV compared to the different Monte Carlo models tuned to the Z-pole data (*cf.* Section 4.4). At 91.2 GeV, JETSET PS agrees well with the data for all, b and udsc quarks. This is not the case for HERWIG, whose distributions are too broad. At higher energies, this feature of HERWIG remains, while JETSET PS continues to provide a good description. The matrix element version of JETSET produces too few particles at high energy.

Figure 35a shows the evolution of mean charged particle multiplicity with centre-of-mass energy compared to several QCD models. The parameters of the models are the same at all energies. We find that the energy dependence predicted by the parton shower models JETSET, HERWIG and ARIADNE, which include QCD coherence effects, are in agreement with the measured mean multiplicities. However, parton shower models with no QCD coherence effects, such as COJETS and JETSET ME, do not explain the observed energy dependence. COJETS predicts a faster energy evolution, while JETSET ME, which has low parton multiplicity before fragmentation due to the $\mathcal{O}(\alpha_{\rm s}^2)$ calculation, would need retuning at each centre-of-mass energy.

The mean charged particle multiplicity in gluon jets has been calculated, in the framework of LPHD, to next-to-next-to-next-to leading order (3NLO) [178]:

$$\langle N_{\rm ch}(y) \rangle_{\rm g} = \mathcal{N} y^{-a_1 C^2} \exp\left[2C\sqrt{y} + \delta_{\rm g}(y)\right] \tag{52}$$

where $\mathcal{N}$ is an overall normalization constant, $y = \ln(\mu/\Lambda)$, $C = \sqrt{4N_{\rm C}\,/\beta_0}$ and

$$\delta_{\rm g}(y) = \frac{C}{\sqrt{y}} \left\{ 2a_2 C^2 + \frac{\beta_1}{\beta_0}\left[2 + \ln(2y)\right] \right\} + \frac{C^2}{y} \left\{ a_3 C^2 - \frac{a_1 \beta_1}{\beta_0^2}\left[1 + \ln(2y)\right] \right\} \tag{53}$$

The leading order (LO) prediction is given by $\exp\left[2C\sqrt{y}\right]$. The factor in front of this exponential arises in NLO. The first term in $\delta_{\rm g}(y)$ is the 2NLO contribution, and the second term that of 3NLO. The prediction for quark jets or $\rm e^+e^-$ events, is then

$$\langle N_{\rm ch}(y) \rangle_{\rm F} = \frac{\langle N_{\rm ch}(y) \rangle_{\rm g}}{r(y)} \tag{54}$$

where $r(y)$, the ratio of multiplicities of gluon and quark jets, is given by

$$r(y) = r_0 \left(1 - r_1\gamma_0 - r_2\gamma_0^2 - r_3\gamma_0^3\right) \ . \tag{55}$$

Here γ_0 is an anomalous dimension, which is related to α_s by

$$\gamma_0 = \sqrt{\frac{2\alpha_s N_c}{\pi}} \tag{56}$$

and $r_0 = N_c/C_F = 4$. The coefficients a_i and r_i, $i = 1, 2, 3$ have been calculated in Reference 179 and are given in Table 70.

Figure 35b shows the mean charged particle multiplicity as measured by this experiment together with measurements of other e^+e^- experiments at lower [180–184] centre-of-mass energies. The prediction of JETSET PS is also shown. Fits of LO through 3NLO with $N_f = 3$ or 5 are performed to the data from TASSO, AMY and this experiment using $\mu = \sqrt{s}$. The result for 3NLO with $N_f = 3$ is shown in Figure 35b. The results of all of the fits are given in Table 71 in terms of the value of $\alpha_s(m_Z)$ calculated from

$$\alpha_s(\mu) = \frac{2\pi}{\beta_0 y}\left[1 - \frac{\beta_1 \ln(2\ln(\mu/\Lambda))}{\beta_0^2 \ln(\mu/\Lambda)}\right] . \tag{57}$$

The description of N_{ch} *vs.* $\sqrt{s}$ is good in all cases, the resulting curves being nearly indistinguishable. Also the choice of number of active flavours makes little difference. However the value of α_s obtained in the fit increases steadily from LO to 3NLO, and the values of α_s from the 3NLO fits are consistent with that obtained from event shapes.

6.2 Inclusive Particle Spectrum

The suppression of low momentum hadron production as a consequence of colour coherence is studied in terms of the variable ξ. The observed distribution is corrected for the effect of background, detector resolution and acceptance. At $\sqrt{s} = 91.2$ GeV this is done using a matrix unfolding method as for the charged particle multiplicity distribution. For the other energies it is done on a bin-by-bin basis using Monte Carlo events.

The corrected spectra for all flavours as well as for non-b and b quarks at $\sqrt{s} = 91.2$ GeV are shown in Figure 36 and summarised in Table 72. JETSET overestimates the central region. This may be due to its tuning, which only uses the charged-particle multiplicity distribution and global event-shape data. The description provided by HERWIG is in general poorer, particularly for the b-flavour events. The corrected distributions at $\sqrt{s} = 188.6$ and 206.2 GeV are shown in Figure 37. The corrected distributions at $\sqrt{s} > 130$ GeV are summarised in Tables 73–75. The asymptotic shape of the ξ spectrum is predicted to be Gaussian [50,185–187]. However, at finite energies the shape is affected by destructive interference in soft gluon emission. With next-to-leading order corrections [188], one expects a skewed platykurtic shape (often called a skewed Gaussian) for the ξ distribution. This implies a narrower ξ-peak shifted towards higher ξ-values, skewed and flattened towards lower ξ-values, with the high-ξ tail falling off faster than Gaussian. The smooth lines in Figure 37 are the results of fits to the corrected distributions of both a Gaussian and the Fong-Webber parametrisation of the skewed Gaussian [188], which reproduces the expected MLLA shape around the peak value, The fit range is restricted to values of ξ where the distribution is within 60% of its maximum value. In the fit, the systematic uncertainties are taken to be fully correlated. Both parametrisations give a reasonable description of the data. The Fong-Webber curve also provides a good description for large ξ where the Gaussian is systematically too high. However, at small ξ the Gaussian fits better.

The results of the fits at $\sqrt{s} = 91.2$ GeV are shown in Table 76. The systematic uncertainty is estimated by repeating the fits changing (a) the quality cuts on track selection; (b) the

hadronic selection criteria to vary the backgrounds within one standard deviation; (c) the model, using HERWIG for detector corrections instead of PYTHIA. Half of the maximum spread is assigned as the systematic uncertainty. As expected, the values obtained from the Fong-Webber fits are systematically higher than those obtained using the Gaussian parametrisation. The difference is about 0.03, independent of flavour. Thus the flavour dependence of $\xi^\star$ is independent of the choice of the fit function.

We observe a flavour dependence of the peak position, $\xi^\star$, more clearly shown by the ratios,

$$\begin{aligned} \xi^\star_{\rm udsc}/\xi^\star_{\rm all} &= 1.008 \pm 0.003 \pm 0.002 \\ \xi^\star_{\rm b}/\xi^\star_{\rm all} &= 0.975 \pm 0.003 \pm 0.008 \quad , \end{aligned}$$

where the first uncertainty is statistical and the second systematic. The small size of the resulting systematic uncertainty is due to the fact that most of the systematic uncertainty cancels when forming these ratios. Moreover, these ratios are insensitive to the fit parametrisation, the small difference being assigned as an additional systematic uncertainty.

The peak positions $\xi^\star$ of the ξ distribution as well as the χ^2/d.o.f and the confidence level of the fits obtained with the skewed Gaussian for all the energy points are summarised in Table 77. The systematic uncertainty includes, in addition to those mentioned above, a contribution of half the difference between the result using the Gaussian and the Fong-Webber parametrisations.

Figure 38 shows the measured values of $\xi^\star$ together with earlier measurements [189–191] as a function of centre-of-mass energy. The energy evolution of $\xi^\star$ has been fitted using the QCD prediction

$$\xi^\star(s) = y\left(\frac{1}{2} + \sqrt{\frac{C}{y}} - \frac{C}{y}\right), \tag{58}$$

where $y = \ln(\mu/\Lambda)$ and $C = a^2/(16N_{\rm c}\beta_0)$ with $a = [11N_{\rm c}/3] + [(2N_{\rm f})/(3N_{\rm c}^2)]$. We choose $\mu = \sqrt{s}/2$. The first term is given by the double logarithm approximation (DLA), and the correction terms arise in the next-to-leading order [50–52] (MLLA) QCD predictions. In the fits, the systematic uncertainties among the TASSO points are treated as fully correlated. The same is true of the L3 points with $\sqrt{s} > 130$ GeV. We find that the data are in better agreement with QCD predictions computed to next-to leading orders. The fit of the L3 and TASSO data to the DLA parametrisation gives a χ^2 of 110 for 13 degrees of freedom whereas the MLLA predictions give a fit with χ^2 of 26 for 13 degrees of freedom, corresponding to a confidence level of 2%.

It should be recalled that the suppression of hadron production at very small momenta resulting in a bell shape of the ξ distribution is expected on purely kinematical grounds due to finite hadron masses. Soft gluon coherence, however, increases this suppression and is manifested in the energy dependence of $\xi^\star$. The change with energy would be approximately two times larger without any destructive interference.

7 Summary

Distributions of event-shape variables in hadronic events from e^+e^- annihilation at centre-of-mass energies from 30 GeV to 209 GeV have been measured. These distributions as well as the energy dependence of their first moments are well described by parton shower models.

Jet fractions have been measured using the JADE, Durham and Cambridge algorithms as a function of the jet resolution parameters. The parton shower models are in good agreement with

the measured jet fractions. The energy evolution of the 3-jet fraction at a fixed jet resolution parameter is in agreement with $\mathcal{O}(\alpha_s^2)$ QCD calculations.

The energy dependence of the first two moments has been compared to second order perturbative QCD with power law corrections for the non-perturbative effects. The fits to the six event-shape variables give consistent values of α_s, which are somewhat lower than that obtained by the event-shape analysis. However, the values of α_0 are not consistent, differing by as much as 40% from their average. Further, the contribution from a $\mathcal{O}(\frac{1}{s})$ term in describing the second moments of $1-T$ and C is not small in contradiction to expectations. This implies that the power law correction can at best be described as semi-quantitative.

The event-shape distributions are compared to second order QCD calculations combined with resummed leading and next-to-leading logarithmic terms. The data are well described by these calculations at all energies. The measurements demonstrate the running of α_s as expected in QCD with a value of $\alpha_s(m_Z) = 0.1227 \pm 0.0012(\mathrm{exp}) \pm 0.0058(\mathrm{th})$. The uncertainties on these measurements are dominated by the theoretical uncertainty coming from unknown higher order contributions in the calculations. An improved determination of α_s from these measurements thus awaits improved theoretical calculations.

The energy evolution of the charged particle multiplicity as well as the inclusive charged particle momentum spectrum show evidence of soft gluon suppression. Energy evolution of the peak position $\xi^\star$ of the inclusive ξ spectrum is described adequately by the next-to-leading order QCD calculation including gluon interference effects.

The L3 Collaboration:

P.Achard,[20] O.Adriani,[17] M.Aguilar-Benitez,[25] J.Alcaraz,[25] G.Alemanni,[23] J.Allaby,[18] A.Aloisio,[29] M.G.Alviggi,[29] H.Anderhub,[49] V.P.Andreev,[6,34] F.Anselmo,[8] A.Arefiev,[28] T.Azemoon,[3] T.Aziz,[9] P.Bagnaia,[39] A.Bajo,[25] G.Baksay,[26] L.Baksay,[26] S.V.Baldew,[2] S.Banerjee,[9] Sw.Banerjee,[4] A.Barczyk,[49,47] R.Barillère,[18] P.Bartalini,[23] M.Basile,[8] N.Batalova,[46] R.Battiston,[33] A.Bay,[23] F.Becattini,[17] U.Becker,[13] F.Behner,[49] L.Bellucci,[17] R.Berbeco,[3] J.Berdugo,[25] P.Berges,[13] B.Bertucci,[33] B.L.Betev,[49] M.Biasini,[33] M.Biglietti,[29] A.Biland,[49] J.J.Blaising,[4] S.C.Blyth,[35] G.J.Bobbink,[2] A.Böhm,[1] L.Boldizsar,[12] B.Borgia,[39] S.Bottai,[17] D.Bourilkov,[49] M.Bourquin,[20] S.Braccini,[20] J.G.Branson,[41] F.Brochu,[4] J.D.Burger,[13] W.J.Burger,[33] X.D.Cai,[13] M.Capell,[13] G.Cara Romeo,[8] G.Carlino,[29] A.Cartacci,[17] J.Casaus,[25] F.Cavallari,[39] N.Cavallo,[36] C.Cecchi,[33] M.Cerrada,[25] M.Chamizo,[20] Y.H.Chang,[44] M.Chemarin,[24] A.Chen,[44] G.Chen,[7] G.M.Chen,[7] H.F.Chen,[22] H.S.Chen,[7] G.Chiefari,[29] L.Cifarelli,[40] F.Cindolo,[8] I.Clare,[13] R.Clare,[38] G.Coignet,[4] N.Colino,[25] S.Costantini,[39] B.de la Cruz,[25] S.Cucciarelli,[33] J.A.van Dalen,[31] R.de Asmundis,[29] P.Déglon,[20] J.Debreczeni,[12] A.Degré,[4] K.Dehmelt,[26] K.Deiters,[47] D.della Volpe,[29] E.Delmeire,[20] P.Denes,[37] F.DeNotaristefani,[39] A.De Salvo,[49] M.Diemoz,[39] M.Dierckxsens,[2] C.Dionisi,[39] M.Dittmar,[49] A.Doria,[29] M.T.Dova,[10,♯] D.Duchesneau,[4] M.Duda,[1] B.Echenard,[20] A.Eline,[18] A.El Hage,[1] H.El Mamouni,[24] A.Engler,[35] F.J.Eppling,[13] P.Extermann,[20] M.A.Falagan,[25] S.Falciano,[39] A.Favara,[32] J.Fay,[24] O.Fedin,[34] M.Felcini,[49] T.Ferguson,[35] H.Fesefeldt,[1] E.Fiandrini,[33] J.H.Field,[20] F.Filthaut,[31] P.H.Fisher,[13] W.Fisher,[37] I.Fisk,[41] G.Forconi,[13] K.Freudenreich,[49] C.Furetta,[27] Yu.Galaktionov,[28,13] S.N.Ganguli,[9] P.Garcia-Abia,[25] M.Gataullin,[32] S.Gentile,[39] S.Giagu,[39] Z.F.Gong,[22] G.Grenier,[24] O.Grimm,[49] M.W.Gruenewald,[16] M.Guida,[40] V.K.Gupta,[37] A.Gurtu,[9] L.J.Gutay,[46] D.Haas,[5] D.Hatzifotiadou,[8] T.Hebbeker,[1] A.Hervé,[18] J.Hirschfelder,[35] H.Hofer,[49] M.Hohlmann,[26] G.Holzner,[49] S.R.Hou,[44] Y.Hu,[31] B.N.Jin,[7] L.W.Jones,[3] P.de Jong,[2] I.Josa-Mutuberría,[25] M.Kaur,[14] M.N.Kienzle-Focacci,[20] J.K.Kim,[43] J.Kirkby,[18] W.Kittel,[31] A.Klimentov,[13,28] A.C.König,[31] M.Kopal,[46] V.Koutsenko,[13,28] M.Kräber,[49] R.W.Kraemer,[35] A.Krüger,[48] A.Kunin,[13] P.Ladron de Guevara,[25] I.Laktineh,[24] G.Landi,[17] M.Lebeau,[18] A.Lebedev,[13] P.Lebrun,[24] P.Lecomte,[49] P.Lecoq,[18] P.Le Coultre,[49] J.M.Le Goff,[18] R.Leiste,[48] M.Levtchenko,[27] P.Levtchenko,[34] C.Li,[22] S.Likhoded,[48] C.H.Lin,[44] W.T.Lin,[44] F.L.Linde,[2] L.Lista,[29] Z.A.Liu,[7] W.Lohmann,[48] E.Longo,[39] Y.S.Lu,[7] C.Luci,[39] L.Luminari,[39] W.Lustermann,[49] W.G.Ma,[22] L.Malgeri,[18] A.Malinin,[28] C.Maña,[25] D.Mangeol,[31] J.Mans,[37] J.P.Martin,[24] F.Marzano,[39] K.Mazumdar,[9] R.R.McNeil,[6] S.Mele,[18,29] L.Merola,[29] M.Meschini,[17] W.J.Metzger,[31] A.Mihul,[11] H.Milcent,[18] G.Mirabelli,[39] J.Mnich,[1] G.B.Mohanty,[9] G.S.Muanza,[24] A.J.M.Muijs,[2] B.Musicar,[41] M.Musy,[39] S.Nagy,[15] S.Natale,[20] M.Napolitano,[29] F.Nessi-Tedaldi,[49] H.Newman,[32] A.Nisati,[39] T.Novak,[31] H.Nowak,[48] R.Ofierzynski,[49] G.Organtini,[39] I.Pal,[46] C.Palomares,[25] P.Paolucci,[29] R.Paramatti,[39] G.Passaleva,[17] S.Patricelli,[29] T.Paul,[10] M.Pauluzzi,[33] C.Paus,[13] F.Pauss,[49] M.Pedace,[39] S.Pensotti,[27] D.Perret-Gallix,[4] B.Petersen,[31] D.Piccolo,[29] F.Pierella,[8] M.Pioppi,[33] P.A.Piroué,[37] E.Pistolesi,[27] V.Plyaskin,[28] M.Pohl,[20] V.Pojidaev,[17] J.Pothier,[18] D.Prokofiev,[34] J.Quartieri,[40] G.Rahal-Callot,[49] M.A.Rahaman,[9] P.Raics,[15] N.Raja,[9] R.Ramelli,[49] P.G.Rancoita,[27] R.Ranieri,[17] A.Raspereza,[48] P.Razis,[30] D.Ren,[49] M.Rescigno,[39] S.Reucroft,[10] S.Riemann,[48] K.Riles,[3] B.P.Roe,[3] L.Romero,[25] A.Rosca,[48] C.Rosemann,[1] C.Rosenbleck,[1] S.Rosier-Lees,[4] S.Roth,[1] J.A.Rubio,[18] G.Ruggiero,[17] H.Rykaczewski,[49] A.Sakharov,[49] S.Saremi,[6] S.Sarkar,[39] J.Salicio,[18] E.Sanchez,[25] C.Schäfer,[18] V.Schegelsky,[34] H.Schopper,[21] D.J.Schotanus,[31] C.Sciacca,[29] L.Servoli,[33] S.Shevchenko,[32] N.Shivarov,[42] V.Shoutko,[13] E.Shumilov,[28] A.Shvorob,[32] D.Son,[43] C.Souga,[24] P.Spillantini,[17] M.Steuer,[13] D.P.Stickland,[37] B.Stoyanov,[42] A.Straessner,[20] K.Sudhakar,[9] G.Sultanov,[42] L.Z.Sun,[22] S.Sushkov,[1] H.Suter,[49] J.D.Swain,[10] Z.Szillasi,[26,¶] X.W.Tang,[7] P.Tarjan,[15] L.Tauscher,[5] L.Taylor,[10] B.Tellili,[24] D.Teyssier,[24] C.Timmermans,[31] Samuel C.C.Ting,[13] S.M.Ting,[13] S.C.Tonwar,[9] J.Tóth,[12] C.Tully,[37] K.L.Tung,[7] J.Ulbricht,[49] E.Valente,[39] R.T.Van de Walle,[31] R.Vasquez,[46] V.Veszpremi,[26] G.Vesztergombi,[12] I.Vetlitsky,[28] D.Vicinanza,[40] G.Viertel,[49] S.Villa,[38] M.Vivargent,[4] S.Vlachos,[5] I.Vodopianov,[26] H.Vogel,[35] H.Vogt,[48] I.Vorobiev,[35,28] A.A.Vorobyov,[34] M.Wadhwa,[5] Q.Wang,[31] X.L.Wang,[22] Z.M.Wang,[22] M.Weber,[18] H.Wilkens,[31] S.Wynhoff,[37] L.Xia,[32] Z.Z.Xu,[22] J.Yamamoto,[3] B.Z.Yang,[22] C.G.Yang,[7] H.J.Yang,[3] M.Yang,[7] S.C.Yeh,[45] An.Zalite,[34] Yu.Zalite,[34] Z.P.Zhang,[22] J.Zhao,[22] G.Y.Zhu,[7] R.Y.Zhu,[32] H.L.Zhuang,[7] A.Zichichi,[8,18,19] B.Zimmermann,[49] M.Zöller.[1]

1 III. Physikalisches Institut, RWTH, D-52056 Aachen, Germany[§]
2 National Institute for High Energy Physics, NIKHEF, and University of Amsterdam, NL-1009 DB Amsterdam, The Netherlands
3 University of Michigan, Ann Arbor, MI 48109, USA
4 Laboratoire d'Annecy-le-Vieux de Physique des Particules, LAPP,IN2P3-CNRS, BP 110, F-74941 Annecy-le-Vieux CEDEX, France
5 Institute of Physics, University of Basel, CH-4056 Basel, Switzerland
6 Louisiana State University, Baton Rouge, LA 70803, USA
7 Institute of High Energy Physics, IHEP, 100039 Beijing, China[△]
8 University of Bologna and INFN-Sezione di Bologna, I-40126 Bologna, Italy
9 Tata Institute of Fundamental Research, Mumbai (Bombay) 400 005, India
10 Northeastern University, Boston, MA 02115, USA
11 Institute of Atomic Physics and University of Bucharest, R-76900 Bucharest, Romania
12 Central Research Institute for Physics of the Hungarian Academy of Sciences, H-1525 Budapest 114, Hungary[‡]
13 Massachusetts Institute of Technology, Cambridge, MA 02139, USA
14 Panjab University, Chandigarh 160 014, India
15 KLTE-ATOMKI, H-4010 Debrecen, Hungary[¶]
16 Department of Experimental Physics, University College Dublin, Belfield, Dublin 4, Ireland
17 INFN Sezione di Firenze and University of Florence, I-50125 Florence, Italy
18 European Laboratory for Particle Physics, CERN, CH-1211 Geneva 23, Switzerland
19 World Laboratory, FBLJA Project, CH-1211 Geneva 23, Switzerland
20 University of Geneva, CH-1211 Geneva 4, Switzerland
21 University of Hamburg, D-22761 Hamburg, Germany
22 Chinese University of Science and Technology, USTC, Hefei, Anhui 230 029, China[△]
23 University of Lausanne, CH-1015 Lausanne, Switzerland
24 Institut de Physique Nucléaire de Lyon, IN2P3-CNRS,Université Claude Bernard, F-69622 Villeurbanne, France
25 Centro de Investigaciones Energéticas, Medioambientales y Tecnológicas, CIEMAT, E-28040 Madrid, Spain[♭]
26 Florida Institute of Technology, Melbourne, FL 32901, USA
27 INFN-Sezione di Milano, I-20133 Milan, Italy
28 Institute of Theoretical and Experimental Physics, ITEP, Moscow, Russia
29 INFN-Sezione di Napoli and University of Naples, I-80125 Naples, Italy
30 Department of Physics, University of Cyprus, Nicosia, Cyprus
31 University of Nijmegen and NIKHEF, NL-6525 ED Nijmegen, The Netherlands
32 California Institute of Technology, Pasadena, CA 91125, USA
33 INFN-Sezione di Perugia and Università Degli Studi di Perugia, I-06100 Perugia, Italy
34 Nuclear Physics Institute, St. Petersburg, Russia
35 Carnegie Mellon University, Pittsburgh, PA 15213, USA
36 INFN-Sezione di Napoli and University of Potenza, I-85100 Potenza, Italy
37 Princeton University, Princeton, NJ 08544, USA
38 University of Californa, Riverside, CA 92521, USA
39 INFN-Sezione di Roma and University of Rome, "La Sapienza", I-00185 Rome, Italy
40 University and INFN, Salerno, I-84100 Salerno, Italy
41 University of California, San Diego, CA 92093, USA
42 Bulgarian Academy of Sciences, Central Lab. of Mechatronics and Instrumentation, BU-1113 Sofia, Bulgaria
43 The Center for High Energy Physics, Kyungpook National University, 702-701 Taegu, Republic of Korea
44 National Central University, Chung-Li, Taiwan, China
45 Department of Physics, National Tsing Hua University, Taiwan, China
46 Purdue University, West Lafayette, IN 47907, USA
47 Paul Scherrer Institut, PSI, CH-5232 Villigen, Switzerland
48 DESY, D-15738 Zeuthen, Germany
49 Eidgenössische Technische Hochschule, ETH Zürich, CH-8093 Zürich, Switzerland
§ Supported by the German Bundesministerium für Bildung, Wissenschaft, Forschung und Technologie.
‡ Supported by the Hungarian OTKA fund under contract numbers T019181, F023259 and T037350.
¶ Also supported by the Hungarian OTKA fund under contract number T026178.
♭ Supported also by the Comisión Interministerial de Ciencia y Tecnología.
♯ Also supported by CONICET and Universidad Nacional de La Plata, CC 67, 1900 La Plata, Argentina.
△ Supported by the National Natural Science Foundation of China.

References

[1] M. Gell-Mann, Acta Phys. Austriaca Suppl. **IX** (1972) 733.

[2] H. Fritzsch and M. Gell-Mann, 16th International Conference on High Energy Physics, Batavia, 1972; editors J. D. Jackson and

[3] A. Roberts, National Accelerator Laboratory (1972).

[4] H. Fritzsch, M. Gell-Mann and H. Leytwyler, Phys. Lett. **B47** (1973) 365.

[5] D.J. Gross and F. Wilczek, Phys. Rev. Lett. **30** (1973) 1343.

[6] D.J. Gross and F. Wilczek, Phys. Rev. **D8** (1973) 3633.

[7] H.D. Politzer, Phys. Rev. Lett. **30** (1973) 1346.

[8] G. 't Hooft, Nucl. Phys. **B33** (1971) 173.

[9] S. Weinberg, Phys. Rev. Lett. **31** (1973) 494.

[10] L3 Collaboration, B. Adeva *et al.*, Nucl. Inst. Meth. **A289** (1990) 35.

[11] M. Chemarin *et al.*, Nucl. Inst. Meth. **A349** (1994) 345.

[12] I.C. Brock *et al.*, Nucl. Inst. Meth. **A381** (1996) 236.

[13] H. Anderhub *et al.*, Nucl. Inst. Meth. **A515** (2003) 31.

[14] M. Acciarri *et al.*, Nucl. Inst. Meth. **A351** (1994) 300.

[15] A. Adam *et al.*, Nucl. Inst. Meth. **A383** (1996) 342.

[16] G. Basti *et al.*, Nucl. Inst. Meth. **A374** (1996) 293.

[17] B.R. Webber, Phys. Lett. **B339** (1994) 148.

[18] Yu.L. Dokshitzer and B.R. Webber, Phys. Lett. **B352** (1995) 451.

[19] Yu.L. Dokshitzer *et al.*, Nucl. Phys. **B511** (1997) 396.

[20] Yu.L. Dokshitzer *et al.*, J. High Energy Phys. **05** (1998) 3.

[21] Yu.L. Dokshitzer *et al.*, Eur. Phys. J. Direct **C3** (1999) 1; *Erratum* **C3** (2001) 1.

[22] Z. Kunzst and P. Nason, *Z Physics at LEP1*, CERN Yellow Report 89-08 (1989) Vol. I, p. 373.

[23] R.K. Ellis, D.A. Ross and A.E. Terrano, Nucl. Phys. **B178** (1981) 421.

[24] S. Catani *et al.*, Phys. Lett. **B263** (1991) 491.

[25] S. Catani *et al.*, Phys. Lett. **B272** (1991) 368.

[26] S. Catani *et al.*, Phys. Lett. **B295** (1992) 269.

[27] Yu.L. Dokshitzer *et al.*, J. High Energy Phys. **01** (1998) 11.

[28] S. Catani *et al.*, Nucl. Phys. **B407** (1993) 3.

[29] S. Catani *et al.*, Phys. Lett. **B427** (1998) 377.

[30] L3 Collaboration, B. Adeva *et al.*, Z. Phys. **C55** (1992) 39.

[31] L3 Collaboration, B. Adeva *et al.*, Phys. Lett. **B284** (1992) 471.

[32] L3 Collaboration, O. Adriani *et al.*, Phys. Rep. **236** (1993) 1.

[33] L3 Collaboration, M. Acciarri *et al.*, Phys. Lett. **B371** (1996) 137.

[34] L3 Collaboration, M. Acciarri *et al.*, Phys. Lett. **B404** (1997) 390.

[35] L3 Collaboration, M. Acciarri *et al.*, Phys. Lett. **B444** (1998) 569.

[36] L3 Collaboration, M. Acciarri *et al.*, Phys. Lett. **B489** (2000) 65.

[37] L3 Collaboration, P. Achard *et al.*, Phys. Lett. **B536** (2002) 217.

[38] L3 Collaboration, M. Acciarri *et al.*, Phys. Lett. **B411** (1997) 339.

[39] Z. Nagy and Z. Trócsányi, Nucl. Phys. Proc. Suppl. **64** (1998) 63.

[40] Z. Nagy and Z. Trócsányi, Phys. Rev. **D59** (1999) 014020; *Erratum* Phys. Rev. **D62** (2000) 099902.

[41] K. Konishi, A. Ukawa and G. Veneziano, Nucl. Phys. **B157** (1979) 45.

[42] R. Odorico, Nucl. Phys. **B172** (1980) 157.

[43] G.C. Fox and S. Wolfram, Nucl. Phys. **B168** (1980) 285.

[44] T.D. Gottschalk, Nucl. Phys. **B214** (1983) 201.

[45] G. Marchesini and B.R. Webber, Nucl. Phys. **B238** (1984) 1.

[46] J. Kalinowski, K. Konishi and T.R. Taylor, Nucl. Phys. **B181** (1981) 221.

[47] J. Kalinowski *et al.*, Nucl. Phys. **B181** (1981) 253.

[48] J.F. Gunion and J. Kalinowski, Phys. Rev. **D29** (1984) 1545.

[49] J.F. Gunion, J. Kalinowski and L. Szymanowski, Phys. Rev. **D32** (1985) 2303.

[50] A.H. Mueller, Nucl. Phys. **B213** (1983) 85.

[51] Yu.L. Dokshitzer *et al.*, Rev. Mod. Phys. **60** (1988) 373.

[52] Yu.L. Dokshitzer *et al.*, *Basics of Perturbative* QCD, Editions Frontières, Gif-sur-Yvette, 1991.

[53] Yu.L. Dokshitzer and B.R. Webber, Phys. Lett. **B352** (1995) 451; preprint Cavendish HEP-97-2 (1997).

[54] Ya.I. Azimov *et al.*, Z. Phys. **C27** (1985) 65.

[55] Ya.I. Azimov *et al.*, Z. Phys. **C31** (1986) 213.

[56] MARK-I Collaboration, G. Hanson *et al.*, Phys. Rev. Lett. **35** (1975) 1609.

[57] MARK-J Collaboration, D.P. Barber *et al.*, Phys. Rev. Lett. **43** (1979) 830.

[58] TASSO Collaboration, R. Brandelik *et al.*, Phys. Lett. **B86** (1979) 243.

[59] PLUTO Collaboration, C. Berger *et al.*, Phys. Lett. **B86** (1979) 418.

[60] JADE W. Bartel *et al.*, Phys. Lett. **B91** (1980) 142.

[61] JADE Collaboration, W. Bartel *et al.*, Phys. Lett. **B101** (1981) 129.

[62] JADE Collaboration, W. Bartel *et al.*, Z. Phys. **C21** (1983) 37.

[63] AMY Collaboration, I.H. Park *et al.*, Phys. Rev. Lett. **62** (1989) 1713.

[64] P. Mättig, Phys. Rep. **177** (1989) 141.

[65] T. Hebbeker, Phys. Rep. **217** (1992) 69.

[66] S. Bethke and J.E. Pilcher, Ann. Rev. Nucl. Part. Sci. **42** (1992) 251.

[67] M. Schmelling, Phys. Scr. **51** (1995) 683.

[68] P.N. Burrows, Proc. of XXIV SLAC Summer Institute on Particle Physics (1996) 101.

[69] D. Duchesneau, J.H. Field and H. Jeremie, C. R. Physique **3** (2002) 1211.

[70] H1 Collaboration, C. Adloff *et al.*, Eur. Phys. J. **C19** (2001) 289.

[71] ZEUS Collaboration, S. Chekanov *et al.*, Phys. Lett. **B547** (2002) 164.

[72] CDF Collaboration, C. Affolder *et al.*, Phys. Rev. Lett. **88** (2002) 042001.

[73] For a review see: T. Sjöstrand *et al.*, "Z Physics at LEP 1", eds. G. Altarelli *et al.*, CERN Report CERN-89-08, Vol. 3 (1989) 143.

[74] A. Bassetto, M. Ciafaloni and G. Marchesini, Phys. Rep. **100** (1983) 201.

[75] Yu.L. Dokshitzer *et al.*, Rev. Mod. Phys. **60** (1988) 373.

[76] B. R. Webber, Ann. Rev. Nucl. Part. Sci. **36** (1986) 253.

[77] V.N. Gribov and L.N. Lipatov, Sov. J. Nucl. Phys. **15** (1972) 438.

[78] V.N. Gribov and L.N. Lipatov, Sov. J. Nucl. Phys. **15** (1972) 675.

[79] Yu. L. Dokshitzer, Sov. J. Phys. JETP **46** (1977) 641.

[80] G. Altarelli and G. Parisi, Nucl. Phys. **B126** (1977) 298.

[81] A. Krzywicki and B. Petersson, Phys. Rev. **D6** (1972) 924.

[82] J. Finkelstein and R. Peccei, Phys. Rev. **D6** (1972) 2606.

[83] F. Niedermayer, Nucl. Phys. **B79** (1974) 355.

[84] A. Casher, J. Kogut and L. Susskind, Phys. Rev. **D10** (1974) 732.

[85] R.D. Field and R.P. Feynman, Nucl. Phys. **B136** (1978) 1.

[86] P. Hoyer *et al.*, Nucl. Phys. **B161** (1979) 349.

[87] A. Ali *et al.*, Nucl. Phys. **B168** (1980) 409.

[88] A. Ali *et al.*, Phys. Lett. **B93** (1980) 155.

[89] X. Artru and G. Mennessier, Nucl. Phys. **B70** (1974) 93.

[90] B. Andersson, G. Gustafson and T. Sjöstrand, Z. Phys. **C6** (1980) 235.

[91] B. Andersson *et al.*, Phys. Rep. **97** (1983) 31.

[92] X. Artru, Phys. Rep. **97** (1983) 147.

[93] R.D. Field and S. Wolfram, Nucl. Phys. **B213** (1983) 65.

[94] B.R. Webber, Nucl. Phys. **B238** (1984) 492.

[95] Jetset 7.4 and Pythia 5.7 Monte Carlo Programs: T. Sjöstrand, Comp. Phys. Comm. **82** (1994) 74; CERN-TH-7112/93 (1993), revised August 1995.

[96] Ariadne Monte Carlo Program: L. Lönnblad, Comp. Phys. Comm. **71** (1992) 15.

[97] G. Marchesini and B. Webber, Nucl. Phys. **B310** (1988) 461.

[98] I.G. Knowles, Nucl. Phys. **B310** (1988) 571.

[99] Herwig 5.9 Monte Carlo Program: G. Marchesini *et al.*, Comp. Phys. Comm. **67** (1992) 465.

[100] Cojets 6.23 Monte Carlo Program: R. Odorico, Comp. Phys. Comm. **32** (1984) 139; *Erratum* Comp. Phys. Comm. **34** (1985) 43.

[101] R. Odorico, Nucl. Phys. **B228** (1983) 381.

[102] R. Mazzanti and R. Odorico, Nucl. Phys. **B370** (1992) 23 and Bologna preprint DFUB 92/1.

[103] Pythia 6.2 Monte Carlo Program: T. Sjöstrand *et al.*, Comp. Phys. Comm. **135**(2001) 238.

[104] F.A. Berends, R. Kleiss and S. Jadach, Nucl. Phys. **B202** (1982) 63.

[105] F.A. Berends, R. Kleiss and S. Jadach, Comp. Phys. Comm. **29** (1983) 185.

[106] C. Peterson *et al.*, Phys. Rev. **D27** (1983) 105.

[107] B. Andersson, G. Gustafson and B. Söderberg. Z. Phys. **C20** (1983) 317.

[108] Ya.I. Azimov, Phys. Lett. **B165** (1985) 147.

[109] P.M. Stevenson, Phys. Rev. **D23** (1981) 2916.

[110] J.H. Field, Ann. Phys. **226** (1993) 209.

[111] S. Bethke, Z. Phys. **C43** (1989) 331.

[112] R. Y. Zhu, Ph.D. thesis, MIT (1983).

[113] D. Amati and G. Veneziano, Phys. Lett. **B83** (1979) 87.

[114] KK2f 4.14 Monte Carlo Program: S. Jadach, B.F.L. Ward and Z. Wąs, Comp. Phys. Comm. **130** (2000) 260.

[115] S. Jadach, B.F.L. Ward and Z. Wąs, Phys. Rev. **D63** (2001) 113009.

[116] GEANT 3.15 detector simulation program: R. Brun *et al.*, "GEANT 3", CERN DD/EE/84-1 (Revised), September 1987.

[117] GHEISHA program: H. Fesefeldt, RWTH Aachen Report PITHA 85/02 (1985).

[118] PHOJET Monte Carlo Program: R. Engel, Z. Phys. **C66** (1995) 203.

[119] R. Engel, J. Ranft and S. Roesler, Phys. Rev. **D52** (1995) 1459.

[120] KORALZ Monte Carlo Program: S. Jadach, B.F.L. Ward and Z. Wąs, Comp. Phys. Comm. **79** (1994) 503.

[121] J.H. Field, Phys. Lett. **B323** (1994) 432.

[122] BHAGENE Monte Carlo Program: J.H. Field and T. Riemann, Comp. Phys. Comm. **94** (1996) 53.

[123] BHWIDE Monte Carlo Program: S. Jadach *et al.*, Phys. Lett. **B390** (1997) 298.

[124] KORALW Monte Carlo Program: M. Skrzypek *et al.*, Comp. Phys. Comm. **94** (1996) 216.

[125] M. Skrzypek *et al.*, Phys. Lett. **B372** (1996) 289.

[126] Yu.L. Dokshitzer, Contribution to the Workshop on Jets at LEP and HERA (1990).

[127] N. Brown and W. J. Stirling, Rutherford Preprint RAL-91-049.

[128] S. Catani *et al.*, Phys. Lett. **B269** (1991) 432.

[129] S. Bethke *et al.*, Nucl. Phys. **B370** (1992) 310.

[130] L3 Collaboration, M. Acciarri *et al.*, Phys. Lett. **B411** (1997) 373.

[131] S. Brandt *et al.*, Phys. Lett. **12** (1964) 57.

[132] E. Fahri, Phys. Rev. Lett. **39** (1977) 1587.

[133] T. Chandramohan and L. Clavelli, Nucl. Phys. **B184** (1981) 365.

[134] MARK-II Collaboration, A. Peterson *et al.*, Phys. Rev. **D37** (1988) 1.

[135] TASSO Collaboration, W. Braunschweig *et al.*, Z. Phys. **C45** (1989) 11.

[136] G. Parisi, Phys. Lett. **B74** (1978) 65.

[137] J.F. Donoghue, F.E. Low, and S.Y. Pi, Phys. Rev. **D20** (1979) 2759.

[138] MARK-J Collaboration, D.P. Barber *et al.*, Phys. Lett. **B89** (1979) 139.

[139] JADE Collaboration, W. Bartel *et al.*, Z. Phys. **C33** (1986) 23.

[140] JADE Collaboration, S. Bethke *et al.*, Phys. Lett. **B213** (1988) 235.

[141] G.C. Fox and F. Wolfram, Phys. Rev. Lett. **41** (1978) 1581.

[142] G.C. Fox and F. Wolfram, Nucl. Phys. **B149** (1979) 413.

[143] G.C. Fox and F. Wolfram, Phys. Lett. **B82** (1979) 134.

[144] J.D. Bjorken and S.J. Brodsky, Phys. Rev. **D1** (1970) 1416.

[145] H. Georgi *et al.*, Phys. Rev. Lett. **39** (1977) 1237.

[146] S. Brandt *et al.*, Z. Phys. **C1** (1979) 61.

[147] L3 Collaboration, O. Adriani *et al.*, Phys. Lett. **B292** (1992) 472

[148] MINUIT, CERN program library D506: F. James and M. Roos, Comp. Phys. Comm. **10** (1975) 343.

[149] Herwig 6.2 Monte Carlo Program: Gennaro Corcella *et al.*, J. High Energy Phys. **01**(2001) 10.

[150] The LEP heavy flavour group, preprint LEPHF/96-01, ALEPH Note 96-099, DELPHI 96-67 PHYS 627, L3 Note 1969, OPAL Technical Note TN391 (1996).

[151] L. Lönnblad and T. Sjöstrand, Phys. Lett. **B351** (1995) 293.

[152] L. Lönnblad and T. Sjöstrand, Eur. Phys. J. **C2** (1998) 165.

[153] Yu.L. Dokshitzer *et al.*, J. High Energy Phys. **08**(1997) 001; preprint hep-ph/9707323 (1997).

[154] MARK-II Collaboration, S. Bethke *et al.*, Z. Phys. **C43** (1989) 325.

[155] TASSO Collaboration, W. Braunschweig *et al.*, Phys. Lett. **B214** (1988) 286.

[156] VENUS Collaboration, K. Abe *et al.*, Phys. Lett. **B240** (1990) 232.

[157] S. Catani and M. Seymour, Phys. Lett. **B378** (1996) 287.

[158] G.P. Salam and Z. Trócsányi, private communication.

[159] Yu.L. Dokshitzer and B.R. Webber, Phys. Lett. **B404** (1997) 321.

[160] B.R. Webber, Nucl. Phys. Proc. Suppl. **71** (1999) 66.

[161] G. Salam, private communication.

[162] Particle Data Group, K. Hagiwara *et al.*, Phys. Rev. **D15** (2002) 010001.

[163] ALEPH Coll., D. Buskulic *et al.*, Z. Phys. **C73** (1997) 409.

[164] ALEPH Coll., R. Barate *et al.*, Phys. Rep. **294** (1998) 1.

[165] ALEPH Coll., A. Heister *et al.*, preprint CERN-EP/2003-084, submitted to E. Phys. J.

[166] DELPHI Coll., P. Abreu *et al.*, Phys. Lett. **B456** (1999) 322.

[167] DELPHI Coll., P. Abreu *et al.*, E. Phys. J. **C14** (2000) 557.

[168] DELPHI Coll., J. Abdallah *et al.*, preprint CERN-EP-2004-007, accepted by E. Phys. J.

[169] OPAL Coll., P.D. Acton et al., Z. Phys. **C59** (1993) 1.

[170] OPAL Coll., G. Alexander *et al.*, Z. Phys. **C72** (1996) 191.

[171] OPAL Coll., K. Ackerstaff *et al.*, Z. Phys. **C75** (1997) 193.

[172] OPAL Coll., G. Abbiendi *et al.*, Eur. Phys. J **C16** (2000) 185.

[173] SLD Coll., K. Abe *et al..*, Phys. Rev. **D51** (1995) 962.

[174] L3 Collaboration, M. Acciarri *et al.*, Phys. Lett. **B507** (2001) 47.

[175] L3 Collaboration, M. Acciarri *et al.*, Eur. Phys. J. **C16** (2000) 1.

[176] L3 Collaboration, P. Achard *et al.*, Phys. Lett. **B577** (2003) 109.

[177] G. D'Agostini, Nucl. Inst. Meth. **A362** (1995) 487.

[178] I.M. Dremin and J.W. Gary, Phys. Lett. **B459** (1999) 341.

[179] A. Capella *et al.*, Phys. Rev. **D61** (2000) 074009.

[180] JADE Collaboration, W. Bartel *et al.*, Z. Phys. **C20** (1983) 187.

[181] TASSO Collaboration, W. Braunschweig *et al.*, Z. Phys. **C45** (1989) 193.

[182] TASSO Collaboration, W. Braunschweig *et al.*, Z. Phys. **C47** (1990) 187.

[183] AMY Collaboration, Y.K. Li *et al.*, Phys. Rev. **D41** (1990) 2675.

[184] AMY Collaboration, H.W. Zheng *et al.*, Phys. Rev. **D42** (1990) 737.

[185] A.H. Mueller, in *Proc. 1981 International Symposium on Lepton and Photon Interactions at High Energies*, ed. W. Pfeil (Bonn, 1981), p. 689.

[186] Yu.L. Dokshitzer, V.S. Fadin and V.A. Khoze, Phys. Lett. **B115** (1982) 242.

[187] A.H. Mueller, Nucl. Phys. **B241** (1984) 141.

[188] C.P. Fong and B.R. Webber, Phys. Lett. **B229** (1989) 289.

[189] L3 Collaboration, B. Adeva *et al.*, Phys. Lett. **B259** (1991) 199.

[190] L3 Collaboration, M. Acciarri *et al.*, Phys. Lett. **B444** (1998) 569.

[191] TASSO Collaboration, W. Braunschweig *et al.*, Z. Phys. **C47** (1990) 187.

Type of Event	$\sqrt{s}$ (GeV)	$\langle\sqrt{s}\rangle$ (GeV)	Integrated Luminosity (pb^{-1})	Selection Efficiency (%)	Sample Purity (%)	Selected events
Reduced Centre-of-Mass Energy	30–50	41.4	142.4	48.3	68.4	1247
	50–60	55.3	142.4	41.0	78.0	1047
	60–70	65.4	142.4	35.2	86.0	1575
	70–80	75.7	142.4	29.9	89.0	2938
	80–84	82.3	142.4	27.4	90.5	2091
	84–86	85.1	142.4	27.5	87.0	1607
Z pole	91.2	91.2	8.3	98.5	99.8	248100
High Energy	129.9–130.4	130.1	6.1	90.0	80.6	556
	135.9–140.1	136.1	5.9	89.0	81.5	414
	161.2–164.7	161.3	10.8	89.0	81.2	424
	170.3–172.5	172.3	10.2	84.8	82.6	325
	180.8–184.2	182.8	55.3	84.2	82.4	1500
	188.4–189.9	188.6	176.8	87.8	81.1	4479
	191.4–196.0	194.4	112.2	82.8	81.4	2403
	199.2–203.8	200.2	117.0	85.7	80.6	2456
	201.5–209.1	206.2	207.6	86.0	78.8	4146

Table 1: Summary of integrated luminosity, selection efficiency, sample purity and number of selected hadronic events at the different energies used in this analysis. The energies below $\sqrt{s} = 91.2$ GeV are obtained from the full data sample at the Z pole, by selecting events with an isolated high energy photon.

$\sqrt{s}$ (GeV)		SRC				ECLU			
		RMS	σ_1	σ_2	f_1	RMS	σ_1	σ_2	f_1
91.2	$E_{\rm vis}/\sqrt{s}$	0.135	0.125	0.225	0.86	0.099	0.059	0.118	0.63
	$\Delta\theta$ (mrad)	44.3	34.9	60.0	0.71	45.1	33.1	59.4	0.64
	$\Delta\phi$ (mrad)	57.5	36.8	88.3	0.70	51.4	31.8	85.6	0.75
188.6	$E_{\rm vis}/\sqrt{s}$	0.120	0.107	0.173	0.85	0.095	0.040	0.121	0.49
	$\Delta\theta$ (mrad)	57.4	33.5	103.8	0.79	60.7	33.4	108.3	0.75
	$\Delta\phi$ (mrad)	47.9	32.0	85.6	0.79	43.3	25.8	69.7	0.78

Table 2: Resolution of total energy measurement and jet angles as obtained in the hadronic data at $\sqrt{s} = 91.2$ GeV and $\sqrt{s} = 188.6$ GeV. The RMS is of the data. the σ are the standard deviations from a fit to a sum of two Gaussian functions. The fraction of events in the narrower Gaussian, f_1, is also given.

Model	Parameter	Fit Value
JETSET 7.4 PS	$\Lambda_{\rm LLA}$ (GeV)	0.311 ± 0.034
	σ_Q (GeV)	0.411 ± 0.034
	b (GeV^{-2})	0.886 ± 0.120
ARIADNE 4.06	$\Lambda_{\rm AR}$ (GeV)	0.254 ± 0.024
	σ_Q (GeV)	0.384 ± 0.025
	b (GeV^{-2})	0.772 ± 0.075
JETSET 7.4 ME	$\Lambda_{\rm ME}$ (GeV)	0.152 ± 0.007
	σ_Q (GeV)	0.430 ± 0.026
	b (GeV^{-2})	0.310 ± 0.016
HERWIG 5.9	$\Lambda_{\rm MLLA}$ (GeV)	0.184 ± 0.015
	CLMAX (GeV)	3.911 ± 0.196
	CLPOW	2.000 ± 0.482

Table 3: Tuned parameters for the Monte Carlo models [95, 96, 99] used in this study.

Model	Parameter	Fit value
No BE	$\Lambda_{\rm LLA}$ (GeV)	0.266 ± 0.008
All	$\sigma_{\rm Q}$ (GeV)	0.393 ± 0.004
flavours	b	0.874 ± 0.014
No BE	$\Lambda_{\rm LLA}$ (GeV)	0.258 ± 0.002
udsc	$\sigma_{\rm Q}$ (GeV)	0.390 ± 0.015
flavours	b	0.776 ± 0.006
	$\Lambda_{\rm LLA}$ (GeV)	$0.270\ ^{+\ 0.002}_{-\ 0.004}$
$\rm BE_{32}$	$\sigma_{\rm Q}$ (GeV)	0.420 ± 0.008
All	b	0.750 ± 0.031
flavours	$\lambda_{\rm BE}$	$1.100\ ^{+\ 0.1}_{-\ 0.5}$
	$r_{\rm BE}^{-1}$ (GeV)	0.400 ± 0.051
	$\Lambda_{\rm LLA}$ (GeV)	0.268 ± 0.003
$\rm BE_{32}$	$\sigma_{\rm Q}$ (GeV)	0.421 ± 0.004
udsc	b	0.741 ± 0.010
flavours	$\lambda_{\rm BE}$	$0.900\ ^{+\ 0.2}_{-\ 0.1}$
	$r_{\rm BE}^{-1}$ (GeV)	0.425 ± 0.041

Table 4: Tuned parameters for the PYTHIA 6.2 parton shower program [103] for udsc-quarks and for all flavours, without Bose-Einstein correlations and with these correlations using the $\rm BE_{32}$ Gaussian model [152]. The cut-off parameter and the Lund fragmentaion parameter were kept fixed at $Q_0 = 1.0$ GeV and $a = 0.5$ and the Peterson fragmentation parameters for heavy quarks at $\epsilon_{\rm c} = 0.03$ and $\epsilon_{\rm b} = 0.002$.

		Fit Value	
	Parameter	All flavours	udsc flavours
No BE	$\Lambda_{\rm AR}$ (GeV)	0.223 ± 0.002	$0.225\ ^{+\ 0.002}_{-\ 0.003}$
	$p_{\rm t}$ cut-off (GeV)	$0.65\ ^{+\ 0.05}_{-\ 0.02}$	0.60 ± 0.03
	$\sigma_{\rm Q}$ (GeV)	0.424 ± 0.002	0.436 ± 0.004
	a	0.106 ± 0.006	$0.112\ ^{+\ 0.006}_{-\ 0.012}$
	b	$0.62\ ^{+\ 0.02}_{-\ 0.04}$	0.62 ± 0.02
$\rm BE_{32}$	$\Lambda_{\rm AR}$ (GeV)	0.227 ± 0.002	0.227 ± 0.003
	$p_{\rm t}$ cut-off (GeV)	$0.60\ ^{+\ 0.08}_{-\ 0.05}$	0.60 ± 0.05
	$\sigma_{\rm Q}$ (GeV)	0.45 ± 0.02	0.47 ± 0.03
	a	0.106 ± 0.006	0.106 ± 0.006
	b	0.64 ± 0.02	0.58 ± 0.04
	$\lambda_{\rm BE}$	1.0 ± 0.2	1.0 ± 0.2
	$r_{\rm BE}^{-1}$ (GeV)	0.30 ± 0.05	0.35 ± 0.10

Table 5: Tuned parameters for ARIADNE 4.12 [96] with hadronisation by PYTHIA 6.2 [103] for udsc-quarks and for all flavours, without Bose-Einstein correlations and using the $\rm BE_{32}$ Gaussian model [152].

	Fit Value	
Parameter	no BE	BE_{32}
$\Lambda_{\rm MLLA}$ (GeV)	0.163 ± 0.006	0.168 ± 0.006
CLSMR(1)	0.20 ± 0.08	0.15 ± 0.05
CLSMR(2)	0.30 ± 0.10	0.30 ± 0.10
CLMAX	4.0 ± 0.2	4.16 ± 0.05
PSPLT(1)	0.92 ± 0.09	0.98 ± 0.07
PSPLT(2)	0.43 ± 0.05	0.43 ± 0.05
CLPOW	1.47 ± 0.14	1.40 ± 0.05
$M_{\rm g}$ (GeV)	0.75 ± 0.03	0.75 ± 0.02
$\lambda_{\rm BE}$	–	$1.1\ ^{+\ 0.1}_{-\ 0.2}$
$r_{\rm BE}^{-1}$ (GeV)	–	0.40 ± 0.05

Table 6: Tuned parameters for HERWIG 6.2 [149] using the PYTHIA 6.2 [103] particle decay routines without Bose-Einstein correlations and using the BE_{32} Gaussian model [152]. In both cases the parameter DECWT is fixed at the value 0.70.

$y_{\rm cut}^{\rm J}$	2-Jet Fraction	3-Jet Fraction	4-Jet Fraction	5-Jet Fraction
0.001	$0.013 \pm 0.006 \pm 0.002$	$0.161 \pm 0.019 \pm 0.002$	$0.316 \pm 0.024 \pm 0.002$	$0.271 \pm 0.022 \pm 0.004$
0.002	$0.065 \pm 0.013 \pm 0.002$	$0.341 \pm 0.026 \pm 0.003$	$0.355 \pm 0.025 \pm 0.004$	$0.187 \pm 0.018 \pm 0.004$
0.004	$0.148 \pm 0.018 \pm 0.002$	$0.478 \pm 0.031 \pm 0.003$	$0.293 \pm 0.022 \pm 0.002$	$0.070 \pm 0.010 \pm 0.002$
0.006	$0.222 \pm 0.022 \pm 0.002$	$0.535 \pm 0.032 \pm 0.005$	$0.204 \pm 0.018 \pm 0.004$	$0.035 \pm 0.007 \pm 0.002$
0.008	$0.287 \pm 0.024 \pm 0.002$	$0.529 \pm 0.031 \pm 0.003$	$0.155 \pm 0.016 \pm 0.005$	$0.029 \pm 0.007 \pm 0.001$
0.010	$0.323 \pm 0.026 \pm 0.003$	$0.525 \pm 0.031 \pm 0.002$	$0.133 \pm 0.014 \pm 0.003$	$0.019 \pm 0.005 \pm 0.001$
0.020	$0.491 \pm 0.032 \pm 0.007$	$0.445 \pm 0.028 \pm 0.005$	$0.061 \pm 0.009 \pm 0.003$	$0.003 \pm 0.002 \pm 0.001$
0.040	$0.678 \pm 0.037 \pm 0.007$	$0.310 \pm 0.023 \pm 0.007$	$0.013 \pm 0.004 \pm 0.001$	
0.060	$0.775 \pm 0.039 \pm 0.005$	$0.221 \pm 0.018 \pm 0.005$	$0.004 \pm 0.002 \pm 0.001$	
0.080	$0.839 \pm 0.040 \pm 0.003$	$0.159 \pm 0.015 \pm 0.003$	$0.002 \pm 0.002 \pm 0.001$	
0.100	$0.889 \pm 0.041 \pm 0.003$	$0.110 \pm 0.012 \pm 0.003$	$0.001 \pm 0.001 \pm 0.000$	
0.120	$0.920 \pm 0.042 \pm 0.002$	$0.078 \pm 0.010 \pm 0.002$	$0.002 \pm 0.002 \pm 0.001$	
0.140	$0.930 \pm 0.042 \pm 0.002$	$0.070 \pm 0.010 \pm 0.002$		
0.160	$0.949 \pm 0.042 \pm 0.002$	$0.051 \pm 0.008 \pm 0.002$		
0.180	$0.970 \pm 0.043 \pm 0.001$	$0.030 \pm 0.006 \pm 0.001$		
0.200	$0.977 \pm 0.043 \pm 0.001$	$0.023 \pm 0.005 \pm 0.001$		
0.220	$0.986 \pm 0.043 \pm 0.001$	$0.014 \pm 0.004 \pm 0.001$		
0.240	$0.992 \pm 0.043 \pm 0.001$	$0.008 \pm 0.003 \pm 0.001$		
0.260	$0.994 \pm 0.043 \pm 0.001$	$0.006 \pm 0.003 \pm 0.001$		
0.280	$0.996 \pm 0.043 \pm 0.001$	$0.004 \pm 0.003 \pm 0.001$		

Table 7: Jet fraction using the JADE algorithm as a function of the jet resolution parameter $y_{\rm cut}^{\rm J}$ at $\sqrt{s} = 130.1$ GeV. The first uncertainty is statistical, the second systematic.

$y_{\rm cut}^{\rm J}$	2-Jet Fraction	3-Jet Fraction	4-Jet Fraction	5-Jet Fraction
0.001	$0.019 \pm 0.007 \pm 0.001$	$0.175 \pm 0.022 \pm 0.003$	$0.305 \pm 0.028 \pm 0.004$	$0.236 \pm 0.024 \pm 0.001$
0.002	$0.061 \pm 0.013 \pm 0.003$	$0.344 \pm 0.031 \pm 0.006$	$0.326 \pm 0.028 \pm 0.009$	$0.157 \pm 0.019 \pm 0.005$
0.004	$0.149 \pm 0.021 \pm 0.002$	$0.464 \pm 0.034 \pm 0.002$	$0.272 \pm 0.025 \pm 0.005$	$0.092 \pm 0.014 \pm 0.002$
0.006	$0.206 \pm 0.024 \pm 0.003$	$0.512 \pm 0.036 \pm 0.004$	$0.224 \pm 0.023 \pm 0.004$	$0.047 \pm 0.010 \pm 0.004$
0.008	$0.266 \pm 0.027 \pm 0.003$	$0.523 \pm 0.036 \pm 0.001$	$0.175 \pm 0.020 \pm 0.005$	$0.034 \pm 0.009 \pm 0.001$
0.010	$0.319 \pm 0.030 \pm 0.005$	$0.504 \pm 0.035 \pm 0.004$	$0.148 \pm 0.018 \pm 0.002$	$0.030 \pm 0.008 \pm 0.002$
0.020	$0.507 \pm 0.037 \pm 0.004$	$0.406 \pm 0.031 \pm 0.005$	$0.080 \pm 0.012 \pm 0.003$	$0.008 \pm 0.004 \pm 0.001$
0.040	$0.683 \pm 0.042 \pm 0.005$	$0.294 \pm 0.026 \pm 0.005$	$0.024 \pm 0.007 \pm 0.002$	
0.060	$0.774 \pm 0.045 \pm 0.003$	$0.218 \pm 0.022 \pm 0.004$	$0.008 \pm 0.004 \pm 0.001$	
0.080	$0.825 \pm 0.046 \pm 0.003$	$0.175 \pm 0.019 \pm 0.003$		
0.100	$0.865 \pm 0.047 \pm 0.003$	$0.135 \pm 0.016 \pm 0.003$		
0.120	$0.900 \pm 0.048 \pm 0.003$	$0.100 \pm 0.014 \pm 0.003$		
0.140	$0.919 \pm 0.049 \pm 0.004$	$0.081 \pm 0.012 \pm 0.004$		
0.160	$0.940 \pm 0.049 \pm 0.002$	$0.060 \pm 0.010 \pm 0.002$		
0.180	$0.966 \pm 0.050 \pm 0.001$	$0.034 \pm 0.007 \pm 0.001$		
0.200	$0.978 \pm 0.050 \pm 0.001$	$0.022 \pm 0.006 \pm 0.001$		
0.220	$0.983 \pm 0.050 \pm 0.002$	$0.017 \pm 0.005 \pm 0.002$		
0.240	$0.984 \pm 0.050 \pm 0.001$	$0.016 \pm 0.005 \pm 0.001$		
0.260	$0.990 \pm 0.050 \pm 0.001$	$0.010 \pm 0.004 \pm 0.001$		
0.280	$0.997 \pm 0.050 \pm 0.001$	$0.003 \pm 0.002 \pm 0.001$		

Table 8: Jet fraction using the JADE algorithm as a function of the jet resolution parameter $y_{\rm cut}^{\rm J}$ at $\sqrt{s} = 136.1$ GeV. The first uncertainty is statistical, the second systematic.

$y_{\rm cut}^{\rm J}$	2-Jet Fraction	3-Jet Fraction	4-Jet Fraction	5-Jet Fraction
0.001	$0.062 \pm 0.016 \pm 0.006$	$0.228 \pm 0.029 \pm 0.009$	$0.313 \pm 0.030 \pm 0.005$	$0.262 \pm 0.026 \pm 0.001$
0.002	$0.108 \pm 0.021 \pm 0.007$	$0.369 \pm 0.035 \pm 0.011$	$0.366 \pm 0.031 \pm 0.006$	$0.132 \pm 0.018 \pm 0.010$
0.004	$0.196 \pm 0.027 \pm 0.006$	$0.493 \pm 0.039 \pm 0.010$	$0.257 \pm 0.025 \pm 0.005$	$0.054 \pm 0.013 \pm 0.008$
0.006	$0.278 \pm 0.032 \pm 0.004$	$0.504 \pm 0.038 \pm 0.007$	$0.199 \pm 0.022 \pm 0.004$	$0.019 \pm 0.009 \pm 0.004$
0.008	$0.337 \pm 0.035 \pm 0.007$	$0.503 \pm 0.037 \pm 0.006$	$0.153 \pm 0.020 \pm 0.008$	$0.007 \pm 0.007 \pm 0.002$
0.010	$0.387 \pm 0.037 \pm 0.007$	$0.489 \pm 0.036 \pm 0.003$	$0.120 \pm 0.018 \pm 0.006$	$0.004 \pm 0.006 \pm 0.001$
0.020	$0.529 \pm 0.042 \pm 0.010$	$0.420 \pm 0.033 \pm 0.009$	$0.051 \pm 0.013 \pm 0.002$	
0.040	$0.681 \pm 0.046 \pm 0.009$	$0.313 \pm 0.028 \pm 0.012$	$0.007 \pm 0.007 \pm 0.003$	
0.060	$0.768 \pm 0.049 \pm 0.007$	$0.226 \pm 0.024 \pm 0.007$	$0.006 \pm 0.005 \pm 0.001$	
0.080	$0.826 \pm 0.051 \pm 0.005$	$0.174 \pm 0.021 \pm 0.005$		
0.100	$0.870 \pm 0.052 \pm 0.005$	$0.130 \pm 0.018 \pm 0.005$		
0.120	$0.906 \pm 0.053 \pm 0.004$	$0.094 \pm 0.015 \pm 0.004$		
0.140	$0.924 \pm 0.053 \pm 0.004$	$0.076 \pm 0.013 \pm 0.004$		
0.160	$0.950 \pm 0.054 \pm 0.003$	$0.050 \pm 0.010 \pm 0.003$		
0.180	$0.962 \pm 0.054 \pm 0.003$	$0.038 \pm 0.009 \pm 0.003$		
0.200	$0.984 \pm 0.054 \pm 0.002$	$0.016 \pm 0.006 \pm 0.002$		
0.220	$0.990 \pm 0.054 \pm 0.002$	$0.010 \pm 0.004 \pm 0.002$		
0.240	$0.992 \pm 0.055 \pm 0.002$	$0.008 \pm 0.004 \pm 0.002$		
0.260	$0.994 \pm 0.055 \pm 0.001$	$0.006 \pm 0.003 \pm 0.001$		
0.280	$0.992 \pm 0.055 \pm 0.001$	$0.008 \pm 0.003 \pm 0.001$		

Table 9: Jet fraction using the JADE algorithm as a function of the jet resolution parameter $y_{\rm cut}^{\rm J}$ at $\sqrt{s} = 161.3$ GeV. The first uncertainty is statistical, the second systematic.

$y_{\rm cut}^{\rm J}$	2-Jet Fraction	3-Jet Fraction	4-Jet Fraction	5-Jet Fraction
0.001	$0.055 \pm 0.020 \pm 0.003$	$0.186 \pm 0.030 \pm 0.004$	$0.340 \pm 0.036 \pm 0.007$	$0.253 \pm 0.029 \pm 0.021$
0.002	$0.115 \pm 0.026 \pm 0.009$	$0.342 \pm 0.037 \pm 0.012$	$0.290 \pm 0.031 \pm 0.012$	$0.183 \pm 0.025 \pm 0.009$
0.004	$0.170 \pm 0.029 \pm 0.010$	$0.455 \pm 0.041 \pm 0.028$	$0.255 \pm 0.029 \pm 0.009$	$0.083 \pm 0.020 \pm 0.006$
0.006	$0.245 \pm 0.034 \pm 0.006$	$0.466 \pm 0.040 \pm 0.019$	$0.200 \pm 0.026 \pm 0.009$	$0.049 \pm 0.017 \pm 0.006$
0.008	$0.287 \pm 0.036 \pm 0.008$	$0.463 \pm 0.040 \pm 0.011$	$0.177 \pm 0.026 \pm 0.007$	$0.037 \pm 0.016 \pm 0.007$
0.010	$0.323 \pm 0.038 \pm 0.012$	$0.448 \pm 0.039 \pm 0.009$	$0.157 \pm 0.025 \pm 0.007$	$0.038 \pm 0.017 \pm 0.009$
0.020	$0.491 \pm 0.045 \pm 0.013$	$0.399 \pm 0.036 \pm 0.010$	$0.068 \pm 0.021 \pm 0.014$	$0.040 \pm 0.020 \pm 0.011$
0.040	$0.656 \pm 0.050 \pm 0.020$	$0.270 \pm 0.031 \pm 0.010$	$0.074 \pm 0.027 \pm 0.015$	
0.060	$0.762 \pm 0.055 \pm 0.011$	$0.230 \pm 0.029 \pm 0.010$	$0.008 \pm 0.017 \pm 0.006$	
0.080	$0.860 \pm 0.058 \pm 0.007$	$0.140 \pm 0.023 \pm 0.008$		
0.100	$0.907 \pm 0.059 \pm 0.011$	$0.093 \pm 0.019 \pm 0.011$		
0.120	$0.924 \pm 0.060 \pm 0.006$	$0.076 \pm 0.017 \pm 0.006$		
0.140	$0.956 \pm 0.061 \pm 0.008$	$0.044 \pm 0.013 \pm 0.008$		
0.160	$0.972 \pm 0.062 \pm 0.004$	$0.028 \pm 0.010 \pm 0.004$		
0.180	$0.984 \pm 0.062 \pm 0.006$	$0.016 \pm 0.008 \pm 0.004$		
0.200	$0.986 \pm 0.062 \pm 0.005$	$0.014 \pm 0.007 \pm 0.004$		
0.220	$0.988 \pm 0.062 \pm 0.004$	$0.012 \pm 0.007 \pm 0.003$		
0.240	$0.989 \pm 0.062 \pm 0.003$	$0.011 \pm 0.006 \pm 0.003$		
0.260	$0.990 \pm 0.062 \pm 0.004$	$0.010 \pm 0.005 \pm 0.003$		
0.280	$0.996 \pm 0.063 \pm 0.001$	$0.004 \pm 0.004 \pm 0.001$		

Table 10: Jet fraction using the JADE algorithm as a function of the jet resolution parameter $y_{\rm cut}^{\rm J}$ at $\sqrt{s} = 172.3$ GeV. The first uncertainty is statistical, the second systematic.

$y_{\rm cut}^{\rm J}$	2-Jet Fraction	3-Jet Fraction	4-Jet Fraction	5-Jet Fraction
0.001	$0.028 \pm 0.004 \pm 0.002$	$0.209 \pm 0.012 \pm 0.002$	$0.345 \pm 0.016 \pm 0.004$	$0.230 \pm 0.014 \pm 0.004$
0.002	$0.069 \pm 0.007 \pm 0.002$	$0.363 \pm 0.016 \pm 0.004$	$0.345 \pm 0.016 \pm 0.005$	$0.169 \pm 0.014 \pm 0.002$
0.004	$0.154 \pm 0.011 \pm 0.003$	$0.477 \pm 0.019 \pm 0.002$	$0.284 \pm 0.016 \pm 0.007$	$0.077 \pm 0.011 \pm 0.007$
0.006	$0.231 \pm 0.013 \pm 0.005$	$0.498 \pm 0.019 \pm 0.002$	$0.216 \pm 0.015 \pm 0.004$	$0.045 \pm 0.010 \pm 0.004$
0.008	$0.293 \pm 0.015 \pm 0.005$	$0.493 \pm 0.019 \pm 0.002$	$0.177 \pm 0.014 \pm 0.004$	$0.026 \pm 0.009 \pm 0.006$
0.010	$0.365 \pm 0.017 \pm 0.006$	$0.472 \pm 0.019 \pm 0.004$	$0.144 \pm 0.013 \pm 0.004$	$0.018 \pm 0.009 \pm 0.002$
0.020	$0.514 \pm 0.020 \pm 0.006$	$0.413 \pm 0.018 \pm 0.004$	$0.067 \pm 0.011 \pm 0.005$	$0.006 \pm 0.005 \pm 0.001$
0.040	$0.692 \pm 0.023 \pm 0.002$	$0.298 \pm 0.016 \pm 0.002$	$0.003 \pm 0.007 \pm 0.001$	$0.007 \pm 0.010 \pm 0.002$
0.060	$0.784 \pm 0.025 \pm 0.004$	$0.209 \pm 0.014 \pm 0.003$	$0.007 \pm 0.008 \pm 0.003$	
0.080	$0.839 \pm 0.026 \pm 0.002$	$0.154 \pm 0.012 \pm 0.003$	$0.007 \pm 0.008 \pm 0.002$	
0.100	$0.886 \pm 0.027 \pm 0.002$	$0.114 \pm 0.010 \pm 0.002$		
0.120	$0.923 \pm 0.027 \pm 0.001$	$0.077 \pm 0.008 \pm 0.001$		
0.140	$0.939 \pm 0.028 \pm 0.002$	$0.061 \pm 0.007 \pm 0.002$		
0.160	$0.957 \pm 0.028 \pm 0.001$	$0.043 \pm 0.006 \pm 0.001$		
0.180	$0.971 \pm 0.028 \pm 0.002$	$0.029 \pm 0.005 \pm 0.002$		
0.200	$0.980 \pm 0.028 \pm 0.003$	$0.020 \pm 0.005 \pm 0.001$		
0.220	$0.982 \pm 0.028 \pm 0.002$	$0.018 \pm 0.004 \pm 0.002$		
0.240	$0.985 \pm 0.028 \pm 0.001$	$0.015 \pm 0.004 \pm 0.001$		
0.260	$0.991 \pm 0.029 \pm 0.001$	$0.009 \pm 0.003 \pm 0.001$		
0.280	$0.997 \pm 0.029 \pm 0.001$	$0.003 \pm 0.002 \pm 0.001$		

Table 11: Jet fraction using the JADE algorithm as a function of the jet resolution parameter $y_{\rm cut}^{\rm J}$ at $\sqrt{s} = 182.8$ GeV. The first uncertainty is statistical, the second systematic.

$y_{\rm cut}^{\rm J}$	2-Jet Fraction	3-Jet Fraction	4-Jet Fraction	5-Jet Fraction
0.001	$0.038 \pm 0.003 \pm 0.001$	$0.215 \pm 0.008 \pm 0.005$	$0.318 \pm 0.009 \pm 0.002$	$0.252 \pm 0.009 \pm 0.004$
0.002	$0.082 \pm 0.005 \pm 0.003$	$0.356 \pm 0.010 \pm 0.006$	$0.345 \pm 0.010 \pm 0.009$	$0.166 \pm 0.008 \pm 0.004$
0.004	$0.162 \pm 0.007 \pm 0.004$	$0.472 \pm 0.012 \pm 0.006$	$0.286 \pm 0.009 \pm 0.010$	$0.070 \pm 0.007 \pm 0.005$
0.006	$0.235 \pm 0.009 \pm 0.007$	$0.503 \pm 0.012 \pm 0.004$	$0.220 \pm 0.009 \pm 0.006$	$0.042 \pm 0.007 \pm 0.002$
0.008	$0.289 \pm 0.010 \pm 0.008$	$0.510 \pm 0.012 \pm 0.004$	$0.174 \pm 0.008 \pm 0.007$	$0.026 \pm 0.006 \pm 0.004$
0.010	$0.334 \pm 0.010 \pm 0.009$	$0.511 \pm 0.012 \pm 0.007$	$0.142 \pm 0.008 \pm 0.005$	$0.012 \pm 0.005 \pm 0.003$
0.020	$0.507 \pm 0.013 \pm 0.008$	$0.439 \pm 0.011 \pm 0.008$	$0.054 \pm 0.006 \pm 0.002$	
0.040	$0.678 \pm 0.015 \pm 0.005$	$0.312 \pm 0.010 \pm 0.004$	$0.010 \pm 0.005 \pm 0.002$	$0.000 \pm 0.001 \pm 0.000$
0.060	$0.780 \pm 0.016 \pm 0.007$	$0.220 \pm 0.008 \pm 0.007$		
0.080	$0.834 \pm 0.016 \pm 0.005$	$0.165 \pm 0.007 \pm 0.005$	$0.001 \pm 0.006 \pm 0.001$	
0.100	$0.876 \pm 0.016 \pm 0.006$	$0.123 \pm 0.006 \pm 0.005$	$0.001 \pm 0.002 \pm 0.001$	
0.120	$0.910 \pm 0.017 \pm 0.006$	$0.089 \pm 0.005 \pm 0.007$	$0.000 \pm 0.001 \pm 0.000$	
0.140	$0.932 \pm 0.017 \pm 0.004$	$0.068 \pm 0.005 \pm 0.004$		
0.160	$0.953 \pm 0.017 \pm 0.003$	$0.047 \pm 0.004 \pm 0.003$		
0.180	$0.966 \pm 0.017 \pm 0.002$	$0.034 \pm 0.004 \pm 0.002$		
0.200	$0.976 \pm 0.017 \pm 0.004$	$0.024 \pm 0.003 \pm 0.003$		
0.220	$0.983 \pm 0.018 \pm 0.002$	$0.017 \pm 0.003 \pm 0.002$		
0.240	$0.987 \pm 0.018 \pm 0.002$	$0.013 \pm 0.002 \pm 0.002$		
0.260	$0.993 \pm 0.018 \pm 0.003$	$0.007 \pm 0.002 \pm 0.001$		
0.280	$0.997 \pm 0.018 \pm 0.002$	$0.003 \pm 0.001 \pm 0.001$		

Table 12: Jet fraction using the JADE algorithm as a function of the jet resolution parameter $y_{\rm cut}^{\rm J}$ at $\sqrt{s} = 188.6$ GeV. The first uncertainty is statistical, the second systematic.

$y_{\rm cut}^{\rm J}$	2-Jet Fraction	3-Jet Fraction	4-Jet Fraction	5-Jet Fraction
0.001	$0.031 \pm 0.004 \pm 0.002$	$0.213 \pm 0.010 \pm 0.004$	$0.332 \pm 0.012 \pm 0.007$	$0.244 \pm 0.012 \pm 0.011$
0.002	$0.078 \pm 0.006 \pm 0.004$	$0.351 \pm 0.012 \pm 0.004$	$0.375 \pm 0.014 \pm 0.009$	$0.142 \pm 0.012 \pm 0.008$
0.004	$0.154 \pm 0.008 \pm 0.008$	$0.483 \pm 0.015 \pm 0.004$	$0.275 \pm 0.014 \pm 0.010$	$0.078 \pm 0.012 \pm 0.009$
0.006	$0.218 \pm 0.010 \pm 0.010$	$0.531 \pm 0.016 \pm 0.007$	$0.217 \pm 0.013 \pm 0.006$	$0.034 \pm 0.012 \pm 0.004$
0.008	$0.273 \pm 0.011 \pm 0.011$	$0.547 \pm 0.016 \pm 0.012$	$0.173 \pm 0.013 \pm 0.008$	$0.007 \pm 0.009 \pm 0.003$
0.010	$0.321 \pm 0.012 \pm 0.010$	$0.527 \pm 0.016 \pm 0.011$	$0.151 \pm 0.013 \pm 0.005$	$0.001 \pm 0.007 \pm 0.001$
0.020	$0.499 \pm 0.015 \pm 0.008$	$0.454 \pm 0.016 \pm 0.009$	$0.044 \pm 0.012 \pm 0.005$	$0.003 \pm 0.008 \pm 0.003$
0.040	$0.669 \pm 0.018 \pm 0.006$	$0.324 \pm 0.014 \pm 0.008$	$0.008 \pm 0.007 \pm 0.003$	
0.060	$0.777 \pm 0.020 \pm 0.004$	$0.223 \pm 0.012 \pm 0.005$		
0.080	$0.833 \pm 0.021 \pm 0.007$	$0.167 \pm 0.010 \pm 0.007$		
0.100	$0.878 \pm 0.021 \pm 0.008$	$0.122 \pm 0.009 \pm 0.008$		
0.120	$0.910 \pm 0.022 \pm 0.008$	$0.090 \pm 0.008 \pm 0.008$		
0.140	$0.935 \pm 0.022 \pm 0.009$	$0.065 \pm 0.007 \pm 0.009$		
0.160	$0.950 \pm 0.022 \pm 0.007$	$0.050 \pm 0.006 \pm 0.007$		
0.180	$0.959 \pm 0.022 \pm 0.007$	$0.041 \pm 0.005 \pm 0.007$		
0.200	$0.969 \pm 0.023 \pm 0.007$	$0.031 \pm 0.005 \pm 0.007$		
0.220	$0.983 \pm 0.023 \pm 0.007$	$0.017 \pm 0.004 \pm 0.004$		
0.240	$0.987 \pm 0.023 \pm 0.004$	$0.013 \pm 0.004 \pm 0.003$		
0.260	$0.992 \pm 0.023 \pm 0.002$	$0.008 \pm 0.003 \pm 0.002$		
0.280	$0.998 \pm 0.023 \pm 0.001$	$0.002 \pm 0.002 \pm 0.001$		

Table 13: Jet fraction using the JADE algorithm as a function of the jet resolution parameter $y_{\rm cut}^{\rm J}$ at $\sqrt{s} = 194.4$ GeV. The first uncertainty is statistical, the second systematic.

$y_{\rm cut}^{\rm J}$	2-Jet Fraction	3-Jet Fraction	4-Jet Fraction	5-Jet Fraction
0.001	$0.036 \pm 0.004 \pm 0.002$	$0.207 \pm 0.009 \pm 0.007$	$0.324 \pm 0.012 \pm 0.006$	$0.248 \pm 0.012 \pm 0.006$
0.002	$0.072 \pm 0.006 \pm 0.003$	$0.351 \pm 0.012 \pm 0.005$	$0.338 \pm 0.013 \pm 0.006$	$0.171 \pm 0.012 \pm 0.004$
0.004	$0.155 \pm 0.009 \pm 0.007$	$0.473 \pm 0.015 \pm 0.004$	$0.282 \pm 0.013 \pm 0.006$	$0.073 \pm 0.010 \pm 0.007$
0.006	$0.226 \pm 0.010 \pm 0.007$	$0.507 \pm 0.015 \pm 0.012$	$0.229 \pm 0.013 \pm 0.012$	$0.023 \pm 0.009 \pm 0.008$
0.008	$0.285 \pm 0.012 \pm 0.010$	$0.522 \pm 0.016 \pm 0.012$	$0.182 \pm 0.013 \pm 0.012$	$0.010 \pm 0.008 \pm 0.009$
0.010	$0.329 \pm 0.013 \pm 0.011$	$0.519 \pm 0.016 \pm 0.009$	$0.148 \pm 0.012 \pm 0.006$	$0.004 \pm 0.008 \pm 0.004$
0.020	$0.493 \pm 0.015 \pm 0.011$	$0.435 \pm 0.015 \pm 0.009$	$0.072 \pm 0.012 \pm 0.006$	
0.040	$0.662 \pm 0.018 \pm 0.009$	$0.322 \pm 0.014 \pm 0.009$	$0.015 \pm 0.012 \pm 0.004$	
0.060	$0.744 \pm 0.019 \pm 0.014$	$0.237 \pm 0.012 \pm 0.006$	$0.020 \pm 0.015 \pm 0.011$	
0.080	$0.817 \pm 0.020 \pm 0.012$	$0.177 \pm 0.011 \pm 0.010$	$0.006 \pm 0.015 \pm 0.008$	
0.100	$0.871 \pm 0.021 \pm 0.012$	$0.129 \pm 0.009 \pm 0.010$		
0.120	$0.898 \pm 0.021 \pm 0.007$	$0.102 \pm 0.009 \pm 0.007$		
0.140	$0.922 \pm 0.022 \pm 0.005$	$0.078 \pm 0.008 \pm 0.005$		
0.160	$0.945 \pm 0.022 \pm 0.005$	$0.055 \pm 0.007 \pm 0.005$		
0.180	$0.954 \pm 0.022 \pm 0.004$	$0.046 \pm 0.007 \pm 0.004$		
0.200	$0.968 \pm 0.023 \pm 0.005$	$0.032 \pm 0.006 \pm 0.004$		
0.220	$0.978 \pm 0.023 \pm 0.004$	$0.023 \pm 0.005 \pm 0.003$		
0.240	$0.982 \pm 0.023 \pm 0.002$	$0.018 \pm 0.004 \pm 0.002$		
0.260	$0.987 \pm 0.023 \pm 0.003$	$0.013 \pm 0.004 \pm 0.003$		
0.280	$0.995 \pm 0.023 \pm 0.001$	$0.005 \pm 0.003 \pm 0.001$		

Table 14: Jet fraction using the JADE algorithm as a function of the jet resolution parameter $y_{\rm cut}^{\rm J}$ at $\sqrt{s} = 200.2$ GeV. The first uncertainty is statistical, the second systematic.

$y_{\rm cut}^{\rm J}$	2-Jet Fraction	3-Jet Fraction	4-Jet Fraction	5-Jet Fraction
0.001	$0.030 \pm 0.003 \pm 0.002$	$0.216 \pm 0.008 \pm 0.004$	$0.337 \pm 0.010 \pm 0.004$	$0.240 \pm 0.009 \pm 0.005$
0.002	$0.075 \pm 0.004 \pm 0.003$	$0.367 \pm 0.010 \pm 0.006$	$0.341 \pm 0.010 \pm 0.008$	$0.157 \pm 0.009 \pm 0.008$
0.004	$0.149 \pm 0.007 \pm 0.005$	$0.478 \pm 0.011 \pm 0.002$	$0.279 \pm 0.010 \pm 0.009$	$0.080 \pm 0.009 \pm 0.003$
0.006	$0.213 \pm 0.008 \pm 0.008$	$0.510 \pm 0.012 \pm 0.004$	$0.222 \pm 0.010 \pm 0.008$	$0.052 \pm 0.008 \pm 0.005$
0.008	$0.272 \pm 0.009 \pm 0.010$	$0.518 \pm 0.012 \pm 0.007$	$0.180 \pm 0.010 \pm 0.007$	$0.025 \pm 0.007 \pm 0.008$
0.010	$0.323 \pm 0.010 \pm 0.010$	$0.513 \pm 0.012 \pm 0.008$	$0.149 \pm 0.010 \pm 0.006$	$0.014 \pm 0.007 \pm 0.005$
0.020	$0.496 \pm 0.012 \pm 0.009$	$0.451 \pm 0.012 \pm 0.007$	$0.054 \pm 0.009 \pm 0.007$	
0.040	$0.674 \pm 0.014 \pm 0.008$	$0.321 \pm 0.011 \pm 0.005$	$0.006 \pm 0.008 \pm 0.003$	
0.060	$0.769 \pm 0.015 \pm 0.006$	$0.231 \pm 0.010 \pm 0.004$		
0.080	$0.826 \pm 0.016 \pm 0.007$	$0.174 \pm 0.009 \pm 0.009$		
0.100	$0.873 \pm 0.016 \pm 0.007$	$0.127 \pm 0.008 \pm 0.007$		
0.120	$0.901 \pm 0.017 \pm 0.007$	$0.098 \pm 0.007 \pm 0.007$		
0.140	$0.928 \pm 0.017 \pm 0.005$	$0.072 \pm 0.006 \pm 0.005$		
0.160	$0.943 \pm 0.017 \pm 0.006$	$0.057 \pm 0.006 \pm 0.006$		
0.180	$0.960 \pm 0.017 \pm 0.004$	$0.040 \pm 0.005 \pm 0.004$		
0.200	$0.970 \pm 0.018 \pm 0.002$	$0.030 \pm 0.005 \pm 0.002$		
0.220	$0.976 \pm 0.018 \pm 0.001$	$0.024 \pm 0.004 \pm 0.001$		
0.240	$0.986 \pm 0.018 \pm 0.002$	$0.014 \pm 0.004 \pm 0.002$		
0.260	$0.988 \pm 0.018 \pm 0.002$	$0.012 \pm 0.003 \pm 0.002$		
0.280	$0.994 \pm 0.018 \pm 0.001$	$0.006 \pm 0.002 \pm 0.001$		

Table 15: Jet fraction using the JADE algorithm as a function of the jet resolution parameter $y_{\rm cut}^{\rm J}$ at $\sqrt{s} = 206.2$ GeV. The first uncertainty is statistical, the second systematic.

$y_{\rm cut}^{\rm D}$	2-Jet Fraction	3-Jet Fraction	4-Jet Fraction	5-Jet Fraction
0.001	$0.234 \pm 0.022 \pm 0.003$	$0.367 \pm 0.026 \pm 0.006$	$0.271 \pm 0.022 \pm 0.005$	$0.089 \pm 0.012 \pm 0.003$
0.002	$0.395 \pm 0.028 \pm 0.005$	$0.369 \pm 0.026 \pm 0.003$	$0.195 \pm 0.018 \pm 0.007$	$0.031 \pm 0.007 \pm 0.002$
0.004	$0.502 \pm 0.031 \pm 0.008$	$0.374 \pm 0.026 \pm 0.005$	$0.116 \pm 0.014 \pm 0.003$	$0.008 \pm 0.004 \pm 0.001$
0.006	$0.580 \pm 0.034 \pm 0.006$	$0.349 \pm 0.025 \pm 0.004$	$0.068 \pm 0.010 \pm 0.003$	$0.003 \pm 0.002 \pm 0.001$
0.008	$0.624 \pm 0.035 \pm 0.005$	$0.322 \pm 0.024 \pm 0.005$	$0.054 \pm 0.009 \pm 0.002$	
0.010	$0.654 \pm 0.036 \pm 0.006$	$0.305 \pm 0.023 \pm 0.006$	$0.041 \pm 0.008 \pm 0.002$	
0.020	$0.770 \pm 0.039 \pm 0.007$	$0.218 \pm 0.018 \pm 0.007$	$0.012 \pm 0.004 \pm 0.001$	
0.040	$0.876 \pm 0.041 \pm 0.003$	$0.119 \pm 0.013 \pm 0.003$	$0.004 \pm 0.003 \pm 0.001$	
0.060	$0.914 \pm 0.042 \pm 0.003$	$0.085 \pm 0.010 \pm 0.003$	$0.001 \pm 0.001 \pm 0.001$	
0.080	$0.941 \pm 0.042 \pm 0.002$	$0.058 \pm 0.009 \pm 0.002$	$0.001 \pm 0.001 \pm 0.001$	
0.100	$0.954 \pm 0.042 \pm 0.001$	$0.046 \pm 0.008 \pm 0.001$		
0.120	$0.962 \pm 0.043 \pm 0.001$	$0.038 \pm 0.007 \pm 0.001$		
0.140	$0.973 \pm 0.043 \pm 0.001$	$0.027 \pm 0.006 \pm 0.001$		
0.160	$0.978 \pm 0.043 \pm 0.001$	$0.022 \pm 0.005 \pm 0.001$		
0.180	$0.983 \pm 0.043 \pm 0.001$	$0.017 \pm 0.005 \pm 0.001$		
0.200	$0.992 \pm 0.043 \pm 0.001$	$0.009 \pm 0.004 \pm 0.001$		
0.220	$0.994 \pm 0.043 \pm 0.001$	$0.006 \pm 0.003 \pm 0.001$		
0.240	$0.997 \pm 0.043 \pm 0.001$	$0.003 \pm 0.002 \pm 0.001$		
0.260	$0.998 \pm 0.043 \pm 0.001$	$0.002 \pm 0.002 \pm 0.001$		
0.280	$1.000 \pm 0.043 \pm 0.001$			

Table 16: Jet fraction using the $k_{\rm t}$ algorithm as a function of the jet resolution parameter $y_{\rm cut}^{\rm D}$ at $\sqrt{s} = 130.1$ GeV. The first uncertainty is statistical, the second systematic.

$y_{\rm cut}^{\rm D}$	2-Jet Fraction	3-Jet Fraction	4-Jet Fraction	5-Jet Fraction
0.001	$0.224 \pm 0.025 \pm 0.008$	$0.370 \pm 0.030 \pm 0.006$	$0.219 \pm 0.023 \pm 0.004$	$0.115 \pm 0.017 \pm 0.002$
0.002	$0.374 \pm 0.031 \pm 0.009$	$0.369 \pm 0.030 \pm 0.010$	$0.185 \pm 0.021 \pm 0.006$	$0.053 \pm 0.011 \pm 0.001$
0.004	$0.515 \pm 0.036 \pm 0.007$	$0.352 \pm 0.029 \pm 0.009$	$0.101 \pm 0.015 \pm 0.007$	$0.032 \pm 0.009 \pm 0.003$
0.006	$0.586 \pm 0.039 \pm 0.004$	$0.316 \pm 0.027 \pm 0.003$	$0.079 \pm 0.013 \pm 0.004$	$0.020 \pm 0.007 \pm 0.002$
0.008	$0.622 \pm 0.040 \pm 0.003$	$0.303 \pm 0.027 \pm 0.002$	$0.062 \pm 0.012 \pm 0.004$	$0.013 \pm 0.006 \pm 0.002$
0.010	$0.649 \pm 0.041 \pm 0.003$	$0.290 \pm 0.026 \pm 0.003$	$0.051 \pm 0.010 \pm 0.004$	$0.011 \pm 0.006 \pm 0.002$
0.020	$0.763 \pm 0.045 \pm 0.003$	$0.209 \pm 0.021 \pm 0.003$	$0.026 \pm 0.008 \pm 0.003$	$0.002 \pm 0.002 \pm 0.001$
0.040	$0.853 \pm 0.047 \pm 0.006$	$0.141 \pm 0.016 \pm 0.007$	$0.006 \pm 0.003 \pm 0.001$	
0.060	$0.890 \pm 0.048 \pm 0.004$	$0.110 \pm 0.014 \pm 0.004$		
0.080	$0.923 \pm 0.049 \pm 0.002$	$0.077 \pm 0.011 \pm 0.002$		
0.100	$0.947 \pm 0.049 \pm 0.002$	$0.053 \pm 0.009 \pm 0.002$		
0.120	$0.960 \pm 0.050 \pm 0.003$	$0.040 \pm 0.008 \pm 0.003$		
0.140	$0.973 \pm 0.050 \pm 0.002$	$0.027 \pm 0.006 \pm 0.002$		
0.160	$0.981 \pm 0.050 \pm 0.002$	$0.019 \pm 0.005 \pm 0.002$		
0.180	$0.988 \pm 0.050 \pm 0.002$	$0.012 \pm 0.004 \pm 0.002$		
0.200	$0.991 \pm 0.050 \pm 0.001$	$0.010 \pm 0.004 \pm 0.001$		
0.220	$0.995 \pm 0.050 \pm 0.001$	$0.005 \pm 0.003 \pm 0.001$		
0.240	$0.995 \pm 0.050 \pm 0.001$	$0.005 \pm 0.003 \pm 0.001$		
0.260	$0.997 \pm 0.050 \pm 0.002$	$0.003 \pm 0.002 \pm 0.001$		
0.280	$1.000 \pm 0.050 \pm 0.003$			

Table 17: Jet fraction using the $k_{\rm t}$ algorithm as a function of the jet resolution parameter $y_{\rm cut}^{\rm D}$ at $\sqrt{s} = 136.1$ GeV. The first uncertainty is statistical, the second systematic.

$y_{\rm cut}^{\rm D}$	2-Jet Fraction	3-Jet Fraction	4-Jet Fraction	5-Jet Fraction
0.001	$0.252 \pm 0.030 \pm 0.008$	$0.382 \pm 0.033 \pm 0.001$	$0.253 \pm 0.026 \pm 0.006$	$0.107 \pm 0.017 \pm 0.002$
0.002	$0.343 \pm 0.034 \pm 0.012$	$0.470 \pm 0.035 \pm 0.010$	$0.160 \pm 0.022 \pm 0.006$	$0.027 \pm 0.010 \pm 0.004$
0.004	$0.491 \pm 0.039 \pm 0.013$	$0.403 \pm 0.033 \pm 0.010$	$0.106 \pm 0.019 \pm 0.004$	
0.006	$0.577 \pm 0.042 \pm 0.013$	$0.370 \pm 0.031 \pm 0.014$	$0.052 \pm 0.014 \pm 0.006$	
0.008	$0.619 \pm 0.044 \pm 0.014$	$0.349 \pm 0.030 \pm 0.014$	$0.032 \pm 0.012 \pm 0.002$	
0.010	$0.656 \pm 0.045 \pm 0.013$	$0.323 \pm 0.029 \pm 0.015$	$0.021 \pm 0.011 \pm 0.003$	
0.020	$0.763 \pm 0.048 \pm 0.004$	$0.228 \pm 0.024 \pm 0.005$	$0.009 \pm 0.008 \pm 0.003$	
0.040	$0.866 \pm 0.051 \pm 0.005$	$0.130 \pm 0.018 \pm 0.005$	$0.004 \pm 0.005 \pm 0.001$	
0.060	$0.908 \pm 0.052 \pm 0.007$	$0.092 \pm 0.015 \pm 0.007$		
0.080	$0.932 \pm 0.053 \pm 0.005$	$0.068 \pm 0.013 \pm 0.005$		
0.100	$0.947 \pm 0.054 \pm 0.003$	$0.053 \pm 0.011 \pm 0.003$		
0.120	$0.967 \pm 0.054 \pm 0.004$	$0.033 \pm 0.009 \pm 0.004$		
0.140	$0.984 \pm 0.054 \pm 0.002$	$0.016 \pm 0.006 \pm 0.002$		
0.160	$0.988 \pm 0.054 \pm 0.001$	$0.012 \pm 0.005 \pm 0.001$		
0.180	$0.991 \pm 0.054 \pm 0.001$	$0.009 \pm 0.004 \pm 0.001$		
0.200	$0.991 \pm 0.055 \pm 0.001$	$0.009 \pm 0.004 \pm 0.001$		
0.220	$0.991 \pm 0.055 \pm 0.001$	$0.009 \pm 0.004 \pm 0.001$		
0.240	$0.991 \pm 0.055 \pm 0.001$	$0.009 \pm 0.004 \pm 0.001$		
0.260	$0.991 \pm 0.055 \pm 0.001$	$0.009 \pm 0.004 \pm 0.001$		
0.280	$0.991 \pm 0.054 \pm 0.001$	$0.009 \pm 0.004 \pm 0.001$		

Table 18: Jet fraction using the $k_{\rm t}$ algorithm as a function of the jet resolution parameter $y_{\rm cut}^{\rm D}$ at $\sqrt{s} = 161.3$ GeV. The first uncertainty is statistical, the second systematic.

$y_{\rm cut}^{\rm D}$	2-Jet Fraction	3-Jet Fraction	4-Jet Fraction	5-Jet Fraction
0.001	$0.252 \pm 0.033 \pm 0.009$	$0.363 \pm 0.036 \pm 0.013$	$0.255 \pm 0.030 \pm 0.014$	$0.095 \pm 0.021 \pm 0.005$
0.002	$0.365 \pm 0.038 \pm 0.005$	$0.361 \pm 0.035 \pm 0.010$	$0.193 \pm 0.028 \pm 0.007$	$0.036 \pm 0.017 \pm 0.007$
0.004	$0.458 \pm 0.041 \pm 0.010$	$0.335 \pm 0.033 \pm 0.013$	$0.135 \pm 0.027 \pm 0.007$	$0.011 \pm 0.014 \pm 0.004$
0.006	$0.454 \pm 0.038 \pm 0.016$	$0.273 \pm 0.028 \pm 0.029$	$0.047 \pm 0.018 \pm 0.014$	$0.014 \pm 0.014 \pm 0.005$
0.008	$0.619 \pm 0.048 \pm 0.021$	$0.293 \pm 0.032 \pm 0.005$	$0.033 \pm 0.020 \pm 0.010$	$0.048 \pm 0.025 \pm 0.014$
0.010	$0.657 \pm 0.049 \pm 0.019$	$0.252 \pm 0.030 \pm 0.004$	$0.032 \pm 0.021 \pm 0.006$	$0.052 \pm 0.025 \pm 0.014$
0.020	$0.707 \pm 0.050 \pm 0.025$	$0.185 \pm 0.026 \pm 0.006$	$0.093 \pm 0.042 \pm 0.021$	$0.015 \pm 0.009 \pm 0.007$
0.040	$0.793 \pm 0.054 \pm 0.027$	$0.140 \pm 0.023 \pm 0.004$	$0.067 \pm 0.044 \pm 0.024$	
0.060	$0.913 \pm 0.060 \pm 0.006$	$0.087 \pm 0.019 \pm 0.006$		
0.080	$0.951 \pm 0.061 \pm 0.004$	$0.049 \pm 0.014 \pm 0.004$		
0.100	$0.972 \pm 0.062 \pm 0.006$	$0.028 \pm 0.011 \pm 0.006$		
0.120	$0.978 \pm 0.062 \pm 0.002$	$0.022 \pm 0.009 \pm 0.003$		
0.140	$0.980 \pm 0.062 \pm 0.004$	$0.020 \pm 0.007 \pm 0.003$		
0.160	$0.982 \pm 0.062 \pm 0.004$	$0.018 \pm 0.006 \pm 0.003$		
0.180	$0.985 \pm 0.062 \pm 0.005$	$0.015 \pm 0.006 \pm 0.004$		
0.200	$0.987 \pm 0.062 \pm 0.005$	$0.013 \pm 0.007 \pm 0.004$		
0.220	$0.993 \pm 0.062 \pm 0.002$	$0.007 \pm 0.005 \pm 0.002$		
0.240	$0.994 \pm 0.062 \pm 0.002$	$0.006 \pm 0.004 \pm 0.002$		
0.260	$0.994 \pm 0.062 \pm 0.002$	$0.006 \pm 0.005 \pm 0.002$		
0.280	$0.994 \pm 0.062 \pm 0.002$	$0.006 \pm 0.006 \pm 0.002$		

Table 19: Jet fraction using the $k_{\rm t}$ algorithm as a function of the jet resolution parameter $y_{\rm cut}^{\rm D}$ at $\sqrt{s} = 172.3$ GeV. The first uncertainty is statistical, the second systematic.

$y_{\rm cut}^{\rm D}$	2-Jet Fraction	3-Jet Fraction	4-Jet Fraction	5-Jet Fraction
0.001	$0.265 \pm 0.014 \pm 0.005$	$0.385 \pm 0.017 \pm 0.003$	$0.241 \pm 0.015 \pm 0.008$	$0.082 \pm 0.011 \pm 0.003$
0.002	$0.392 \pm 0.017 \pm 0.007$	$0.396 \pm 0.017 \pm 0.004$	$0.159 \pm 0.014 \pm 0.011$	$0.040 \pm 0.010 \pm 0.004$
0.004	$0.524 \pm 0.020 \pm 0.009$	$0.347 \pm 0.016 \pm 0.003$	$0.112 \pm 0.013 \pm 0.009$	$0.014 \pm 0.009 \pm 0.002$
0.006	$0.594 \pm 0.021 \pm 0.007$	$0.320 \pm 0.016 \pm 0.003$	$0.080 \pm 0.013 \pm 0.007$	$0.001 \pm 0.007 \pm 0.001$
0.008	$0.640 \pm 0.022 \pm 0.006$	$0.287 \pm 0.015 \pm 0.004$	$0.071 \pm 0.013 \pm 0.003$	$0.002 \pm 0.007 \pm 0.002$
0.010	$0.668 \pm 0.023 \pm 0.003$	$0.271 \pm 0.015 \pm 0.004$	$0.061 \pm 0.013 \pm 0.005$	
0.020	$0.785 \pm 0.025 \pm 0.004$	$0.201 \pm 0.013 \pm 0.002$	$0.014 \pm 0.010 \pm 0.004$	$0.001 \pm 0.003 \pm 0.001$
0.040	$0.876 \pm 0.026 \pm 0.003$	$0.123 \pm 0.011 \pm 0.001$	$0.000 \pm 0.007 \pm 0.000$	
0.060	$0.915 \pm 0.027 \pm 0.002$	$0.085 \pm 0.009 \pm 0.002$		
0.080	$0.943 \pm 0.028 \pm 0.003$	$0.057 \pm 0.007 \pm 0.003$		
0.100	$0.957 \pm 0.028 \pm 0.002$	$0.043 \pm 0.006 \pm 0.002$		
0.120	$0.969 \pm 0.028 \pm 0.002$	$0.031 \pm 0.005 \pm 0.002$		
0.140	$0.980 \pm 0.028 \pm 0.002$	$0.020 \pm 0.004 \pm 0.002$		
0.160	$0.980 \pm 0.028 \pm 0.002$	$0.020 \pm 0.004 \pm 0.002$		
0.180	$0.984 \pm 0.028 \pm 0.002$	$0.016 \pm 0.004 \pm 0.002$		
0.200	$0.987 \pm 0.029 \pm 0.001$	$0.013 \pm 0.004 \pm 0.001$		
0.220	$0.991 \pm 0.029 \pm 0.002$	$0.009 \pm 0.003 \pm 0.002$		
0.240	$0.998 \pm 0.029 \pm 0.001$	$0.002 \pm 0.002 \pm 0.001$		
0.260	$0.998 \pm 0.029 \pm 0.001$	$0.002 \pm 0.002 \pm 0.001$		
0.280	$1.000 \pm 0.029 \pm 0.001$			

Table 20: Jet fraction using the $k_{\rm t}$ algorithm as a function of the jet resolution parameter $y_{\rm cut}^{\rm D}$ at $\sqrt{s} = 182.8$ GeV. The first uncertainty is statistical, the second systematic.

$y_{\rm cut}^{\rm D}$	2-Jet Fraction	3-Jet Fraction	4-Jet Fraction	5-Jet Fraction
0.001	$0.267 \pm 0.009 \pm 0.005$	$0.386 \pm 0.010 \pm 0.003$	$0.231 \pm 0.009 \pm 0.007$	$0.095 \pm 0.007 \pm 0.005$
0.002	$0.395 \pm 0.011 \pm 0.007$	$0.399 \pm 0.010 \pm 0.005$	$0.161 \pm 0.008 \pm 0.006$	$0.043 \pm 0.007 \pm 0.004$
0.004	$0.520 \pm 0.013 \pm 0.009$	$0.373 \pm 0.010 \pm 0.007$	$0.099 \pm 0.008 \pm 0.005$	$0.007 \pm 0.005 \pm 0.003$
0.006	$0.582 \pm 0.013 \pm 0.010$	$0.346 \pm 0.010 \pm 0.007$	$0.068 \pm 0.007 \pm 0.006$	
0.008	$0.634 \pm 0.014 \pm 0.010$	$0.325 \pm 0.010 \pm 0.006$	$0.040 \pm 0.007 \pm 0.005$	$0.001 \pm 0.004 \pm 0.002$
0.010	$0.670 \pm 0.014 \pm 0.008$	$0.298 \pm 0.009 \pm 0.005$	$0.031 \pm 0.006 \pm 0.004$	
0.020	$0.786 \pm 0.015 \pm 0.009$	$0.206 \pm 0.008 \pm 0.008$	$0.007 \pm 0.006 \pm 0.005$	
0.040	$0.867 \pm 0.016 \pm 0.005$	$0.133 \pm 0.007 \pm 0.005$		
0.060	$0.907 \pm 0.017 \pm 0.004$	$0.093 \pm 0.006 \pm 0.004$		
0.080	$0.935 \pm 0.017 \pm 0.004$	$0.065 \pm 0.005 \pm 0.003$		
0.100	$0.951 \pm 0.017 \pm 0.004$	$0.049 \pm 0.004 \pm 0.004$		
0.120	$0.965 \pm 0.017 \pm 0.003$	$0.035 \pm 0.004 \pm 0.003$		
0.140	$0.974 \pm 0.017 \pm 0.004$	$0.026 \pm 0.003 \pm 0.004$		
0.160	$0.982 \pm 0.018 \pm 0.003$	$0.019 \pm 0.003 \pm 0.003$		
0.180	$0.986 \pm 0.018 \pm 0.002$	$0.014 \pm 0.003 \pm 0.002$		
0.200	$0.989 \pm 0.018 \pm 0.002$	$0.011 \pm 0.002 \pm 0.002$		
0.220	$0.992 \pm 0.018 \pm 0.001$	$0.008 \pm 0.002 \pm 0.001$		
0.240	$0.996 \pm 0.018 \pm 0.002$	$0.004 \pm 0.002 \pm 0.001$		
0.260	$0.997 \pm 0.018 \pm 0.001$	$0.002 \pm 0.002 \pm 0.001$		
0.280	$0.998 \pm 0.018 \pm 0.001$	$0.001 \pm 0.001 \pm 0.001$		

Table 21: Jet fraction using the $k_{\rm t}$ algorithm as a function of the jet resolution parameter $y_{\rm cut}^{\rm D}$ at $\sqrt{s} = 188.6$ GeV. The first uncertainty is statistical, the second systematic.

$y_{\rm cut}^{\rm D}$	2-Jet Fraction	3-Jet Fraction	4-Jet Fraction	5-Jet Fraction
0.001	$0.259 \pm 0.011 \pm 0.011$	$0.397 \pm 0.013 \pm 0.007$	$0.228 \pm 0.012 \pm 0.017$	$0.080 \pm 0.011 \pm 0.010$
0.002	$0.389 \pm 0.013 \pm 0.013$	$0.416 \pm 0.014 \pm 0.009$	$0.161 \pm 0.014 \pm 0.016$	$0.028 \pm 0.011 \pm 0.005$
0.004	$0.511 \pm 0.015 \pm 0.015$	$0.404 \pm 0.014 \pm 0.011$	$0.079 \pm 0.015 \pm 0.021$	$0.002 \pm 0.006 \pm 0.005$
0.006	$0.581 \pm 0.017 \pm 0.014$	$0.368 \pm 0.014 \pm 0.009$	$0.051 \pm 0.016 \pm 0.011$	
0.008	$0.630 \pm 0.017 \pm 0.010$	$0.326 \pm 0.014 \pm 0.012$	$0.045 \pm 0.017 \pm 0.018$	
0.010	$0.679 \pm 0.018 \pm 0.013$	$0.303 \pm 0.014 \pm 0.006$	$0.018 \pm 0.016 \pm 0.013$	
0.020	$0.766 \pm 0.019 \pm 0.013$	$0.215 \pm 0.012 \pm 0.011$	$0.019 \pm 0.018 \pm 0.018$	
0.040	$0.872 \pm 0.021 \pm 0.013$	$0.128 \pm 0.010 \pm 0.011$		
0.060	$0.907 \pm 0.022 \pm 0.013$	$0.093 \pm 0.008 \pm 0.013$		
0.080	$0.935 \pm 0.022 \pm 0.012$	$0.065 \pm 0.007 \pm 0.012$		
0.100	$0.950 \pm 0.022 \pm 0.012$	$0.050 \pm 0.006 \pm 0.012$		
0.120	$0.960 \pm 0.022 \pm 0.009$	$0.040 \pm 0.005 \pm 0.009$		
0.140	$0.968 \pm 0.023 \pm 0.008$	$0.032 \pm 0.005 \pm 0.008$		
0.160	$0.978 \pm 0.023 \pm 0.007$	$0.022 \pm 0.004 \pm 0.006$		
0.180	$0.984 \pm 0.023 \pm 0.005$	$0.016 \pm 0.004 \pm 0.005$		
0.200	$0.988 \pm 0.023 \pm 0.005$	$0.012 \pm 0.004 \pm 0.003$		
0.220	$0.996 \pm 0.023 \pm 0.004$	$0.004 \pm 0.003 \pm 0.001$		
0.240	$0.996 \pm 0.023 \pm 0.002$	$0.004 \pm 0.002 \pm 0.001$		
0.260	$0.998 \pm 0.023 \pm 0.003$	$0.002 \pm 0.002 \pm 0.001$		
0.280	$0.999 \pm 0.023 \pm 0.002$	$0.001 \pm 0.001 \pm 0.001$		

Table 22: Jet fraction using the $k_{\rm t}$ algorithm as a function of the jet resolution parameter $y_{\rm cut}^{\rm D}$ at $\sqrt{s} = 194.4$ GeV. The first uncertainty is statistical, the second systematic.

$y_{\rm cut}^{\rm D}$	2-Jet Fraction	3-Jet Fraction	4-Jet Fraction	5-Jet Fraction
0.001	$0.267 \pm 0.011 \pm 0.007$	$0.369 \pm 0.013 \pm 0.009$	$0.245 \pm 0.013 \pm 0.008$	$0.104 \pm 0.011 \pm 0.004$
0.002	$0.372 \pm 0.013 \pm 0.010$	$0.398 \pm 0.014 \pm 0.011$	$0.179 \pm 0.013 \pm 0.010$	$0.048 \pm 0.010 \pm 0.007$
0.004	$0.492 \pm 0.015 \pm 0.013$	$0.396 \pm 0.014 \pm 0.007$	$0.104 \pm 0.013 \pm 0.007$	$0.006 \pm 0.008 \pm 0.007$
0.006	$0.573 \pm 0.016 \pm 0.015$	$0.368 \pm 0.014 \pm 0.006$	$0.054 \pm 0.012 \pm 0.011$	$0.005 \pm 0.007 \pm 0.004$
0.008	$0.619 \pm 0.017 \pm 0.015$	$0.340 \pm 0.014 \pm 0.008$	$0.041 \pm 0.012 \pm 0.009$	
0.010	$0.661 \pm 0.018 \pm 0.016$	$0.313 \pm 0.014 \pm 0.011$	$0.026 \pm 0.012 \pm 0.011$	
0.020	$0.764 \pm 0.019 \pm 0.013$	$0.226 \pm 0.012 \pm 0.010$	$0.010 \pm 0.014 \pm 0.006$	
0.040	$0.852 \pm 0.021 \pm 0.014$	$0.144 \pm 0.010 \pm 0.010$	$0.004 \pm 0.005 \pm 0.003$	
0.060	$0.893 \pm 0.021 \pm 0.010$	$0.106 \pm 0.009 \pm 0.009$	$0.001 \pm 0.001 \pm 0.001$	
0.080	$0.926 \pm 0.022 \pm 0.009$	$0.074 \pm 0.008 \pm 0.009$		
0.100	$0.944 \pm 0.022 \pm 0.008$	$0.056 \pm 0.007 \pm 0.008$		
0.120	$0.963 \pm 0.022 \pm 0.005$	$0.037 \pm 0.006 \pm 0.005$		
0.140	$0.967 \pm 0.023 \pm 0.004$	$0.033 \pm 0.005 \pm 0.003$		
0.160	$0.977 \pm 0.023 \pm 0.005$	$0.023 \pm 0.005 \pm 0.005$		
0.180	$0.982 \pm 0.023 \pm 0.003$	$0.018 \pm 0.005 \pm 0.003$		
0.200	$0.990 \pm 0.023 \pm 0.002$	$0.010 \pm 0.004 \pm 0.002$		
0.220	$0.992 \pm 0.023 \pm 0.003$	$0.008 \pm 0.004 \pm 0.002$		
0.240	$0.996 \pm 0.023 \pm 0.002$	$0.004 \pm 0.003 \pm 0.002$		
0.260	$0.997 \pm 0.023 \pm 0.001$	$0.003 \pm 0.002 \pm 0.001$		
0.280	$0.997 \pm 0.023 \pm 0.002$	$0.003 \pm 0.002 \pm 0.001$		

Table 23: Jet fraction using the $k_{\rm t}$ algorithm as a function of the jet resolution parameter $y_{\rm cut}^{\rm D}$ at $\sqrt{s} = 200.2$ GeV. The first uncertainty is statistical, the second systematic.

$y_{\rm cut}^{\rm D}$	2-Jet Fraction	3-Jet Fraction	4-Jet Fraction	5-Jet Fraction
0.001	$0.251 \pm 0.008 \pm 0.005$	$0.394 \pm 0.010 \pm 0.005$	$0.237 \pm 0.010 \pm 0.011$	$0.093 \pm 0.008 \pm 0.004$
0.002	$0.379 \pm 0.010 \pm 0.008$	$0.412 \pm 0.011 \pm 0.006$	$0.169 \pm 0.010 \pm 0.009$	$0.034 \pm 0.008 \pm 0.004$
0.004	$0.509 \pm 0.012 \pm 0.011$	$0.390 \pm 0.011 \pm 0.007$	$0.090 \pm 0.010 \pm 0.013$	$0.011 \pm 0.007 \pm 0.002$
0.006	$0.583 \pm 0.013 \pm 0.013$	$0.367 \pm 0.011 \pm 0.006$	$0.048 \pm 0.009 \pm 0.014$	$0.002 \pm 0.005 \pm 0.002$
0.008	$0.627 \pm 0.014 \pm 0.013$	$0.343 \pm 0.011 \pm 0.008$	$0.030 \pm 0.009 \pm 0.013$	
0.010	$0.666 \pm 0.014 \pm 0.012$	$0.316 \pm 0.011 \pm 0.009$	$0.018 \pm 0.009 \pm 0.010$	
0.020	$0.765 \pm 0.015 \pm 0.009$	$0.234 \pm 0.010 \pm 0.004$	$0.001 \pm 0.009 \pm 0.001$	
0.040	$0.855 \pm 0.016 \pm 0.007$	$0.144 \pm 0.008 \pm 0.003$	$0.001 \pm 0.013 \pm 0.001$	
0.060	$0.900 \pm 0.017 \pm 0.007$	$0.100 \pm 0.007 \pm 0.007$		
0.080	$0.926 \pm 0.017 \pm 0.006$	$0.074 \pm 0.006 \pm 0.006$		
0.100	$0.942 \pm 0.017 \pm 0.005$	$0.058 \pm 0.006 \pm 0.005$		
0.120	$0.955 \pm 0.017 \pm 0.003$	$0.045 \pm 0.005 \pm 0.003$		
0.140	$0.966 \pm 0.018 \pm 0.004$	$0.034 \pm 0.005 \pm 0.004$		
0.160	$0.974 \pm 0.018 \pm 0.003$	$0.026 \pm 0.004 \pm 0.003$		
0.180	$0.981 \pm 0.018 \pm 0.004$	$0.019 \pm 0.004 \pm 0.004$		
0.200	$0.983 \pm 0.018 \pm 0.003$	$0.016 \pm 0.004 \pm 0.003$		
0.220	$0.991 \pm 0.018 \pm 0.001$	$0.008 \pm 0.003 \pm 0.002$		
0.240	$0.995 \pm 0.018 \pm 0.002$	$0.005 \pm 0.002 \pm 0.001$		
0.260	$0.996 \pm 0.018 \pm 0.003$	$0.004 \pm 0.003 \pm 0.001$		
0.280	$0.997 \pm 0.018 \pm 0.003$	$0.002 \pm 0.002 \pm 0.001$		

Table 24: Jet fraction using the $k_{\rm t}$ algorithm as a function of the jet resolution parameter $y_{\rm cut}^{\rm D}$ at $\sqrt{s} = 206.2$ GeV. The first uncertainty is statistical, the second systematic.

$y_{\rm cut}^{\rm D}$	2-Jet Fraction	3-Jet Fraction	4-Jet Fraction	5-Jet Fraction
0.001	$0.336 \pm 0.013 \pm 0.008$	$0.380 \pm 0.013 \pm 0.007$	$0.214 \pm 0.013 \pm 0.010$	$0.064 \pm 0.010 \pm 0.004$
0.002	$0.435 \pm 0.014 \pm 0.010$	$0.379 \pm 0.014 \pm 0.011$	$0.157 \pm 0.013 \pm 0.013$	$0.024 \pm 0.009 \pm 0.006$
0.004	$0.538 \pm 0.016 \pm 0.013$	$0.367 \pm 0.014 \pm 0.011$	$0.088 \pm 0.012 \pm 0.010$	$0.005 \pm 0.008 \pm 0.004$
0.006	$0.605 \pm 0.017 \pm 0.015$	$0.339 \pm 0.014 \pm 0.008$	$0.050 \pm 0.011 \pm 0.010$	$0.006 \pm 0.007 \pm 0.005$
0.008	$0.647 \pm 0.018 \pm 0.014$	$0.317 \pm 0.014 \pm 0.008$	$0.035 \pm 0.011 \pm 0.007$	
0.010	$0.680 \pm 0.018 \pm 0.015$	$0.294 \pm 0.013 \pm 0.011$	$0.026 \pm 0.011 \pm 0.010$	
0.020	$0.781 \pm 0.020 \pm 0.013$	$0.212 \pm 0.012 \pm 0.009$	$0.005 \pm 0.007 \pm 0.004$	$0.001 \pm 0.002 \pm 0.001$
0.040	$0.862 \pm 0.021 \pm 0.012$	$0.137 \pm 0.010 \pm 0.010$	$0.002 \pm 0.004 \pm 0.001$	
0.060	$0.900 \pm 0.022 \pm 0.010$	$0.100 \pm 0.009 \pm 0.009$	$0.001 \pm 0.001 \pm 0.001$	
0.080	$0.929 \pm 0.022 \pm 0.008$	$0.071 \pm 0.007 \pm 0.008$		
0.100	$0.945 \pm 0.022 \pm 0.007$	$0.055 \pm 0.007 \pm 0.007$		
0.120	$0.963 \pm 0.022 \pm 0.006$	$0.037 \pm 0.006 \pm 0.006$		
0.140	$0.967 \pm 0.023 \pm 0.005$	$0.033 \pm 0.005 \pm 0.004$		
0.160	$0.977 \pm 0.023 \pm 0.005$	$0.023 \pm 0.005 \pm 0.004$		
0.180	$0.979 \pm 0.023 \pm 0.004$	$0.021 \pm 0.005 \pm 0.004$		
0.200	$0.988 \pm 0.023 \pm 0.003$	$0.012 \pm 0.004 \pm 0.003$		
0.220	$0.991 \pm 0.023 \pm 0.002$	$0.009 \pm 0.004 \pm 0.002$		
0.240	$0.993 \pm 0.023 \pm 0.002$	$0.007 \pm 0.003 \pm 0.002$		
0.260	$0.994 \pm 0.023 \pm 0.002$	$0.006 \pm 0.003 \pm 0.002$		
0.280	$0.995 \pm 0.023 \pm 0.002$	$0.005 \pm 0.003 \pm 0.002$		

Table 25: Jet fraction using the Cambridge algorithm as a function of the jet resolution parameter $y_{\rm cut}^{\rm D}$ at $\sqrt{s} = 200.2$ GeV. The first uncertainty is statistical, the second systematic.

$y_{\rm cut}^{\rm D}$	2-Jet Fraction	3-Jet Fraction	4-Jet Fraction	5-Jet Fraction
0.001	$0.339 \pm 0.010 \pm 0.007$	$0.401 \pm 0.011 \pm 0.008$	$0.183 \pm 0.009 \pm 0.012$	$0.073 \pm 0.008 \pm 0.007$
0.002	$0.434 \pm 0.011 \pm 0.009$	$0.408 \pm 0.011 \pm 0.007$	$0.132 \pm 0.009 \pm 0.011$	$0.024 \pm 0.007 \pm 0.003$
0.004	$0.551 \pm 0.013 \pm 0.011$	$0.374 \pm 0.011 \pm 0.006$	$0.070 \pm 0.009 \pm 0.011$	$0.005 \pm 0.006 \pm 0.003$
0.006	$0.608 \pm 0.013 \pm 0.012$	$0.344 \pm 0.011 \pm 0.007$	$0.045 \pm 0.009 \pm 0.013$	$0.002 \pm 0.005 \pm 0.002$
0.008	$0.651 \pm 0.014 \pm 0.012$	$0.320 \pm 0.011 \pm 0.006$	$0.029 \pm 0.009 \pm 0.012$	
0.010	$0.688 \pm 0.014 \pm 0.012$	$0.292 \pm 0.010 \pm 0.006$	$0.020 \pm 0.009 \pm 0.010$	
0.020	$0.779 \pm 0.015 \pm 0.008$	$0.213 \pm 0.009 \pm 0.004$	$0.008 \pm 0.009 \pm 0.006$	
0.040	$0.861 \pm 0.016 \pm 0.007$	$0.133 \pm 0.008 \pm 0.003$	$0.006 \pm 0.014 \pm 0.006$	
0.060	$0.906 \pm 0.017 \pm 0.006$	$0.094 \pm 0.007 \pm 0.006$		
0.080	$0.930 \pm 0.017 \pm 0.005$	$0.070 \pm 0.006 \pm 0.005$		
0.100	$0.945 \pm 0.017 \pm 0.004$	$0.055 \pm 0.005 \pm 0.005$		
0.120	$0.957 \pm 0.018 \pm 0.003$	$0.043 \pm 0.005 \pm 0.003$		
0.140	$0.966 \pm 0.018 \pm 0.003$	$0.034 \pm 0.005 \pm 0.003$		
0.160	$0.972 \pm 0.018 \pm 0.002$	$0.028 \pm 0.004 \pm 0.003$		
0.180	$0.980 \pm 0.018 \pm 0.003$	$0.020 \pm 0.004 \pm 0.003$		
0.200	$0.982 \pm 0.018 \pm 0.002$	$0.017 \pm 0.004 \pm 0.002$		
0.220	$0.989 \pm 0.018 \pm 0.002$	$0.011 \pm 0.003 \pm 0.002$		
0.240	$0.993 \pm 0.018 \pm 0.001$	$0.007 \pm 0.002 \pm 0.002$		
0.260	$0.993 \pm 0.018 \pm 0.002$	$0.007 \pm 0.003 \pm 0.001$		
0.280	$0.998 \pm 0.018 \pm 0.003$	$0.002 \pm 0.001 \pm 0.001$		

Table 26: Jet fraction using the Cambridge algorithm as a function of the jet resolution parameter $y_{\rm cut}^{\rm D}$ at $\sqrt{s} = 206.2$ GeV. The first uncertainty is statistical, the second systematic.

	$\frac{1}{\sigma} \cdot \frac{\mathrm{d}\sigma}{\mathrm{d}(1-T)}$		
$1-T$	at $\sqrt{s} = 41.4$ GeV	at $\sqrt{s} = 55.3$ GeV	at $\sqrt{s} = 65.4$ GeV
0.000–0.025	$1.636 \pm 0.322 \pm 0.591$	$3.604 \pm 0.491 \pm 1.252$	$4.737 \pm 0.392 \pm 1.292$
0.025–0.045	$9.120 \pm 0.914 \pm 1.122$	$14.245 \pm 1.066 \pm 2.225$	$12.412 \pm 0.716 \pm 1.566$
0.045–0.065	$9.768 \pm 1.084 \pm 1.612$	$8.897 \pm 0.789 \pm 0.920$	$9.618 \pm 0.606 \pm 1.444$
0.065–0.085	$7.872 \pm 0.919 \pm 1.014$	$6.593 \pm 0.714 \pm 1.244$	$7.229 \pm 0.600 \pm 0.534$
0.085–0.115	$4.156 \pm 0.478 \pm 0.272$	$2.989 \pm 0.439 \pm 0.588$	$3.604 \pm 0.317 \pm 0.768$
0.115–0.145	$3.547 \pm 0.452 \pm 0.699$	$2.237 \pm 0.310 \pm 1.434$	$1.722 \pm 0.217 \pm 0.507$
0.145–0.175	$2.240 \pm 0.393 \pm 0.376$	$2.229 \pm 0.371 \pm 0.539$	$1.172 \pm 0.180 \pm 0.240$
0.175–0.210	$1.244 \pm 0.292 \pm 0.329$	$1.112 \pm 0.254 \pm 0.231$	$0.902 \pm 0.161 \pm 0.222$
0.210–0.250	$0.882 \pm 0.189 \pm 0.182$	$0.531 \pm 0.166 \pm 0.160$	$0.809 \pm 0.149 \pm 0.144$
0.250–0.290	$0.598 \pm 0.185 \pm 0.133$	$0.420 \pm 0.146 \pm 0.121$	$0.417 \pm 0.087 \pm 0.207$
0.290–0.330	$0.283 \pm 0.137 \pm 0.147$	$0.140 \pm 0.084 \pm 0.072$	$0.269 \pm 0.089 \pm 0.057$
0.330–0.370	$0.218 \pm 0.065 \pm 0.086$	$0.168 \pm 0.073 \pm 0.064$	$0.253 \pm 0.080 \pm 0.089$
0.370–0.420	$0.056 \pm 0.032 \pm 0.055$	$0.046 \pm 0.033 \pm 0.023$	$0.000 \pm 0.000 \pm 0.000$
First Moment	$0.0971 \pm 0.0030 \pm 0.0034$	$0.0811 \pm 0.0027 \pm 0.0029$	$0.0796 \pm 0.0021 \pm 0.0051$
Second Moment	$0.0143 \pm 0.0009 \pm 0.0015$	$0.0109 \pm 0.0008 \pm 0.0006$	$0.0109 \pm 0.0006 \pm 0.0010$

Table 27: Differential distribution for event thrust at $\sqrt{s} = 41.4$, 55.3 and 65.4 GeV. The first uncertainty is statistical, the second systematic.

	$\frac{1}{\sigma} \cdot \frac{\mathrm{d}\sigma}{\mathrm{d}(1-T)}$		
$1-T$	at $\sqrt{s} = 75.7$ GeV	at $\sqrt{s} = 82.3$ GeV	at $\sqrt{s} = 85.1$ GeV
0.000–0.025	$5.754 \pm 0.287 \pm 1.262$	$6.277 \pm 0.364 \pm 1.402$	$7.602 \pm 0.480 \pm 1.411$
0.025–0.045	$15.307 \pm 0.564 \pm 1.003$	$15.551 \pm 0.655 \pm 0.472$	$15.215 \pm 0.753 \pm 0.801$
0.045–0.065	$7.994 \pm 0.406 \pm 1.077$	$8.884 \pm 0.509 \pm 0.346$	$8.031 \pm 0.619 \pm 0.908$
0.065–0.085	$5.056 \pm 0.338 \pm 0.325$	$4.322 \pm 0.384 \pm 1.376$	$3.804 \pm 0.427 \pm 0.533$
0.085–0.115	$3.569 \pm 0.239 \pm 0.418$	$3.408 \pm 0.286 \pm 0.117$	$3.078 \pm 0.342 \pm 0.267$
0.115–0.145	$1.932 \pm 0.183 \pm 0.269$	$1.485 \pm 0.203 \pm 0.346$	$1.641 \pm 0.260 \pm 1.148$
0.145–0.175	$1.462 \pm 0.157 \pm 0.162$	$1.460 \pm 0.169 \pm 0.314$	$1.563 \pm 0.237 \pm 0.398$
0.175–0.210	$0.944 \pm 0.121 \pm 0.173$	$0.894 \pm 0.143 \pm 0.210$	$1.116 \pm 0.190 \pm 0.319$
0.210–0.250	$0.491 \pm 0.082 \pm 0.120$	$0.617 \pm 0.140 \pm 0.126$	$0.502 \pm 0.159 \pm 0.147$
0.250–0.290	$0.397 \pm 0.084 \pm 0.094$	$0.354 \pm 0.110 \pm 0.113$	$0.296 \pm 0.114 \pm 0.042$
0.290–0.330	$0.186 \pm 0.058 \pm 0.036$	$0.104 \pm 0.055 \pm 0.033$	$0.191 \pm 0.073 \pm 0.080$
0.330–0.370	$0.092 \pm 0.039 \pm 0.027$	$0.078 \pm 0.033 \pm 0.025$	$0.047 \pm 0.034 \pm 0.025$
0.370–0.420	$0.009 \pm 0.009 \pm 0.005$	$0.000 \pm 0.000 \pm 0.000$	$0.000 \pm 0.000 \pm 0.000$
First Moment	$0.0731 \pm 0.0015 \pm 0.0045$	$0.0700 \pm 0.0018 \pm 0.0046$	$0.0691 \pm 0.0022 \pm 0.0088$
Second Moment	$0.0093 \pm 0.0004 \pm 0.0010$	$0.0086 \pm 0.0005 \pm 0.0010$	$0.0086 \pm 0.0006 \pm 0.0020$

Table 28: Differential distribution for event thrust at $\sqrt{s} = 75.7$, 82.3 and 85.1 GeV. The first uncertainty is statistical, the second systematic.

	$\frac{1}{\sigma} \cdot \frac{\mathrm{d}\sigma}{\mathrm{d}(1-T)}$		
$1-T$	at $\sqrt{s} = 130.1$ GeV	at $\sqrt{s} = 136.1$ GeV	at $\sqrt{s} = 161.3$ GeV
0.000–0.025	$14.875 \pm 1.223 \pm 1.053$	$14.171 \pm 1.371 \pm 0.929$	$19.149 \pm 1.709 \pm 0.557$
0.025–0.050	$11.125 \pm 0.900 \pm 0.613$	$11.992 \pm 1.107 \pm 0.920$	$8.102 \pm 0.922 \pm 0.564$
0.050–0.075	$5.057 \pm 0.615 \pm 0.376$	$4.622 \pm 0.688 \pm 0.331$	$3.535 \pm 0.582 \pm 0.253$
0.075–0.100	$2.763 \pm 0.439 \pm 0.144$	$2.174 \pm 0.464 \pm 0.104$	$3.123 \pm 0.543 \pm 0.202$
0.100–0.125	$2.046 \pm 0.352 \pm 0.189$	$2.099 \pm 0.439 \pm 0.144$	$1.626 \pm 0.397 \pm 0.159$
0.125–0.150	$1.552 \pm 0.303 \pm 0.063$	$0.941 \pm 0.310 \pm 0.100$	$1.331 \pm 0.362 \pm 0.087$
0.150–0.175	$0.833 \pm 0.216 \pm 0.082$	$1.327 \pm 0.327 \pm 0.212$	$0.943 \pm 0.305 \pm 0.183$
0.175–0.200	$0.367 \pm 0.136 \pm 0.012$	$1.153 \pm 0.293 \pm 0.088$	$0.635 \pm 0.247 \pm 0.033$
0.200–0.225	$0.461 \pm 0.141 \pm 0.039$	$0.452 \pm 0.188 \pm 0.033$	$0.840 \pm 0.274 \pm 0.077$
0.225–0.250	$0.257 \pm 0.107 \pm 0.052$	$0.274 \pm 0.132 \pm 0.069$	$0.166 \pm 0.141 \pm 0.070$
0.250–0.275	$0.329 \pm 0.127 \pm 0.063$	$0.046 \pm 0.046 \pm 0.001$	$0.195 \pm 0.126 \pm 0.058$
0.275–0.300	$0.125 \pm 0.087 \pm 0.047$	$0.218 \pm 0.105 \pm 0.119$	$0.202 \pm 0.122 \pm 0.010$
0.300–0.325	$0.050 \pm 0.050 \pm 0.001$	$0.179 \pm 0.090 \pm 0.013$	$0.132 \pm 0.100 \pm 0.007$
0.325–0.350	$0.054 \pm 0.054 \pm 0.009$	$0.161 \pm 0.114 \pm 0.178$	$0.023 \pm 0.059 \pm 0.003$
0.350–0.375	$0.034 \pm 0.034 \pm 0.022$	$0.107 \pm 0.075 \pm 0.119$	$0.000 \pm 0.000 \pm 0.000$
0.375–0.400	$0.072 \pm 0.051 \pm 0.057$	$0.085 \pm 0.085 \pm 0.029$	$0.000 \pm 0.000 \pm 0.000$
First Moment	$0.0556 \pm 0.0022 \pm 0.0014$	$0.0614 \pm 0.0030 \pm 0.0012$	$0.0513 \pm 0.0030 \pm 0.0008$
Second Moment	$0.0064 \pm 0.0005 \pm 0.0002$	$0.0080 \pm 0.0008 \pm 0.0007$	$0.0059 \pm 0.0007 \pm 0.0002$

Table 29: Differential distribution for event thrust at $\sqrt{s} = 130.1$, 136.1 and 161.3 GeV. The first uncertainty is statistical, the second systematic.

	$\frac{1}{\sigma} \cdot \frac{\mathrm{d}\sigma}{\mathrm{d}(1-T)}$		
$1-T$	at $\sqrt{s} = 172.3$ GeV	at $\sqrt{s} = 182.8$ GeV	at $\sqrt{s} = 188.6$ GeV
0.000–0.025	$17.499 \pm 1.879 \pm 0.867$	$16.920 \pm 0.740 \pm 1.403$	$16.067 \pm 0.471 \pm 0.436$
0.025–0.050	$8.458 \pm 1.016 \pm 0.874$	$9.107 \pm 0.534 \pm 0.851$	$9.908 \pm 0.330 \pm 0.175$
0.050–0.075	$4.705 \pm 0.774 \pm 0.336$	$5.099 \pm 0.400 \pm 0.494$	$4.641 \pm 0.223 \pm 0.132$
0.075–0.100	$2.454 \pm 0.569 \pm 0.327$	$2.655 \pm 0.295 \pm 0.065$	$2.940 \pm 0.183 \pm 0.079$
0.100–0.125	$2.087 \pm 0.557 \pm 0.192$	$1.896 \pm 0.253 \pm 0.066$	$1.721 \pm 0.141 \pm 0.053$
0.125–0.150	$1.550 \pm 0.490 \pm 0.277$	$1.328 \pm 0.214 \pm 0.196$	$1.494 \pm 0.134 \pm 0.140$
0.150–0.175	$0.957 \pm 0.378 \pm 0.249$	$0.750 \pm 0.173 \pm 0.073$	$0.952 \pm 0.109 \pm 0.038$
0.175–0.200	$0.759 \pm 0.343 \pm 0.137$	$0.598 \pm 0.148 \pm 0.100$	$0.736 \pm 0.094 \pm 0.076$
0.200–0.225	$0.706 \pm 0.308 \pm 0.202$	$0.563 \pm 0.137 \pm 0.020$	$0.511 \pm 0.083 \pm 0.011$
0.225–0.250	$0.213 \pm 0.185 \pm 0.083$	$0.299 \pm 0.109 \pm 0.032$	$0.424 \pm 0.079 \pm 0.037$
0.250–0.275	$0.257 \pm 0.195 \pm 0.200$	$0.247 \pm 0.106 \pm 0.113$	$0.288 \pm 0.076 \pm 0.124$
0.275–0.300	$0.206 \pm 0.173 \pm 0.180$	$0.245 \pm 0.105 \pm 0.083$	$0.194 \pm 0.075 \pm 0.073$
0.300–0.325	$0.045 \pm 0.108 \pm 0.001$	$0.194 \pm 0.116 \pm 0.075$	$0.076 \pm 0.072 \pm 0.057$
0.325–0.350	$0.103 \pm 0.128 \pm 0.067$	$0.100 \pm 0.102 \pm 0.077$	$0.019 \pm 0.049 \pm 0.044$
0.350–0.375	$0.000 \pm 0.000 \pm 0.000$	$0.000 \pm 0.000 \pm 0.000$	$0.020 \pm 0.029 \pm 0.059$
0.375–0.400	$0.000 \pm 0.000 \pm 0.000$	$0.000 \pm 0.000 \pm 0.000$	$0.010 \pm 0.012 \pm 0.006$
First Moment	$0.0542 \pm 0.0037 \pm 0.0022$	$0.0539 \pm 0.0020 \pm 0.0011$	$0.0548 \pm 0.0013 \pm 0.0013$
Second Moment	$0.0064 \pm 0.0009 \pm 0.0005$	$0.0064 \pm 0.0005 \pm 0.0001$	$0.0064 \pm 0.0004 \pm 0.0005$

Table 30: Differential distribution for event thrust at $\sqrt{s} = 172.3$, 182.8 and 188.6 GeV. The first uncertainty is statistical, the second systematic.

	$\frac{1}{\sigma} \cdot \frac{\mathrm{d}\sigma}{\mathrm{d}(1-T)}$		
$1-T$	at $\sqrt{s} = 194.4$ GeV	at $\sqrt{s} = 200.2$ GeV	at $\sqrt{s} = 206.2$ GeV
0.000–0.025	$16.177 \pm 0.571 \pm 0.436$	$16.119 \pm 0.578 \pm 0.444$	$16.202 \pm 0.466 \pm 0.509$
0.025–0.050	$9.285 \pm 0.416 \pm 0.248$	$9.277 \pm 0.420 \pm 0.270$	$9.321 \pm 0.326 \pm 0.297$
0.050–0.075	$5.302 \pm 0.340 \pm 0.261$	$4.534 \pm 0.305 \pm 0.175$	$4.637 \pm 0.240 \pm 0.169$
0.075–0.100	$2.823 \pm 0.253 \pm 0.175$	$2.947 \pm 0.280 \pm 0.200$	$3.013 \pm 0.198 \pm 0.106$
0.100–0.125	$1.837 \pm 0.224 \pm 0.152$	$1.904 \pm 0.204 \pm 0.129$	$1.707 \pm 0.155 \pm 0.101$
0.125–0.150	$1.229 \pm 0.188 \pm 0.159$	$1.636 \pm 0.195 \pm 0.263$	$1.553 \pm 0.151 \pm 0.085$
0.150–0.175	$0.902 \pm 0.161 \pm 0.049$	$1.041 \pm 0.159 \pm 0.174$	$1.031 \pm 0.122 \pm 0.073$
0.175–0.200	$0.732 \pm 0.134 \pm 0.213$	$0.693 \pm 0.139 \pm 0.111$	$0.624 \pm 0.106 \pm 0.055$
0.200–0.225	$0.569 \pm 0.125 \pm 0.101$	$0.497 \pm 0.127 \pm 0.095$	$0.686 \pm 0.118 \pm 0.117$
0.225–0.250	$0.454 \pm 0.119 \pm 0.163$	$0.659 \pm 0.152 \pm 0.032$	$0.466 \pm 0.125 \pm 0.043$
0.250–0.275	$0.366 \pm 0.128 \pm 0.105$	$0.242 \pm 0.136 \pm 0.152$	$0.208 \pm 0.128 \pm 0.012$
0.275–0.300	$0.130 \pm 0.103 \pm 0.091$	$0.328 \pm 0.168 \pm 0.099$	$0.193 \pm 0.129 \pm 0.100$
0.300–0.325	$0.096 \pm 0.119 \pm 0.023$	$0.000 \pm 0.000 \pm 0.000$	$0.357 \pm 0.122 \pm 0.120$
0.325–0.350	$0.081 \pm 0.058 \pm 0.046$	$0.110 \pm 0.093 \pm 0.067$	$0.003 \pm 0.045 \pm 0.015$
0.350–0.375	$0.015 \pm 0.026 \pm 0.007$	$0.000 \pm 0.000 \pm 0.000$	$0.000 \pm 0.000 \pm 0.000$
0.375–0.400	$0.000 \pm 0.000 \pm 0.000$	$0.011 \pm 0.014 \pm 0.018$	$0.000 \pm 0.000 \pm 0.000$
First Moment	$0.0551 \pm 0.0021 \pm 0.0014$	$0.0582 \pm 0.0021 \pm 0.0015$	$0.0569 \pm 0.0017 \pm 0.0016$
Second Moment	$0.0063 \pm 0.0006 \pm 0.0004$	$0.0073 \pm 0.0006 \pm 0.0004$	$0.0070 \pm 0.0005 \pm 0.0005$

Table 31: Differential distribution for event thrust at $\sqrt{s} = 194.4$, 200.2 and 206.2 GeV. The first uncertainty is statistical, the second systematic.

	$\frac{1}{\sigma} \cdot \frac{\mathrm{d}\sigma}{\mathrm{d}\rho_{\mathrm{H}}}$		
ρ_{H}	at $\sqrt{s} = 41.4$ GeV	at $\sqrt{s} = 55.3$ GeV	at $\sqrt{s} = 65.4$ GeV
0.000–0.015	$0.183 \pm 0.038 \pm 0.858$	$1.329 \pm 0.195 \pm 0.622$	$2.063 \pm 0.190 \pm 0.924$
0.015–0.027	$6.119 \pm 0.642 \pm 0.465$	$13.192 \pm 1.067 \pm 3.301$	$14.082 \pm 0.856 \pm 0.654$
0.027–0.039	$12.263 \pm 1.432 \pm 3.194$	$19.031 \pm 1.637 \pm 2.785$	$20.593 \pm 1.349 \pm 1.384$
0.039–0.051	$16.680 \pm 1.925 \pm 2.251$	$11.201 \pm 1.317 \pm 3.402$	$12.065 \pm 0.940 \pm 1.158$
0.051–0.066	$10.037 \pm 1.223 \pm 0.515$	$9.616 \pm 1.190 \pm 5.665$	$7.040 \pm 0.705 \pm 0.482$
0.066–0.084	$5.589 \pm 0.819 \pm 0.901$	$4.482 \pm 0.658 \pm 1.981$	$5.751 \pm 0.557 \pm 0.262$
0.084–0.102	$6.752 \pm 0.967 \pm 1.918$	$3.114 \pm 0.597 \pm 0.390$	$3.361 \pm 0.450 \pm 0.207$
0.102–0.126	$2.550 \pm 0.432 \pm 0.578$	$3.591 \pm 0.606 \pm 0.951$	$1.803 \pm 0.270 \pm 0.530$
0.126–0.153	$2.029 \pm 0.430 \pm 0.510$	$1.312 \pm 0.333 \pm 0.463$	$0.928 \pm 0.182 \pm 0.217$
0.153–0.183	$1.615 \pm 0.328 \pm 0.312$	$0.559 \pm 0.215 \pm 0.153$	$1.116 \pm 0.243 \pm 0.218$
0.183–0.216	$0.683 \pm 0.210 \pm 0.194$	$0.691 \pm 0.192 \pm 0.203$	$0.517 \pm 0.117 \pm 0.067$
0.216–0.252	$0.211 \pm 0.130 \pm 0.204$	$0.213 \pm 0.117 \pm 0.062$	$0.405 \pm 0.095 \pm 0.090$
0.252–0.300	$0.193 \pm 0.099 \pm 0.113$	$0.191 \pm 0.079 \pm 0.098$	$0.107 \pm 0.047 \pm 0.179$
First Moment	$0.0747 \pm 0.0023 \pm 0.0023$	$0.0632 \pm 0.0021 \pm 0.0023$	$0.0603 \pm 0.0015 \pm 0.0047$
Second Moment	$0.0080 \pm 0.0006 \pm 0.0005$	$0.0063 \pm 0.0005 \pm 0.0008$	$0.0060 \pm 0.0003 \pm 0.0011$

Table 32: Differential distribution for scaled heavy jet mass at $\sqrt{s} = 41.4$, 55.3 and 65.4 GeV. The first uncertainty is statistical, the second systematic.

	$\frac{1}{\sigma} \cdot \frac{\mathrm{d}\sigma}{\mathrm{d}\rho_{\mathrm{H}}}$		
ρ_{H}	at $\sqrt{s} = 75.7$ GeV	at $\sqrt{s} = 82.3$ GeV	at $\sqrt{s} = 85.1$ GeV
0.000–0.015	$3.092 \pm 0.166 \pm 1.346$	$3.493 \pm 0.220 \pm 1.479$	$5.058 \pm 0.339 \pm 2.311$
0.015–0.027	$22.135 \pm 0.853 \pm 1.200$	$21.585 \pm 0.976 \pm 0.641$	$24.679 \pm 1.247 \pm 1.747$
0.027–0.039	$15.391 \pm 0.773 \pm 0.976$	$18.963 \pm 1.044 \pm 1.066$	$15.534 \pm 1.135 \pm 1.193$
0.039–0.051	$10.937 \pm 0.687 \pm 2.336$	$10.236 \pm 0.787 \pm 0.875$	$8.703 \pm 0.983 \pm 1.224$
0.051–0.066	$6.363 \pm 0.494 \pm 1.029$	$5.674 \pm 0.560 \pm 1.575$	$4.801 \pm 0.687 \pm 0.316$
0.066–0.084	$4.329 \pm 0.357 \pm 1.063$	$3.804 \pm 0.407 \pm 0.896$	$3.787 \pm 0.531 \pm 0.673$
0.084–0.102	$3.554 \pm 0.350 \pm 0.398$	$2.835 \pm 0.341 \pm 0.275$	$2.764 \pm 0.386 \pm 0.916$
0.102–0.126	$2.110 \pm 0.231 \pm 0.270$	$1.717 \pm 0.245 \pm 0.305$	$1.764 \pm 0.328 \pm 0.235$
0.126–0.153	$1.010 \pm 0.139 \pm 0.171$	$1.406 \pm 0.207 \pm 0.154$	$1.732 \pm 0.300 \pm 0.330$
0.153–0.183	$0.915 \pm 0.135 \pm 0.107$	$0.435 \pm 0.145 \pm 0.146$	$0.978 \pm 0.210 \pm 0.328$
0.183–0.216	$0.415 \pm 0.105 \pm 0.188$	$1.017 \pm 0.210 \pm 0.279$	$0.394 \pm 0.129 \pm 0.064$
0.216–0.252	$0.347 \pm 0.081 \pm 0.107$	$0.119 \pm 0.049 \pm 0.020$	$0.305 \pm 0.104 \pm 0.090$
0.252–0.300	$0.066 \pm 0.025 \pm 0.016$	$0.074 \pm 0.041 \pm 0.043$	$0.099 \pm 0.048 \pm 0.028$
First Moment	$0.0560 \pm 0.0011 \pm 0.0027$	$0.0546 \pm 0.0015 \pm 0.0035$	$0.0544 \pm 0.0017 \pm 0.0085$
Second Moment	$0.0053 \pm 0.0002 \pm 0.0007$	$0.0052 \pm 0.0003 \pm 0.0007$	$0.0054 \pm 0.0004 \pm 0.0014$

Table 33: Differential distribution for scaled heavy jet mass at $\sqrt{s} = 75.7$, 82.3 and 85.1 GeV. The first uncertainty is statistical, the second systematic.

	$\frac{1}{\sigma} \cdot \frac{\mathrm{d}\sigma}{\mathrm{d}\rho_{\mathrm{H}}}$		
ρ_{H}	at $\sqrt{s} = 130.1$ GeV	at $\sqrt{s} = 136.1$ GeV	at $\sqrt{s} = 161.3$ GeV
0.000–0.015	16.201 ± 1.462 ± 1.335	15.749 ± 1.715 ± 1.470	24.327 ± 2.252 ± 0.887
0.015–0.030	18.462 ± 1.621 ± 0.676	22.091 ± 2.114 ± 1.609	14.684 ± 1.771 ± 1.083
0.030–0.045	10.243 ± 1.201 ± 0.510	8.738 ± 1.266 ± 0.641	7.505 ± 1.167 ± 0.301
0.045–0.060	6.326 ± 0.939 ± 0.457	4.134 ± 0.888 ± 0.455	4.597 ± 0.944 ± 0.402
0.060–0.075	3.810 ± 0.687 ± 0.030	3.169 ± 0.740 ± 0.612	3.471 ± 0.835 ± 0.346
0.075–0.090	3.533 ± 0.649 ± 0.200	3.110 ± 0.755 ± 0.323	3.026 ± 0.759 ± 0.504
0.090–0.105	1.987 ± 0.487 ± 0.254	1.982 ± 0.573 ± 0.162	1.736 ± 0.585 ± 0.344
0.105–0.120	1.731 ± 0.448 ± 0.259	1.525 ± 0.498 ± 0.138	1.727 ± 0.584 ± 0.279
0.120–0.135	0.640 ± 0.260 ± 0.082	1.235 ± 0.449 ± 0.251	1.184 ± 0.489 ± 0.064
0.135–0.150	1.045 ± 0.316 ± 0.107	1.744 ± 0.513 ± 0.240	1.097 ± 0.443 ± 0.058
0.150–0.165	0.256 ± 0.149 ± 0.072	1.084 ± 0.375 ± 0.023	0.981 ± 0.451 ± 0.224
0.165–0.180	0.859 ± 0.275 ± 0.190	0.375 ± 0.222 ± 0.032	0.656 ± 0.351 ± 0.062
0.180–0.195	0.422 ± 0.186 ± 0.104	0.493 ± 0.243 ± 0.046	0.631 ± 0.317 ± 0.094
0.195–0.210	0.180 ± 0.114 ± 0.006	0.650 ± 0.254 ± 0.069	0.604 ± 0.291 ± 0.265
0.210–0.225	0.183 ± 0.129 ± 0.002	0.082 ± 0.082 ± 0.020	0.153 ± 0.162 ± 0.007
0.225–0.240	0.340 ± 0.172 ± 0.112	0.086 ± 0.086 ± 0.091	0.047 ± 0.102 ± 0.004
0.240–0.255	0.314 ± 0.181 ± 0.114	0.072 ± 0.072 ± 0.033	0.000 ± 0.000 ± 0.000
0.255–0.270	0.067 ± 0.067 ± 0.042	0.089 ± 0.089 ± 0.026	0.176 ± 0.149 ± 0.084
0.270–0.285	0.067 ± 0.067 ± 0.023	0.158 ± 0.115 ± 0.131	0.065 ± 0.087 ± 0.002
0.285–0.300	0.000 ± 0.000 ± 0.000	0.100 ± 0.100 ± 0.061	0.000 ± 0.000 ± 0.000
First Moment	0.0452 ±0.0018± 0.0007	0.0467 ±0.0022± 0.0005	0.0421 ±0.0025± 0.0007
Second Moment	0.0041 ±0.0003± 0.0001	0.0045 ±0.0004± 0.0001	0.0040 ±0.0004± 0.0001

Table 34: Differential distribution for scaled heavy jet mass at $\sqrt{s} = 130.1$, 136.1 and 161.3 GeV. The first uncertainty is statistical, the second systematic.

	$\frac{1}{\sigma} \cdot \frac{\mathrm{d}\sigma}{\mathrm{d}\rho_{\mathrm{H}}}$		
ρ_{H}	at $\sqrt{s} = 172.3$ GeV	at $\sqrt{s} = 182.8$ GeV	at $\sqrt{s} = 188.6$ GeV
0.000–0.015	$20.528 \pm 2.362 \pm 0.824$	$21.698 \pm 0.974 \pm 2.301$	$20.410 \pm 0.620 \pm 0.687$
0.015–0.030	$14.956 \pm 1.896 \pm 1.607$	$15.979 \pm 0.996 \pm 1.428$	$16.738 \pm 0.606 \pm 0.365$
0.030–0.045	$9.336 \pm 1.486 \pm 0.294$	$9.381 \pm 0.748 \pm 0.703$	$8.711 \pm 0.417 \pm 0.250$
0.045–0.060	$4.641 \pm 1.102 \pm 0.946$	$5.032 \pm 0.553 \pm 0.471$	$5.259 \pm 0.332 \pm 0.243$
0.060–0.075	$4.249 \pm 1.046 \pm 0.485$	$3.422 \pm 0.465 \pm 0.490$	$3.489 \pm 0.272 \pm 0.065$
0.075–0.090	$3.184 \pm 0.951 \pm 0.621$	$2.524 \pm 0.400 \pm 0.043$	$2.641 \pm 0.242 \pm 0.081$
0.090–0.105	$2.702 \pm 0.841 \pm 0.401$	$1.987 \pm 0.356 \pm 0.183$	$2.037 \pm 0.209 \pm 0.087$
0.105–0.120	$2.160 \pm 0.785 \pm 0.161$	$1.457 \pm 0.310 \pm 0.175$	$1.799 \pm 0.201 \pm 0.210$
0.120–0.135	$0.920 \pm 0.530 \pm 0.643$	$1.171 \pm 0.281 \pm 0.145$	$1.058 \pm 0.165 \pm 0.028$
0.135–0.150	$2.023 \pm 0.707 \pm 0.800$	$1.089 \pm 0.260 \pm 0.179$	$1.158 \pm 0.165 \pm 0.011$
0.150–0.165	$0.564 \pm 0.428 \pm 0.280$	$0.831 \pm 0.241 \pm 0.080$	$0.657 \pm 0.118 \pm 0.053$
0.165–0.180	$0.334 \pm 0.317 \pm 0.004$	$0.346 \pm 0.167 \pm 0.083$	$0.805 \pm 0.131 \pm 0.087$
0.180–0.195	$0.342 \pm 0.305 \pm 0.085$	$0.448 \pm 0.158 \pm 0.018$	$0.554 \pm 0.112 \pm 0.083$
0.195–0.210	$0.177 \pm 0.229 \pm 0.055$	$0.345 \pm 0.144 \pm 0.071$	$0.336 \pm 0.099 \pm 0.070$
0.210–0.225	$0.000 \pm 0.000 \pm 0.000$	$0.157 \pm 0.105 \pm 0.060$	$0.344 \pm 0.087 \pm 0.036$
0.225–0.240	$0.201 \pm 0.198 \pm 0.092$	$0.061 \pm 0.083 \pm 0.088$	$0.116 \pm 0.071 \pm 0.022$
0.240–0.255	$0.000 \pm 0.000 \pm 0.000$	$0.338 \pm 0.133 \pm 0.104$	$0.232 \pm 0.081 \pm 0.002$
0.255–0.270	$0.101 \pm 0.146 \pm 0.001$	$0.228 \pm 0.107 \pm 0.128$	$0.156 \pm 0.060 \pm 0.020$
0.270–0.285	$0.113 \pm 0.148 \pm 0.035$	$0.175 \pm 0.098 \pm 0.027$	$0.099 \pm 0.054 \pm 0.066$
0.285–0.300	$0.136 \pm 0.154 \pm 0.123$	$0.000 \pm 0.000 \pm 0.000$	$0.069 \pm 0.041 \pm 0.021$
First Moment	$0.0440 \pm 0.0028 \pm 0.0008$	$0.0424 \pm 0.0014 \pm 0.0004$	$0.0442 \pm 0.0009 \pm 0.0009$
Second Moment	$0.0040 \pm 0.0005 \pm 0.0003$	$0.0040 \pm 0.0003 \pm 0.0002$	$0.0043 \pm 0.0002 \pm 0.0002$

Table 35: Differential distribution for scaled heavy jet mass at $\sqrt{s} = 172.3$, 182.8 and 188.6 GeV. The first uncertainty is statistical, the second systematic.

	$\frac{1}{\sigma} \cdot \frac{\mathrm{d}\sigma}{\mathrm{d}\rho_{\mathrm{H}}}$		
ρ_{H}	at $\sqrt{s} = 194.4$ GeV	at $\sqrt{s} = 200.2$ GeV	at $\sqrt{s} = 206.2$ GeV
0.000–0.015	$20.870 \pm 0.769 \pm 0.662$	$20.671 \pm 0.765 \pm 0.753$	$21.199 \pm 0.633 \pm 0.788$
0.015–0.030	$16.523 \pm 0.771 \pm 0.644$	$16.098 \pm 0.768 \pm 0.439$	$15.088 \pm 0.576 \pm 0.357$
0.030–0.045	$8.747 \pm 0.588 \pm 0.549$	$8.739 \pm 0.577 \pm 0.393$	$9.048 \pm 0.452 \pm 0.384$
0.045–0.060	$5.854 \pm 0.512 \pm 0.461$	$4.727 \pm 0.435 \pm 0.302$	$5.218 \pm 0.354 \pm 0.208$
0.060–0.075	$3.817 \pm 0.422 \pm 0.256$	$3.701 \pm 0.393 \pm 0.220$	$3.669 \pm 0.300 \pm 0.082$
0.075–0.090	$2.036 \pm 0.317 \pm 0.209$	$2.676 \pm 0.346 \pm 0.519$	$3.101 \pm 0.283 \pm 0.233$
0.090–0.105	$2.060 \pm 0.321 \pm 0.174$	$2.640 \pm 0.330 \pm 0.294$	$2.133 \pm 0.243 \pm 0.107$
0.105–0.120	$1.795 \pm 0.290 \pm 0.298$	$1.571 \pm 0.259 \pm 0.168$	$1.634 \pm 0.227 \pm 0.145$
0.120–0.135	$1.065 \pm 0.246 \pm 0.191$	$1.460 \pm 0.318 \pm 0.387$	$1.142 \pm 0.183 \pm 0.110$
0.135–0.150	$0.840 \pm 0.218 \pm 0.216$	$1.098 \pm 0.221 \pm 0.164$	$0.764 \pm 0.153 \pm 0.242$
0.150–0.165	$0.577 \pm 0.195 \pm 0.145$	$0.586 \pm 0.170 \pm 0.137$	$0.738 \pm 0.159 \pm 0.104$
0.165–0.180	$0.394 \pm 0.146 \pm 0.022$	$0.502 \pm 0.179 \pm 0.086$	$0.735 \pm 0.147 \pm 0.076$
0.180–0.195	$0.522 \pm 0.154 \pm 0.123$	$0.218 \pm 0.091 \pm 0.026$	$0.642 \pm 0.150 \pm 0.072$
0.195–0.210	$0.302 \pm 0.129 \pm 0.166$	$0.407 \pm 0.154 \pm 0.075$	$0.444 \pm 0.138 \pm 0.062$
0.210–0.225	$0.592 \pm 0.184 \pm 0.175$	$0.469 \pm 0.160 \pm 0.078$	$0.387 \pm 0.145 \pm 0.164$
0.225–0.240	$0.388 \pm 0.131 \pm 0.205$	$0.388 \pm 0.152 \pm 0.090$	$0.119 \pm 0.105 \pm 0.114$
0.240–0.255	$0.111 \pm 0.097 \pm 0.048$	$0.496 \pm 0.171 \pm 0.201$	$0.069 \pm 0.085 \pm 0.030$
0.255–0.270	$0.022 \pm 0.050 \pm 0.006$	$0.000 \pm 0.000 \pm 0.000$	$0.283 \pm 0.098 \pm 0.031$
0.270–0.285	$0.089 \pm 0.070 \pm 0.030$	$0.119 \pm 0.085 \pm 0.047$	$0.139 \pm 0.074 \pm 0.073$
0.285–0.300	$0.064 \pm 0.074 \pm 0.063$	$0.102 \pm 0.081 \pm 0.063$	$0.116 \pm 0.055 \pm 0.023$
First Moment	$0.0439 \pm 0.0014 \pm 0.0014$	$0.0464 \pm 0.0014 \pm 0.0015$	$0.0455 \pm 0.0011 \pm 0.0011$
Second Moment	$0.0042 \pm 0.0003 \pm 0.0002$	$0.0048 \pm 0.0003 \pm 0.0003$	$0.0046 \pm 0.0003 \pm 0.0002$

Table 36: Differential distribution for scaled heavy jet mass at $\sqrt{s} = 194.4$, 200.2 and 206.2 GeV. The first uncertainty is statistical, the second systematic.

	$\frac{1}{\sigma} \cdot \frac{\mathrm{d}\sigma}{\mathrm{d}B_\mathrm{T}}$		
B_T	at $\sqrt{s} = 41.4$ GeV	at $\sqrt{s} = 55.3$ GeV	at $\sqrt{s} = 65.4$ GeV
0.000–0.040	$0.229 \pm 0.098 \pm 0.073$	$0.445 \pm 0.131 \pm 0.243$	$0.232 \pm 0.054 \pm 0.116$
0.040–0.070	$2.056 \pm 0.276 \pm 0.316$	$5.108 \pm 0.492 \pm 1.090$	$6.125 \pm 0.399 \pm 1.515$
0.070–0.100	$7.981 \pm 0.685 \pm 0.974$	$9.488 \pm 0.688 \pm 1.665$	$9.335 \pm 0.493 \pm 0.537$
0.100–0.130	$7.756 \pm 0.749 \pm 0.268$	$5.946 \pm 0.558 \pm 0.559$	$6.114 \pm 0.421 \pm 0.223$
0.130–0.160	$4.514 \pm 0.548 \pm 0.564$	$4.592 \pm 0.538 \pm 0.696$	$4.384 \pm 0.383 \pm 0.487$
0.160–0.190	$3.935 \pm 0.532 \pm 0.921$	$2.816 \pm 0.397 \pm 0.845$	$2.529 \pm 0.274 \pm 0.157$
0.190–0.220	$2.887 \pm 0.485 \pm 0.632$	$2.260 \pm 0.406 \pm 0.270$	$1.289 \pm 0.210 \pm 0.829$
0.220–0.250	$1.817 \pm 0.346 \pm 0.128$	$1.136 \pm 0.245 \pm 0.360$	$1.452 \pm 0.202 \pm 0.222$
0.250–0.280	$0.732 \pm 0.210 \pm 0.217$	$0.704 \pm 0.224 \pm 0.146$	$0.940 \pm 0.159 \pm 0.293$
0.280–0.310	$0.849 \pm 0.274 \pm 0.233$	$0.408 \pm 0.173 \pm 0.149$	$0.384 \pm 0.118 \pm 0.073$
0.310–0.340	$0.372 \pm 0.117 \pm 0.159$	$0.168 \pm 0.083 \pm 0.085$	$0.402 \pm 0.125 \pm 0.121$
0.340–0.400	$0.064 \pm 0.035 \pm 0.021$	$0.058 \pm 0.034 \pm 0.010$	$0.035 \pm 0.022 \pm 0.019$
First Moment	$0.1399 \pm 0.0027 \pm 0.0016$	$0.1223 \pm 0.0025 \pm 0.0054$	$0.1213 \pm 0.0019 \pm 0.0079$
Second Moment	$0.0236 \pm 0.0009 \pm 0.0005$	$0.0187 \pm 0.0008 \pm 0.0012$	$0.0187 \pm 0.0006 \pm 0.0022$

Table 37: Differential distribution for total jet broadening at $\sqrt{s} = 41.4$, 55.3 and 65.4 GeV. The first uncertainty is statistical, the second systematic.

	$\frac{1}{\sigma} \cdot \frac{\mathrm{d}\sigma}{\mathrm{d}B_\mathrm{T}}$		
B_T	at $\sqrt{s} = 75.7$ GeV	at $\sqrt{s} = 82.3$ GeV	at $\sqrt{s} = 85.1$ GeV
0.000–0.040	$0.243 \pm 0.030 \pm 0.121$	$0.324 \pm 0.049 \pm 0.178$	$0.637 \pm 0.086 \pm 0.315$
0.040–0.070	$8.069 \pm 0.316 \pm 0.997$	$8.448 \pm 0.376 \pm 1.156$	$9.054 \pm 0.464 \pm 1.153$
0.070–0.100	$8.805 \pm 0.344 \pm 0.227$	$9.377 \pm 0.430 \pm 0.158$	$8.500 \pm 0.493 \pm 1.133$
0.100–0.130	$5.694 \pm 0.300 \pm 0.278$	$5.446 \pm 0.339 \pm 0.940$	$5.978 \pm 0.439 \pm 0.376$
0.130–0.160	$3.663 \pm 0.246 \pm 0.349$	$3.437 \pm 0.296 \pm 0.398$	$2.353 \pm 0.337 \pm 0.448$
0.160–0.190	$2.536 \pm 0.211 \pm 0.113$	$2.341 \pm 0.242 \pm 0.596$	$2.510 \pm 0.283 \pm 0.650$
0.190–0.220	$1.384 \pm 0.154 \pm 0.327$	$1.551 \pm 0.186 \pm 0.139$	$1.557 \pm 0.245 \pm 0.286$
0.220–0.250	$1.420 \pm 0.168 \pm 0.389$	$0.999 \pm 0.186 \pm 0.153$	$1.465 \pm 0.260 \pm 0.313$
0.250–0.280	$0.723 \pm 0.123 \pm 0.119$	$0.886 \pm 0.185 \pm 0.189$	$0.609 \pm 0.187 \pm 0.177$
0.280–0.310	$0.488 \pm 0.113 \pm 0.140$	$0.267 \pm 0.115 \pm 0.138$	$0.248 \pm 0.115 \pm 0.040$
0.310–0.340	$0.184 \pm 0.079 \pm 0.064$	$0.115 \pm 0.064 \pm 0.064$	$0.185 \pm 0.092 \pm 0.096$
0.340–0.400	$0.022 \pm 0.013 \pm 0.009$	$0.017 \pm 0.012 \pm 0.010$	$0.012 \pm 0.012 \pm 0.015$
First Moment	$0.1157 \pm 0.0015 \pm 0.0048$	$0.1116 \pm 0.0017 \pm 0.0057$	$0.1102 \pm 0.0021 \pm 0.0086$
Second Moment	$0.0172 \pm 0.0005 \pm 0.0014$	$0.0160 \pm 0.0006 \pm 0.0015$	$0.0158 \pm 0.0007 \pm 0.0022$

Table 38: Differential distribution for total jet broadening at $\sqrt{s} = 75.7$, 82.3 and 85.1 GeV. The first uncertainty is statistical, the second systematic.

	$\frac{1}{\sigma} \cdot \frac{\mathrm{d}\sigma}{\mathrm{d}B_\mathrm{T}}$		
B_T	at $\sqrt{s} = 130.1$ GeV	at $\sqrt{s} = 136.1$ GeV	at $\sqrt{s} = 161.3$ GeV
0.000–0.020	$0.082 \pm 0.086 \pm 0.037$	$0.103 \pm 0.077 \pm 0.090$	$0.117 \pm 0.090 \pm 0.069$
0.020–0.040	$4.010 \pm 0.684 \pm 0.468$	$5.454 \pm 0.965 \pm 0.863$	$9.224 \pm 1.407 \pm 0.577$
0.040–0.060	$11.651 \pm 1.173 \pm 0.360$	$11.111 \pm 1.340 \pm 0.898$	$9.486 \pm 1.353 \pm 0.934$
0.060–0.080	$8.865 \pm 0.932 \pm 0.289$	$8.945 \pm 1.077 \pm 0.286$	$8.450 \pm 1.071 \pm 0.344$
0.080–0.100	$7.778 \pm 0.884 \pm 0.880$	$7.419 \pm 1.042 \pm 0.468$	$5.530 \pm 0.841 \pm 0.214$
0.100–0.120	$4.239 \pm 0.638 \pm 0.388$	$3.464 \pm 0.669 \pm 0.235$	$4.231 \pm 0.740 \pm 0.197$
0.120–0.140	$3.780 \pm 0.591 \pm 0.246$	$3.259 \pm 0.652 \pm 0.210$	$3.080 \pm 0.613 \pm 0.490$
0.140–0.160	$2.509 \pm 0.455 \pm 0.091$	$2.237 \pm 0.531 \pm 0.106$	$3.025 \pm 0.597 \pm 0.137$
0.160–0.180	$2.031 \pm 0.404 \pm 0.147$	$1.568 \pm 0.421 \pm 0.101$	$1.894 \pm 0.473 \pm 0.248$
0.180–0.200	$1.820 \pm 0.375 \pm 0.127$	$1.865 \pm 0.447 \pm 0.280$	$1.293 \pm 0.396 \pm 0.173$
0.200–0.220	$0.897 \pm 0.241 \pm 0.053$	$1.516 \pm 0.411 \pm 0.237$	$1.069 \pm 0.375 \pm 0.143$
0.220–0.240	$0.790 \pm 0.208 \pm 0.099$	$1.074 \pm 0.317 \pm 0.141$	$1.338 \pm 0.379 \pm 0.228$
0.240–0.260	$0.363 \pm 0.146 \pm 0.097$	$0.661 \pm 0.239 \pm 0.066$	$0.408 \pm 0.218 \pm 0.164$
0.260–0.280	$0.629 \pm 0.186 \pm 0.166$	$0.548 \pm 0.205 \pm 0.080$	$0.067 \pm 0.128 \pm 0.019$
0.280–0.300	$0.227 \pm 0.113 \pm 0.030$	$0.198 \pm 0.115 \pm 0.041$	$0.710 \pm 0.238 \pm 0.224$
0.300–0.320	$0.052 \pm 0.053 \pm 0.020$	$0.252 \pm 0.137 \pm 0.083$	$0.000 \pm 0.000 \pm 0.000$
0.320–0.340	$0.086 \pm 0.061 \pm 0.020$	$0.217 \pm 0.108 \pm 0.138$	$0.078 \pm 0.127 \pm 0.016$
0.340–0.360	$0.092 \pm 0.065 \pm 0.045$	$0.108 \pm 0.077 \pm 0.020$	$0.000 \pm 0.000 \pm 0.000$
First Moment	$0.0976 \pm 0.0023 \pm 0.0008$	$0.0999 \pm 0.0029 \pm 0.0012$	$0.0923 \pm 0.0032 \pm 0.0018$
Second Moment	$0.0131 \pm 0.0006 \pm 0.0002$	$0.0141 \pm 0.0008 \pm 0.0004$	$0.0121 \pm 0.0008 \pm 0.0004$

Table 39: Differential distribution for total jet broadening at $\sqrt{s} = 130.1$, 136.1 and 161.3 GeV. The first uncertainty is statistical, the second systematic.

	$\frac{1}{\sigma} \cdot \frac{\mathrm{d}\sigma}{\mathrm{d}B_\mathrm{T}}$		
B_T	at $\sqrt{s} = 172.3$ GeV	at $\sqrt{s} = 182.8$ GeV	at $\sqrt{s} = 188.6$ GeV
0.000–0.020	$0.410 \pm 0.189 \pm 0.117$	$0.343 \pm 0.086 \pm 0.471$	$0.418 \pm 0.061 \pm 0.065$
0.020–0.040	$8.824 \pm 1.579 \pm 1.483$	$8.245 \pm 0.597 \pm 0.670$	$8.634 \pm 0.416 \pm 0.383$
0.040–0.060	$10.568 \pm 1.517 \pm 0.462$	$10.962 \pm 0.680 \pm 0.389$	$10.279 \pm 0.423 \pm 0.276$
0.060–0.080	$6.654 \pm 1.043 \pm 0.747$	$7.658 \pm 0.549 \pm 0.191$	$8.186 \pm 0.332 \pm 0.100$
0.080–0.100	$6.733 \pm 1.046 \pm 1.026$	$5.831 \pm 0.470 \pm 0.391$	$5.241 \pm 0.257 \pm 0.196$
0.100–0.120	$3.987 \pm 0.814 \pm 0.155$	$4.179 \pm 0.392 \pm 0.240$	$4.633 \pm 0.242 \pm 0.156$
0.120–0.140	$3.130 \pm 0.715 \pm 0.333$	$3.865 \pm 0.377 \pm 0.316$	$3.143 \pm 0.201 \pm 0.111$
0.140–0.160	$1.937 \pm 0.580 \pm 0.147$	$2.068 \pm 0.287 \pm 0.073$	$2.525 \pm 0.180 \pm 0.038$
0.160–0.180	$1.847 \pm 0.574 \pm 0.291$	$1.787 \pm 0.264 \pm 0.076$	$1.644 \pm 0.155 \pm 0.016$
0.180–0.200	$1.482 \pm 0.510 \pm 0.249$	$1.763 \pm 0.264 \pm 0.144$	$1.527 \pm 0.150 \pm 0.122$
0.200–0.220	$1.510 \pm 0.536 \pm 0.604$	$0.783 \pm 0.192 \pm 0.138$	$1.179 \pm 0.131 \pm 0.053$
0.220–0.240	$0.530 \pm 0.338 \pm 0.240$	$0.637 \pm 0.180 \pm 0.242$	$1.119 \pm 0.132 \pm 0.106$
0.240–0.260	$0.274 \pm 0.267 \pm 0.076$	$0.691 \pm 0.190 \pm 0.043$	$0.677 \pm 0.125 \pm 0.141$
0.260–0.280	$0.223 \pm 0.265 \pm 0.167$	$0.656 \pm 0.208 \pm 0.144$	$0.399 \pm 0.126 \pm 0.143$
0.280–0.300	$0.734 \pm 0.415 \pm 0.630$	$0.314 \pm 0.167 \pm 0.035$	$0.144 \pm 0.098 \pm 0.089$
0.300–0.320	$0.865 \pm 0.383 \pm 0.649$	$0.212 \pm 0.154 \pm 0.075$	$0.228 \pm 0.108 \pm 0.058$
0.320–0.340	$0.000 \pm 0.000 \pm 0.000$	$0.000 \pm 0.000 \pm 0.000$	$0.000 \pm 0.000 \pm 0.000$
0.340–0.360	$0.294 \pm 0.337 \pm 0.193$	$0.008 \pm 0.073 \pm 0.000$	$0.013 \pm 0.050 \pm 0.110$
First Moment	$0.0950 \pm 0.0046 \pm 0.0031$	$0.0918 \pm 0.0020 \pm 0.0015$	$0.0918 \pm 0.0013 \pm 0.0018$
Second Moment	$0.0136 \pm 0.0014 \pm 0.0006$	$0.0121 \pm 0.0006 \pm 0.0003$	$0.0121 \pm 0.0004 \pm 0.0005$

Table 40: Differential distribution for total jet broadening at $\sqrt{s} = 172.3$, 182.8 and 188.6 GeV. The first uncertainty is statistical, the second systematic.

	$\frac{1}{\sigma} \cdot \frac{\mathrm{d}\sigma}{\mathrm{d}B_\mathrm{T}}$		
B_T	at $\sqrt{s} = 194.4$ GeV	at $\sqrt{s} = 200.2$ GeV	at $\sqrt{s} = 206.2$ GeV
0.000–0.020	$0.376 \pm 0.078 \pm 0.124$	$0.449 \pm 0.085 \pm 0.109$	$0.491 \pm 0.064 \pm 0.101$
0.020–0.040	$8.334 \pm 0.480 \pm 0.415$	$8.633 \pm 0.495 \pm 0.405$	$8.694 \pm 0.386 \pm 0.387$
0.040–0.060	$10.931 \pm 0.531 \pm 0.377$	$10.228 \pm 0.507 \pm 0.201$	$10.221 \pm 0.401 \pm 0.228$
0.060–0.080	$7.336 \pm 0.419 \pm 0.283$	$7.197 \pm 0.415 \pm 0.180$	$7.299 \pm 0.322 \pm 0.124$
0.080–0.100	$6.187 \pm 0.384 \pm 0.236$	$5.780 \pm 0.368 \pm 0.118$	$5.821 \pm 0.285 \pm 0.260$
0.100–0.120	$4.157 \pm 0.316 \pm 0.188$	$4.282 \pm 0.326 \pm 0.327$	$4.079 \pm 0.241 \pm 0.176$
0.120–0.140	$3.356 \pm 0.299 \pm 0.230$	$2.929 \pm 0.266 \pm 0.270$	$3.432 \pm 0.229 \pm 0.179$
0.140–0.160	$2.245 \pm 0.271 \pm 0.184$	$2.839 \pm 0.269 \pm 0.203$	$2.411 \pm 0.196 \pm 0.135$
0.160–0.180	$2.367 \pm 0.271 \pm 0.187$	$2.384 \pm 0.253 \pm 0.134$	$1.725 \pm 0.174 \pm 0.108$
0.180–0.200	$0.992 \pm 0.176 \pm 0.132$	$1.430 \pm 0.207 \pm 0.123$	$1.568 \pm 0.169 \pm 0.151$
0.200–0.220	$1.011 \pm 0.199 \pm 0.085$	$1.073 \pm 0.202 \pm 0.150$	$1.441 \pm 0.182 \pm 0.146$
0.220–0.240	$0.816 \pm 0.183 \pm 0.113$	$1.191 \pm 0.236 \pm 0.177$	$0.960 \pm 0.174 \pm 0.053$
0.240–0.260	$1.141 \pm 0.286 \pm 0.289$	$0.429 \pm 0.182 \pm 0.189$	$0.576 \pm 0.174 \pm 0.011$
0.260–0.280	$0.339 \pm 0.194 \pm 0.120$	$0.553 \pm 0.225 \pm 0.114$	$0.632 \pm 0.179 \pm 0.094$
0.280–0.300	$0.099 \pm 0.144 \pm 0.046$	$0.211 \pm 0.183 \pm 0.094$	$0.500 \pm 0.186 \pm 0.175$
0.300–0.320	$0.168 \pm 0.094 \pm 0.025$	$0.281 \pm 0.191 \pm 0.136$	$0.063 \pm 0.082 \pm 0.076$
0.320–0.340	$0.144 \pm 0.125 \pm 0.061$	$0.095 \pm 0.121 \pm 0.100$	$0.040 \pm 0.079 \pm 0.017$
0.340–0.360	$0.000 \pm 0.000 \pm 0.000$	$0.015 \pm 0.024 \pm 0.048$	$0.048 \pm 0.063 \pm 0.029$
First Moment	$0.0920 \pm 0.0022 \pm 0.0028$	$0.0950 \pm 0.0021 \pm 0.0025$	$0.0938 \pm 0.0017 \pm 0.0015$
Second Moment	$0.0122 \pm 0.0006 \pm 0.0010$	$0.0131 \pm 0.0007 \pm 0.0006$	$0.0128 \pm 0.0005 \pm 0.0005$

Table 41: Differential distribution for total jet broadening at $\sqrt{s} = 194.4$, 200.2 and 206.2 GeV. The first uncertainty is statistical, the second systematic.

	$\frac{1}{\sigma} \cdot \frac{\mathrm{d}\sigma}{\mathrm{d}B_{\mathrm{W}}}$		
B_{W}	at $\sqrt{s} = 41.4$ GeV	at $\sqrt{s} = 55.3$ GeV	at $\sqrt{s} = 65.4$ GeV
0.000–0.030	$0.641 \pm 0.167 \pm 0.325$	$1.498 \pm 0.246 \pm 0.742$	$1.264 \pm 0.164 \pm 0.620$
0.030–0.050	$8.586 \pm 0.836 \pm 2.308$	$13.144 \pm 1.014 \pm 2.525$	$13.873 \pm 0.756 \pm 0.784$
0.050–0.075	$12.655 \pm 1.026 \pm 0.338$	$11.029 \pm 0.802 \pm 1.831$	$10.676 \pm 0.583 \pm 0.421$
0.075–0.100	$6.548 \pm 0.676 \pm 0.558$	$6.442 \pm 0.669 \pm 0.470$	$6.186 \pm 0.473 \pm 0.388$
0.100–0.125	$5.168 \pm 0.681 \pm 0.818$	$3.544 \pm 0.475 \pm 0.573$	$4.246 \pm 0.393 \pm 0.873$
0.125–0.150	$2.900 \pm 0.497 \pm 0.436$	$3.117 \pm 0.479 \pm 1.599$	$2.485 \pm 0.312 \pm 0.325$
0.150–0.175	$2.101 \pm 0.402 \pm 0.495$	$1.703 \pm 0.403 \pm 0.202$	$1.445 \pm 0.224 \pm 0.247$
0.175–0.200	$1.856 \pm 0.346 \pm 0.134$	$0.692 \pm 0.283 \pm 0.544$	$1.175 \pm 0.234 \pm 0.697$
0.200–0.225	$0.636 \pm 0.223 \pm 0.242$	$0.751 \pm 0.240 \pm 0.233$	$0.669 \pm 0.156 \pm 0.159$
0.225–0.300	$0.166 \pm 0.080 \pm 0.086$	$0.137 \pm 0.057 \pm 0.061$	$0.167 \pm 0.040 \pm 0.048$
First Moment	$0.0896 \pm 0.0021 \pm 0.0018$	$0.0800 \pm 0.0020 \pm 0.0034$	$0.0806 \pm 0.0014 \pm 0.0060$
Second Moment	$0.0104 \pm 0.0005 \pm 0.0005$	$0.0086 \pm 0.0005 \pm 0.0006$	$0.0088 \pm 0.0003 \pm 0.0013$

Table 42: Differential distribution for wide jet broadening at $\sqrt{s} = 41.4$, 55.3 and 65.4 GeV. The first uncertainty is statistical, the second systematic.

	$\frac{1}{\sigma} \cdot \frac{\mathrm{d}\sigma}{\mathrm{d}B_{\mathrm{W}}}$		
B_{W}	at $\sqrt{s} = 75.7$ GeV	at $\sqrt{s} = 82.3$ GeV	at $\sqrt{s} = 85.1$ GeV
0.000–0.030	$2.299 \pm 0.153 \pm 1.123$	$2.628 \pm 0.204 \pm 1.255$	$3.260 \pm 0.274 \pm 1.577$
0.030–0.050	$16.308 \pm 0.576 \pm 0.614$	$15.538 \pm 0.645 \pm 0.746$	$15.441 \pm 0.763 \pm 1.344$
0.050–0.075	$9.129 \pm 0.384 \pm 0.455$	$9.862 \pm 0.472 \pm 0.655$	$10.235 \pm 0.602 \pm 0.556$
0.075–0.100	$5.427 \pm 0.326 \pm 0.847$	$4.651 \pm 0.372 \pm 1.406$	$3.917 \pm 0.446 \pm 1.180$
0.100–0.125	$3.611 \pm 0.273 \pm 0.275$	$3.800 \pm 0.337 \pm 0.769$	$3.173 \pm 0.396 \pm 0.476$
0.125–0.150	$2.499 \pm 0.222 \pm 0.240$	$2.442 \pm 0.288 \pm 0.277$	$2.226 \pm 0.303 \pm 0.315$
0.150–0.175	$1.297 \pm 0.189 \pm 0.238$	$1.500 \pm 0.210 \pm 0.250$	$1.775 \pm 0.273 \pm 0.369$
0.175–0.200	$1.320 \pm 0.176 \pm 0.248$	$0.883 \pm 0.186 \pm 0.078$	$1.205 \pm 0.248 \pm 0.234$
0.200–0.225	$0.449 \pm 0.114 \pm 0.179$	$1.026 \pm 0.237 \pm 0.203$	$0.686 \pm 0.187 \pm 0.213$
0.225–0.300	$0.154 \pm 0.033 \pm 0.021$	$0.084 \pm 0.032 \pm 0.038$	$0.173 \pm 0.059 \pm 0.057$
First Moment	$0.0758 \pm 0.0011 \pm 0.0046$	$0.0756 \pm 0.0014 \pm 0.0051$	$0.0749 \pm 0.0017 \pm 0.0092$
Second Moment	$0.0081 \pm 0.0003 \pm 0.0008$	$0.0081 \pm 0.0003 \pm 0.0008$	$0.0082 \pm 0.0004 \pm 0.0018$

Table 43: Differential distribution for wide jet broadening at $\sqrt{s} = 75.7$, 82.3 and 85.1 GeV. The first uncertainty is statistical, the second systematic.

	$\frac{1}{\sigma}\cdot\frac{\mathrm{d}\sigma}{\mathrm{d}B_{\mathrm{W}}}$		
B_{W}	at $\sqrt{s} = 130.1$ GeV	at $\sqrt{s} = 136.1$ GeV	at $\sqrt{s} = 161.3$ GeV
0.000–0.015	$0.157 \pm 0.126 \pm 0.053$	$0.235 \pm 0.257 \pm 0.077$	$2.601 \pm 0.768 \pm 0.708$
0.015–0.030	$12.915 \pm 1.493 \pm 0.732$	$14.660 \pm 1.837 \pm 1.348$	$16.194 \pm 2.091 \pm 0.795$
0.030–0.045	$14.268 \pm 1.332 \pm 0.963$	$15.618 \pm 1.646 \pm 0.640$	$10.741 \pm 1.481 \pm 0.779$
0.045–0.060	$10.861 \pm 1.164 \pm 0.876$	$8.923 \pm 1.262 \pm 0.465$	$10.016 \pm 1.327 \pm 0.223$
0.060–0.075	$6.320 \pm 0.921 \pm 0.272$	$5.144 \pm 0.951 \pm 0.977$	$5.587 \pm 0.992 \pm 0.551$
0.075–0.090	$5.646 \pm 0.851 \pm 0.436$	$5.510 \pm 0.990 \pm 0.430$	$4.394 \pm 0.878 \pm 0.277$
0.090–0.105	$4.097 \pm 0.714 \pm 0.153$	$3.752 \pm 0.833 \pm 0.161$	$4.149 \pm 0.862 \pm 0.249$
0.105–0.120	$3.866 \pm 0.683 \pm 0.530$	$2.436 \pm 0.631 \pm 0.348$	$3.511 \pm 0.795 \pm 0.310$
0.120–0.135	$2.078 \pm 0.483 \pm 0.210$	$2.427 \pm 0.635 \pm 0.074$	$2.089 \pm 0.608 \pm 0.197$
0.135–0.150	$1.974 \pm 0.453 \pm 0.287$	$1.802 \pm 0.532 \pm 0.192$	$2.024 \pm 0.585 \pm 0.070$
0.150–0.165	$1.160 \pm 0.337 \pm 0.076$	$1.292 \pm 0.394 \pm 0.348$	$1.162 \pm 0.486 \pm 0.421$
0.165–0.180	$0.647 \pm 0.235 \pm 0.054$	$1.660 \pm 0.502 \pm 0.265$	$0.779 \pm 0.402 \pm 0.044$
0.180–0.195	$0.802 \pm 0.261 \pm 0.059$	$1.177 \pm 0.358 \pm 0.188$	$1.449 \pm 0.507 \pm 0.043$
0.195–0.210	$0.877 \pm 0.246 \pm 0.108$	$0.656 \pm 0.258 \pm 0.052$	$0.800 \pm 0.347 \pm 0.169$
0.210–0.225	$0.230 \pm 0.126 \pm 0.001$	$0.587 \pm 0.229 \pm 0.011$	$0.581 \pm 0.279 \pm 0.042$
0.225–0.240	$0.514 \pm 0.200 \pm 0.124$	$0.259 \pm 0.150 \pm 0.100$	$0.092 \pm 0.128 \pm 0.008$
0.240–0.255	$0.197 \pm 0.123 \pm 0.048$	$0.144 \pm 0.102 \pm 0.056$	$0.114 \pm 0.121 \pm 0.041$
0.255–0.270	$0.057 \pm 0.058 \pm 0.008$	$0.170 \pm 0.136 \pm 0.075$	$0.053 \pm 0.086 \pm 0.002$
0.270–0.285	$0.000 \pm 0.000 \pm 0.000$	$0.072 \pm 0.072 \pm 0.041$	$0.330 \pm 0.172 \pm 0.155$
0.285–0.300	$0.000 \pm 0.000 \pm 0.000$	$0.144 \pm 0.144 \pm 0.098$	$0.000 \pm 0.000 \pm 0.000$
First Moment	$0.0681 \pm 0.0019 \pm 0.0006$	$0.0699 \pm 0.0024 \pm 0.0007$	$0.0666 \pm 0.0027 \pm 0.0010$
Second Moment	$0.0069 \pm 0.0004 \pm 0.0001$	$0.0076 \pm 0.0005 \pm 0.0002$	$0.0070 \pm 0.0005 \pm 0.0002$

Table 44: Differential distribution for wide jet broadening at $\sqrt{s} = 130.1$, 136.1 and 161.3 GeV. The first uncertainty is statistical, the second systematic.

	$\frac{1}{\sigma}\cdot\frac{\mathrm{d}\sigma}{\mathrm{d}B_{\mathrm{W}}}$		
B_{W}	at $\sqrt{s} = 172.3$ GeV	at $\sqrt{s} = 182.8$ GeV	at $\sqrt{s} = 188.6$ GeV
0.000–0.015	$2.337 \pm 0.943 \pm 0.433$	$1.727 \pm 0.262 \pm 1.415$	$2.170 \pm 0.244 \pm 0.237$
0.015–0.030	$15.587 \pm 2.244 \pm 1.365$	$16.496 \pm 0.966 \pm 0.402$	$15.348 \pm 0.587 \pm 0.353$
0.030–0.045	$11.428 \pm 1.577 \pm 0.771$	$12.573 \pm 0.814 \pm 0.592$	$12.889 \pm 0.515 \pm 0.440$
0.045–0.060	$8.594 \pm 1.426 \pm 0.877$	$8.528 \pm 0.663 \pm 0.295$	$8.460 \pm 0.384 \pm 0.198$
0.060–0.075	$8.232 \pm 1.376 \pm 0.656$	$6.961 \pm 0.612 \pm 0.839$	$6.632 \pm 0.343 \pm 0.322$
0.075–0.090	$4.833 \pm 1.082 \pm 0.614$	$4.354 \pm 0.487 \pm 0.238$	$4.898 \pm 0.300 \pm 0.149$
0.090–0.105	$3.079 \pm 0.878 \pm 0.046$	$3.945 \pm 0.467 \pm 0.254$	$3.648 \pm 0.271 \pm 0.184$
0.105–0.120	$2.021 \pm 0.738 \pm 0.457$	$3.230 \pm 0.424 \pm 0.332$	$2.908 \pm 0.239 \pm 0.137$
0.120–0.135	$1.842 \pm 0.698 \pm 0.236$	$1.965 \pm 0.340 \pm 0.133$	$1.899 \pm 0.200 \pm 0.071$
0.135–0.150	$2.506 \pm 0.805 \pm 0.508$	$1.745 \pm 0.327 \pm 0.150$	$1.786 \pm 0.196 \pm 0.072$
0.150–0.165	$2.968 \pm 0.867 \pm 0.767$	$1.325 \pm 0.294 \pm 0.294$	$1.793 \pm 0.209 \pm 0.122$
0.165–0.180	$0.748 \pm 0.501 \pm 0.464$	$1.225 \pm 0.273 \pm 0.136$	$1.156 \pm 0.158 \pm 0.072$
0.180–0.195	$1.099 \pm 0.512 \pm 0.308$	$0.873 \pm 0.244 \pm 0.047$	$0.951 \pm 0.145 \pm 0.143$
0.195–0.210	$0.909 \pm 0.459 \pm 0.246$	$0.584 \pm 0.185 \pm 0.136$	$0.872 \pm 0.135 \pm 0.062$
0.210–0.225	$0.079 \pm 0.203 \pm 0.001$	$0.211 \pm 0.128 \pm 0.015$	$0.375 \pm 0.097 \pm 0.022$
0.225–0.240	$0.000 \pm 0.000 \pm 0.000$	$0.182 \pm 0.116 \pm 0.128$	$0.253 \pm 0.089 \pm 0.108$
0.240–0.255	$0.331 \pm 0.241 \pm 0.052$	$0.568 \pm 0.155 \pm 0.064$	$0.335 \pm 0.087 \pm 0.055$
0.255–0.270	$0.075 \pm 0.113 \pm 0.034$	$0.045 \pm 0.068 \pm 0.089$	$0.110 \pm 0.050 \pm 0.082$
0.270–0.285	$0.000 \pm 0.000 \pm 0.000$	$0.089 \pm 0.055 \pm 0.021$	$0.060 \pm 0.030 \pm 0.003$
0.285–0.300	$0.000 \pm 0.000 \pm 0.000$	$0.039 \pm 0.035 \pm 0.039$	$0.125 \pm 0.050 \pm 0.035$
First Moment	$0.0664 \pm 0.0031 \pm 0.0023$	$0.0654 \pm 0.0015 \pm 0.0010$	$0.0669 \pm 0.0009 \pm 0.0010$
Second Moment	$0.0068 \pm 0.0006 \pm 0.0005$	$0.0067 \pm 0.0003 \pm 0.0002$	$0.0071 \pm 0.0002 \pm 0.0002$

Table 45: Differential distribution for wide jet broadening at $\sqrt{s} = 172.3$, 182.8 and 188.6 GeV. The first uncertainty is statistical, the second systematic.

	$\frac{1}{\sigma}\cdot\frac{\mathrm{d}\sigma}{\mathrm{d}B_{\mathrm{W}}}$		
B_{W}	at $\sqrt{s} = 194.4$ GeV	at $\sqrt{s} = 200.2$ GeV	at $\sqrt{s} = 206.2$ GeV
0.000–0.015	$2.446 \pm 0.261 \pm 0.243$	$3.055 \pm 0.310 \pm 0.216$	$2.690 \pm 0.226 \pm 0.302$
0.015–0.030	$15.023 \pm 0.740 \pm 0.609$	$14.545 \pm 0.722 \pm 0.506$	$14.846 \pm 0.576 \pm 0.679$
0.030–0.045	$12.061 \pm 0.612 \pm 0.394$	$12.038 \pm 0.617 \pm 0.392$	$11.911 \pm 0.476 \pm 0.200$
0.045–0.060	$9.734 \pm 0.555 \pm 0.363$	$8.410 \pm 0.525 \pm 0.354$	$8.842 \pm 0.420 \pm 0.256$
0.060–0.075	$6.486 \pm 0.479 \pm 0.350$	$6.472 \pm 0.474 \pm 0.398$	$6.541 \pm 0.373 \pm 0.340$
0.075–0.090	$4.938 \pm 0.429 \pm 0.287$	$5.464 \pm 0.438 \pm 0.217$	$5.080 \pm 0.329 \pm 0.215$
0.090–0.105	$3.758 \pm 0.389 \pm 0.329$	$3.203 \pm 0.345 \pm 0.267$	$3.618 \pm 0.291 \pm 0.145$
0.105–0.120	$3.145 \pm 0.370 \pm 0.233$	$3.097 \pm 0.345 \pm 0.311$	$3.343 \pm 0.282 \pm 0.124$
0.120–0.135	$2.200 \pm 0.318 \pm 0.282$	$2.536 \pm 0.327 \pm 0.155$	$2.171 \pm 0.240 \pm 0.115$
0.135–0.150	$1.734 \pm 0.289 \pm 0.076$	$2.702 \pm 0.334 \pm 0.255$	$2.000 \pm 0.234 \pm 0.093$
0.150–0.165	$1.585 \pm 0.285 \pm 0.186$	$1.326 \pm 0.259 \pm 0.262$	$1.376 \pm 0.201 \pm 0.326$
0.165–0.180	$0.736 \pm 0.206 \pm 0.130$	$1.051 \pm 0.241 \pm 0.192$	$0.842 \pm 0.174 \pm 0.091$
0.180–0.195	$0.958 \pm 0.211 \pm 0.206$	$0.925 \pm 0.208 \pm 0.148$	$0.800 \pm 0.188 \pm 0.118$
0.195–0.210	$0.576 \pm 0.192 \pm 0.230$	$0.032 \pm 0.009 \pm 0.089$	$0.944 \pm 0.173 \pm 0.098$
0.210–0.225	$0.620 \pm 0.176 \pm 0.112$	$0.595 \pm 0.189 \pm 0.089$	$0.723 \pm 0.163 \pm 0.154$
0.225–0.240	$0.537 \pm 0.153 \pm 0.218$	$0.775 \pm 0.188 \pm 0.140$	$0.384 \pm 0.141 \pm 0.124$
0.240–0.255	$0.000 \pm 0.000 \pm 0.000$	$0.207 \pm 0.121 \pm 0.092$	$0.260 \pm 0.107 \pm 0.016$
0.255–0.270	$0.073 \pm 0.068 \pm 0.075$	$0.199 \pm 0.108 \pm 0.071$	$0.247 \pm 0.082 \pm 0.073$
0.270–0.285	$0.057 \pm 0.043 \pm 0.033$	$0.027 \pm 0.038 \pm 0.006$	$0.019 \pm 0.032 \pm 0.028$
0.285–0.300	$0.000 \pm 0.000 \pm 0.000$	$0.009 \pm 0.023 \pm 0.001$	$0.030 \pm 0.026 \pm 0.023$
First Moment	$0.0663 \pm 0.0014 \pm 0.0016$	$0.0688 \pm 0.0013 \pm 0.0016$	$0.0682 \pm 0.0011 \pm 0.0009$
Second Moment	$0.0069 \pm 0.0003 \pm 0.0003$	$0.0075 \pm 0.0003 \pm 0.0003$	$0.0074 \pm 0.0003 \pm 0.0001$

Table 46: Differential distribution for wide jet broadening at $\sqrt{s} = 194.4$, 200.2 and 206.2 GeV. The first uncertainty is statistical, the second systematic.

	$\frac{1}{\sigma} \cdot \frac{\mathrm{d}\sigma}{\mathrm{d}C}$		
C	at $\sqrt{s} = 130.1$ GeV	at $\sqrt{s} = 136.1$ GeV	at $\sqrt{s} = 161.3$ GeV
0.000–0.050	$0.632 \pm 0.166 \pm 0.176$	$0.637 \pm 0.282 \pm 0.197$	$2.593 \pm 0.480 \pm 0.143$
0.050–0.100	$4.864 \pm 0.497 \pm 0.412$	$5.005 \pm 0.591 \pm 0.212$	$5.547 \pm 0.664 \pm 0.335$
0.100–0.150	$3.906 \pm 0.392 \pm 0.128$	$3.858 \pm 0.459 \pm 0.291$	$2.821 \pm 0.408 \pm 0.277$
0.150–0.200	$2.657 \pm 0.315 \pm 0.153$	$3.039 \pm 0.394 \pm 0.283$	$1.867 \pm 0.299 \pm 0.085$
0.200–0.250	$1.554 \pm 0.242 \pm 0.104$	$1.056 \pm 0.239 \pm 0.059$	$1.112 \pm 0.227 \pm 0.035$
0.250–0.300	$1.481 \pm 0.239 \pm 0.088$	$1.202 \pm 0.256 \pm 0.079$	$1.046 \pm 0.225 \pm 0.084$
0.300–0.350	$0.901 \pm 0.178 \pm 0.090$	$0.721 \pm 0.199 \pm 0.084$	$0.923 \pm 0.210 \pm 0.079$
0.350–0.400	$0.604 \pm 0.140 \pm 0.079$	$0.641 \pm 0.181 \pm 0.033$	$1.038 \pm 0.221 \pm 0.066$
0.400–0.450	$1.040 \pm 0.192 \pm 0.144$	$0.839 \pm 0.206 \pm 0.027$	$0.572 \pm 0.167 \pm 0.025$
0.450–0.500	$0.530 \pm 0.128 \pm 0.011$	$0.446 \pm 0.147 \pm 0.026$	$0.562 \pm 0.160 \pm 0.058$
0.500–0.550	$0.461 \pm 0.118 \pm 0.012$	$0.505 \pm 0.155 \pm 0.091$	$0.466 \pm 0.147 \pm 0.025$
0.550–0.600	$0.334 \pm 0.097 \pm 0.061$	$0.497 \pm 0.144 \pm 0.084$	$0.256 \pm 0.118 \pm 0.036$
0.600–0.650	$0.180 \pm 0.071 \pm 0.029$	$0.418 \pm 0.137 \pm 0.109$	$0.480 \pm 0.145 \pm 0.014$
0.650–0.700	$0.261 \pm 0.076 \pm 0.014$	$0.452 \pm 0.122 \pm 0.016$	$0.352 \pm 0.122 \pm 0.037$
0.700–0.750	$0.313 \pm 0.086 \pm 0.033$	$0.241 \pm 0.087 \pm 0.004$	$0.148 \pm 0.080 \pm 0.021$
0.750–0.800	$0.147 \pm 0.062 \pm 0.039$	$0.169 \pm 0.071 \pm 0.045$	$0.191 \pm 0.089 \pm 0.043$
0.800–0.850	$0.053 \pm 0.038 \pm 0.001$	$0.095 \pm 0.062 \pm 0.041$	$0.024 \pm 0.054 \pm 0.007$
0.850–0.900	$0.040 \pm 0.029 \pm 0.010$	$0.157 \pm 0.066 \pm 0.061$	$0.003 \pm 0.032 \pm 0.003$
0.900–0.950	$0.000 \pm 0.000 \pm 0.000$	$0.022 \pm 0.022 \pm 0.016$	$0.000 \pm 0.000 \pm 0.000$
0.950–1.000	$0.040 \pm 0.040 \pm 0.023$	$0.000 \pm 0.000 \pm 0.000$	$0.000 \pm 0.000 \pm 0.000$
First Moment	$0.2277 \pm 0.0072 \pm 0.0053$	$0.2357 \pm 0.0089 \pm 0.0039$	$0.2052 \pm 0.0098 \pm 0.0028$
Second Moment	$0.0848 \pm 0.0050 \pm 0.0027$	$0.0938 \pm 0.0064 \pm 0.0018$	$0.0757 \pm 0.0064 \pm 0.0019$

Table 47: Differential distribution for C-parameter at $\sqrt{s} = 130.1$, 136.1 and 161.3 GeV. The first uncertainty is statistical, the second systematic.

	$\frac{1}{\sigma} \cdot \frac{\mathrm{d}\sigma}{\mathrm{d}C}$		
C	at $\sqrt{s} = 172.3$ GeV	at $\sqrt{s} = 182.8$ GeV	at $\sqrt{s} = 188.6$ GeV
0.000–0.050	$2.733 \pm 0.577 \pm 0.389$	$1.563 \pm 0.154 \pm 0.525$	$1.916 \pm 0.123 \pm 0.101$
0.050–0.100	$4.694 \pm 0.675 \pm 0.351$	$5.526 \pm 0.302 \pm 0.160$	$4.844 \pm 0.182 \pm 0.142$
0.100–0.150	$2.475 \pm 0.408 \pm 0.412$	$3.047 \pm 0.220 \pm 0.147$	$3.358 \pm 0.139 \pm 0.076$
0.150–0.200	$2.200 \pm 0.355 \pm 0.134$	$2.202 \pm 0.185 \pm 0.251$	$2.016 \pm 0.102 \pm 0.063$
0.200–0.250	$1.665 \pm 0.320 \pm 0.207$	$1.469 \pm 0.151 \pm 0.072$	$1.557 \pm 0.090 \pm 0.038$
0.250–0.300	$0.991 \pm 0.250 \pm 0.056$	$1.274 \pm 0.140 \pm 0.107$	$1.268 \pm 0.082 \pm 0.041$
0.300–0.350	$0.897 \pm 0.238 \pm 0.155$	$1.049 \pm 0.131 \pm 0.098$	$1.073 \pm 0.077 \pm 0.058$
0.350–0.400	$0.784 \pm 0.229 \pm 0.144$	$0.624 \pm 0.100 \pm 0.026$	$0.794 \pm 0.066 \pm 0.019$
0.400–0.450	$0.446 \pm 0.178 \pm 0.067$	$0.730 \pm 0.108 \pm 0.074$	$0.563 \pm 0.056 \pm 0.018$
0.450–0.500	$0.599 \pm 0.202 \pm 0.078$	$0.607 \pm 0.098 \pm 0.047$	$0.522 \pm 0.055 \pm 0.012$
0.500–0.550	$0.563 \pm 0.194 \pm 0.112$	$0.377 \pm 0.080 \pm 0.066$	$0.553 \pm 0.056 \pm 0.054$
0.550–0.600	$0.166 \pm 0.131 \pm 0.019$	$0.400 \pm 0.085 \pm 0.006$	$0.387 \pm 0.048 \pm 0.027$
0.600–0.650	$0.475 \pm 0.170 \pm 0.056$	$0.241 \pm 0.068 \pm 0.092$	$0.401 \pm 0.048 \pm 0.033$
0.650–0.700	$0.169 \pm 0.117 \pm 0.066$	$0.225 \pm 0.061 \pm 0.007$	$0.330 \pm 0.046 \pm 0.047$
0.700–0.750	$0.060 \pm 0.087 \pm 0.028$	$0.333 \pm 0.078 \pm 0.042$	$0.254 \pm 0.049 \pm 0.044$
0.750–0.800	$0.344 \pm 0.170 \pm 0.131$	$0.231 \pm 0.099 \pm 0.038$	$0.111 \pm 0.065 \pm 0.031$
0.800–0.850	$0.533 \pm 0.291 \pm 0.246$	$0.039 \pm 0.072 \pm 0.001$	$0.030 \pm 0.044 \pm 0.044$
0.850–0.900	$0.086 \pm 0.130 \pm 0.070$	$0.064 \pm 0.059 \pm 0.065$	$0.024 \pm 0.030 \pm 0.050$
0.900–0.950	$0.123 \pm 0.130 \pm 0.068$	$0.000 \pm 0.000 \pm 0.000$	$0.000 \pm 0.000 \pm 0.000$
0.950–1.000	$0.000 \pm 0.000 \pm 0.000$	$0.000 \pm 0.000 \pm 0.000$	$0.002 \pm 0.003 \pm 0.001$
First Moment	$0.2281 \pm 0.0159 \pm 0.0033$	$0.2157 \pm 0.0063 \pm 0.0073$	$0.2160 \pm 0.0040 \pm 0.0041$
Second Moment	$0.0979 \pm 0.0133 \pm 0.0029$	$0.0804 \pm 0.0051 \pm 0.0032$	$0.0795 \pm 0.0032 \pm 0.0038$

Table 48: Differential distribution for C-parameter at $\sqrt{s} = 172.3$, 182.8 and 188.6 GeV. The first uncertainty is statistical, the second systematic.

	$\frac{1}{\sigma} \cdot \frac{\mathrm{d}\sigma}{\mathrm{d}C}$		
C	at $\sqrt{s} = 194.4$ GeV	at $\sqrt{s} = 200.2$ GeV	at $\sqrt{s} = 206.2$ GeV
0.000–0.050	$1.858 \pm 0.135 \pm 0.073$	$2.208 \pm 0.152 \pm 0.105$	$2.178 \pm 0.117 \pm 0.121$
0.050–0.100	$5.000 \pm 0.231 \pm 0.163$	$4.622 \pm 0.219 \pm 0.135$	$4.801 \pm 0.174 \pm 0.130$
0.100–0.150	$3.191 \pm 0.170 \pm 0.109$	$2.911 \pm 0.166 \pm 0.047$	$2.831 \pm 0.128 \pm 0.046$
0.150–0.200	$2.004 \pm 0.139 \pm 0.067$	$2.069 \pm 0.140 \pm 0.068$	$2.178 \pm 0.112 \pm 0.134$
0.200–0.250	$1.657 \pm 0.128 \pm 0.053$	$1.690 \pm 0.130 \pm 0.092$	$1.636 \pm 0.098 \pm 0.065$
0.250–0.300	$1.339 \pm 0.123 \pm 0.095$	$1.093 \pm 0.108 \pm 0.075$	$1.217 \pm 0.086 \pm 0.052$
0.300–0.350	$0.954 \pm 0.102 \pm 0.102$	$0.943 \pm 0.099 \pm 0.084$	$0.934 \pm 0.077 \pm 0.022$
0.350–0.400	$0.871 \pm 0.099 \pm 0.047$	$0.865 \pm 0.097 \pm 0.050$	$0.845 \pm 0.074 \pm 0.030$
0.400–0.450	$0.624 \pm 0.088 \pm 0.048$	$0.650 \pm 0.084 \pm 0.070$	$0.687 \pm 0.068 \pm 0.063$
0.450–0.500	$0.675 \pm 0.096 \pm 0.072$	$0.632 \pm 0.083 \pm 0.066$	$0.483 \pm 0.060 \pm 0.034$
0.500–0.550	$0.351 \pm 0.069 \pm 0.036$	$0.609 \pm 0.087 \pm 0.068$	$0.475 \pm 0.061 \pm 0.055$
0.550–0.600	$0.326 \pm 0.066 \pm 0.034$	$0.460 \pm 0.079 \pm 0.038$	$0.452 \pm 0.059 \pm 0.034$
0.600–0.650	$0.287 \pm 0.068 \pm 0.040$	$0.308 \pm 0.069 \pm 0.026$	$0.445 \pm 0.060 \pm 0.060$
0.650–0.700	$0.407 \pm 0.072 \pm 0.031$	$0.323 \pm 0.072 \pm 0.040$	$0.352 \pm 0.065 \pm 0.025$
0.700–0.750	$0.369 \pm 0.108 \pm 0.072$	$0.448 \pm 0.105 \pm 0.095$	$0.285 \pm 0.083 \pm 0.056$
0.750–0.800	$0.036 \pm 0.056 \pm 0.004$	$0.163 \pm 0.113 \pm 0.119$	$0.152 \pm 0.091 \pm 0.051$
0.800–0.850	$0.030 \pm 0.032 \pm 0.018$	$0.000 \pm 0.000 \pm 0.000$	$0.050 \pm 0.039 \pm 0.113$
0.850–0.900	$0.018 \pm 0.034 \pm 0.011$	$0.000 \pm 0.000 \pm 0.000$	$0.000 \pm 0.000 \pm 0.000$
0.900–0.950	$0.004 \pm 0.013 \pm 0.003$	$0.000 \pm 0.000 \pm 0.000$	$0.000 \pm 0.000 \pm 0.000$
0.950–1.000	$0.000 \pm 0.000 \pm 0.000$	$0.005 \pm 0.007 \pm 0.008$	$0.000 \pm 0.000 \pm 0.000$
First Moment	$0.2158 \pm 0.0058 \pm 0.0039$	$0.2244 \pm 0.0059 \pm 0.0068$	$0.2195 \pm 0.0049 \pm 0.0035$
Second Moment	$0.0778 \pm 0.0045 \pm 0.0025$	$0.0864 \pm 0.0049 \pm 0.0048$	$0.0828 \pm 0.0040 \pm 0.0033$

Table 49: Differential distribution for C-parameter at $\sqrt{s} = 194.4$, 200.2 and 206.2 GeV. The first uncertainty is statistical, the second systematic.

	$\frac{1}{\sigma}\cdot\frac{\mathrm{d}\sigma}{\mathrm{d}D}$		
D	at $\sqrt{s} = 130.1$ GeV	at $\sqrt{s} = 136.1$ GeV	at $\sqrt{s} = 161.3$ GeV
0.000–0.016	$32.260 \pm 2.111 \pm 1.450$	$33.049 \pm 2.488 \pm 1.294$	$36.816 \pm 2.836 \pm 0.746$
0.016–0.032	$10.027 \pm 1.099 \pm 0.838$	$10.402 \pm 1.287 \pm 0.562$	$6.917 \pm 1.016 \pm 0.324$
0.032–0.048	$5.896 \pm 0.823 \pm 0.158$	$4.132 \pm 0.828 \pm 0.220$	$4.376 \pm 0.799 \pm 0.480$
0.048–0.064	$3.080 \pm 0.559 \pm 0.198$	$3.099 \pm 0.675 \pm 0.110$	$4.035 \pm 0.753 \pm 0.151$
0.064–0.080	$2.224 \pm 0.461 \pm 0.109$	$1.323 \pm 0.443 \pm 0.088$	$3.172 \pm 0.652 \pm 0.351$
0.080–0.096	$1.449 \pm 0.366 \pm 0.093$	$1.266 \pm 0.467 \pm 0.098$	$1.368 \pm 0.443 \pm 0.062$
0.096–0.112	$1.330 \pm 0.371 \pm 0.239$	$1.077 \pm 0.388 \pm 0.010$	$1.078 \pm 0.392 \pm 0.278$
0.112–0.128	$1.443 \pm 0.375 \pm 0.269$	$1.308 \pm 0.418 \pm 0.118$	$0.572 \pm 0.300 \pm 0.048$
0.128–0.144	$0.531 \pm 0.233 \pm 0.145$	$0.726 \pm 0.346 \pm 0.141$	$0.567 \pm 0.293 \pm 0.038$
0.144–0.160	$0.842 \pm 0.311 \pm 0.222$	$0.271 \pm 0.202 \pm 0.041$	$0.918 \pm 0.349 \pm 0.121$
0.160–0.176	$1.038 \pm 0.343 \pm 0.197$	$0.217 \pm 0.153 \pm 0.011$	$0.200 \pm 0.183 \pm 0.012$
0.176–0.192	$0.397 \pm 0.175 \pm 0.018$	$0.278 \pm 0.197 \pm 0.002$	$0.340 \pm 0.237 \pm 0.112$
0.192–0.208	$0.276 \pm 0.163 \pm 0.001$	$0.000 \pm 0.000 \pm 0.000$	$0.000 \pm 0.000 \pm 0.000$
0.208–0.224	$0.070 \pm 0.070 \pm 0.028$	$0.358 \pm 0.231 \pm 0.094$	$0.263 \pm 0.214 \pm 0.063$
0.224–0.240	$0.080 \pm 0.080 \pm 0.001$	$0.648 \pm 0.291 \pm 0.057$	$0.355 \pm 0.227 \pm 0.206$
0.240–0.256	$0.396 \pm 0.183 \pm 0.029$	$1.048 \pm 0.389 \pm 0.326$	$0.130 \pm 0.168 \pm 0.011$
0.256–0.272	$0.207 \pm 0.147 \pm 0.053$	$0.087 \pm 0.087 \pm 0.001$	$0.169 \pm 0.182 \pm 0.087$
0.272–0.288	$0.165 \pm 0.117 \pm 0.094$	$0.487 \pm 0.253 \pm 0.077$	$0.150 \pm 0.162 \pm 0.008$
0.288–0.304	$0.000 \pm 0.000 \pm 0.000$	$0.249 \pm 0.181 \pm 0.048$	$0.000 \pm 0.000 \pm 0.000$
0.304–0.320	$0.155 \pm 0.116 \pm 0.068$	$0.000 \pm 0.000 \pm 0.000$	$0.171 \pm 0.172 \pm 0.008$
0.320–0.336	$0.000 \pm 0.000 \pm 0.000$	$0.214 \pm 0.163 \pm 0.117$	$0.000 \pm 0.000 \pm 0.000$
0.336–0.352	$0.135 \pm 0.096 \pm 0.069$	$0.000 \pm 0.000 \pm 0.000$	$0.000 \pm 0.000 \pm 0.000$
0.352–0.368	$0.000 \pm 0.000 \pm 0.000$	$0.477 \pm 0.337 \pm 0.187$	$0.319 \pm 0.215 \pm 0.188$
0.368–0.384	$0.188 \pm 0.134 \pm 0.121$	$0.000 \pm 0.000 \pm 0.000$	$0.000 \pm 0.000 \pm 0.000$
0.384–0.400	$0.000 \pm 0.000 \pm 0.000$	$0.229 \pm 0.229 \pm 0.106$	$0.000 \pm 0.000 \pm 0.000$
First Moment	$0.0404 \pm 0.0024 \pm 0.0007$	$0.0566 \pm 0.0052 \pm 0.0017$	$0.0390 \pm 0.0038 \pm 0.0009$
Second Moment	$0.0051 \pm 0.0016 \pm 0.0001$	$0.0138 \pm 0.0025 \pm 0.0006$	$0.0066 \pm 0.0017 \pm 0.0002$

Table 50: Differential distribution for D-parameter at $\sqrt{s} = 130.1$, 136.1 and 161.3 GeV. The first uncertainty is statistical, the second systematic.

	$\frac{1}{\sigma} \cdot \frac{\mathrm{d}\sigma}{\mathrm{d}D}$		
D	at $\sqrt{s} = 172.3$ GeV	at $\sqrt{s} = 182.8$ GeV	at $\sqrt{s} = 188.6$ GeV
0.000–0.016	$32.580 \pm 2.939 \pm 1.329$	$33.692 \pm 1.281 \pm 1.815$	$34.263 \pm 0.826 \pm 0.524$
0.016–0.032	$8.480 \pm 1.241 \pm 0.554$	$9.029 \pm 0.643 \pm 0.532$	$8.535 \pm 0.361 \pm 0.229$
0.032–0.048	$4.472 \pm 0.894 \pm 0.151$	$5.082 \pm 0.476 \pm 0.390$	$5.421 \pm 0.286 \pm 0.105$
0.048–0.064	$3.290 \pm 0.781 \pm 0.075$	$3.314 \pm 0.391 \pm 0.301$	$3.062 \pm 0.219 \pm 0.179$
0.064–0.080	$0.910 \pm 0.429 \pm 0.013$	$2.181 \pm 0.328 \pm 0.094$	$2.086 \pm 0.191 \pm 0.161$
0.080–0.096	$2.109 \pm 0.625 \pm 0.437$	$1.622 \pm 0.293 \pm 0.250$	$1.662 \pm 0.173 \pm 0.124$
0.096–0.112	$1.199 \pm 0.473 \pm 0.156$	$1.212 \pm 0.266 \pm 0.253$	$1.337 \pm 0.168 \pm 0.083$
0.112–0.128	$0.448 \pm 0.345 \pm 0.208$	$0.720 \pm 0.217 \pm 0.020$	$1.203 \pm 0.168 \pm 0.195$
0.128–0.144	$0.453 \pm 0.341 \pm 0.271$	$1.090 \pm 0.266 \pm 0.029$	$0.851 \pm 0.149 \pm 0.062$
0.144–0.160	$1.296 \pm 0.539 \pm 0.316$	$0.370 \pm 0.184 \pm 0.024$	$0.405 \pm 0.120 \pm 0.005$
0.160–0.176	$0.171 \pm 0.257 \pm 0.003$	$0.999 \pm 0.259 \pm 0.191$	$0.721 \pm 0.144 \pm 0.128$
0.176–0.192	$0.207 \pm 0.271 \pm 0.198$	$0.239 \pm 0.172 \pm 0.111$	$0.643 \pm 0.149 \pm 0.189$
0.192–0.208	$0.605 \pm 0.394 \pm 0.075$	$0.082 \pm 0.147 \pm 0.001$	$0.359 \pm 0.120 \pm 0.064$
0.208–0.224	$0.290 \pm 0.336 \pm 0.082$	$0.243 \pm 0.171 \pm 0.226$	$0.352 \pm 0.117 \pm 0.056$
0.224–0.240	$0.055 \pm 0.186 \pm 0.105$	$0.088 \pm 0.155 \pm 0.116$	$0.132 \pm 0.105 \pm 0.135$
0.240–0.256	$0.495 \pm 0.366 \pm 0.216$	$0.311 \pm 0.188 \pm 0.084$	$0.012 \pm 0.070 \pm 0.124$
0.256–0.272	$0.273 \pm 0.289 \pm 0.122$	$0.146 \pm 0.176 \pm 0.061$	$0.341 \pm 0.137 \pm 0.143$
0.272–0.288	$0.124 \pm 0.274 \pm 0.191$	$0.237 \pm 0.183 \pm 0.068$	$0.104 \pm 0.089 \pm 0.008$
0.288–0.304	$0.127 \pm 0.238 \pm 0.002$	$0.165 \pm 0.163 \pm 0.234$	$0.028 \pm 0.089 \pm 0.019$
0.304–0.320	$0.765 \pm 0.516 \pm 0.139$	$0.006 \pm 0.119 \pm 0.000$	$0.204 \pm 0.113 \pm 0.002$
0.320–0.336	$0.000 \pm 0.000 \pm 0.000$	$0.035 \pm 0.122 \pm 0.039$	$0.101 \pm 0.094 \pm 0.049$
0.336–0.352	$0.000 \pm 0.000 \pm 0.000$	$0.031 \pm 0.129 \pm 0.036$	$0.000 \pm 0.000 \pm 0.000$
0.352–0.368	$0.000 \pm 0.000 \pm 0.000$	$0.604 \pm 0.258 \pm 0.161$	$0.000 \pm 0.000 \pm 0.000$
0.368–0.384	$0.000 \pm 0.000 \pm 0.000$	$0.000 \pm 0.000 \pm 0.000$	$0.240 \pm 0.109 \pm 0.080$
0.384–0.400	$0.318 \pm 0.406 \pm 0.115$	$0.168 \pm 0.158 \pm 0.100$	$0.066 \pm 0.077 \pm 0.013$
First Moment	$0.0752 \pm 0.0119 \pm 0.0075$	$0.0457 \pm 0.0037 \pm 0.0059$	$0.0415 \pm 0.0020 \pm 0.0028$
Second Moment	$0.0277 \pm 0.0072 \pm 0.0014$	$0.0089 \pm 0.0018 \pm 0.0035$	$0.0067 \pm 0.0009 \pm 0.0017$

Table 51: Differential distribution for D-parameter at $\sqrt{s} = 172.3$, 182.8 and 188.6 GeV. The first uncertainty is statistical, the second systematic.

	$\frac{1}{\sigma}\cdot\frac{\mathrm{d}\sigma}{\mathrm{d}D}$		
D	at $\sqrt{s} = 194.4$ GeV	at $\sqrt{s} = 200.2$ GeV	at $\sqrt{s} = 206.2$ GeV
0.000–0.016	$34.894 \pm 1.033 \pm 0.772$	$33.486 \pm 1.015 \pm 0.586$	$33.974 \pm 0.795 \pm 0.595$
0.016–0.032	$9.195 \pm 0.517 \pm 0.296$	$9.230 \pm 0.510 \pm 0.537$	$8.981 \pm 0.387 \pm 0.218$
0.032–0.048	$4.744 \pm 0.377 \pm 0.218$	$4.744 \pm 0.417 \pm 0.340$	$4.963 \pm 0.293 \pm 0.128$
0.048–0.064	$3.568 \pm 0.341 \pm 0.159$	$3.175 \pm 0.319 \pm 0.137$	$2.969 \pm 0.241 \pm 0.132$
0.064–0.080	$1.975 \pm 0.284 \pm 0.198$	$2.321 \pm 0.288 \pm 0.147$	$2.618 \pm 0.239 \pm 0.096$
0.080–0.096	$1.683 \pm 0.274 \pm 0.327$	$2.172 \pm 0.281 \pm 0.108$	$1.530 \pm 0.210 \pm 0.130$
0.096–0.112	$1.633 \pm 0.295 \pm 0.228$	$1.350 \pm 0.257 \pm 0.120$	$1.647 \pm 0.221 \pm 0.137$
0.112–0.128	$1.086 \pm 0.255 \pm 0.099$	$0.860 \pm 0.261 \pm 0.362$	$0.923 \pm 0.179 \pm 0.107$
0.128–0.144	$0.961 \pm 0.254 \pm 0.181$	$0.742 \pm 0.222 \pm 0.152$	$1.093 \pm 0.206 \pm 0.154$
0.144–0.160	$0.469 \pm 0.215 \pm 0.232$	$0.855 \pm 0.244 \pm 0.175$	$0.526 \pm 0.172 \pm 0.091$
0.160–0.176	$0.437 \pm 0.231 \pm 0.175$	$0.712 \pm 0.224 \pm 0.145$	$0.499 \pm 0.170 \pm 0.088$
0.176–0.192	$0.295 \pm 0.208 \pm 0.123$	$0.855 \pm 0.273 \pm 0.138$	$0.667 \pm 0.189 \pm 0.145$
0.192–0.208	$0.171 \pm 0.167 \pm 0.057$	$0.418 \pm 0.204 \pm 0.146$	$0.234 \pm 0.156 \pm 0.080$
0.208–0.224	$0.288 \pm 0.183 \pm 0.071$	$0.308 \pm 0.215 \pm 0.101$	$0.547 \pm 0.187 \pm 0.163$
0.224–0.240	$0.418 \pm 0.206 \pm 0.125$	$0.215 \pm 0.169 \pm 0.141$	$0.337 \pm 0.167 \pm 0.085$
0.240–0.256	$0.045 \pm 0.134 \pm 0.212$	$0.461 \pm 0.221 \pm 0.170$	$0.301 \pm 0.157 \pm 0.137$
0.256–0.272	$0.266 \pm 0.171 \pm 0.109$	$0.018 \pm 0.025 \pm 0.188$	$0.000 \pm 0.000 \pm 0.000$
0.272–0.288	$0.000 \pm 0.000 \pm 0.000$	$0.000 \pm 0.000 \pm 0.000$	$0.057 \pm 0.128 \pm 0.103$
0.288–0.304	$0.000 \pm 0.000 \pm 0.000$	$0.098 \pm 0.144 \pm 0.032$	$0.045 \pm 0.108 \pm 0.044$
0.304–0.320	$0.036 \pm 0.104 \pm 0.026$	$0.000 \pm 0.000 \pm 0.000$	$0.124 \pm 0.117 \pm 0.078$
0.320–0.336	$0.022 \pm 0.060 \pm 0.059$	$0.149 \pm 0.147 \pm 0.102$	$0.148 \pm 0.115 \pm 0.100$
0.336–0.352	$0.074 \pm 0.103 \pm 0.024$	$0.054 \pm 0.112 \pm 0.113$	$0.018 \pm 0.017 \pm 0.059$
0.352–0.368	$0.000 \pm 0.000 \pm 0.000$	$0.048 \pm 0.075 \pm 0.038$	$0.000 \pm 0.000 \pm 0.000$
0.368–0.384	$0.000 \pm 0.000 \pm 0.000$	$0.025 \pm 0.093 \pm 0.010$	$0.000 \pm 0.000 \pm 0.000$
0.384–0.400	$0.039 \pm 0.046 \pm 0.086$	$0.000 \pm 0.000 \pm 0.000$	$0.000 \pm 0.000 \pm 0.000$
First Moment	$0.0387 \pm 0.0023 \pm 0.0047$	$0.0435 \pm 0.0028 \pm 0.0037$	$0.0429 \pm 0.0029 \pm 0.0033$
Second Moment	$0.0056 \pm 0.0010 \pm 0.0016$	$0.0064 \pm 0.0010 \pm 0.0021$	$0.0064 \pm 0.0012 \pm 0.0020$

Table 52: Differential distribution for D-parameter at $\sqrt{s} = 194.4$, 200.2 and 206.2 GeV. The first uncertainty is statistical, the second systematic.

T	$\frac{1}{\sigma}\cdot\frac{\mathrm{d}\sigma}{\mathrm{d}T}$ (udsc)	$\frac{1}{\sigma}\cdot\frac{\mathrm{d}\sigma}{\mathrm{d}T}$ (b)
0.575–0.600	0.001 ± 0.000 ± 0.000	0.001 ± 0.000 ± 0.001
0.600–0.625	0.008 ± 0.000 ± 0.002	0.005 ± 0.001 ± 0.001
0.625–0.650	0.025 ± 0.001 ± 0.001	0.034 ± 0.002 ± 0.002
0.650–0.675	0.085 ± 0.002 ± 0.007	0.089 ± 0.004 ± 0.008
0.675–0.700	0.155 ± 0.003 ± 0.003	0.166 ± 0.007 ± 0.006
0.700–0.725	0.237 ± 0.003 ± 0.005	0.250 ± 0.008 ± 0.011
0.725–0.750	0.339 ± 0.004 ± 0.006	0.342 ± 0.009 ± 0.010
0.750–0.775	0.477 ± 0.005 ± 0.011	0.488 ± 0.011 ± 0.012
0.775–0.800	0.627 ± 0.005 ± 0.013	0.643 ± 0.013 ± 0.015
0.800–0.825	0.838 ± 0.006 ± 0.014	0.859 ± 0.014 ± 0.018
0.825–0.850	1.169 ± 0.008 ± 0.020	1.195 ± 0.017 ± 0.026
0.850–0.875	1.598 ± 0.009 ± 0.042	1.737 ± 0.020 ± 0.046
0.875–0.900	2.329 ± 0.010 ± 0.038	2.442 ± 0.022 ± 0.049
0.900–0.925	3.614 ± 0.012 ± 0.059	3.855 ± 0.025 ± 0.081
0.925–0.950	6.186 ± 0.014 ± 0.101	6.564 ± 0.029 ± 0.131
0.950–0.975	12.801 ± 0.029 ± 0.210	13.475 ± 0.064 ± 0.268
0.975–1.000	9.513 ± 0.017 ± 0.156	7.855 ± 0.027 ± 0.186
First Moment	0.93441 ±0.00007± 0.00053	0.93174 ±0.00014± 0.00077
Second Moment	0.87680 ±0.00013± 0.00106	0.87181 ±0.00028± 0.00155

Table 53: Differential distribution for event thrust at $\sqrt{s} = 91.2$ GeV for udsc and b events. The first uncertainty is statistical, the second systematic.

ρ_{H}	$\frac{1}{\sigma}\cdot\frac{\mathrm{d}\sigma}{\mathrm{d}\rho_{\mathrm{H}}}$ (udsc)	$\frac{1}{\sigma}\cdot\frac{\mathrm{d}\sigma}{\mathrm{d}\rho_{\mathrm{H}}}$ (b)
0.000–0.015	7.432 ± 0.014 ± 0.157	6.126 ± 0.021 ± 0.171
0.015–0.030	21.946 ± 0.052 ± 0.788	22.363 ± 0.108 ± 0.866
0.030–0.045	11.890 ± 0.028 ± 0.555	11.945 ± 0.055 ± 0.561
0.045–0.060	7.033 ± 0.023 ± 0.193	7.214 ± 0.048 ± 0.216
0.060–0.075	4.595 ± 0.020 ± 0.097	4.824 ± 0.042 ± 0.118
0.075–0.090	3.279 ± 0.017 ± 0.069	3.508 ± 0.039 ± 0.086
0.090–0.105	2.433 ± 0.015 ± 0.051	2.478 ± 0.033 ± 0.061
0.105–0.120	1.890 ± 0.013 ± 0.045	1.950 ± 0.030 ± 0.051
0.120–0.135	1.445 ± 0.012 ± 0.031	1.422 ± 0.025 ± 0.035
0.135–0.150	1.105 ± 0.010 ± 0.023	1.196 ± 0.024 ± 0.029
0.150–0.165	0.917 ± 0.009 ± 0.021	0.866 ± 0.020 ± 0.022
0.165–0.180	0.689 ± 0.008 ± 0.015	0.727 ± 0.018 ± 0.018
0.180–0.195	0.550 ± 0.007 ± 0.012	0.564 ± 0.017 ± 0.014
0.195–0.210	0.425 ± 0.006 ± 0.009	0.424 ± 0.014 ± 0.010
0.210–0.225	0.320 ± 0.005 ± 0.007	0.339 ± 0.013 ± 0.008
0.225–0.240	0.256 ± 0.005 ± 0.005	0.235 ± 0.010 ± 0.006
0.240–0.255	0.183 ± 0.004 ± 0.004	0.192 ± 0.009 ± 0.005
0.255–0.270	0.133 ± 0.003 ± 0.003	0.131 ± 0.007 ± 0.004
0.270–0.285	0.086 ± 0.003 ± 0.004	0.108 ± 0.007 ± 0.008
0.285–0.300	0.059 ± 0.002 ± 0.002	0.055 ± 0.004 ± 0.002
First Moment	0.05160 ±0.00005± 0.00035	0.05270 ±0.00012± 0.00058
Second Moment	0.00487 ±0.00001± 0.00004	0.00499 ±0.00002± 0.00008

Table 54: Differential distribution for scaled heavy jet mass at $\sqrt{s} = 91.2$ GeV for udsc and b events. The first uncertainty is statistical, the second systematic.

B_{T}	$\frac{1}{\sigma}\cdot\frac{\mathrm{d}\sigma}{\mathrm{d}B_{\mathrm{T}}}$ (udsc)	$\frac{1}{\sigma}\cdot\frac{\mathrm{d}\sigma}{\mathrm{d}B_{\mathrm{T}}}$ (b)
0.000–0.020	0.003 ± 0.000 ± 0.014	0.000 ± 0.000 ± 0.000
0.020–0.040	1.588 ± 0.005 ± 0.811	0.009 ± 0.000 ± 0.001
0.040–0.060	10.151 ± 0.029 ± 0.533	3.093 ± 0.019 ± 0.175
0.060–0.080	9.728 ± 0.025 ± 0.511	13.369 ± 0.070 ± 0.508
0.080–0.100	7.282 ± 0.020 ± 0.383	9.338 ± 0.045 ± 0.209
0.100–0.120	5.438 ± 0.017 ± 0.286	6.565 ± 0.038 ± 0.147
0.120–0.140	4.060 ± 0.015 ± 0.213	4.616 ± 0.033 ± 0.103
0.140–0.160	3.033 ± 0.013 ± 0.159	3.445 ± 0.031 ± 0.077
0.160–0.180	2.313 ± 0.012 ± 0.121	2.624 ± 0.027 ± 0.059
0.180–0.200	1.778 ± 0.010 ± 0.093	2.012 ± 0.025 ± 0.045
0.200–0.220	1.396 ± 0.009 ± 0.073	1.511 ± 0.021 ± 0.034
0.220–0.240	1.046 ± 0.008 ± 0.055	1.104 ± 0.018 ± 0.025
0.240–0.260	0.812 ± 0.007 ± 0.043	0.831 ± 0.016 ± 0.023
0.260–0.280	0.580 ± 0.006 ± 0.031	0.659 ± 0.015 ± 0.018
0.280–0.300	0.413 ± 0.005 ± 0.022	0.415 ± 0.011 ± 0.016
0.300–0.320	0.233 ± 0.003 ± 0.012	0.248 ± 0.009 ± 0.013
0.320–0.340	0.105 ± 0.002 ± 0.005	0.126 ± 0.005 ± 0.008
0.340–0.360	0.034 ± 0.001 ± 0.006	0.033 ± 0.002 ± 0.005
0.360–0.380	0.009 ± 0.000 ± 0.002	0.003 ± 0.000 ± 0.002
0.380–0.400	0.000 ± 0.000 ± 0.000	0.001 ± 0.002 ± 0.001
First Moment	0.10677 ±0.00007± 0.00070	0.11614 ±0.00014± 0.00088
Second Moment	0.01502 ±0.00002± 0.00016	0.01669 ±0.00004± 0.00021

Table 55: Differential distribution for total jet broadening at $\sqrt{s} = 91.2$ GeV for udsc and b events. The first uncertainty is statistical, the second systematic.

B_{W}	$\frac{1}{\sigma}\cdot\frac{\mathrm{d}\sigma}{\mathrm{d}B_{\mathrm{W}}}$ (udsc)	$\frac{1}{\sigma}\cdot\frac{\mathrm{d}\sigma}{\mathrm{d}B_{\mathrm{W}}}$ (b)
0.000–0.015	0.043 ± 0.000 ± 0.173	0.000 ± 0.000 ± 0.000
0.015–0.030	9.367 ± 0.028 ± 0.253	1.734 ± 0.009 ± 0.084
0.030–0.045	15.028 ± 0.040 ± 0.411	19.779 ± 0.107 ± 0.815
0.045–0.060	10.693 ± 0.027 ± 0.338	12.239 ± 0.057 ± 0.442
0.060–0.075	7.827 ± 0.024 ± 0.109	8.451 ± 0.047 ± 0.156
0.075–0.090	5.721 ± 0.021 ± 0.079	5.951 ± 0.044 ± 0.109
0.090–0.105	4.282 ± 0.018 ± 0.071	4.538 ± 0.040 ± 0.083
0.105–0.120	3.338 ± 0.016 ± 0.046	3.433 ± 0.036 ± 0.063
0.120–0.135	2.595 ± 0.014 ± 0.036	2.745 ± 0.033 ± 0.050
0.135–0.150	2.046 ± 0.013 ± 0.029	1.993 ± 0.028 ± 0.037
0.150–0.165	1.585 ± 0.011 ± 0.022	1.639 ± 0.026 ± 0.030
0.165–0.180	1.273 ± 0.011 ± 0.018	1.278 ± 0.023 ± 0.023
0.180–0.195	0.967 ± 0.009 ± 0.013	0.933 ± 0.019 ± 0.017
0.195–0.210	0.702 ± 0.007 ± 0.010	0.744 ± 0.018 ± 0.014
0.210–0.225	0.515 ± 0.007 ± 0.008	0.516 ± 0.014 ± 0.012
0.225–0.240	0.344 ± 0.005 ± 0.006	0.347 ± 0.012 ± 0.009
0.240–0.255	0.211 ± 0.004 ± 0.005	0.225 ± 0.009 ± 0.008
0.255–0.270	0.108 ± 0.003 ± 0.003	0.100 ± 0.005 ± 0.004
0.270–0.285	0.022 ± 0.001 ± 0.003	0.019 ± 0.001 ± 0.002
0.285–0.300	0.000 ± 0.000 ± 0.000	0.001 ± 0.000 ± 0.001
First Moment	0.07235 ±0.00005± 0.00033	0.07548 ±0.00012± 0.00051
Second Moment	0.00752 ±0.00001± 0.00005	0.00781 ±0.00002± 0.00009

Table 56: Differential distribution for wide jet broadening at $\sqrt{s} = 91.2$ GeV for udsc and b events. The first uncertainty is statistical, the second systematic.

C	$\frac{1}{\sigma}\cdot\frac{\mathrm{d}\sigma}{\mathrm{d}C}$ (udsc)	$\frac{1}{\sigma}\cdot\frac{\mathrm{d}\sigma}{\mathrm{d}C}$ (b)
0.000–0.050	$0.194 \pm 0.000 \pm 0.119$	$0.013 \pm 0.000 \pm 0.001$
0.050–0.100	$3.040 \pm 0.009 \pm 0.088$	$1.921 \pm 0.012 \pm 0.071$
0.100–0.150	$4.010 \pm 0.011 \pm 0.115$	$4.303 \pm 0.024 \pm 0.149$
0.150–0.200	$2.849 \pm 0.008 \pm 0.069$	$3.142 \pm 0.016 \pm 0.083$
0.200–0.250	$2.071 \pm 0.007 \pm 0.059$	$2.210 \pm 0.013 \pm 0.068$
0.250–0.300	$1.567 \pm 0.006 \pm 0.028$	$1.746 \pm 0.013 \pm 0.037$
0.300–0.350	$1.232 \pm 0.005 \pm 0.022$	$1.290 \pm 0.011 \pm 0.027$
0.350–0.400	$0.984 \pm 0.005 \pm 0.017$	$1.076 \pm 0.011 \pm 0.023$
0.400–0.450	$0.804 \pm 0.004 \pm 0.016$	$0.875 \pm 0.010 \pm 0.020$
0.450–0.500	$0.665 \pm 0.004 \pm 0.012$	$0.695 \pm 0.009 \pm 0.015$
0.500–0.550	$0.560 \pm 0.004 \pm 0.010$	$0.627 \pm 0.009 \pm 0.013$
0.550–0.600	$0.488 \pm 0.003 \pm 0.010$	$0.502 \pm 0.008 \pm 0.011$
0.600–0.650	$0.419 \pm 0.003 \pm 0.007$	$0.423 \pm 0.007 \pm 0.009$
0.650–0.700	$0.358 \pm 0.003 \pm 0.006$	$0.347 \pm 0.006 \pm 0.007$
0.700–0.750	$0.310 \pm 0.003 \pm 0.009$	$0.334 \pm 0.007 \pm 0.011$
0.750–0.800	$0.260 \pm 0.003 \pm 0.005$	$0.288 \pm 0.007 \pm 0.007$
0.800–0.850	$0.124 \pm 0.002 \pm 0.008$	$0.129 \pm 0.004 \pm 0.011$
0.850–0.900	$0.047 \pm 0.001 \pm 0.002$	$0.060 \pm 0.002 \pm 0.003$
0.900–0.950	$0.016 \pm 0.001 \pm 0.002$	$0.017 \pm 0.001 \pm 0.002$
0.950–1.000	$0.003 \pm 0.000 \pm 0.001$	$0.001 \pm 0.000 \pm 0.000$
First Moment	$0.26110 \pm 0.00021 \pm 0.00197$	$0.27462 \pm 0.00045 \pm 0.00261$
Second Moment	$0.10265 \pm 0.00016 \pm 0.00126$	$0.10905 \pm 0.00036 \pm 0.00170$

Table 57: Differential distribution for C-parameter at $\sqrt{s} = 91.2$ GeV for udsc and b events. The first uncertainty is statistical, the second systematic.

D	$\frac{1}{\sigma}\cdot\frac{\mathrm{d}\sigma}{\mathrm{d}D}$ (udsc)	$\frac{1}{\sigma}\cdot\frac{\mathrm{d}\sigma}{\mathrm{d}D}$ (b)
0.000–0.032	17.574 ± 0.038 ± 0.324	16.133 ± 0.071 ± 0.331
0.032–0.064	5.154 ± 0.009 ± 0.095	5.432 ± 0.020 ± 0.111
0.064–0.096	2.622 ± 0.009 ± 0.048	2.858 ± 0.018 ± 0.059
0.096–0.128	1.620 ± 0.007 ± 0.030	1.816 ± 0.017 ± 0.037
0.128–0.160	1.111 ± 0.006 ± 0.025	1.307 ± 0.015 ± 0.032
0.160–0.192	0.785 ± 0.005 ± 0.019	0.944 ± 0.013 ± 0.025
0.192–0.224	0.563 ± 0.005 ± 0.017	0.698 ± 0.012 ± 0.024
0.224–0.256	0.425 ± 0.004 ± 0.013	0.504 ± 0.010 ± 0.017
0.256–0.288	0.322 ± 0.003 ± 0.009	0.368 ± 0.008 ± 0.011
0.288–0.320	0.241 ± 0.003 ± 0.008	0.273 ± 0.007 ± 0.007
0.320–0.352	0.184 ± 0.003 ± 0.006	0.227 ± 0.007 ± 0.006
0.352–0.384	0.150 ± 0.003 ± 0.007	0.160 ± 0.006 ± 0.006
0.384–0.416	0.111 ± 0.002 ± 0.005	0.116 ± 0.005 ± 0.005
0.416–0.448	0.087 ± 0.002 ± 0.006	0.082 ± 0.004 ± 0.006
0.448–0.480	0.068 ± 0.002 ± 0.002	0.077 ± 0.004 ± 0.004
0.480–0.512	0.057 ± 0.002 ± 0.002	0.060 ± 0.004 ± 0.003
0.512–0.544	0.044 ± 0.001 ± 0.001	0.049 ± 0.004 ± 0.003
0.544–0.576	0.035 ± 0.001 ± 0.002	0.033 ± 0.003 ± 0.002
0.576–0.608	0.027 ± 0.001 ± 0.001	0.030 ± 0.003 ± 0.002
0.608–0.640	0.019 ± 0.001 ± 0.001	0.017 ± 0.002 ± 0.001
0.640–0.672	0.017 ± 0.001 ± 0.001	0.023 ± 0.003 ± 0.001
0.672–0.704	0.012 ± 0.001 ± 0.000	0.018 ± 0.002 ± 0.000
0.704–0.736	0.011 ± 0.001 ± 0.001	0.012 ± 0.002 ± 0.002
0.736–0.768	0.008 ± 0.001 ± 0.001	0.005 ± 0.001 ± 0.001
0.768–0.800	0.003 ± 0.000 ± 0.001	0.007 ± 0.001 ± 0.003
First Moment	0.06282 ±0.00011± 0.00098	0.06899 ±0.00025± 0.00117
Second Moment	0.01167 ±0.00005± 0.00030	0.01318 ±0.00011± 0.00036

Table 58: Differential distribution for D-parameter at $\sqrt{s} = 91.2$ GeV for udsc and b events. The first uncertainty is statistical, the second systematic.

y	A_y	B_y	c_y
$1-T$	2.103	40.78	2
ρ_{H}	2.103	22.77	1
B_{T}	4.067	55.27	1
B_{W}	4.067	-16.07	0.5
C	8.638	155.5	3π
D	0	60.40	$195\frac{\alpha_{\mathrm{s}}(\mu)}{2\pi}$

Table 59: Shape-variable dependent coefficients appearing in the equations for measurement of α_{s} using the power correction ansatz [17–20, 53, 159–161].

y	α_0	$\alpha_{\mathrm{s}}(m_{\mathrm{Z}})$	χ^2/d.o.f.
$1-T$	$0.518 \pm 0.051 \pm 0.030$	$0.1164 \pm 0.0046 \pm 0.0038$	17.7/14
ρ_{H}	$0.421 \pm 0.034 \pm 0.015$	$0.1051 \pm 0.0047 \pm 0.0021$	13.4/14
B_{T}	$0.449 \pm 0.039 \pm 0.037$	$0.1163 \pm 0.0032 \pm 0.0027$	8.9/14
B_{W}	$0.342 \pm 0.078 \pm 0.015$	$0.1169 \pm 0.0039 \pm 0.0015$	13.9/14
C	$0.457 \pm 0.030 \pm 0.026$	$0.1164 \pm 0.0030 \pm 0.0036$	11.7/14
D	$0.682 \pm 0.094 \pm 0.018$	$0.1046 \pm 0.0078 \pm 0.0096$	24.3/14
avg.	$0.478 \pm 0.054 \pm 0.024$	$0.1126 \pm 0.0045 \pm 0.0039$	

Table 60: Determination of α_0 and $\alpha_{\mathrm{s}}(m_{\mathrm{Z}})$ from fits to the first moments of the event-shape distributions together with χ^2/d.o.f. (see text). The first uncertainty is statistical, the second systematic. The unweighted averages are also shown. The first uncertainty is the average of the statistical uncertainties, the second the theoretical uncertainty.

y	A_2 (GeV^2)	χ^2/d.o.f.	$\frac{A_2/s}{2\langle y_{\rm pert}\rangle c_y F_y \mathcal{P}}$
$1-T$	5.47 ± 0.17	13.9/15	0.78
$\rho_{\rm H}$	-0.47 ± 0.09	6.0/15	-0.18
$B_{\rm T}$	15.44 ± 0.52	32.9/15	0.56
$B_{\rm W}$	-10.05 ± 0.33	25.2/15	-1.32
C	11.51 ± 0.35	20.2/15	0.51

Table 61: Results of fits of the power correction ansatz to the second moments of event-shape variables. Also shown is the ratio at $\sqrt{s} = m_{\rm Z}$ of the $\mathcal{O}(1/s)$ term to the lowest-order power correction term.

	Leading Log	Next-to-Leading Log	Subleading			
First Order	$\overline{\alpha}_{\rm s} L^2$	$\overline{\alpha}_{\rm s} L$	$\overline{\alpha}_{\rm s}$			
Second Order	$\overline{\alpha}_{\rm s}^2 L^3$	$\overline{\alpha}_{\rm s}^2 L^2$	$\overline{\alpha}_{\rm s}^2 L$	$\overline{\alpha}_{\rm s}^2$		
Third Order	$\overline{\alpha}_{\rm s}^3 L^4$	$\overline{\alpha}_{\rm s}^3 L^3$	$\overline{\alpha}_{\rm s}^3 L^2$	$\overline{\alpha}_{\rm s}^3 L$	$\overline{\alpha}_{\rm s}^3$	
$\vdots$	$\vdots$	$\vdots$	$\vdots$	$\vdots$	$\vdots$	$\ddots$

Table 62: Schematic representation of the fixed-order expansion versus the logarithmic expansion of theoretical predictions to the event-shape variables.

$\langle\sqrt{s}\rangle$		$1-T$	ρ_{H}	B_{T}	B_{W}	C
41.4 GeV	Fit range	0.025–0.290	0.015–0.252	0.040–0.250	0.030–0.220	0.10–0.64
	χ^2/d.o.f.	12.7 / 9	8.6 / 10	6.4 / 6	8.4 / 5	14.7 / 8
55.3 GeV	Fit range	0.025–0.250	0.015–0.252	0.040–0.250	0.030–0.220	0.10–0.64
	χ^2/d.o.f.	7.3 / 8	4.7 / 10	4.1 / 6	1.2 / 5	25.4 / 8
65.4 GeV	Fit range	0.025–0.250	0.015–0.252	0.040–0.250	0.030–0.220	0.10–0.64
	χ^2/d.o.f.	7.6 / 8	18.2 / 10	2.3 / 6	0.9 / 5	22.8 / 8
75.7 GeV	Fit range	0.025–0.250	0.015–0.252	0.040–0.250	0.030–0.220	0.10–0.64
	χ^2/d.o.f.	1.8 / 8	6.0 / 10	4.1 / 6	4.1 / 5	16.8 / 8
82.3 GeV	Fit range	0.025–0.250	0.015–0.252	0.040–0.250	0.030–0.220	0.10–0.64
	χ^2/d.o.f.	3.0 / 8	34.4 / 10	0.6 / 6	1.4 / 5	15.9 / 8
85.1 GeV	Fit range	0.025–0.250	0.015–0.252	0.040–0.250	0.030–0.220	0.10–0.64
	χ^2/d.o.f.	2.9 / 8	9.2 / 10	6.4 / 6	2.4 / 5	8.2 / 8
91.2 GeV	Fit range	0.025–0.290	0.015–0.216	0.070–0.250	0.050–0.175	0.10–0.52
	χ^2/d.o.f.	6.0 / 9	20.1 / 9	1.2 / 7	5.8 / 7	16.3 / 8
130.1 GeV	Fit range	0.000–0.275	0.000–0.150	0.020–0.260	0.015–0.210	0.05–0.50
	χ^2/d.o.f.	6.8 / 10	7.9 / 9	5.7 / 11	11.9 / 12	6.1 / 8
136.1 GeV	Fit range	0.000–0.250	0.000–0.210	0.020–0.260	0.015–0.210	0.05–0.50
	χ^2/d.o.f.	9.4 / 9	8.9 / 13	6.0 / 11	4.9 / 12	11.2 / 9
161.3 GeV	Fit range	0.000–0.250	0.000–0.210	0.020–0.260	0.015–0.210	0.05–0.50
	χ^2/d.o.f.	8.3 / 9	4.9 / 13	6.7 / 12	5.3 / 12	4.8 / 8
172.3 GeV	Fit range	0.000–0.250	0.000–0.210	0.000–0.260	0.000–0.210	0.05–0.50
	χ^2/d.o.f.	2.4 / 9	6.2 / 13	5.5 / 12	7.2 / 13	2.6 / 8
182.8 GeV	Fit range	0.000–0.300	0.000–0.210	0.000–0.260	0.000–0.210	0.05–0.50
	χ^2/d.o.f.	2.6 / 11	4.6 / 13	8.1 / 12	3.9 / 13	4.2 / 8
188.6 GeV	Fit range	0.000–0.300	0.000–0.210	0.000–0.260	0.000–0.210	0.05–0.50
	χ^2/d.o.f.	6.3 / 11	7.9 / 13	19.3 / 12	11.7 / 13	7.5 / 8
194.4 GeV	Fit range	0.000–0.300	0.000–0.210	0.020–0.260	0.015–0.210	0.05–0.50
	χ^2/d.o.f.	3.1 / 11	10.1 / 13	20.2 / 11	9.7 / 12	3.8 / 8
200.2 GeV	Fit range	0.000–0.300	0.000–0.180	0.020–0.260	0.015–0.195	0.05–0.50
	χ^2/d.o.f.	8.1 / 11	6.8 / 11	9.6 / 11	10.3 / 11	2.9 / 8
206.2 GeV	Fit range	0.000–0.250	0.000–0.210	0.020–0.260	0.015–0.210	0.05–0.50
	χ^2/d.o.f.	7.5 / 9	7.7 / 13	5.9 / 11	7.8 / 12	3.4 / 8

Table 63: The fit range used to determine α_{s} from event-shape variables at different centre-of-mass energies. The χ^2/d.o.f. of the fit are also given. The fit ranges are chosen to exclude regions where the statistics is too small.

$\sqrt{s}$ (GeV)	α_s from				
	$1-T$	ρ_H	B_T	B_W	C
41.4	0.1500±0.0062±0.0124	0.1440±0.0044±0.0102	0.1401±0.0063±0.0119	0.1380±0.0067±0.0091	0.1371±0.0070±0.0102
55.3	0.1310±0.0073±0.0127	0.1280±0.0066±0.0064	0.1321±0.0070±0.0099	0.1191±0.0072±0.0088	0.1197±0.0086±0.0118
65.4	0.1458±0.0062±0.0104	0.1397±0.0041±0.0065	0.1354±0.0067±0.0106	0.1190±0.0062±0.0086	0.1258±0.0039±0.0108
75.7	0.1290±0.0070±0.0101	0.1226±0.0045±0.0062	0.1296±0.0074±0.0097	0.1068±0.0060±0.0084	0.1143±0.0072±0.0094
82.3	0.1224±0.0062±0.0094	0.1189±0.0032±0.0075	0.1270±0.0079±0.0095	0.1083±0.0067±0.0087	0.1153±0.0060±0.0091
85.1	0.1184±0.0067±0.0093	0.1114±0.0062±0.0059	0.1259±0.0069±0.0095	0.1092±0.0080±0.0091	0.1115±0.0045±0.0089
91.2	0.1233±0.0025±0.0076	0.1228±0.0013±0.0052	0.1222±0.0020±0.0080	0.1196±0.0022±0.0052	0.1170±0.0016±0.0076
130.1	0.1139±0.0046±0.0056	0.1134±0.0045±0.0038	0.1178±0.0033±0.0064	0.1089±0.0031±0.0088	0.1151±0.0040±0.0066
136.1	0.1166±0.0053±0.0060	0.1112±0.0039±0.0037	0.1166±0.0035±0.0064	0.1072±0.0041±0.0078	0.1089±0.0047±0.0076
161.3	0.1018±0.0056±0.0050	0.1012±0.0056±0.0034	0.1123±0.0042±0.0067	0.1058±0.0059±0.0068	0.1043±0.0060±0.0057
172.3	0.1109±0.0061±0.0064	0.1099±0.0052±0.0033	0.1092±0.0062±0.0061	0.1045±0.0047±0.0065	0.1121±0.0068±0.0057
182.8	0.1132±0.0026±0.0054	0.1075±0.0025±0.0038	0.1134±0.0022±0.0060	0.1063±0.0016±0.0071	0.1081±0.0029±0.0054
188.6	0.1168±0.0018±0.0057	0.1108±0.0016±0.0033	0.1137±0.0018±0.0067	0.1060±0.0016±0.0078	0.1118±0.0023±0.0055
194.4	0.1168±0.0024±0.0056	0.1096±0.0022±0.0039	0.1152±0.0021±0.0065	0.1071±0.0021±0.0062	0.1130±0.0033±0.0056
200.2	0.1178±0.0033±0.0059	0.1114±0.0033±0.0034	0.1164±0.0023±0.0062	0.1088±0.0022±0.0062	0.1147±0.0029±0.0057
206.2	0.1173±0.0021±0.0057	0.1119±0.0019±0.0034	0.1163±0.0021±0.0065	0.1077±0.0019±0.0062	0.1130±0.0028±0.0053

Table 64: Values of α_s measured at different centre-of-mass energies from fits to the event-shape variables. The first uncertainty is statistical, the second systematic.

$\langle\sqrt{s}\rangle$	α_s measurement from T, ρ_H, B_T, B_W, C				
(GeV)	α_s	stat	syst	hadr.	hi. order
41.4	0.1418	±0.0053	±0.0030	±0.0055	±0.0085
55.3	0.1260	±0.0047	±0.0056	±0.0066	±0.0062
65.4	0.1331	±0.0032	±0.0042	±0.0059	±0.0064
75.7	0.1204	±0.0024	±0.0059	±0.0060	±0.0053
82.3	0.1184	±0.0028	±0.0053	±0.0060	±0.0051
85.1	0.1152	±0.0037	±0.0051	±0.0060	±0.0055
91.2	0.1210	±0.0008	±0.0017	±0.0040	±0.0052
130.1	0.1138	±0.0033	±0.0021	±0.0031	±0.0046
136.1	0.1121	±0.0039	±0.0019	±0.0038	±0.0045
161.3	0.1051	±0.0048	±0.0026	±0.0026	±0.0044
172.3	0.1099	±0.0052	±0.0026	±0.0024	±0.0048
182.8	0.1096	±0.0022	±0.0010	±0.0023	±0.0044
188.6	0.1122	±0.0014	±0.0012	±0.0022	±0.0045
194.4	0.1123	±0.0018	±0.0016	±0.0020	±0.0047
200.2	0.1138	±0.0018	±0.0021	±0.0020	±0.0046
206.2	0.1132	±0.0014	±0.0016	±0.0019	±0.0047

Table 65: Combined α_s values from the five event-shape variables with their uncertainties.

	$P_{N_{ch}}$ at $\sqrt{s} = 91.2$ GeV		
N_{ch}	all flavours	udsc flavours	b flavour
2	0.000018 ± 0.000003 ± 0.000009	0.000021 ± 0.000004 ± 0.000002	
4	0.000268 ± 0.000010 ± 0.000051	0.000331 ± 0.000014 ± 0.000027	0.000009 ± 0.000005 ± 0.000030
6	0.002054 ± 0.000028 ± 0.000104	0.002582 ± 0.000041 ± 0.000192	0.000227 ± 0.000028 ± 0.000084
8	0.009328 ± 0.000063 ± 0.000368	0.011335 ± 0.000087 ± 0.000725	0.001944 ± 0.000085 ± 0.000458
10	0.027621 ± 0.000108 ± 0.000755	0.032821 ± 0.000148 ± 0.001766	0.008961 ± 0.000188 ± 0.001311
12	0.058426 ± 0.000150 ± 0.001115	0.066995 ± 0.000199 ± 0.002907	0.026978 ± 0.000324 ± 0.002513
14	0.093836 ± 0.000173 ± 0.001263	0.104305 ± 0.000226 ± 0.003396	0.057434 ± 0.000447 ± 0.003302
16	0.121719 ± 0.000176 ± 0.001274	0.130215 ± 0.000225 ± 0.002797	0.092830 ± 0.000508 ± 0.003038
18	0.133779 ± 0.000168 ± 0.000978	0.137874 ± 0.000213 ± 0.001607	0.121985 ± 0.000507 ± 0.002036
20	0.129539 ± 0.000158 ± 0.000883	0.128385 ± 0.000199 ± 0.000913	0.135052 ± 0.000471 ± 0.001561
22	0.113598 ± 0.000148 ± 0.000419	0.109303 ± 0.000187 ± 0.001652	0.130966 ± 0.000439 ± 0.001776
24	0.092586 ± 0.000138 ± 0.000639	0.086274 ± 0.000171 ± 0.001992	0.115071 ± 0.000421 ± 0.002153
26	0.070832 ± 0.000125 ± 0.000804	0.064172 ± 0.000152 ± 0.002125	0.093411 ± 0.000405 ± 0.002126
28	0.051225 ± 0.000109 ± 0.000998	0.045495 ± 0.000132 ± 0.001995	0.071269 ± 0.000377 ± 0.001965
30	0.035490 ± 0.000093 ± 0.000908	0.030750 ± 0.000110 ± 0.001792	0.051408 ± 0.000338 ± 0.001662
32	0.023541 ± 0.000076 ± 0.000822	0.019974 ± 0.000089 ± 0.001430	0.035160 ± 0.000289 ± 0.001356
34	0.014928 ± 0.000061 ± 0.000634	0.012434 ± 0.000070 ± 0.001128	0.023016 ± 0.000238 ± 0.001026
36	0.009190 ± 0.000047 ± 0.000461	0.007410 ± 0.000054 ± 0.000808	0.014572 ± 0.000192 ± 0.000731
38	0.005395 ± 0.000036 ± 0.000306	0.004343 ± 0.000041 ± 0.000551	0.008841 ± 0.000150 ± 0.000501
40	0.003119 ± 0.000027 ± 0.000221	0.002433 ± 0.000031 ± 0.000355	0.005114 ± 0.000114 ± 0.000357
42	0.001735 ± 0.000020 ± 0.000146	0.001284 ± 0.000021 ± 0.000237	0.002853 ± 0.000084 ± 0.000214
44	0.000903 ± 0.000014 ± 0.000090	0.000651 ± 0.000014 ± 0.000142	0.001503 ± 0.000058 ± 0.000120
46	0.000452 ± 0.000010 ± 0.000056	0.000330 ± 0.000011 ± 0.000086	0.000741 ± 0.000038 ± 0.000080
48	0.000228 ± 0.000007 ± 0.000035	0.000149 ± 0.000007 ± 0.000055	0.000378 ± 0.000026 ± 0.000060
50	0.000102 ± 0.000004 ± 0.000018	0.000072 ± 0.000006 ± 0.000031	0.000165 ± 0.000016 ± 0.000036
52	0.000051 ± 0.000003 ± 0.000013	0.000033 ± 0.000005 ± 0.000018	0.000066 ± 0.000008 ± 0.000020
54	0.000023 ± 0.000003 ± 0.000010	0.000014 ± 0.000003 ± 0.000023	0.000033 ± 0.000005 ± 0.000014
56	0.000013 ± 0.000003 ± 0.000007	0.000011 ± 0.000004 ± 0.000012	0.000010 ± 0.000003 ± 0.000005
First Moment	20.46 ± 0.01 ± 0.11	19.88 ± 0.01 ± 0.21	22.45 ± 0.03 ± 0.19
Second Moment	457.7 ± 0.3 ± 4.9	432.4 ± 0.4 ± 9.2	542.0 ± 1.2 ± 3.0

Table 66: Charged particle multiplicity distributions at $\sqrt{s} = 91.2$ GeV The first uncertainty is statistical, the second systematic.

	$P_{N_{\mathrm{ch}}}$		
N_{ch}	at $\sqrt{s} = 130.1\,\mathrm{GeV}$	at $\sqrt{s} = 136.1\,\mathrm{GeV}$	at $\sqrt{s} = 161.3\,\mathrm{GeV}$
10	$0.009 \pm 0.002 \pm 0.002$	$0.011 \pm 0.002 \pm 0.002$	$0.006 \pm 0.002 \pm 0.001$
12	$0.026 \pm 0.004 \pm 0.004$	$0.032 \pm 0.005 \pm 0.004$	$0.018 \pm 0.003 \pm 0.001$
14	$0.054 \pm 0.007 \pm 0.004$	$0.056 \pm 0.008 \pm 0.001$	$0.038 \pm 0.006 \pm 0.003$
16	$0.085 \pm 0.009 \pm 0.003$	$0.086 \pm 0.010 \pm 0.001$	$0.061 \pm 0.008 \pm 0.002$
18	$0.109 \pm 0.012 \pm 0.004$	$0.099 \pm 0.013 \pm 0.001$	$0.076 \pm 0.012 \pm 0.005$
20	$0.120 \pm 0.013 \pm 0.002$	$0.099 \pm 0.016 \pm 0.002$	$0.093 \pm 0.013 \pm 0.005$
22	$0.116 \pm 0.013 \pm 0.001$	$0.096 \pm 0.018 \pm 0.002$	$0.107 \pm 0.014 \pm 0.002$
24	$0.107 \pm 0.013 \pm 0.002$	$0.094 \pm 0.014 \pm 0.002$	$0.112 \pm 0.016 \pm 0.005$
26	$0.098 \pm 0.013 \pm 0.003$	$0.090 \pm 0.015 \pm 0.002$	$0.108 \pm 0.014 \pm 0.005$
28	$0.079 \pm 0.013 \pm 0.002$	$0.081 \pm 0.015 \pm 0.002$	$0.096 \pm 0.015 \pm 0.002$
30	$0.063 \pm 0.013 \pm 0.004$	$0.071 \pm 0.012 \pm 0.004$	$0.076 \pm 0.015 \pm 0.001$
32	$0.043 \pm 0.010 \pm 0.001$	$0.050 \pm 0.010 \pm 0.002$	$0.058 \pm 0.013 \pm 0.001$
34	$0.033 \pm 0.001 \pm 0.003$	$0.041 \pm 0.009 \pm 0.002$	$0.044 \pm 0.013 \pm 0.001$
36	$0.019 \pm 0.008 \pm 0.003$	$0.034 \pm 0.001 \pm 0.005$	$0.033 \pm 0.011 \pm 0.001$
38	$0.016 \pm 0.001 \pm 0.002$	$0.024 \pm 0.001 \pm 0.002$	$0.024 \pm 0.011 \pm 0.001$
40	$0.009 \pm 0.001 \pm 0.001$	$0.010 \pm 0.001 \pm 0.001$	$0.017 \pm 0.011 \pm 0.002$
42	$0.006 \pm 0.001 \pm 0.001$	$0.007 \pm 0.001 \pm 0.002$	$0.011 \pm 0.000 \pm 0.001$
44	$0.003 \pm 0.001 \pm 0.001$	$0.005 \pm 0.001 \pm 0.001$	$0.007 \pm 0.000 \pm 0.001$
46	$0.001 \pm 0.001 \pm 0.001$	$0.005 \pm 0.001 \pm 0.001$	$0.006 \pm 0.006 \pm 0.001$
48	$0.001 \pm 0.001 \pm 0.001$	$0.001 \pm 0.001 \pm 0.001$	$0.003 \pm 0.003 \pm 0.001$
50	$0.000 \pm 0.000 \pm 0.000$	$0.001 \pm 0.001 \pm 0.001$	$0.002 \pm 0.000 \pm 0.006$
52	$0.000 \pm 0.000 \pm 0.001$	$0.000 \pm 0.000 \pm 0.000$	$0.001 \pm 0.001 \pm 0.001$
First Moment	$23.28 \pm 0.24 \pm 0.10$	$24.13 \pm 0.27 \pm 0.10$	$25.40 \pm 0.36 \pm 0.13$
Second Moment	$587.5 \pm 11.8 \pm 3.7$	$643.3 \pm 14.3 \pm 5.2$	$700.3 \pm 20.8 \pm 10.2$

Table 67: Charged particle multiplicity distribution at $\sqrt{s} = 130.1$, 136.1 and 161.3 GeV. The first uncertainty is statistical, the second systematic.

	$P_{N_{\rm ch}}$		
$N_{\rm ch}$	at $\sqrt{s} = 172.3$ GeV	at $\sqrt{s} = 182.8$ GeV	at $\sqrt{s} = 188.6$ GeV
10	$0.005 \pm 0.001 \pm 0.001$	$0.004 \pm 0.001 \pm 0.001$	$0.004 \pm 0.001 \pm 0.001$
12	$0.013 \pm 0.000 \pm 0.001$	$0.013 \pm 0.002 \pm 0.001$	$0.013 \pm 0.001 \pm 0.001$
14	$0.028 \pm 0.006 \pm 0.001$	$0.029 \pm 0.002 \pm 0.001$	$0.028 \pm 0.002 \pm 0.002$
16	$0.048 \pm 0.008 \pm 0.002$	$0.051 \pm 0.004 \pm 0.003$	$0.048 \pm 0.002 \pm 0.003$
18	$0.072 \pm 0.010 \pm 0.001$	$0.075 \pm 0.005 \pm 0.002$	$0.072 \pm 0.003 \pm 0.002$
20	$0.091 \pm 0.012 \pm 0.004$	$0.089 \pm 0.006 \pm 0.001$	$0.087 \pm 0.003 \pm 0.001$
22	$0.100 \pm 0.013 \pm 0.003$	$0.097 \pm 0.007 \pm 0.002$	$0.097 \pm 0.004 \pm 0.001$
24	$0.097 \pm 0.014 \pm 0.002$	$0.097 \pm 0.007 \pm 0.003$	$0.101 \pm 0.004 \pm 0.001$
26	$0.091 \pm 0.014 \pm 0.001$	$0.094 \pm 0.007 \pm 0.004$	$0.097 \pm 0.005 \pm 0.002$
28	$0.088 \pm 0.013 \pm 0.001$	$0.085 \pm 0.007 \pm 0.003$	$0.088 \pm 0.004 \pm 0.001$
30	$0.079 \pm 0.016 \pm 0.001$	$0.077 \pm 0.007 \pm 0.002$	$0.079 \pm 0.004 \pm 0.002$
32	$0.064 \pm 0.017 \pm 0.001$	$0.065 \pm 0.007 \pm 0.002$	$0.069 \pm 0.004 \pm 0.002$
34	$0.055 \pm 0.014 \pm 0.002$	$0.056 \pm 0.007 \pm 0.002$	$0.057 \pm 0.005 \pm 0.002$
36	$0.041 \pm 0.012 \pm 0.002$	$0.047 \pm 0.006 \pm 0.002$	$0.045 \pm 0.005 \pm 0.002$
38	$0.034 \pm 0.012 \pm 0.002$	$0.034 \pm 0.006 \pm 0.002$	$0.034 \pm 0.005 \pm 0.002$
40	$0.026 \pm 0.001 \pm 0.002$	$0.025 \pm 0.007 \pm 0.001$	$0.026 \pm 0.005 \pm 0.002$
42	$0.018 \pm 0.018 \pm 0.001$	$0.020 \pm 0.006 \pm 0.002$	$0.018 \pm 0.004 \pm 0.001$
44	$0.019 \pm 0.019 \pm 0.001$	$0.013 \pm 0.005 \pm 0.001$	$0.013 \pm 0.004 \pm 0.001$
46	$0.016 \pm 0.010 \pm 0.005$	$0.008 \pm 0.003 \pm 0.001$	$0.009 \pm 0.004 \pm 0.001$
48	$0.007 \pm 0.001 \pm 0.001$	$0.007 \pm 0.001 \pm 0.002$	$0.005 \pm 0.000 \pm 0.001$
50	$0.005 \pm 0.001 \pm 0.002$	$0.005 \pm 0.001 \pm 0.004$	$0.004 \pm 0.004 \pm 0.001$
52	$0.004 \pm 0.001 \pm 0.001$	$0.003 \pm 0.001 \pm 0.001$	$0.002 \pm 0.002 \pm 0.001$
First Moment	$27.00 \pm 0.54 \pm 0.24$	$26.84 \pm 0.22 \pm 0.26$	$26.84 \pm 0.20 \pm 0.25$
Second Moment	$798.4 \pm 33.9 \pm 13.5$	$788.5 \pm 13.2 \pm 16.8$	$785.2 \pm 13.4 \pm 15.8$

Table 68: Charged particle multiplicity distribution at $\sqrt{s} = 172.3$, 182.8 and 188.6 GeV. The first uncertainty is statistical, the second systematic.

	$P_{N_{\mathrm{ch}}}$		
N_{ch}	at $\sqrt{s} = 194.4$ GeV	at $\sqrt{s} = 200.2$ GeV	at $\sqrt{s} = 206.2$ GeV
10	$0.004 \pm 0.001 \pm 0.001$	$0.003 \pm 0.001 \pm 0.001$	$0.003 \pm 0.001 \pm 0.001$
12	$0.013 \pm 0.001 \pm 0.002$	$0.011 \pm 0.001 \pm 0.001$	$0.010 \pm 0.001 \pm 0.001$
14	$0.028 \pm 0.002 \pm 0.003$	$0.024 \pm 0.002 \pm 0.002$	$0.022 \pm 0.001 \pm 0.002$
16	$0.048 \pm 0.003 \pm 0.004$	$0.045 \pm 0.003 \pm 0.002$	$0.040 \pm 0.002 \pm 0.003$
18	$0.069 \pm 0.004 \pm 0.004$	$0.066 \pm 0.004 \pm 0.002$	$0.062 \pm 0.003 \pm 0.002$
20	$0.086 \pm 0.004 \pm 0.003$	$0.083 \pm 0.004 \pm 0.002$	$0.083 \pm 0.003 \pm 0.001$
22	$0.096 \pm 0.005 \pm 0.002$	$0.095 \pm 0.005 \pm 0.002$	$0.093 \pm 0.004 \pm 0.001$
24	$0.098 \pm 0.006 \pm 0.002$	$0.098 \pm 0.006 \pm 0.003$	$0.097 \pm 0.004 \pm 0.001$
26	$0.095 \pm 0.006 \pm 0.002$	$0.097 \pm 0.006 \pm 0.003$	$0.094 \pm 0.004 \pm 0.002$
28	$0.087 \pm 0.006 \pm 0.002$	$0.089 \pm 0.006 \pm 0.002$	$0.088 \pm 0.005 \pm 0.002$
30	$0.076 \pm 0.007 \pm 0.001$	$0.076 \pm 0.006 \pm 0.002$	$0.077 \pm 0.005 \pm 0.001$
32	$0.066 \pm 0.007 \pm 0.002$	$0.065 \pm 0.006 \pm 0.002$	$0.068 \pm 0.005 \pm 0.002$
34	$0.056 \pm 0.006 \pm 0.002$	$0.054 \pm 0.006 \pm 0.002$	$0.058 \pm 0.005 \pm 0.001$
36	$0.045 \pm 0.006 \pm 0.001$	$0.045 \pm 0.006 \pm 0.002$	$0.047 \pm 0.005 \pm 0.002$
38	$0.037 \pm 0.006 \pm 0.002$	$0.035 \pm 0.007 \pm 0.002$	$0.038 \pm 0.005 \pm 0.002$
40	$0.022 \pm 0.001 \pm 0.003$	$0.028 \pm 0.006 \pm 0.002$	$0.031 \pm 0.005 \pm 0.002$
42	$0.021 \pm 0.006 \pm 0.002$	$0.023 \pm 0.005 \pm 0.001$	$0.024 \pm 0.005 \pm 0.002$
44	$0.018 \pm 0.004 \pm 0.004$	$0.019 \pm 0.007 \pm 0.002$	$0.018 \pm 0.004 \pm 0.001$
46	$0.012 \pm 0.007 \pm 0.004$	$0.014 \pm 0.005 \pm 0.001$	$0.014 \pm 0.004 \pm 0.001$
48	$0.012 \pm 0.001 \pm 0.004$	$0.015 \pm 0.003 \pm 0.002$	$0.012 \pm 0.003 \pm 0.001$
50	$0.006 \pm 0.001 \pm 0.001$	$0.006 \pm 0.003 \pm 0.001$	$0.008 \pm 0.005 \pm 0.001$
52	$0.002 \pm 0.001 \pm 0.001$	$0.003 \pm 0.002 \pm 0.002$	$0.006 \pm 0.003 \pm 0.001$
First Moment	$27.14 \pm 0.31 \pm 0.29$	$27.73 \pm 0.27 \pm 0.39$	$28.09 \pm 0.23 \pm 0.24$
Second Moment	$810.6 \pm 19.7 \pm 14.7$	$843.5 \pm 17.9 \pm 26.1$	$865.4 \pm 16.1 \pm 12.5$

Table 69: Charged particle multiplicity distribution at $\sqrt{s} = 194.4$, 200.2 and 206.2 GeV. The first uncertainty is statistical, the second systematic.

N_{f}	a_1	a_2	a_3	r_1	r_2	r_3
3	0.280	−0.379	0.209	0.185	0.426	0.189
4	0.297	−0.339	0.162	0.191	0.468	0.080
5	0.314	−0.301	0.112	0.198	0.510	−0.041

Table 70: The perturbative correction coefficients for various numbers of active flavours from Reference 179.

	$N_{\rm f}$	$\alpha_{\rm s}(m_{\rm Z})$	χ^2/ d.o.f.
LO	3	0.0714 ± 0.0020	4.8 / 12
LO	5	0.0805 ± 0.0010	9.9 / 12
NLO	3	0.0937 ± 0.0040	4.7 / 12
NLO	5	0.1025 ± 0.0037	4.8 / 12
2NLO	3	0.1008 ± 0.0041	4.7 / 12
2NLO	5	0.1128 ± 0.0046	4.9 / 12
3NLO	3	0.1294 ± 0.0038	6.2 / 12
3NLO	5	0.1292 ± 0.0031	5.2 / 12

Table 71: Results of fits to $N_{\rm ch}$ *vs.* $\sqrt{s}$.

	$\frac{1}{\sigma} \cdot \frac{\mathrm{d}\sigma}{\mathrm{d}\xi}$ at $\sqrt{s} = 91.2$ GeV		
ξ	all flavours	udsc flavours	b flavour
0.0–0.2	$0.015 \pm 0.001 \pm 0.001$	$0.018 \pm 0.001 \pm 0.001$	$0.001 \pm 0.001 \pm 0.001$
0.2–0.4	$0.084 \pm 0.001 \pm 0.005$	$0.101 \pm 0.001 \pm 0.006$	$0.015 \pm 0.002 \pm 0.004$
0.4–0.6	$0.220 \pm 0.002 \pm 0.012$	$0.256 \pm 0.002 \pm 0.015$	$0.083 \pm 0.003 \pm 0.013$
0.6–0.8	$0.417 \pm 0.002 \pm 0.009$	$0.471 \pm 0.003 \pm 0.018$	$0.215 \pm 0.005 \pm 0.012$
0.8–1.0	$0.690 \pm 0.003 \pm 0.012$	$0.767 \pm 0.004 \pm 0.025$	$0.411 \pm 0.007 \pm 0.015$
1.0–1.2	$1.047 \pm 0.004 \pm 0.015$	$1.142 \pm 0.005 \pm 0.030$	$0.706 \pm 0.009 \pm 0.019$
1.2–1.4	$1.481 \pm 0.005 \pm 0.011$	$1.582 \pm 0.005 \pm 0.028$	$1.124 \pm 0.011 \pm 0.017$
1.4–1.6	$1.986 \pm 0.005 \pm 0.016$	$2.077 \pm 0.006 \pm 0.026$	$1.687 \pm 0.014 \pm 0.029$
1.6–1.8	$2.550 \pm 0.006 \pm 0.009$	$2.599 \pm 0.007 \pm 0.013$	$2.384 \pm 0.016 \pm 0.030$
1.8–2.0	$3.104 \pm 0.007 \pm 0.021$	$3.092 \pm 0.008 \pm 0.026$	$3.155 \pm 0.019 \pm 0.062$
2.0–2.2	$3.642 \pm 0.007 \pm 0.047$	$3.536 \pm 0.008 \pm 0.056$	$4.088 \pm 0.022 \pm 0.093$
2.2–2.4	$4.211 \pm 0.008 \pm 0.044$	$4.035 \pm 0.009 \pm 0.066$	$4.905 \pm 0.024 \pm 0.106$
2.4–2.6	$4.697 \pm 0.008 \pm 0.038$	$4.458 \pm 0.009 \pm 0.075$	$5.619 \pm 0.026 \pm 0.117$
2.6–2.8	$5.156 \pm 0.008 \pm 0.034$	$4.884 \pm 0.010 \pm 0.085$	$6.221 \pm 0.027 \pm 0.121$
2.8–3.0	$5.555 \pm 0.009 \pm 0.061$	$5.261 \pm 0.010 \pm 0.109$	$6.598 \pm 0.028 \pm 0.128$
3.0–3.2	$5.896 \pm 0.009 \pm 0.020$	$5.610 \pm 0.010 \pm 0.097$	$6.998 \pm 0.029 \pm 0.088$
3.2–3.4	$6.104 \pm 0.009 \pm 0.051$	$5.829 \pm 0.011 \pm 0.111$	$7.128 \pm 0.030 \pm 0.090$
3.4–3.6	$6.253 \pm 0.009 \pm 0.066$	$5.965 \pm 0.011 \pm 0.122$	$7.336 \pm 0.031 \pm 0.089$
3.6–3.8	$6.278 \pm 0.010 \pm 0.066$	$6.024 \pm 0.011 \pm 0.118$	$7.162 \pm 0.030 \pm 0.082$
3.8–4.0	$6.201 \pm 0.010 \pm 0.048$	$5.976 \pm 0.011 \pm 0.107$	$7.052 \pm 0.031 \pm 0.065$
4.0–4.2	$6.000 \pm 0.009 \pm 0.053$	$5.805 \pm 0.011 \pm 0.100$	$6.699 \pm 0.030 \pm 0.068$
4.2–4.4	$5.681 \pm 0.009 \pm 0.049$	$5.519 \pm 0.011 \pm 0.091$	$6.275 \pm 0.030 \pm 0.066$
4.4–4.6	$5.237 \pm 0.009 \pm 0.059$	$5.100 \pm 0.010 \pm 0.081$	$5.716 \pm 0.029 \pm 0.079$
4.6–4.8	$4.629 \pm 0.009 \pm 0.051$	$4.534 \pm 0.010 \pm 0.065$	$4.995 \pm 0.028 \pm 0.072$
4.8–5.0	$3.890 \pm 0.008 \pm 0.073$	$3.817 \pm 0.009 \pm 0.080$	$4.164 \pm 0.026 \pm 0.087$
5.0–5.2	$3.239 \pm 0.008 \pm 0.043$	$3.180 \pm 0.009 \pm 0.049$	$3.410 \pm 0.025 \pm 0.060$
5.2–5.4	$2.615 \pm 0.008 \pm 0.069$	$2.579 \pm 0.009 \pm 0.071$	$2.846 \pm 0.025 \pm 0.092$
5.4–5.6	$1.967 \pm 0.007 \pm 0.076$	$1.927 \pm 0.009 \pm 0.080$	$2.113 \pm 0.025 \pm 0.096$
5.6–5.8	$1.433 \pm 0.011 \pm 0.216$	$1.406 \pm 0.013 \pm 0.215$	$1.483 \pm 0.039 \pm 0.221$
5.8–6.0	$0.804 \pm 0.059 \pm 0.064$	$0.795 \pm 0.072 \pm 0.096$	$0.820 \pm 0.190 \pm 0.202$
6.0–6.2	$0.495 \pm 0.058 \pm 0.040$	$0.489 \pm 0.069 \pm 0.079$	$0.518 \pm 0.248 \pm 0.251$
6.2–6.4	$0.323 \pm 0.045 \pm 0.006$	$0.318 \pm 0.055 \pm 0.055$	$0.384 \pm 0.190 \pm 0.196$
6.4–6.6	$0.208 \pm 0.043 \pm 0.009$	$0.204 \pm 0.051 \pm 0.051$	$0.211 \pm 0.133 \pm 0.133$
6.6–6.8	$0.134 \pm 0.043 \pm 0.014$	$0.132 \pm 0.051 \pm 0.053$	$0.115 \pm 0.117 \pm 0.120$
6.8–7.0	$0.089 \pm 0.042 \pm 0.004$	$0.086 \pm 0.050 \pm 0.050$	$0.080 \pm 0.115 \pm 0.116$
7.0–7.2	$0.062 \pm 0.035 \pm 0.088$	$0.060 \pm 0.040 \pm 0.097$	$0.000 \pm 0.000 \pm 0.088$
7.2–7.4	$0.046 \pm 0.026 \pm 0.004$	$0.044 \pm 0.038 \pm 0.039$	$0.038 \pm 0.056 \pm 0.060$
7.4–7.6	$0.034 \pm 0.020 \pm 0.003$	$0.034 \pm 0.021 \pm 0.022$	$0.010 \pm 0.021 \pm 0.035$
7.6–7.8	$0.026 \pm 0.022 \pm 0.038$	$0.019 \pm 0.028 \pm 0.048$	$0.023 \pm 0.047 \pm 0.059$
7.8–8.0	$0.022 \pm 0.001 \pm 0.001$	$0.021 \pm 0.001 \pm 0.001$	$0.024 \pm 0.001 \pm 0.001$

Table 72: ξ distributions at $\sqrt{s} = 91.2$ GeV. The first uncertainty is statistical, the second systematic.

	$\frac{1}{\sigma} \cdot \frac{d\sigma}{d\xi}$		
ξ	at $\sqrt{s} = 130.1$ GeV	at $\sqrt{s} = 136.1$ GeV	at $\sqrt{s} = 161.3$ GeV
0.0–0.2	$0.040 \pm 0.015 \pm 0.013$	$0.067 \pm 0.020 \pm 0.007$	$0.028 \pm 0.015 \pm 0.006$
0.2–0.4	$0.055 \pm 0.016 \pm 0.031$	$0.084 \pm 0.023 \pm 0.052$	$0.099 \pm 0.028 \pm 0.025$
0.4–0.6	$0.147 \pm 0.044 \pm 0.088$	$0.170 \pm 0.045 \pm 0.067$	$0.144 \pm 0.041 \pm 0.056$
0.6–0.8	$0.349 \pm 0.066 \pm 0.084$	$0.475 \pm 0.085 \pm 0.078$	$0.350 \pm 0.076 \pm 0.099$
0.8–1.0	$0.638 \pm 0.094 \pm 0.049$	$0.713 \pm 0.115 \pm 0.068$	$0.502 \pm 0.105 \pm 0.104$
1.0–1.2	$0.823 \pm 0.109 \pm 0.059$	$1.075 \pm 0.145 \pm 0.108$	$1.074 \pm 0.158 \pm 0.090$
1.2–1.4	$1.289 \pm 0.136 \pm 0.102$	$1.244 \pm 0.155 \pm 0.102$	$1.614 \pm 0.195 \pm 0.107$
1.4–1.6	$2.148 \pm 0.177 \pm 0.126$	$1.849 \pm 0.190 \pm 0.136$	$1.737 \pm 0.204 \pm 0.040$
1.6–1.8	$2.689 \pm 0.198 \pm 0.157$	$2.433 \pm 0.213 \pm 0.179$	$2.379 \pm 0.234 \pm 0.121$
1.8–2.0	$2.662 \pm 0.195 \pm 0.140$	$2.448 \pm 0.212 \pm 0.230$	$2.619 \pm 0.249 \pm 0.081$
2.0–2.2	$3.691 \pm 0.224 \pm 0.164$	$3.101 \pm 0.237 \pm 0.208$	$4.119 \pm 0.302 \pm 0.212$
2.2–2.4	$4.462 \pm 0.251 \pm 0.296$	$4.007 \pm 0.267 \pm 0.197$	$4.337 \pm 0.309 \pm 0.192$
2.4–2.6	$4.581 \pm 0.241 \pm 0.175$	$4.365 \pm 0.277 \pm 0.254$	$5.176 \pm 0.332 \pm 0.265$
2.6–2.8	$5.299 \pm 0.259 \pm 0.189$	$4.945 \pm 0.296 \pm 0.259$	$5.944 \pm 0.348 \pm 0.210$
2.8–3.0	$5.924 \pm 0.271 \pm 0.265$	$5.538 \pm 0.303 \pm 0.312$	$5.877 \pm 0.344 \pm 0.357$
3.0–3.2	$5.874 \pm 0.263 \pm 0.256$	$6.075 \pm 0.313 \pm 0.271$	$7.071 \pm 0.369 \pm 0.304$
3.2–3.4	$6.764 \pm 0.286 \pm 0.178$	$6.337 \pm 0.317 \pm 0.303$	$6.333 \pm 0.348 \pm 0.425$
3.4–3.6	$6.605 \pm 0.284 \pm 0.243$	$7.308 \pm 0.336 \pm 0.393$	$6.696 \pm 0.349 \pm 0.235$
3.6–3.8	$6.918 \pm 0.280 \pm 0.171$	$6.575 \pm 0.320 \pm 0.234$	$7.279 \pm 0.362 \pm 0.330$
3.8–4.0	$6.903 \pm 0.278 \pm 0.174$	$6.911 \pm 0.328 \pm 0.231$	$7.349 \pm 0.361 \pm 0.297$
4.0–4.2	$6.746 \pm 0.273 \pm 0.224$	$6.970 \pm 0.333 \pm 0.336$	$7.448 \pm 0.362 \pm 0.344$
4.2–4.4	$6.118 \pm 0.256 \pm 0.228$	$6.855 \pm 0.314 \pm 0.390$	$7.142 \pm 0.348 \pm 0.173$
4.4–4.6	$6.588 \pm 0.266 \pm 0.319$	$6.623 \pm 0.308 \pm 0.343$	$6.789 \pm 0.341 \pm 0.305$
4.6–4.8	$5.756 \pm 0.253 \pm 0.280$	$6.541 \pm 0.306 \pm 0.371$	$6.323 \pm 0.327 \pm 0.460$
4.8–5.0	$5.416 \pm 0.238 \pm 0.321$	$4.831 \pm 0.260 \pm 0.142$	$6.167 \pm 0.316 \pm 0.282$
5.0–5.2	$4.484 \pm 0.214 \pm 0.175$	$5.002 \pm 0.272 \pm 0.173$	$5.288 \pm 0.293 \pm 0.246$
5.2–5.4	$3.799 \pm 0.198 \pm 0.220$	$3.817 \pm 0.231 \pm 0.244$	$5.347 \pm 0.290 \pm 0.212$
5.4–5.6	$2.942 \pm 0.172 \pm 0.104$	$3.182 \pm 0.209 \pm 0.142$	$4.147 \pm 0.256 \pm 0.243$
5.6–5.8	$2.409 \pm 0.155 \pm 0.150$	$2.574 \pm 0.186 \pm 0.106$	$2.904 \pm 0.219 \pm 0.120$
5.8–6.0	$1.783 \pm 0.135 \pm 0.109$	$1.804 \pm 0.156 \pm 0.066$	$2.431 \pm 0.194 \pm 0.158$
6.0–6.2	$1.179 \pm 0.110 \pm 0.060$	$1.189 \pm 0.126 \pm 0.081$	$1.529 \pm 0.151 \pm 0.077$
6.2–6.4	$0.785 \pm 0.104 \pm 0.094$	$1.055 \pm 0.135 \pm 0.116$	$1.312 \pm 0.146 \pm 0.048$
6.4–6.6	$0.181 \pm 0.057 \pm 0.032$	$0.429 \pm 0.105 \pm 0.051$	$0.880 \pm 0.134 \pm 0.078$
6.6–6.8	$0.000 \pm 0.000 \pm 0.000$	$0.000 \pm 0.000 \pm 0.000$	$0.248 \pm 0.089 \pm 0.058$

Table 73: ξ distributions at $\sqrt{s} = 130.1$, 136.1 and 161.3 GeV. The first uncertainty is statistical, the second systematic.

	$\frac{1}{\sigma} \cdot \frac{d\sigma}{d\xi}$		
ξ	at $\sqrt{s} = 172.3$ GeV	at $\sqrt{s} = 182.8$ GeV	at $\sqrt{s} = 188.6$ GeV
0.0–0.2	$0.056 \pm 0.023 \pm 0.020$	$0.081 \pm 0.013 \pm 0.014$	$0.065 \pm 0.007 \pm 0.008$
0.2–0.4	$0.089 \pm 0.028 \pm 0.027$	$0.091 \pm 0.013 \pm 0.027$	$0.089 \pm 0.008 \pm 0.015$
0.4–0.6	$0.227 \pm 0.055 \pm 0.088$	$0.127 \pm 0.019 \pm 0.067$	$0.163 \pm 0.013 \pm 0.043$
0.6–0.8	$0.385 \pm 0.094 \pm 0.125$	$0.316 \pm 0.038 \pm 0.037$	$0.346 \pm 0.025 \pm 0.055$
0.8–1.0	$0.640 \pm 0.134 \pm 0.178$	$0.593 \pm 0.058 \pm 0.073$	$0.586 \pm 0.036 \pm 0.067$
1.0–1.2	$1.082 \pm 0.188 \pm 0.100$	$0.892 \pm 0.075 \pm 0.035$	$1.050 \pm 0.049 \pm 0.018$
1.2–1.4	$1.384 \pm 0.204 \pm 0.198$	$1.387 \pm 0.094 \pm 0.053$	$1.338 \pm 0.056 \pm 0.020$
1.4–1.6	$2.105 \pm 0.258 \pm 0.192$	$1.881 \pm 0.110 \pm 0.057$	$1.922 \pm 0.065 \pm 0.071$
1.6–1.8	$1.913 \pm 0.252 \pm 0.161$	$2.556 \pm 0.128 \pm 0.136$	$2.395 \pm 0.075 \pm 0.038$
1.8–2.0	$2.847 \pm 0.303 \pm 0.279$	$2.917 \pm 0.136 \pm 0.079$	$3.027 \pm 0.082 \pm 0.054$
2.0–2.2	$3.841 \pm 0.337 \pm 0.262$	$3.522 \pm 0.149 \pm 0.108$	$3.603 \pm 0.093 \pm 0.044$
2.2–2.4	$4.515 \pm 0.363 \pm 0.490$	$4.118 \pm 0.158 \pm 0.094$	$4.388 \pm 0.098 \pm 0.089$
2.4–2.6	$4.665 \pm 0.372 \pm 0.518$	$4.775 \pm 0.169 \pm 0.082$	$4.651 \pm 0.100 \pm 0.073$
2.6–2.8	$4.951 \pm 0.378 \pm 0.342$	$5.536 \pm 0.180 \pm 0.131$	$5.487 \pm 0.109 \pm 0.139$
2.8–3.0	$5.472 \pm 0.390 \pm 0.380$	$5.625 \pm 0.181 \pm 0.176$	$5.629 \pm 0.107 \pm 0.129$
3.0–3.2	$6.489 \pm 0.419 \pm 0.393$	$6.146 \pm 0.187 \pm 0.238$	$6.394 \pm 0.115 \pm 0.142$
3.2–3.4	$6.838 \pm 0.427 \pm 0.633$	$6.938 \pm 0.197 \pm 0.122$	$6.982 \pm 0.118 \pm 0.139$
3.4–3.6	$7.378 \pm 0.434 \pm 0.564$	$6.839 \pm 0.194 \pm 0.230$	$7.271 \pm 0.119 \pm 0.135$
3.6–3.8	$7.182 \pm 0.418 \pm 0.873$	$7.296 \pm 0.198 \pm 0.229$	$7.080 \pm 0.116 \pm 0.187$
3.8–4.0	$7.583 \pm 0.428 \pm 0.912$	$7.430 \pm 0.199 \pm 0.213$	$7.339 \pm 0.119 \pm 0.147$
4.0–4.2	$7.838 \pm 0.427 \pm 0.620$	$7.415 \pm 0.197 \pm 0.216$	$7.516 \pm 0.118 \pm 0.210$
4.2–4.4	$7.918 \pm 0.433 \pm 0.764$	$7.231 \pm 0.192 \pm 0.201$	$7.450 \pm 0.118 \pm 0.195$
4.4–4.6	$6.706 \pm 0.395 \pm 0.598$	$7.202 \pm 0.191 \pm 0.234$	$7.029 \pm 0.114 \pm 0.170$
4.6–4.8	$6.582 \pm 0.387 \pm 0.654$	$7.070 \pm 0.187 \pm 0.399$	$6.938 \pm 0.111 \pm 0.199$
4.8–5.0	$6.411 \pm 0.381 \pm 0.644$	$6.354 \pm 0.179 \pm 0.213$	$6.427 \pm 0.110 \pm 0.133$
5.0–5.2	$6.069 \pm 0.365 \pm 0.523$	$5.646 \pm 0.167 \pm 0.289$	$5.890 \pm 0.107 \pm 0.086$
5.2–5.4	$5.055 \pm 0.340 \pm 0.480$	$5.442 \pm 0.162 \pm 0.197$	$5.220 \pm 0.096 \pm 0.107$
5.4–5.6	$4.189 \pm 0.302 \pm 0.433$	$4.427 \pm 0.146 \pm 0.239$	$4.559 \pm 0.090 \pm 0.130$
5.6–5.8	$3.531 \pm 0.273 \pm 0.288$	$3.845 \pm 0.136 \pm 0.150$	$3.770 \pm 0.081 \pm 0.071$
5.8–6.0	$2.791 \pm 0.242 \pm 0.177$	$2.890 \pm 0.117 \pm 0.100$	$2.987 \pm 0.073 \pm 0.040$
6.0–6.2	$2.155 \pm 0.214 \pm 0.165$	$2.241 \pm 0.100 \pm 0.080$	$2.363 \pm 0.064 \pm 0.076$
6.2–6.4	$1.721 \pm 0.190 \pm 0.122$	$1.659 \pm 0.087 \pm 0.080$	$1.730 \pm 0.054 \pm 0.060$
6.4–6.6	$1.062 \pm 0.160 \pm 0.147$	$1.086 \pm 0.074 \pm 0.076$	$1.209 \pm 0.047 \pm 0.051$
6.6–6.8	$0.290 \pm 0.108 \pm 0.094$	$0.657 \pm 0.070 \pm 0.058$	$0.749 \pm 0.042 \pm 0.019$
6.8–7.0	$0.000 \pm 0.000 \pm 0.000$	$0.020 \pm 0.013 \pm 0.014$	$0.088 \pm 0.016 \pm 0.023$

Table 74: ξ distributions at $\sqrt{s} = 172.3$, 182.8 and 188.6 GeV. The first uncertainty is statistical, the second systematic.

	$\frac{1}{\sigma} \cdot \frac{d\sigma}{d\xi}$		
ξ	at $\sqrt{s} = 194.4$ GeV	at $\sqrt{s} = 200.2$ GeV	at $\sqrt{s} = 206.2$ GeV
0.0–0.2	$0.068 \pm 0.010 \pm 0.014$	$0.078 \pm 0.010 \pm 0.020$	$0.078 \pm 0.008 \pm 0.012$
0.2–0.4	$0.087 \pm 0.011 \pm 0.018$	$0.084 \pm 0.015 \pm 0.015$	$0.100 \pm 0.009 \pm 0.013$
0.4–0.6	$0.180 \pm 0.018 \pm 0.058$	$0.150 \pm 0.017 \pm 0.059$	$0.173 \pm 0.015 \pm 0.059$
0.6–0.8	$0.310 \pm 0.034 \pm 0.058$	$0.318 \pm 0.033 \pm 0.062$	$0.316 \pm 0.024 \pm 0.070$
0.8–1.0	$0.679 \pm 0.051 \pm 0.074$	$0.527 \pm 0.045 \pm 0.071$	$0.632 \pm 0.038 \pm 0.067$
1.0–1.2	$0.937 \pm 0.061 \pm 0.078$	$0.858 \pm 0.060 \pm 0.047$	$0.908 \pm 0.050 \pm 0.071$
1.2–1.4	$1.233 \pm 0.073 \pm 0.097$	$1.295 \pm 0.075 \pm 0.081$	$1.314 \pm 0.067 \pm 0.073$
1.4–1.6	$1.842 \pm 0.090 \pm 0.070$	$1.751 \pm 0.097 \pm 0.148$	$1.715 \pm 0.068 \pm 0.056$
1.6–1.8	$2.319 \pm 0.100 \pm 0.097$	$2.368 \pm 0.119 \pm 0.140$	$2.339 \pm 0.080 \pm 0.064$
1.8–2.0	$2.828 \pm 0.109 \pm 0.142$	$2.572 \pm 0.155 \pm 0.116$	$2.873 \pm 0.088 \pm 0.094$
2.0–2.2	$3.466 \pm 0.121 \pm 0.106$	$3.566 \pm 0.145 \pm 0.244$	$3.444 \pm 0.096 \pm 0.111$
2.2–2.4	$4.090 \pm 0.128 \pm 0.112$	$4.239 \pm 0.143 \pm 0.214$	$4.189 \pm 0.106 \pm 0.150$
2.4–2.6	$4.726 \pm 0.140 \pm 0.201$	$4.998 \pm 0.205 \pm 0.402$	$4.776 \pm 0.113 \pm 0.126$
2.6–2.8	$5.398 \pm 0.147 \pm 0.170$	$4.759 \pm 0.146 \pm 0.219$	$5.356 \pm 0.117 \pm 0.154$
2.8–3.0	$5.418 \pm 0.147 \pm 0.257$	$5.637 \pm 0.149 \pm 0.194$	$5.820 \pm 0.118 \pm 0.132$
3.0–3.2	$6.227 \pm 0.156 \pm 0.125$	$6.133 \pm 0.155 \pm 0.250$	$6.245 \pm 0.125 \pm 0.150$
3.2–3.4	$6.729 \pm 0.167 \pm 0.219$	$6.240 \pm 0.153 \pm 0.215$	$6.884 \pm 0.132 \pm 0.177$
3.4–3.6	$7.163 \pm 0.166 \pm 0.161$	$7.096 \pm 0.162 \pm 0.207$	$7.197 \pm 0.131 \pm 0.250$
3.6–3.8	$7.138 \pm 0.160 \pm 0.253$	$7.308 \pm 0.163 \pm 0.181$	$7.500 \pm 0.130 \pm 0.284$
3.8–4.0	$7.496 \pm 0.168 \pm 0.281$	$7.453 \pm 0.161 \pm 0.276$	$7.692 \pm 0.133 \pm 0.158$
4.0–4.2	$7.565 \pm 0.173 \pm 0.187$	$7.320 \pm 0.164 \pm 0.292$	$7.829 \pm 0.135 \pm 0.236$
4.2–4.4	$7.133 \pm 0.162 \pm 0.283$	$7.353 \pm 0.161 \pm 0.217$	$7.439 \pm 0.130 \pm 0.219$
4.4–4.6	$7.103 \pm 0.156 \pm 0.264$	$7.409 \pm 0.159 \pm 0.276$	$7.535 \pm 0.125 \pm 0.191$
4.6–4.8	$7.048 \pm 0.158 \pm 0.258$	$7.264 \pm 0.176 \pm 0.260$	$7.149 \pm 0.129 \pm 0.214$
4.8–5.0	$6.482 \pm 0.149 \pm 0.204$	$6.764 \pm 0.153 \pm 0.232$	$6.953 \pm 0.123 \pm 0.210$
5.0–5.2	$6.154 \pm 0.143 \pm 0.197$	$6.424 \pm 0.149 \pm 0.215$	$6.436 \pm 0.117 \pm 0.243$
5.2–5.4	$5.547 \pm 0.137 \pm 0.170$	$5.628 \pm 0.167 \pm 0.344$	$5.713 \pm 0.116 \pm 0.169$
5.4–5.6	$4.587 \pm 0.155 \pm 0.183$	$5.030 \pm 0.133 \pm 0.289$	$4.918 \pm 0.097 \pm 0.176$
5.6–5.8	$3.807 \pm 0.111 \pm 0.113$	$4.071 \pm 0.114 \pm 0.143$	$4.350 \pm 0.096 \pm 0.185$
5.8–6.0	$3.129 \pm 0.101 \pm 0.127$	$3.393 \pm 0.103 \pm 0.155$	$3.443 \pm 0.081 \pm 0.156$
6.0–6.2	$2.342 \pm 0.085 \pm 0.145$	$2.751 \pm 0.091 \pm 0.149$	$2.627 \pm 0.081 \pm 0.140$
6.2–6.4	$1.902 \pm 0.081 \pm 0.158$	$1.957 \pm 0.080 \pm 0.172$	$2.014 \pm 0.060 \pm 0.104$
6.4–6.6	$1.306 \pm 0.067 \pm 0.107$	$1.407 \pm 0.068 \pm 0.123$	$1.466 \pm 0.060 \pm 0.075$
6.6–6.8	$0.990 \pm 0.068 \pm 0.090$	$0.948 \pm 0.061 \pm 0.114$	$1.020 \pm 0.048 \pm 0.106$
6.8–7.0	$0.162 \pm 0.029 \pm 0.028$	$0.350 \pm 0.052 \pm 0.058$	$0.451 \pm 0.040 \pm 0.073$

Table 75: ξ distributions at $\sqrt{s} = 194.4$, 200.2 and 206.2 GeV. The first uncertainty is statistical, the second systematic.

Sample	Gaussian	Fong-Webber
All	$3.712 \pm 0.008 \pm 0.018$	$3.741 \pm 0.007 \pm 0.011$
udsc	$3.743 \pm 0.009 \pm 0.022$	$3.770 \pm 0.008 \pm 0.010$
b	$3.613 \pm 0.007 \pm 0.029$	$3.656 \pm 0.007 \pm 0.037$

Table 76: The peak position, $\xi^\star$, of the ξ distribution from the Gaussian and Fong-Webber fits at $\sqrt{s} = 91.2$ GeV. The first uncertainty is statistical, the second systematic.

$\langle\sqrt{s}\rangle$ (GeV)	χ^2/d.o.f.	$\xi^\star$
91.2	9.4 / 10	$3.74 \pm 0.01 \pm 0.02$
130.1	9.9 / 12	$3.85 \pm 0.03 \pm 0.05$
136.1	15.4 / 10	$3.96 \pm 0.05 \pm 0.05$
161.3	9.6 / 12	$3.91 \pm 0.05 \pm 0.04$
172.3	7.4 / 11	$4.06 \pm 0.05 \pm 0.05$
182.8	11.4 / 12	$4.08 \pm 0.02 \pm 0.04$
188.6	31.1 / 14	$4.06 \pm 0.01 \pm 0.03$
194.4	16.7 / 14	$4.13 \pm 0.02 \pm 0.03$
200.2	10.7 / 14	$4.17 \pm 0.02 \pm 0.04$
206.2	17.0 / 12	$4.13 \pm 0.01 \pm 0.03$

Table 77: The peak position, $\xi^\star$, of the ξ distribution from the Fong-Webber fits at different centre-of-mass energies. The χ^2 and number of degrees of freedom of the fits are also shown.

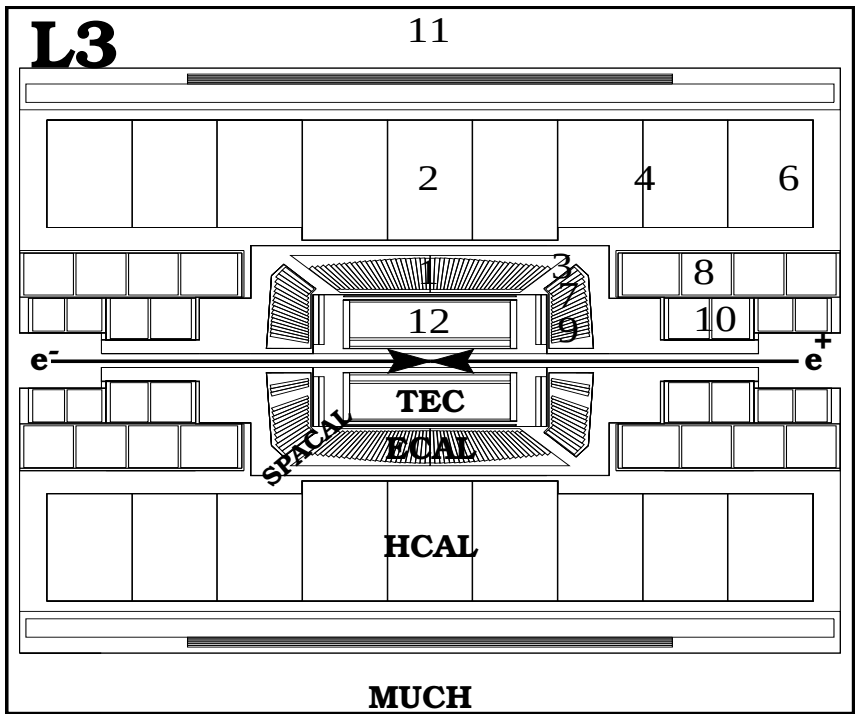

Figure 1: The eleven regions of L3 detectors as used in the energy measurement for the LEP2 configuration. A twelfth region, 5, was present only in earlier set-ups.

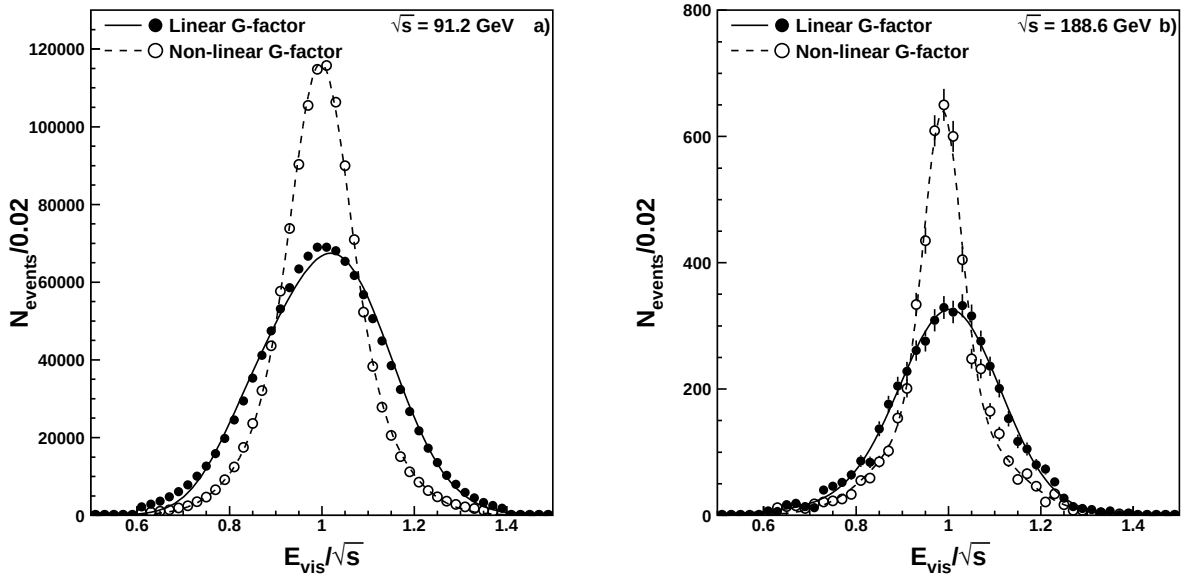

Figure 2: Distributions of scaled visible energy for clusters with linear and non-linear G-factors in data at (a) $\sqrt{s} = 91.2$ GeV and (b) $\sqrt{s} = 188.6$ GeV. The points correspond to the measurements and the smooth curves are from fits of a sum of Gaussian distributions as described in the text.

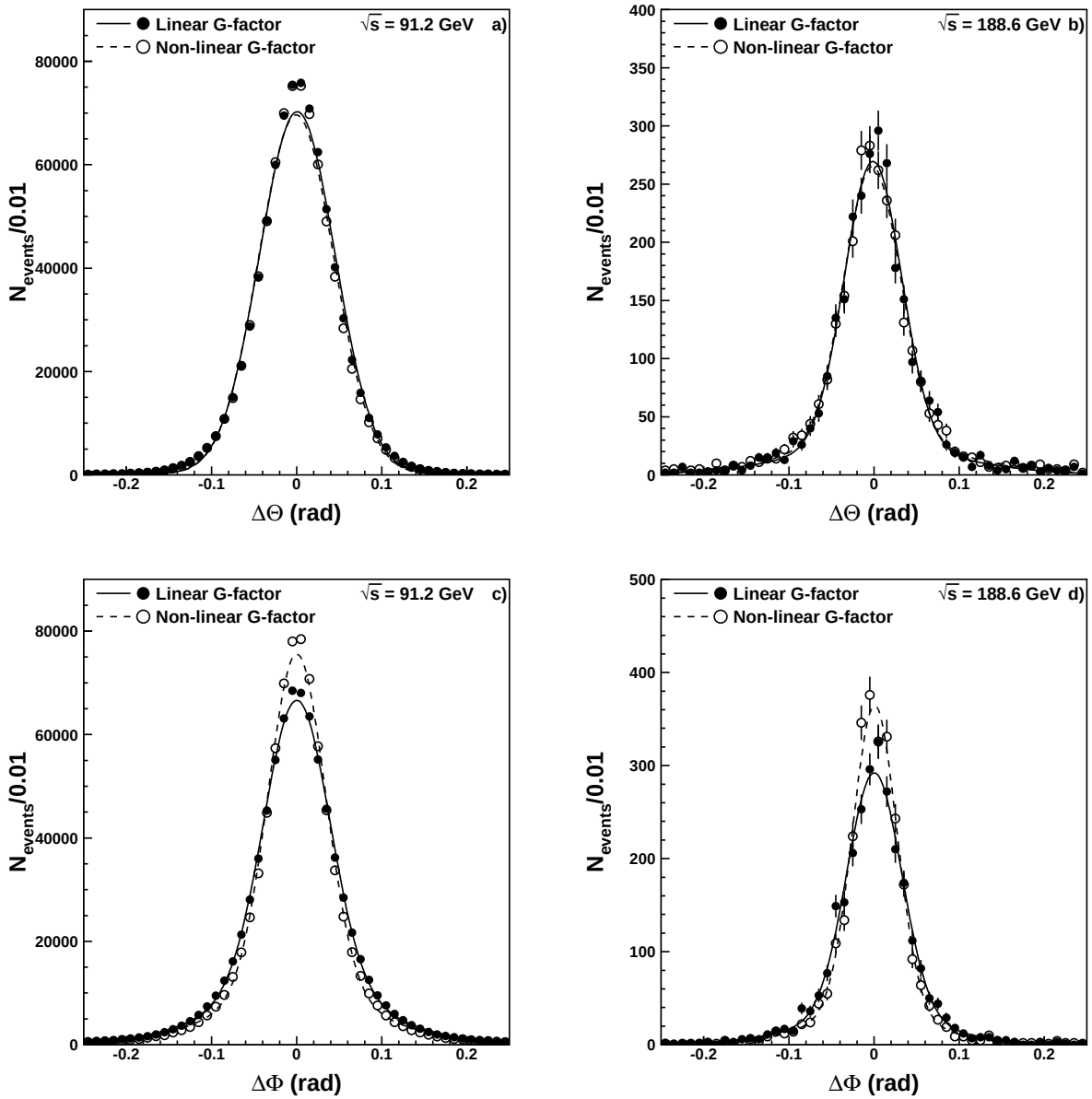

Figure 3: Jet angular resolutions obtained from the differences of (a,b) polar ($\Delta\Theta = |\Theta_2 - \Theta_1| - \pi$) and (c,d) azimuthal ($\Delta\Phi = |\Phi_2 - \Phi_1| - \pi$) angles of the two jets in two-jet events at (a,c) $\sqrt{s} = 91.2$ GeV and (b,d) $\sqrt{s} = 188.6$ GeV with non-linear G-factors.

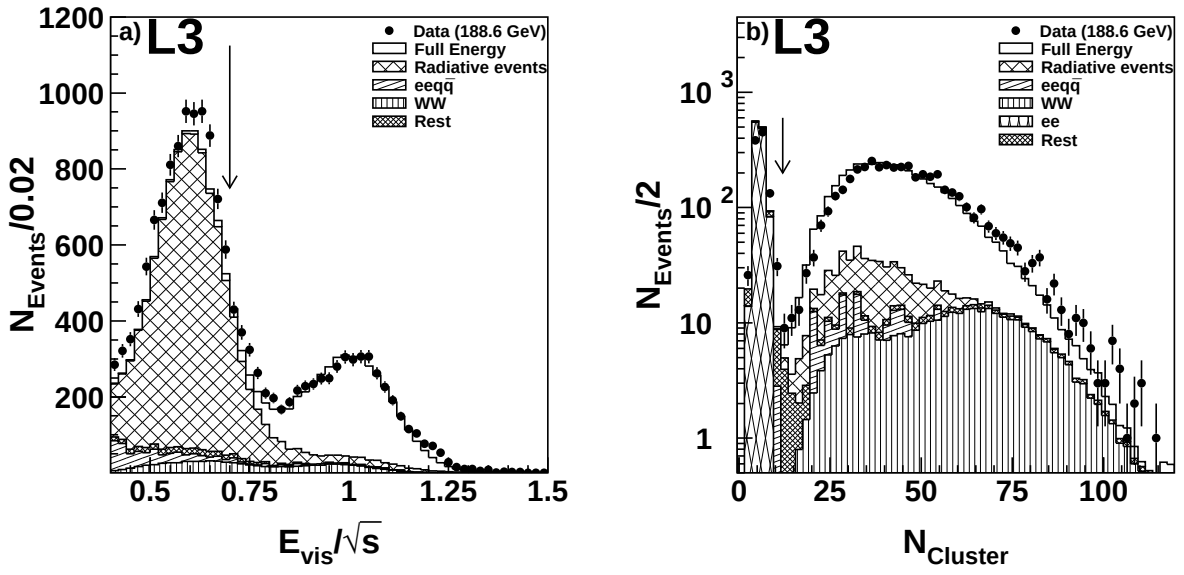

Figure 4: Distributions of (a) visible energy and (b) number of calorimetric clusters at $\sqrt{s} =$ 188.6 GeV. The arrows indicate the selection cuts.

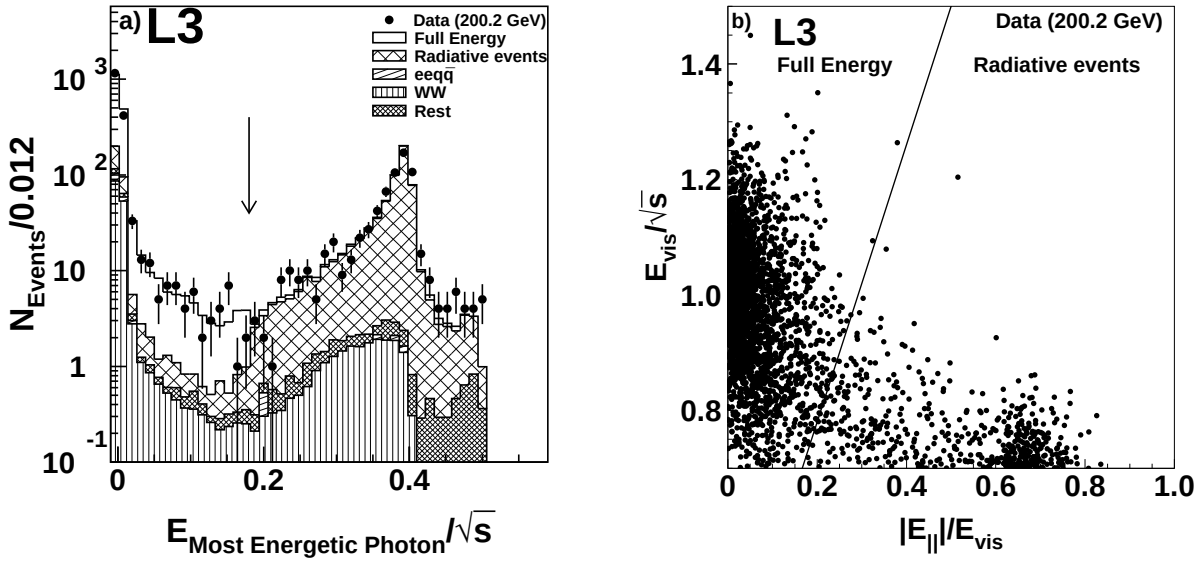

Figure 5: (a) Distribution of the energy of the most energetic photon candidate at $\sqrt{s} =$ 200.2 GeV. The arrow indicates the selection cut. (b) Plot of visible energy *vs.* energy imbalance along the beam direction for $\sqrt{s} = 200.2$ GeV. the cut used to remove radiative events is indicated.

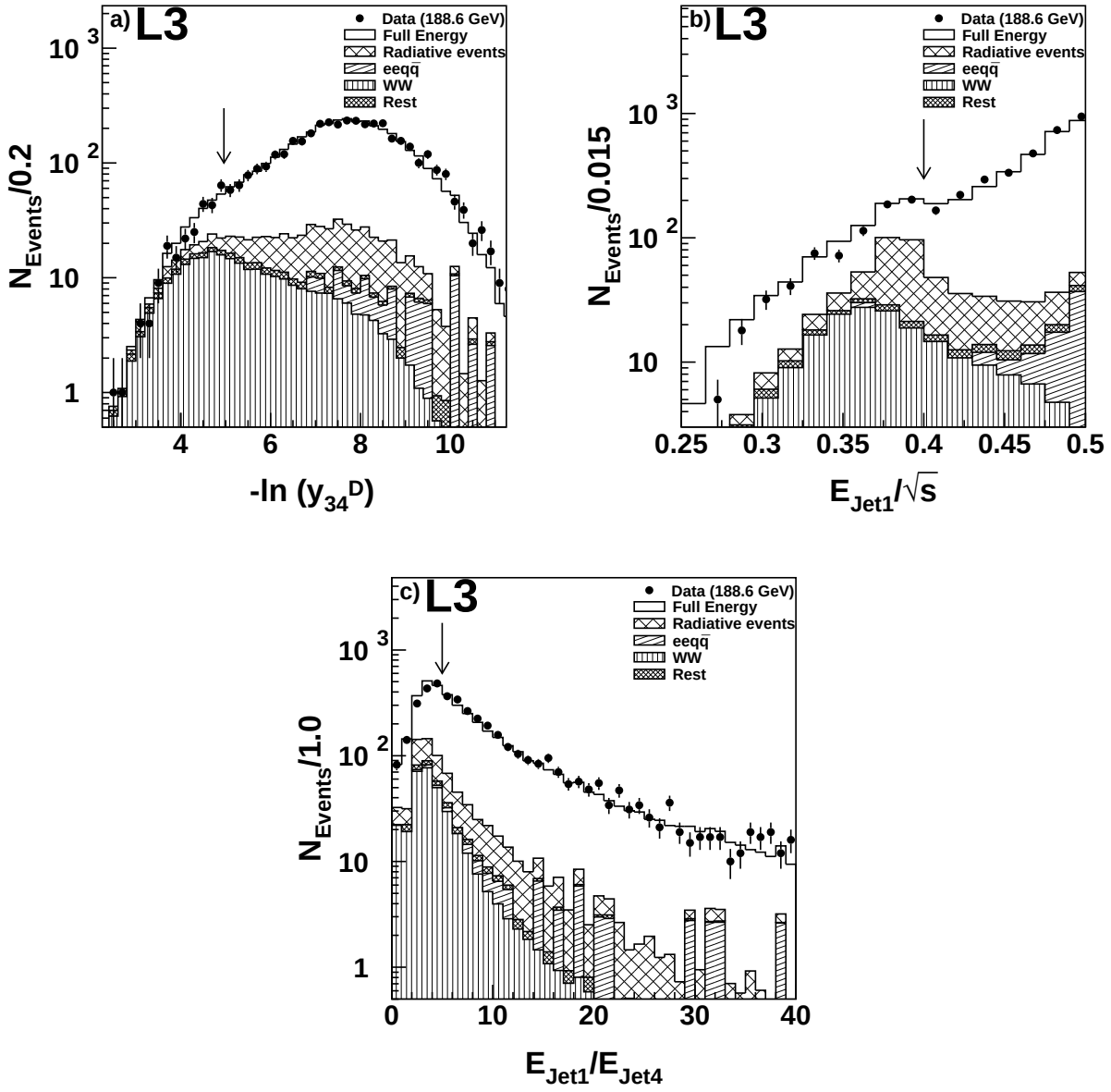

Figure 6: For events at $\sqrt{s} = 188.6$ GeV, (a) distribution of y_{34}^{D}, the value of the Durham jet resolution parameter at which the classification of an event changes from 3-jet to 4-jet. (b) distribution of the energy of the most energetic jet after the kinematic fit. (c) ratio of energy of the most energetic jet to that of the least energetic jet after the kinematic fit. The arrows indicate the selection cuts.

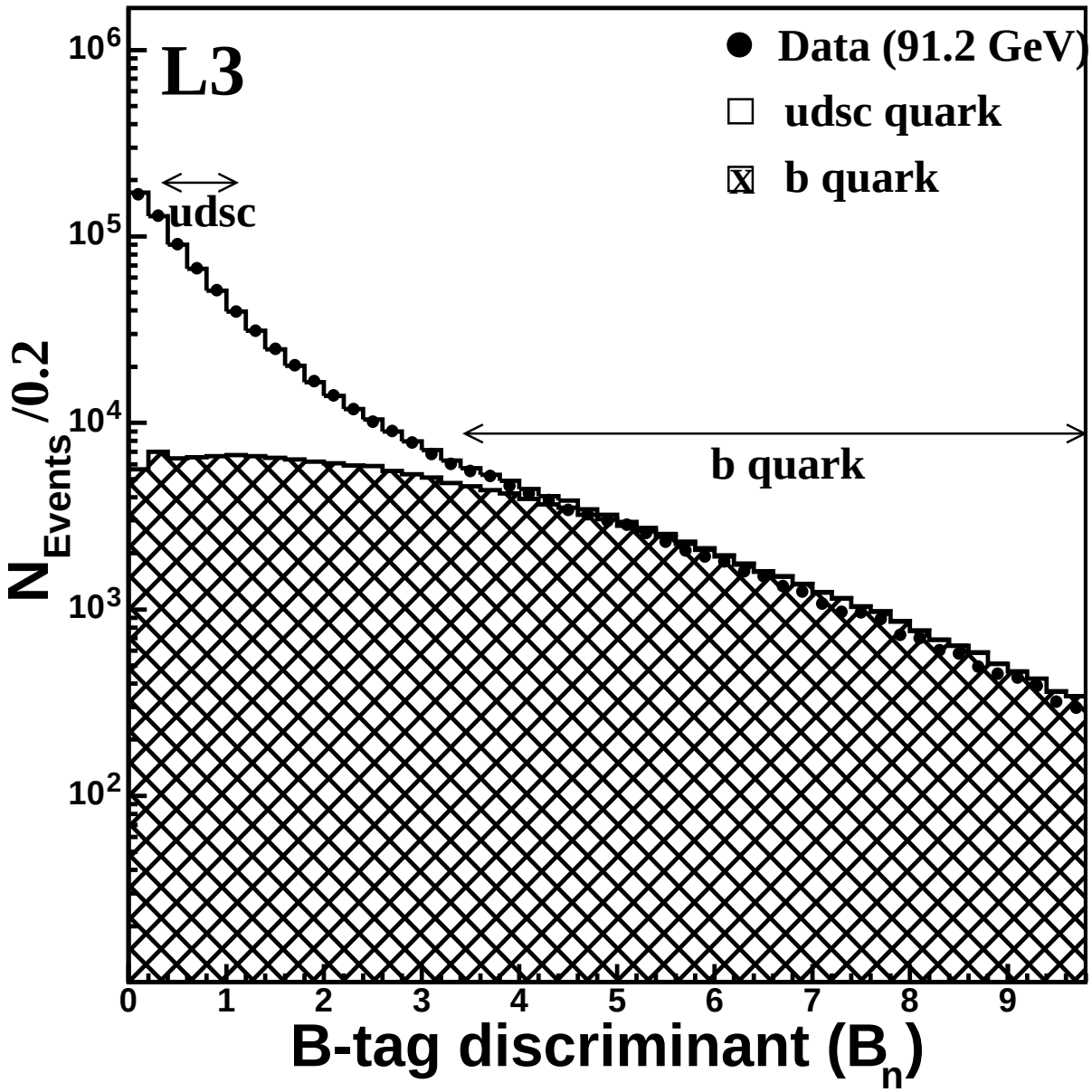

Figure 7: Weighted discriminant for b-tagging, B_n, for the Z-pole data compared to the expectation of the JETSET PS Monte Carlo program. The cuts used to select udsc- and b-enriched samples are indicated.

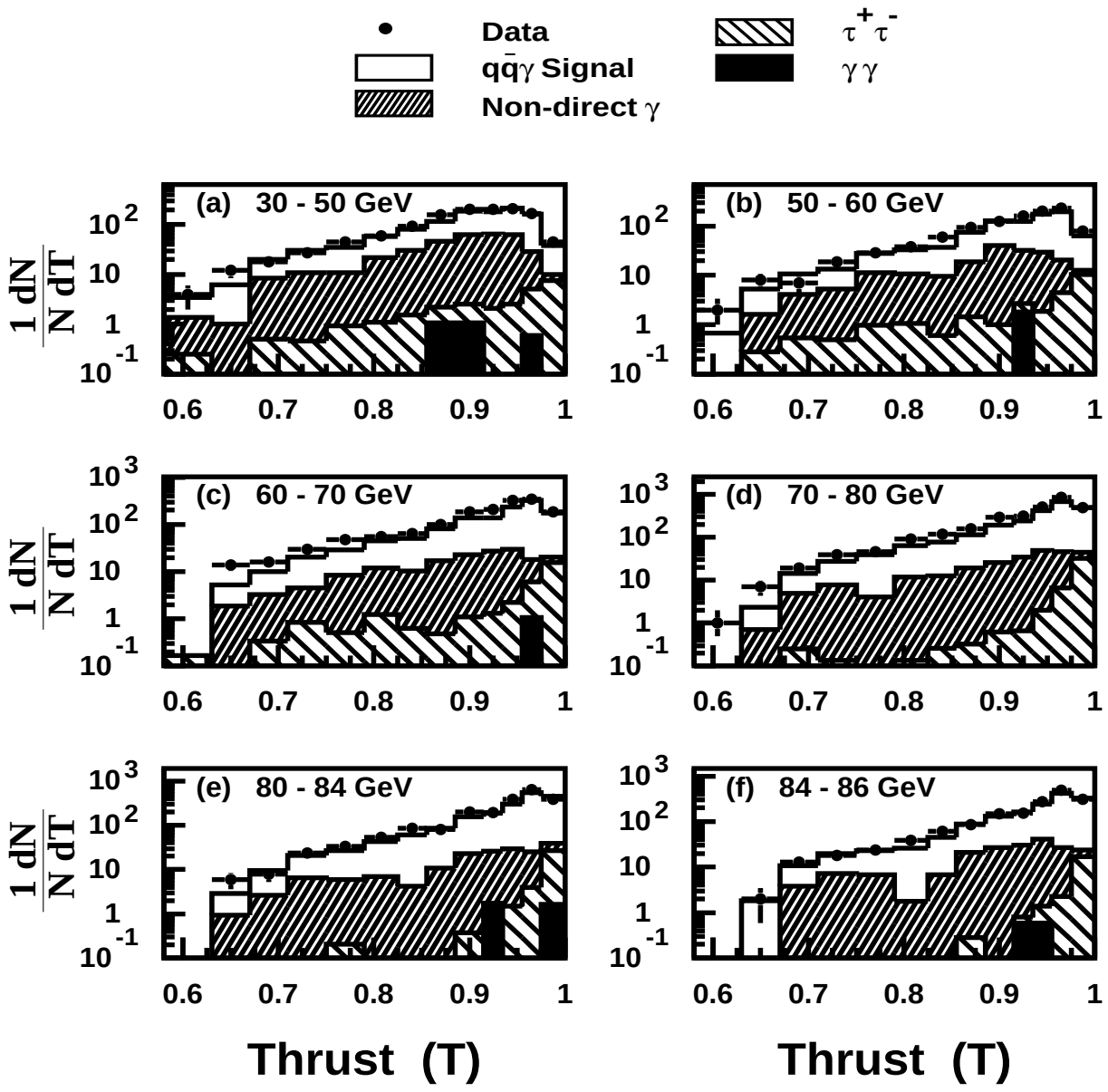

Figure 8: Measured thrust distributions at different reduced centre-of-mass energies (a) 30–50 GeV, (b) 50–60 GeV, (c) 60–70 GeV, (d) 70–80 GeV, (e) 80–84 GeV, (f) 84–86 GeV. The solid lines correspond to the overall expectations from theory. The shaded areas refer to different backgrounds and the clear area refers to the signal predicted by JETSET.

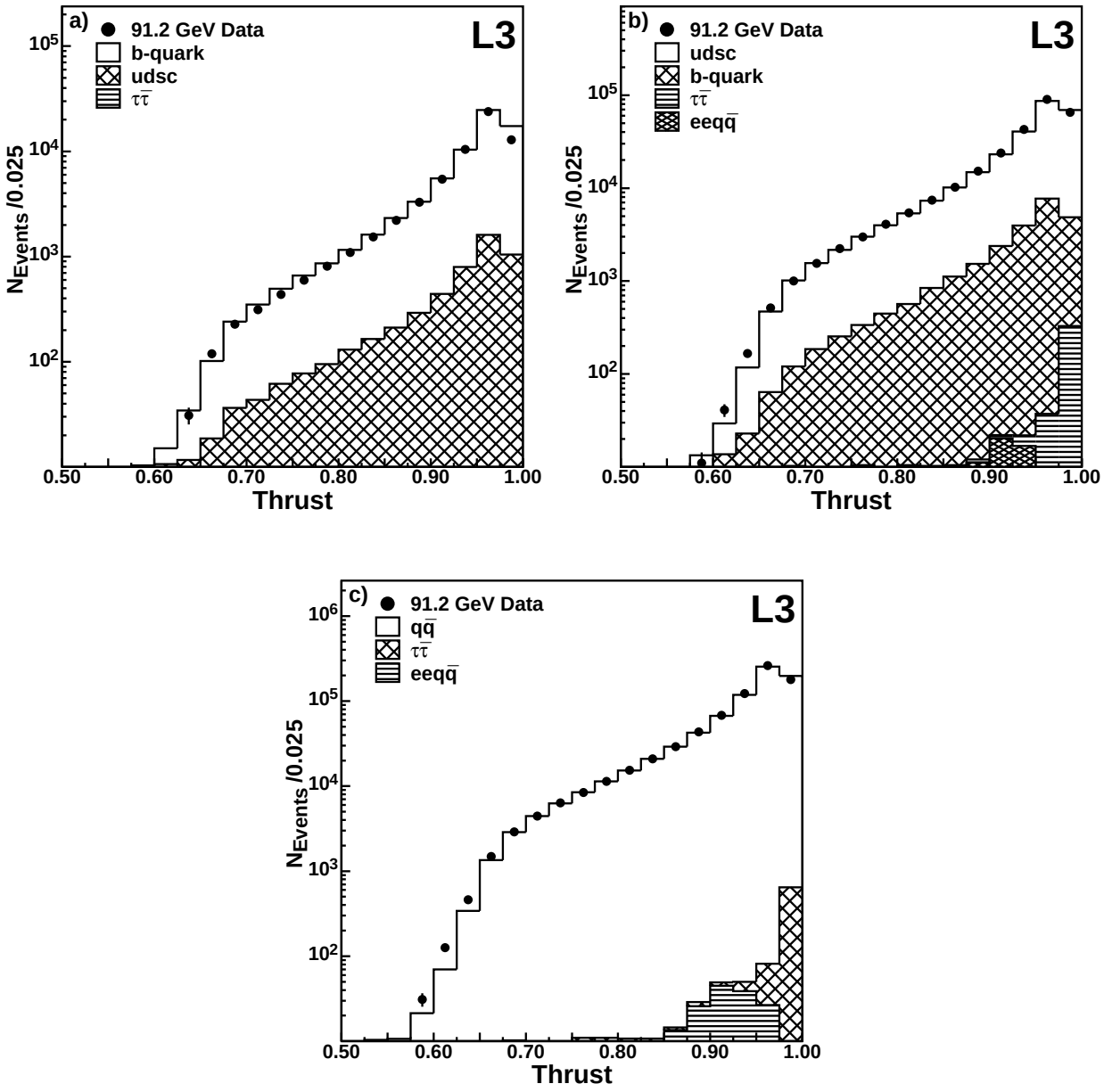

Figure 9: Measured thrust distributions at the Z-pole for the (a) b- and (b) udsc-flavour-tagged samples, as well as for (c) all events. The solid lines correspond to the overall expectations from theory. The shaded areas refer to different backgrounds and the clear area refers to the signal predicted by JETSET.

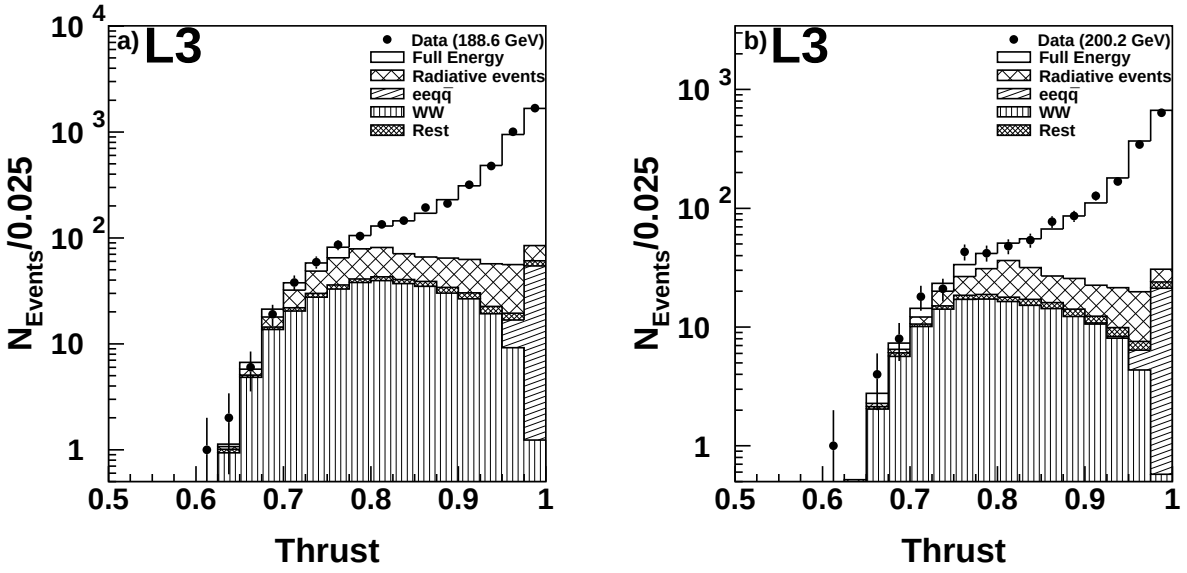

Figure 10: Measured thrust distributions at $\sqrt{s} = 188.6$ GeV and $\sqrt{s} = 200.2$ GeV The solid lines correspond to the overall expectations from theory. The shaded areas refer to different backgrounds and the clear area refers to the signal predicted by JETSET.

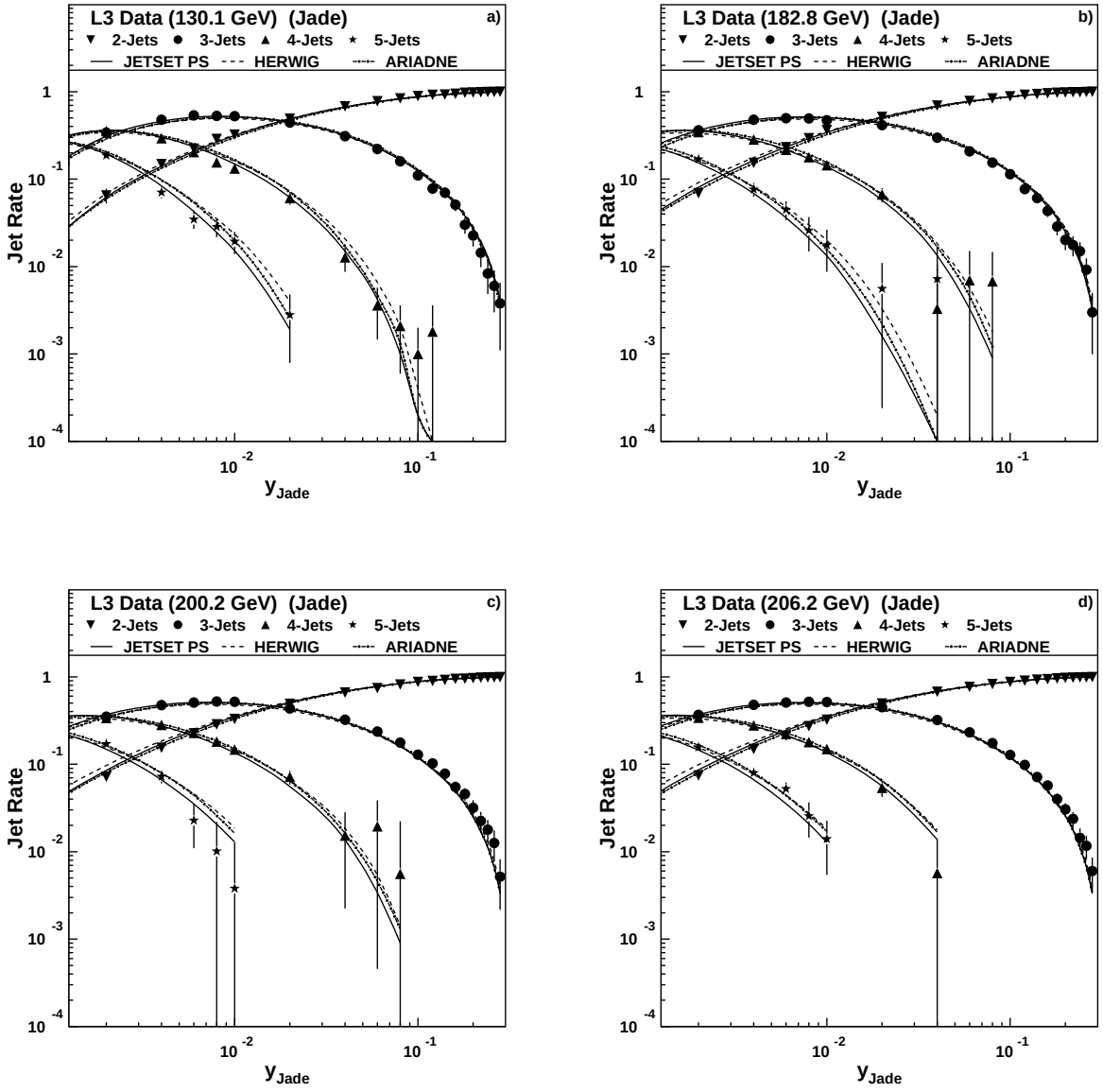

Figure 11: Fraction of 2-, 3-, 4- and 5-jet events as a function of jet resolution parameter $y_{\mathrm{cut}}^{\mathrm{J}}$ at $\sqrt{s} = 130.1, 182.8, 200.2$ and 206.2 GeV for the JADE algorithm.

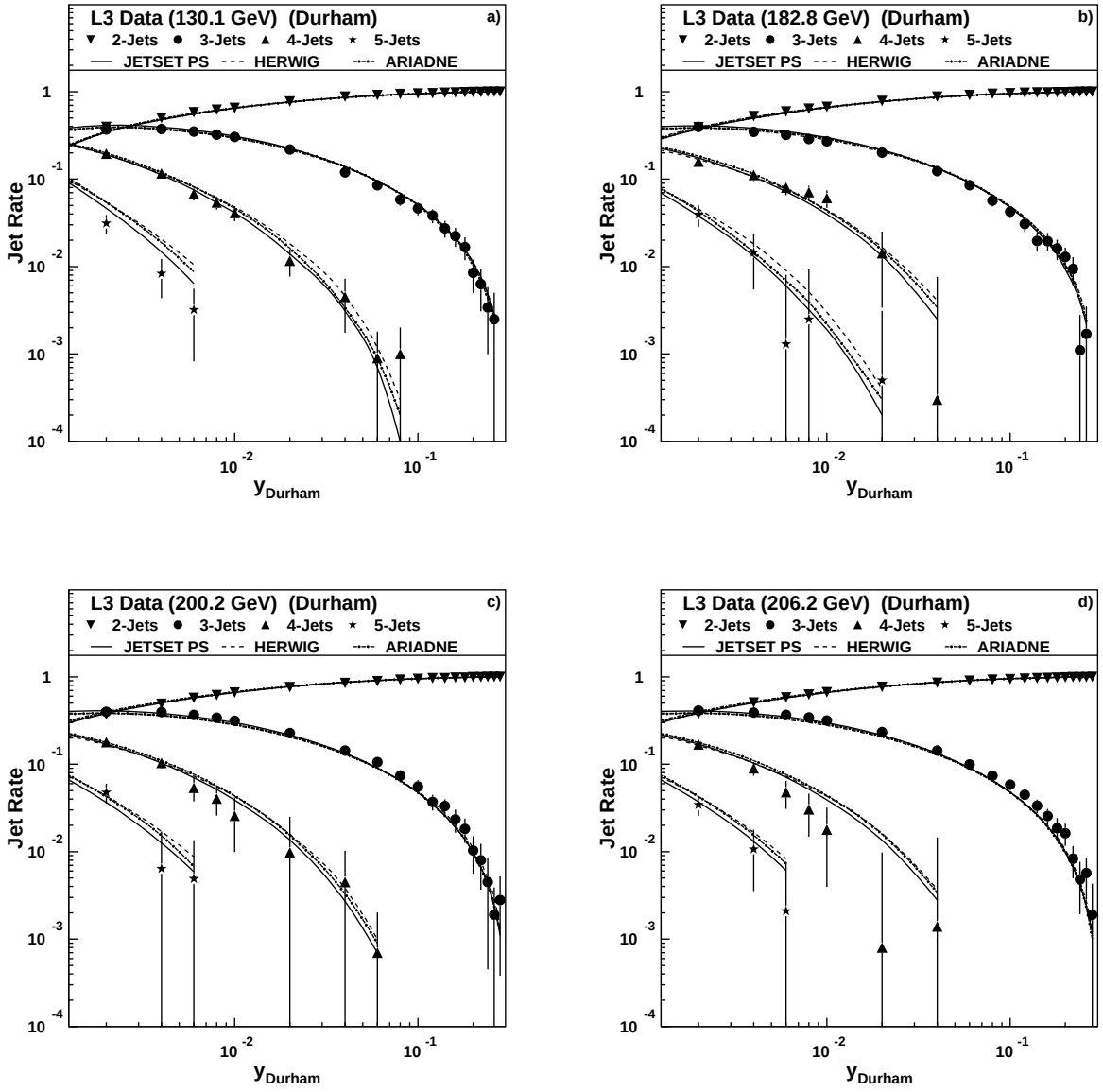

Figure 12: Fraction of 2-, 3-, 4- and 5-jet events as a function of jet resolution parameter $y_{\mathrm{cut}}^{\mathrm{D}}$ at $\sqrt{s} = 130.1, 182.8, 200.2$ and 206.2 GeV for the Durham algorithm.

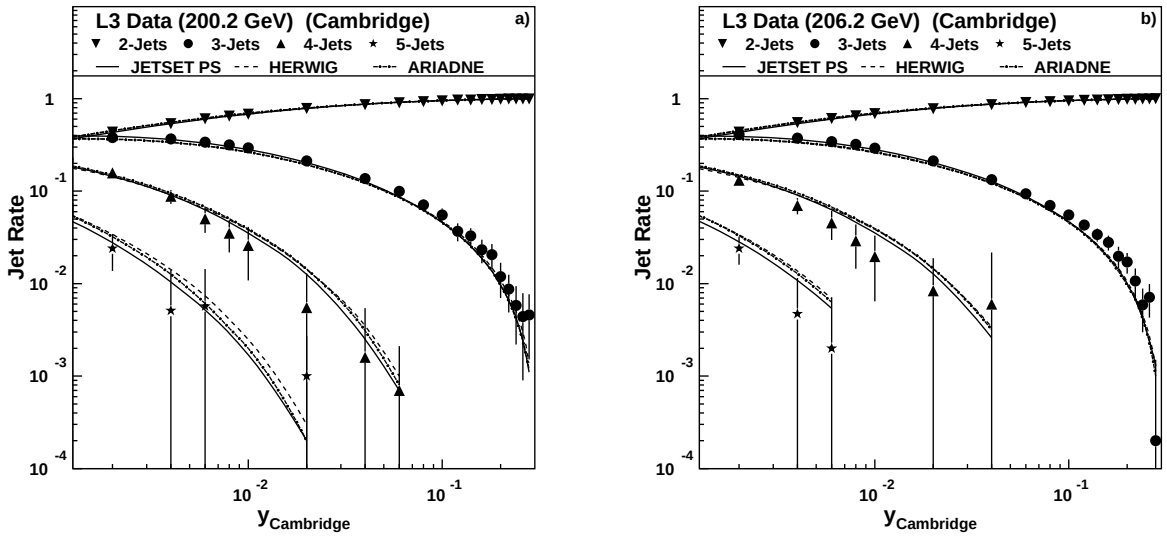

Figure 13: Fraction of 2-, 3-, 4- and 5-jet events as a function of the jet resolution parameter $y_{\rm cut}^{\rm D}$ at $\sqrt{s} = 200.2$ and 206.2 GeV for the Cambridge algorithm.

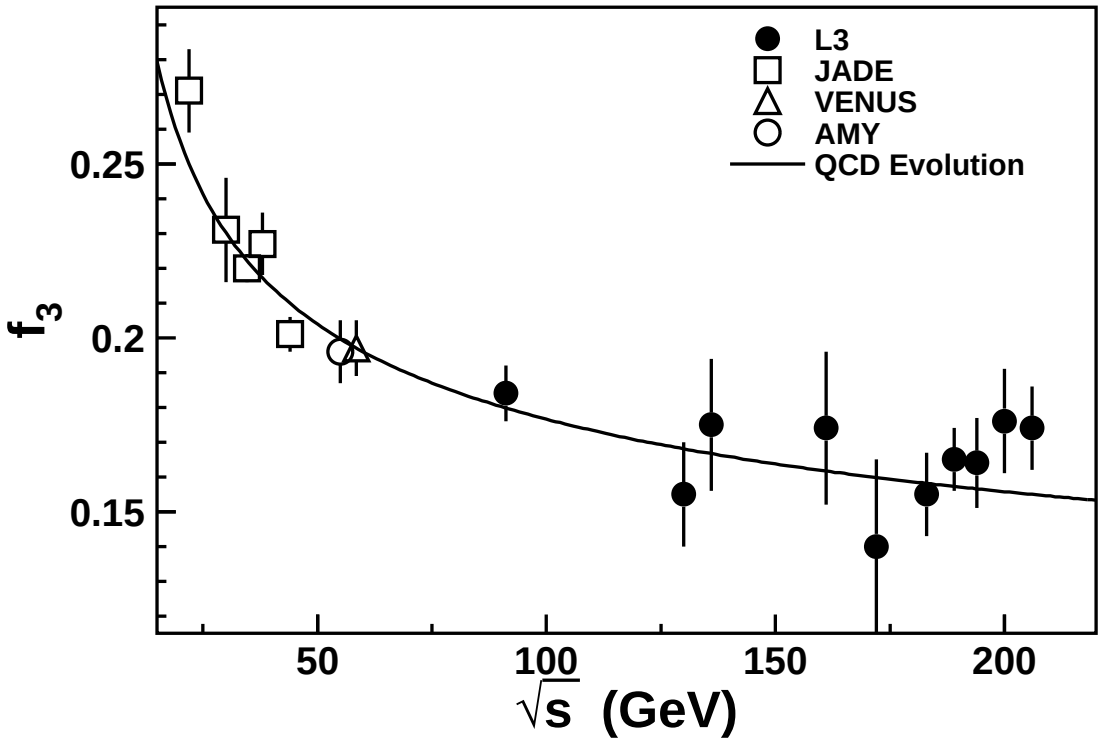

Figure 14: Energy evolution of the 3-jet fraction at $y_{\rm cut}^{\rm J} = 0.08$ with the JADE algorithm.

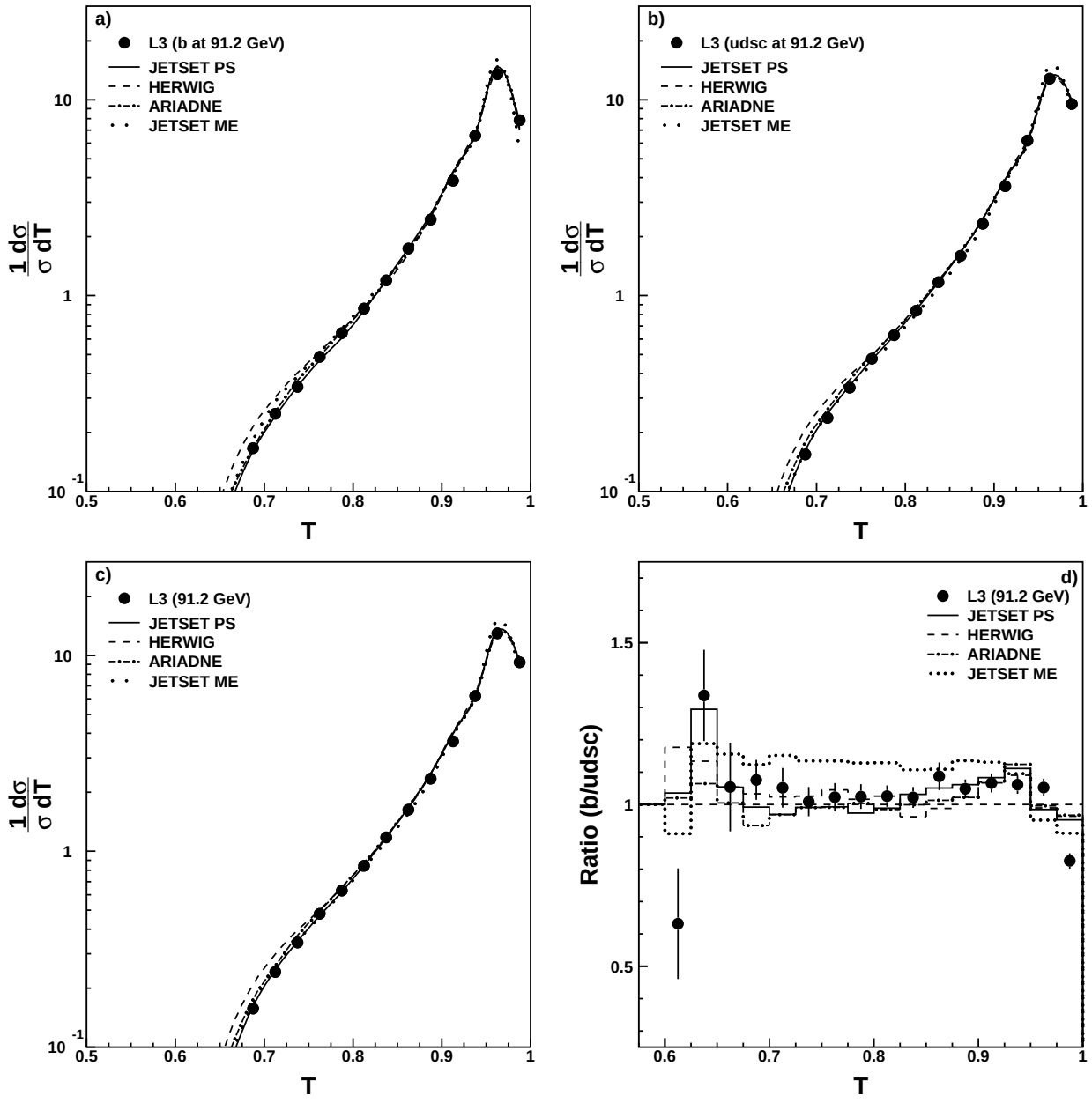

Figure 15: Thrust distributions at $\sqrt{s} = 91.2$ GeV for b, udsc, and all quark flavours and the ratio b/udsc compared to several QCD models.

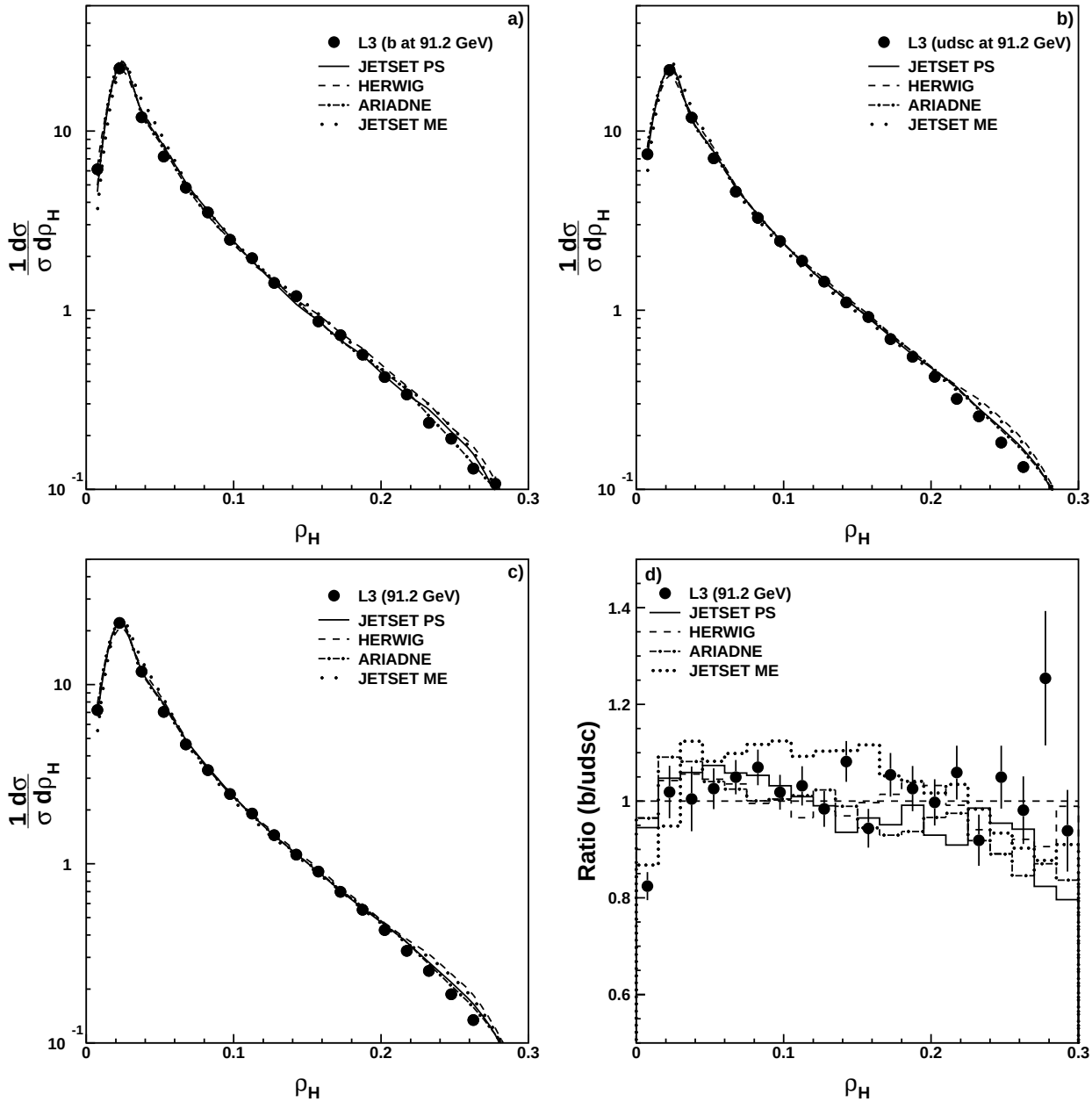

Figure 16: Scaled heavy jet mass distributions at $\sqrt{s} = 91.2$ GeV for b, udsc, and all quark flavours and the ratio b/udsc compared to several QCD models.

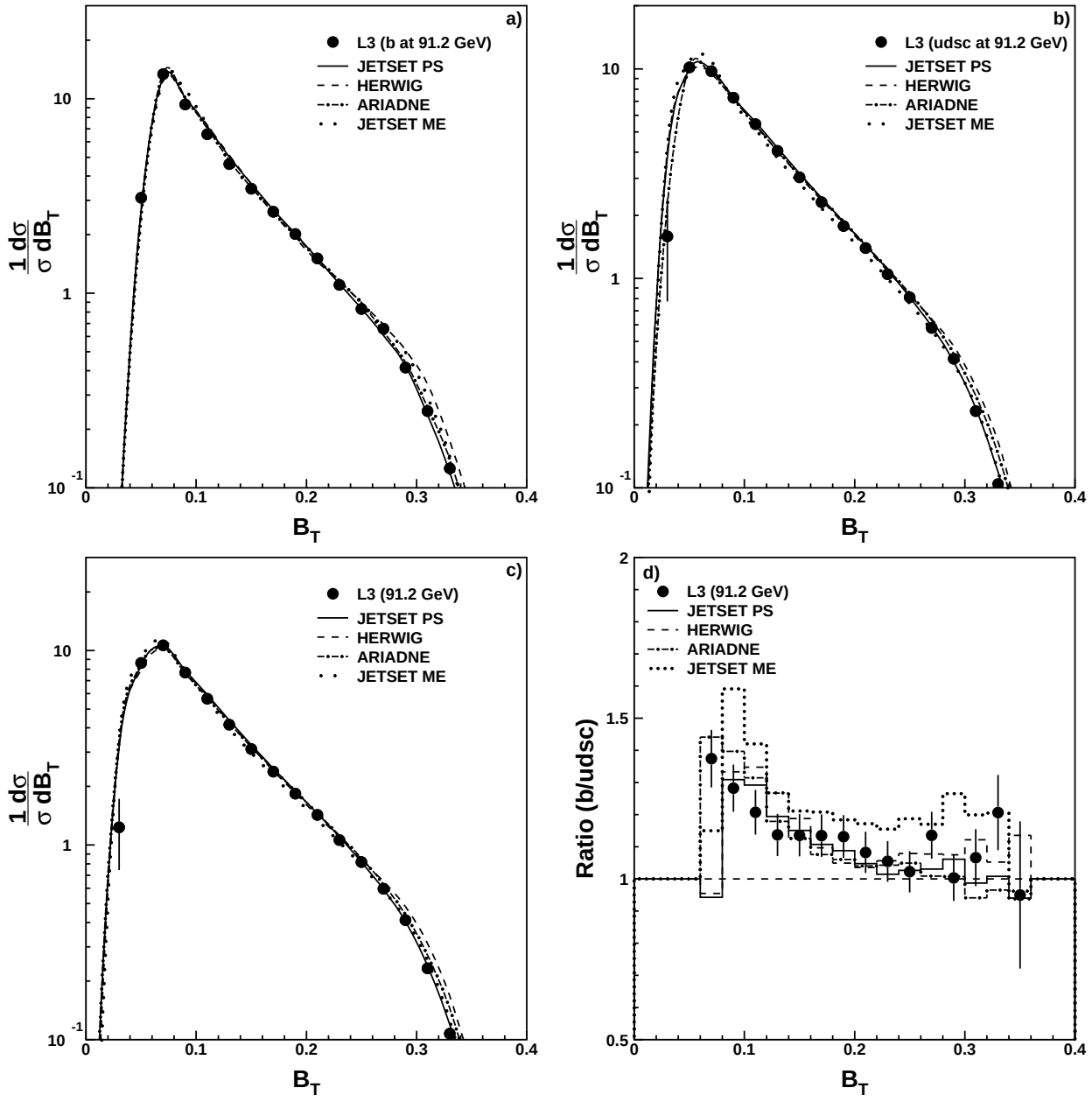

Figure 17: Total jet broadening distributions at $\sqrt{s} = 91.2$ GeV for b, udsc, and all quark flavours and the ratio b/udsc compared to several QCD models.

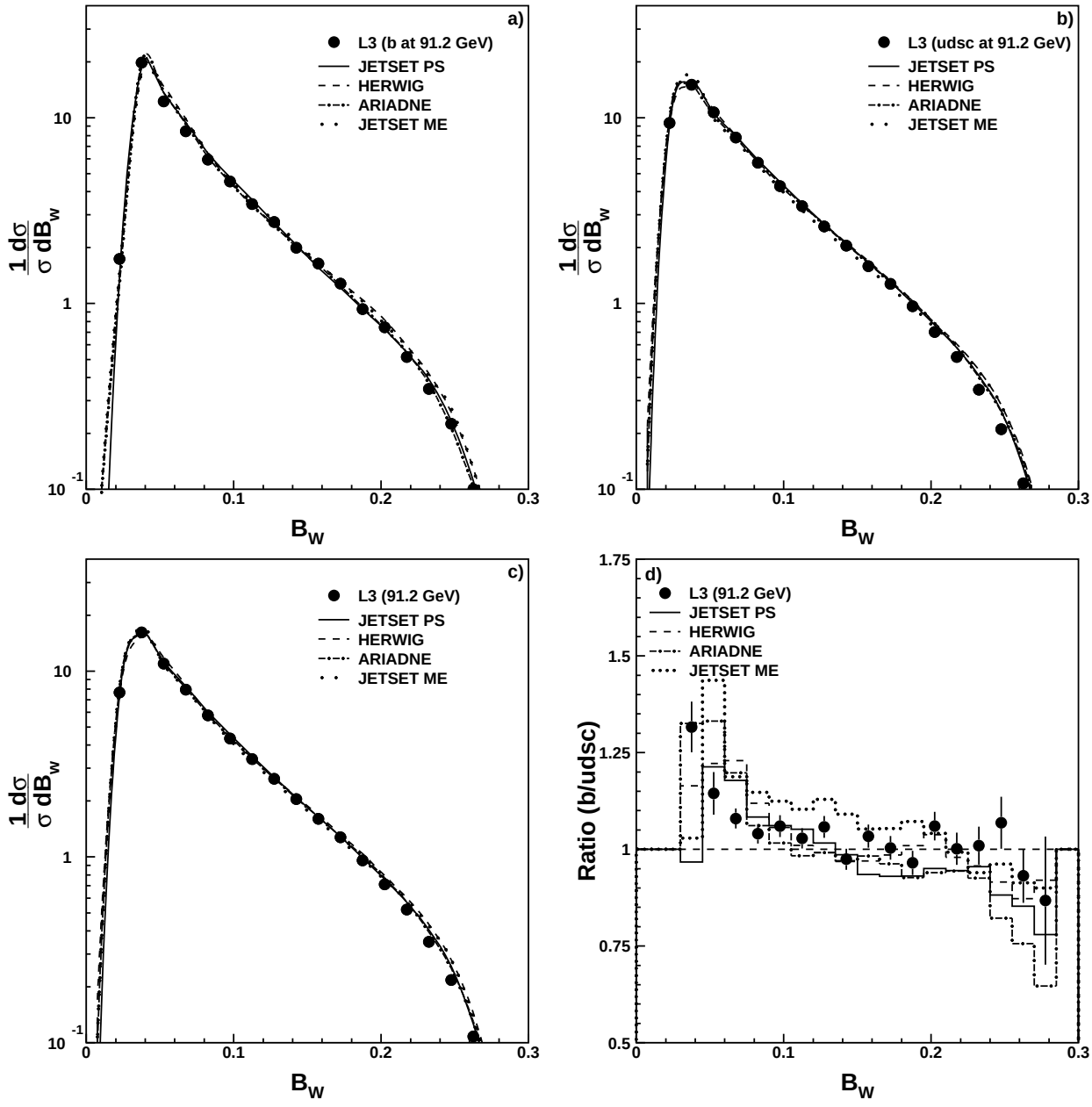

Figure 18: Wide jet broadening distributions at $\sqrt{s} = 91.2$ GeV for b, udsc, and all quark flavours and the ratio b/udsc compared to several QCD models.

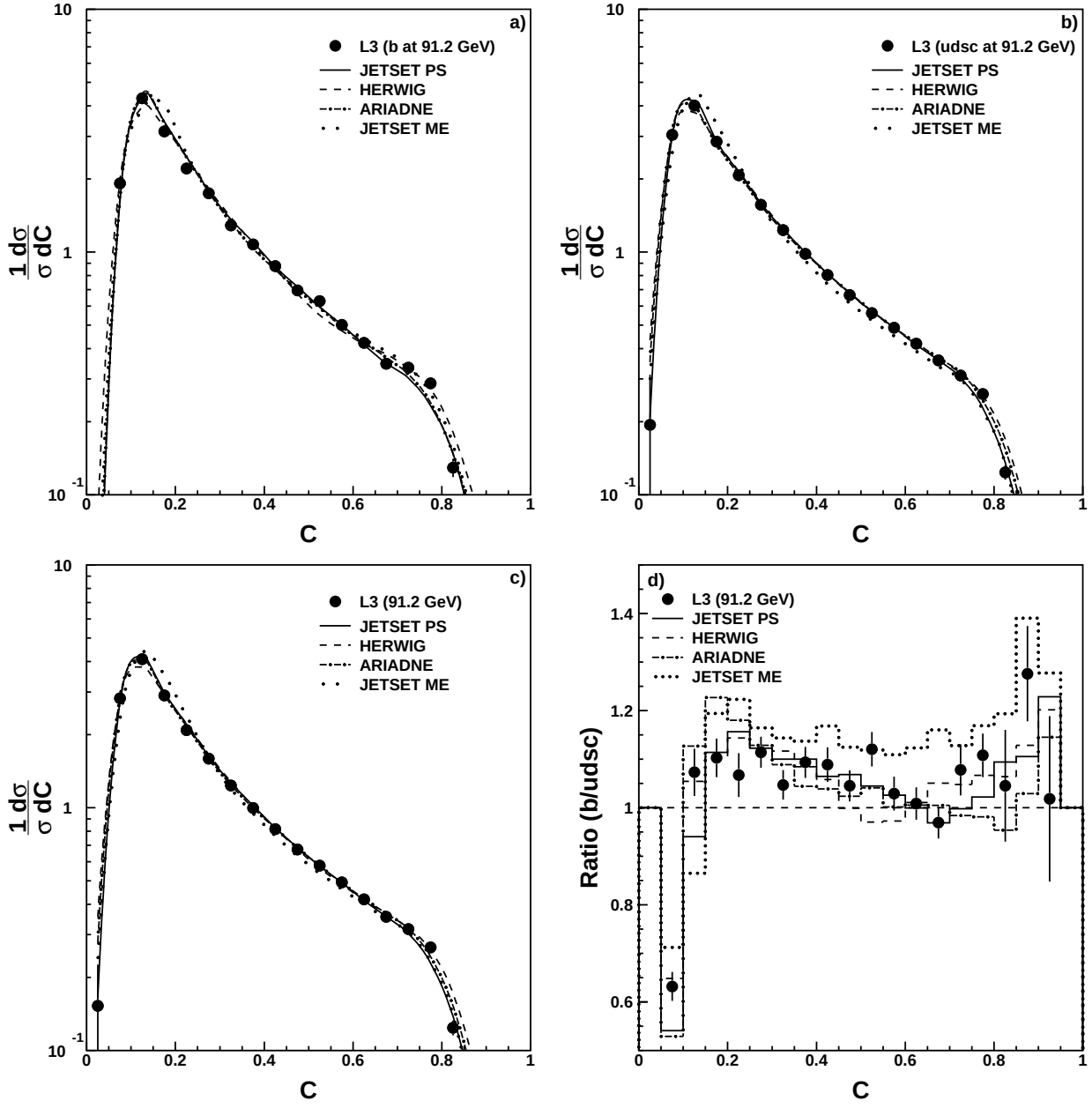

Figure 19: C-parameter distributions at $\sqrt{s} = 91.2$ GeV for b, udsc, and all quark flavours and the ratio b/udsc compared to several QCD models.

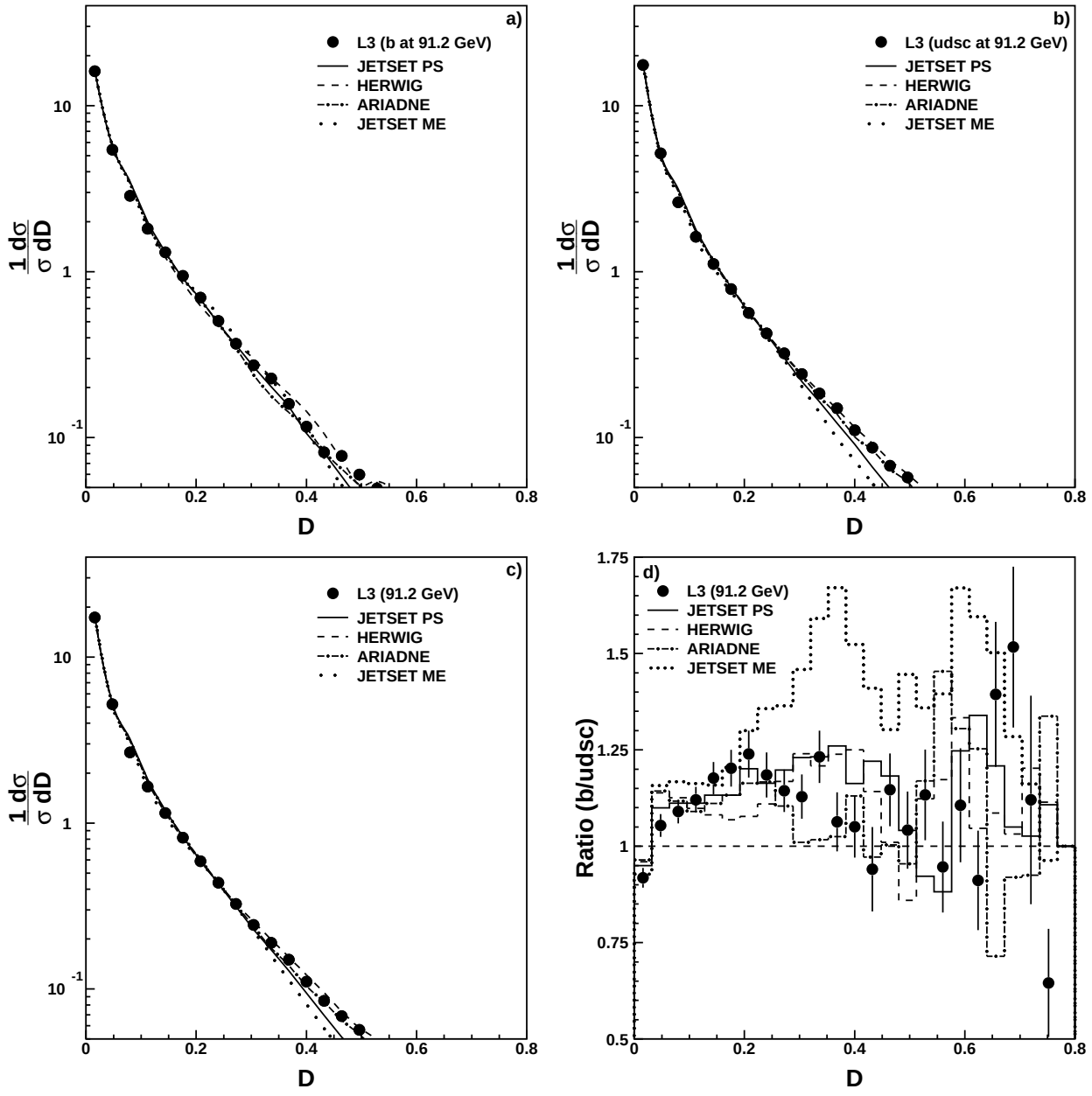

Figure 20: D-parameter distributions at $\sqrt{s} = 91.2$ GeV for b, udsc, and all quark flavours and the ratio b/udsc compared to several QCD models.

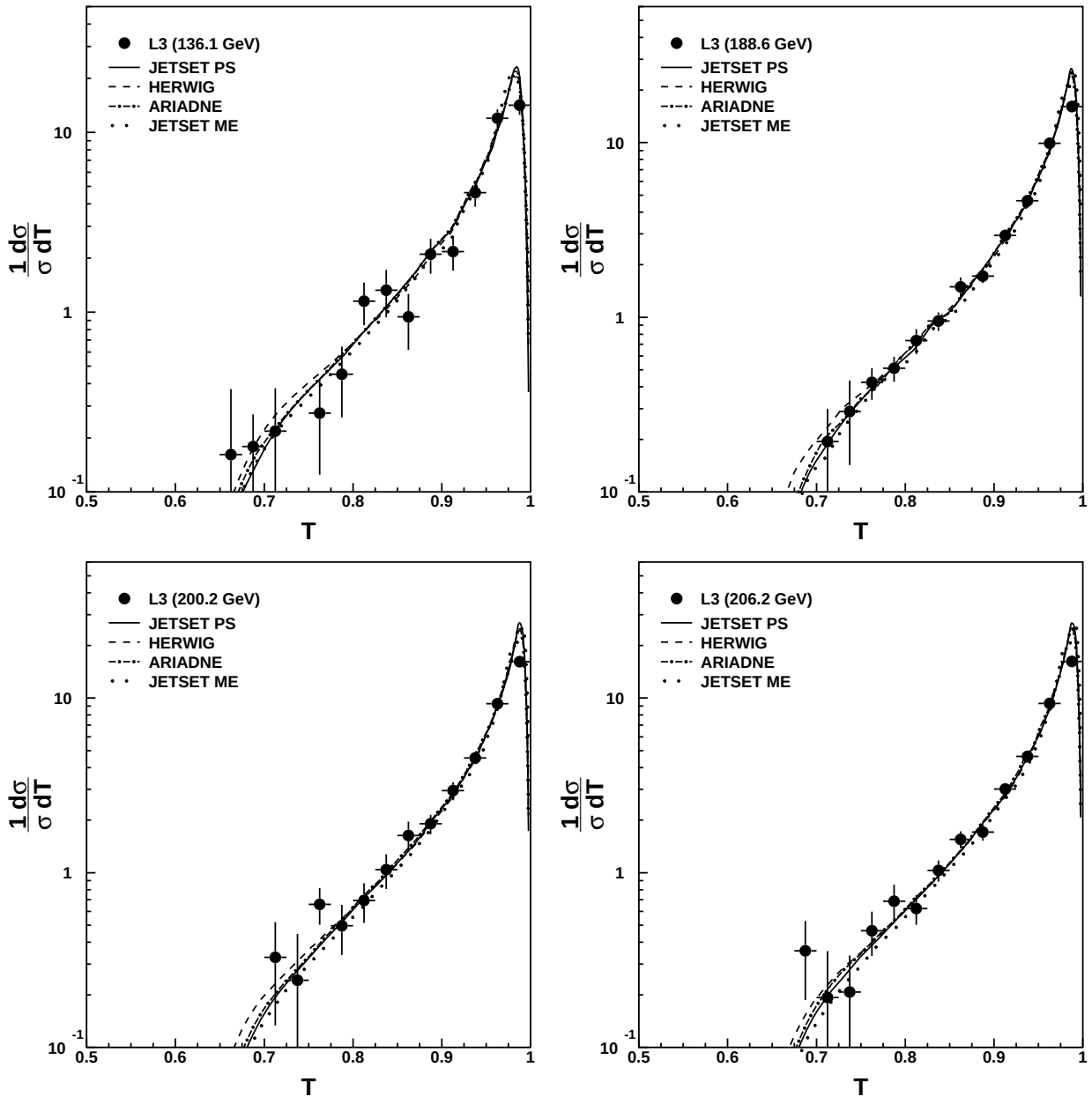

Figure 21: Thrust distributions at $\langle\sqrt{s}\rangle = 136.1, 188.6, 200.2$ and 206.2 GeV compared to several QCD models.

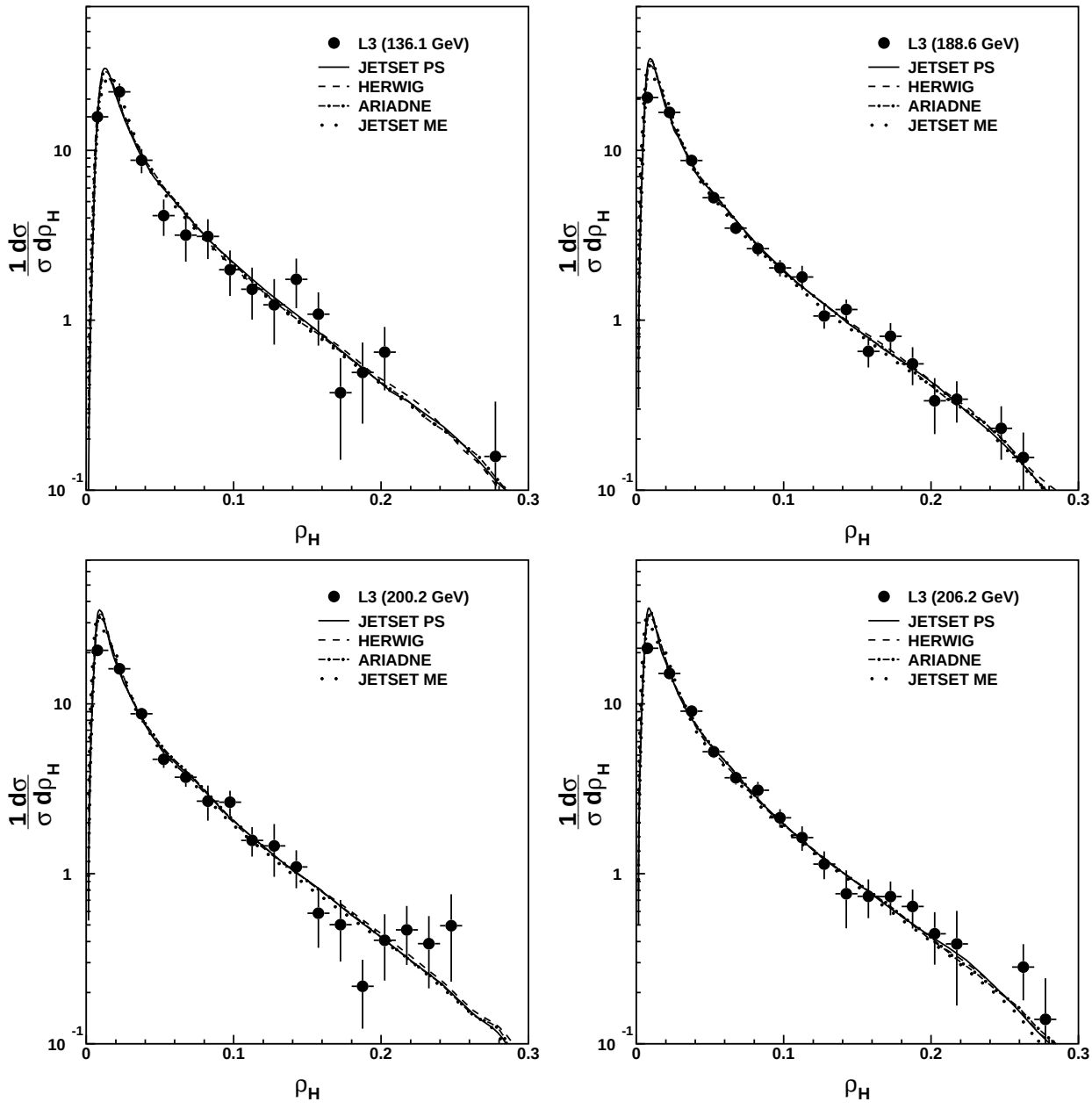

Figure 22: Scaled heavy jet mass distributions at $\langle\sqrt{s}\rangle = 136.1, 188.6, 200.2$ and 206.2 GeV compared to several QCD models.

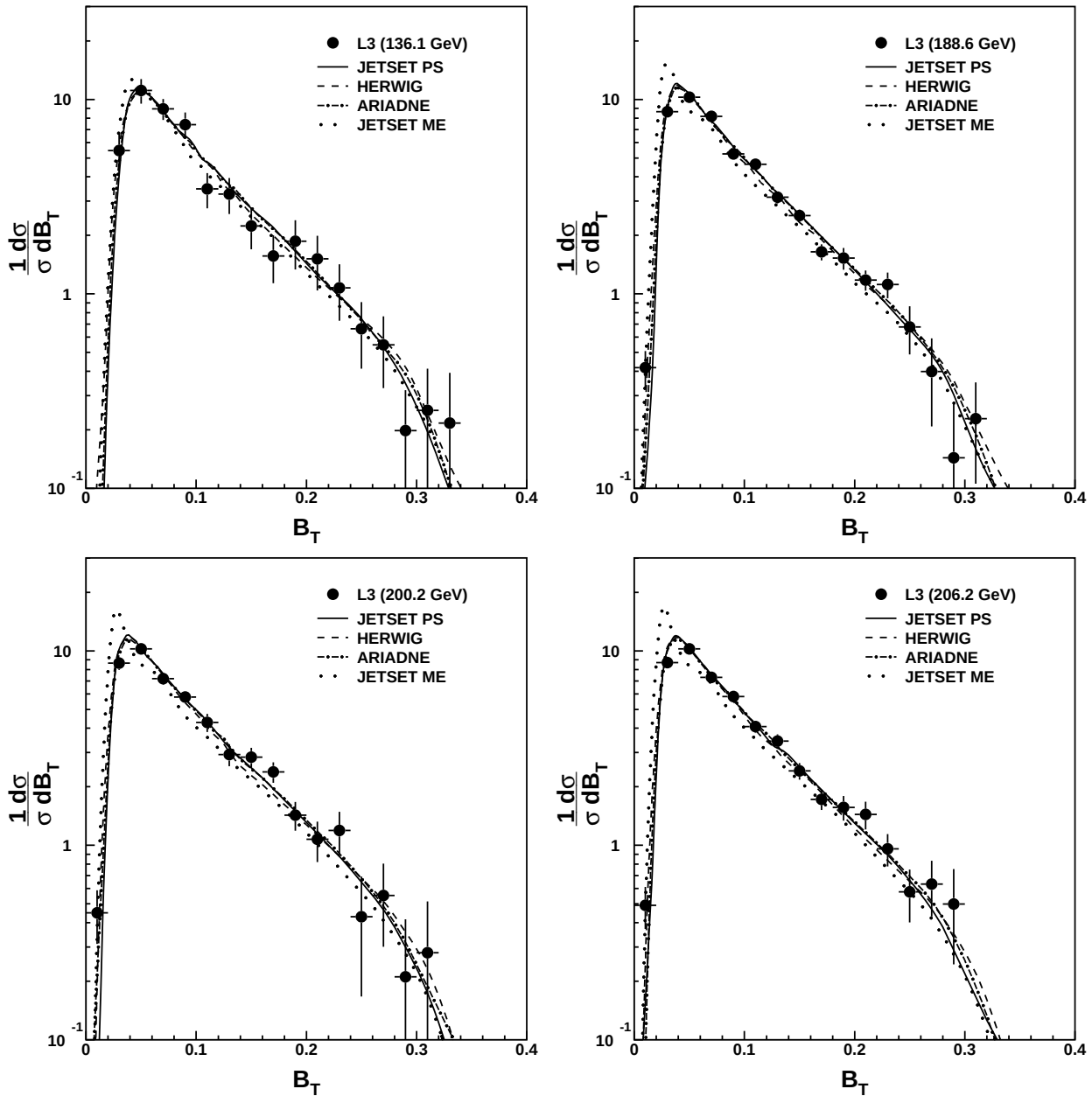

Figure 23: Total jet broadening distributions at $\langle\sqrt{s}\rangle = 136.1, 188.6, 200.2$ and 206.2 GeV compared to several QCD models.

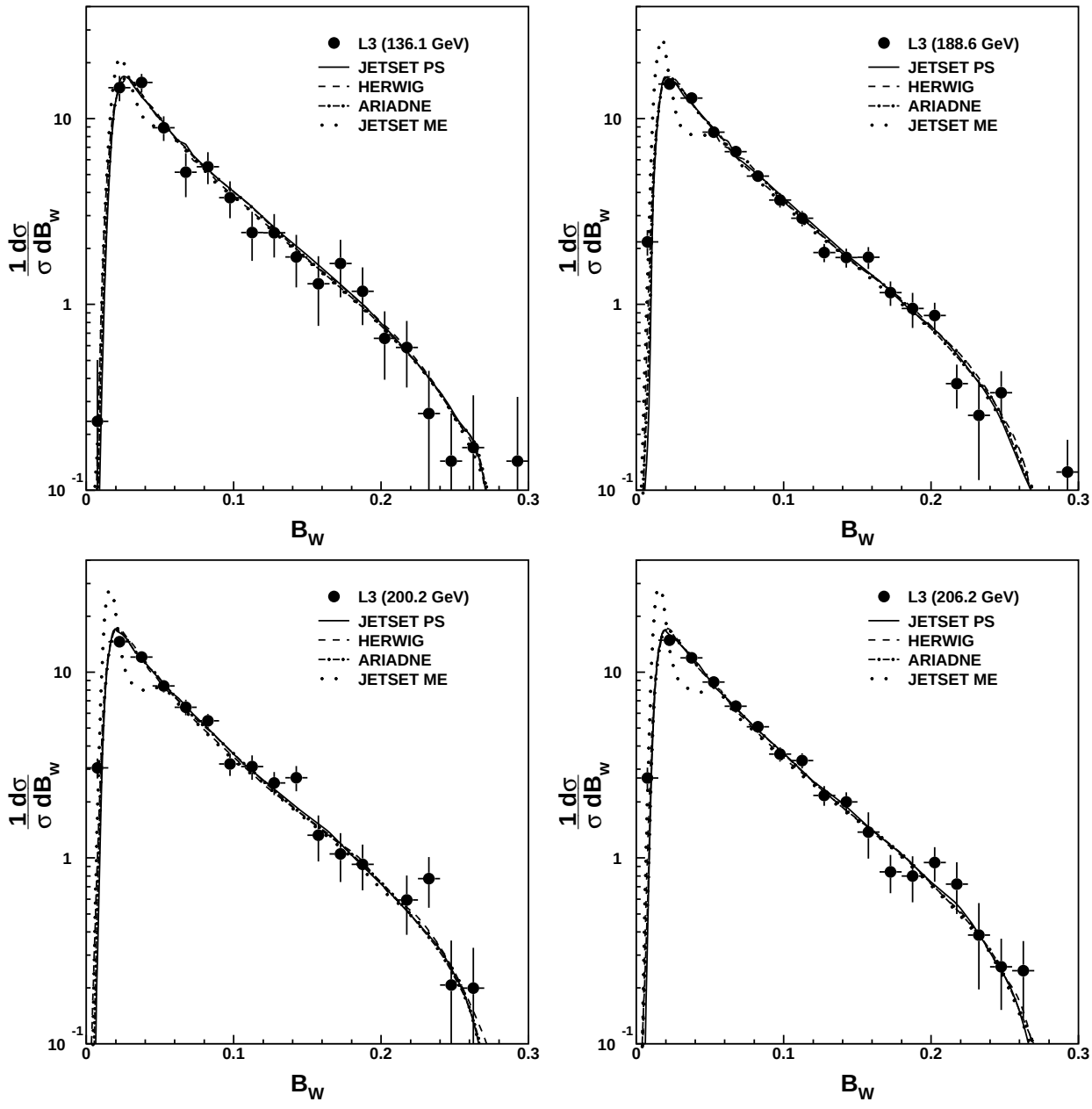

Figure 24: Wide jet broadening distributions at $\langle\sqrt{s}\rangle = 136.1, 188.6, 200.2$ and 206.2 GeV compared to several QCD models.

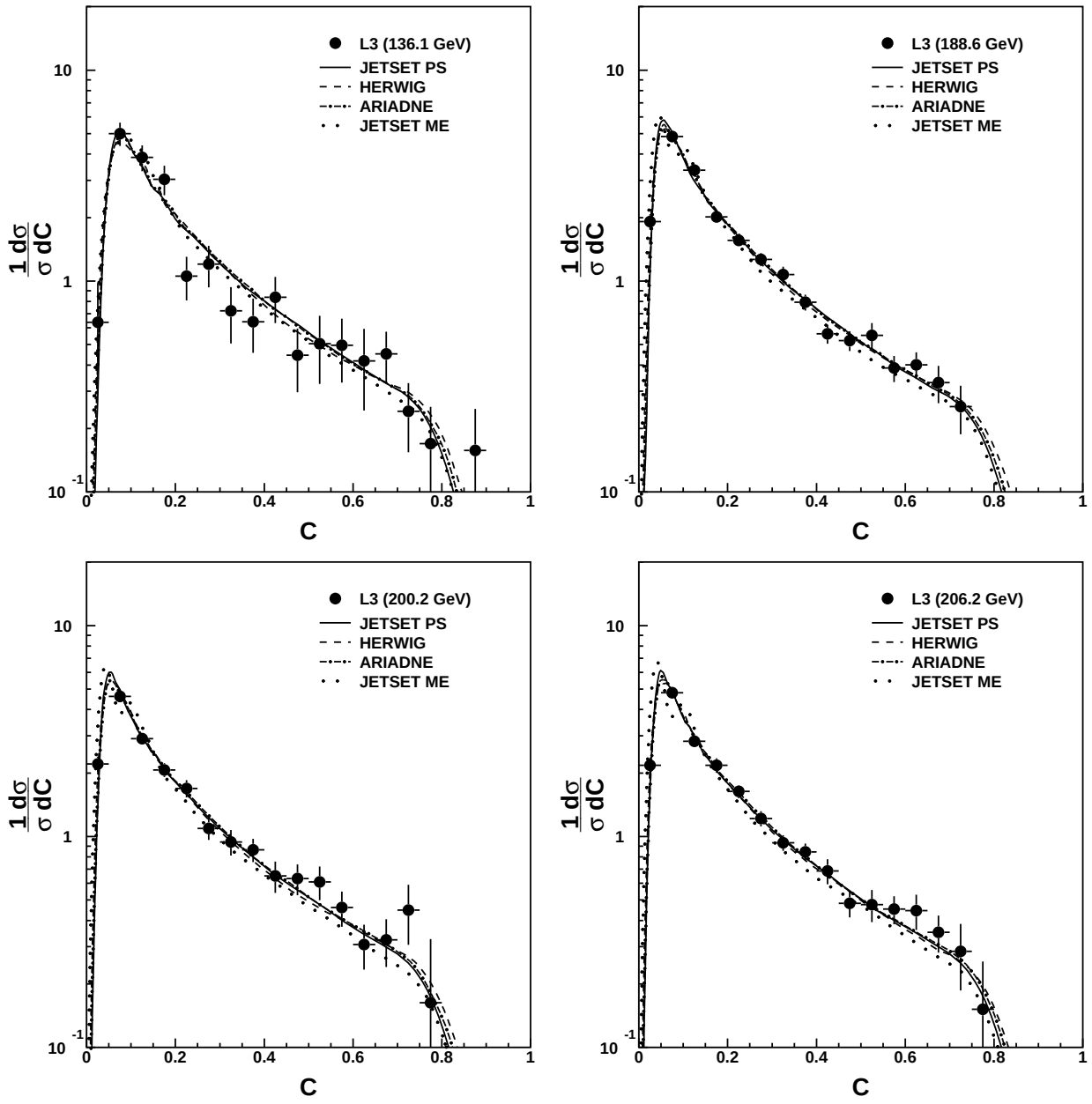

Figure 25: C-parameter distributions at $\langle\sqrt{s}\,\rangle = 136.1, 188.6, 200.2$ and 206.2 GeV compared to several QCD models.

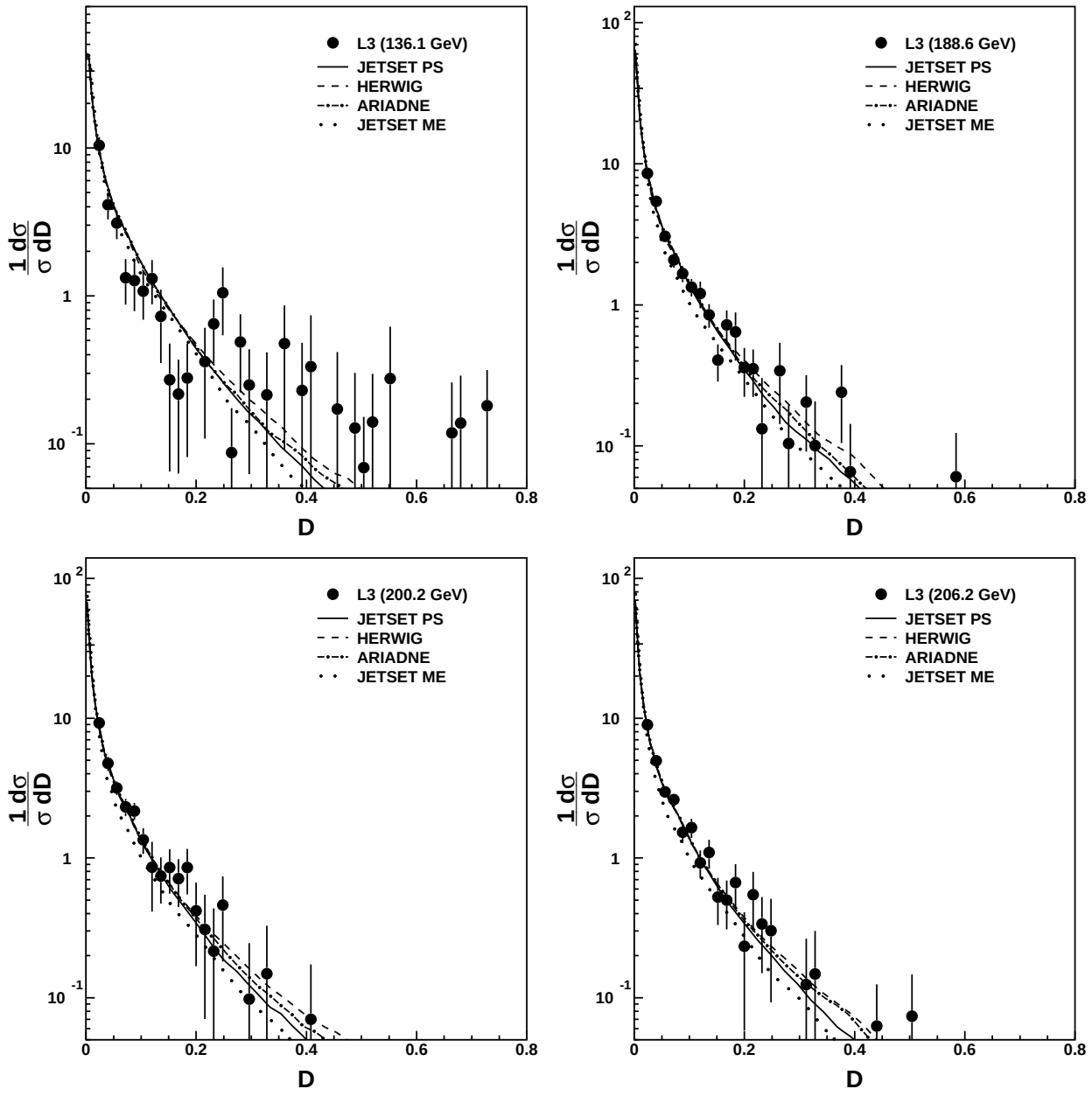

Figure 26: D-parameter distributions at $\langle\sqrt{s}\,\rangle = 136.1, 188.6, 200.2$ and 206.2 GeV compared to several QCD models.

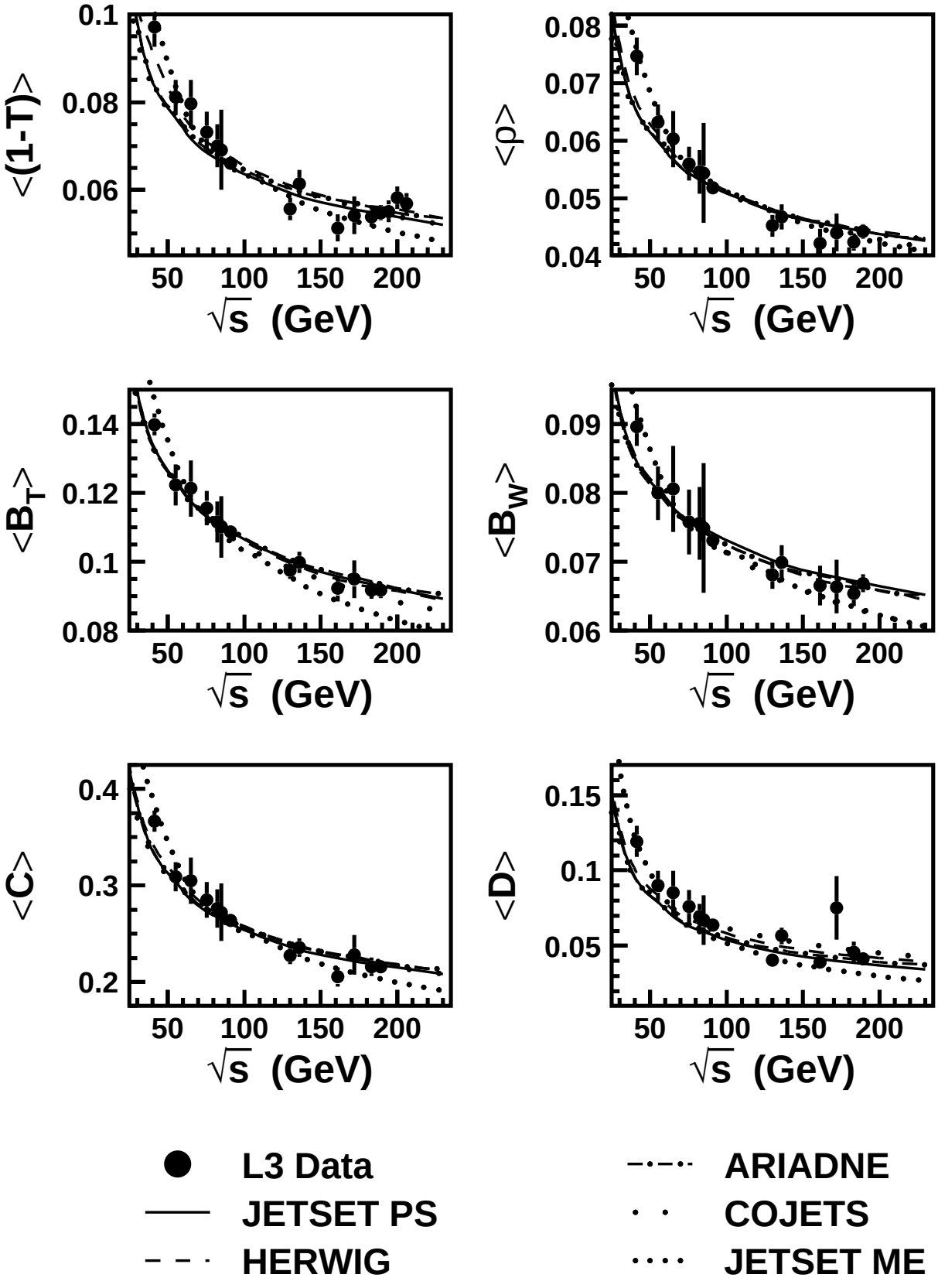

Figure 27: The first moments of the six event-shape variables, $1-T$, ρ_{H}, B_{T}, B_{W}, C and D, as a function of the centre-of-mass energy, compared with several QCD models.

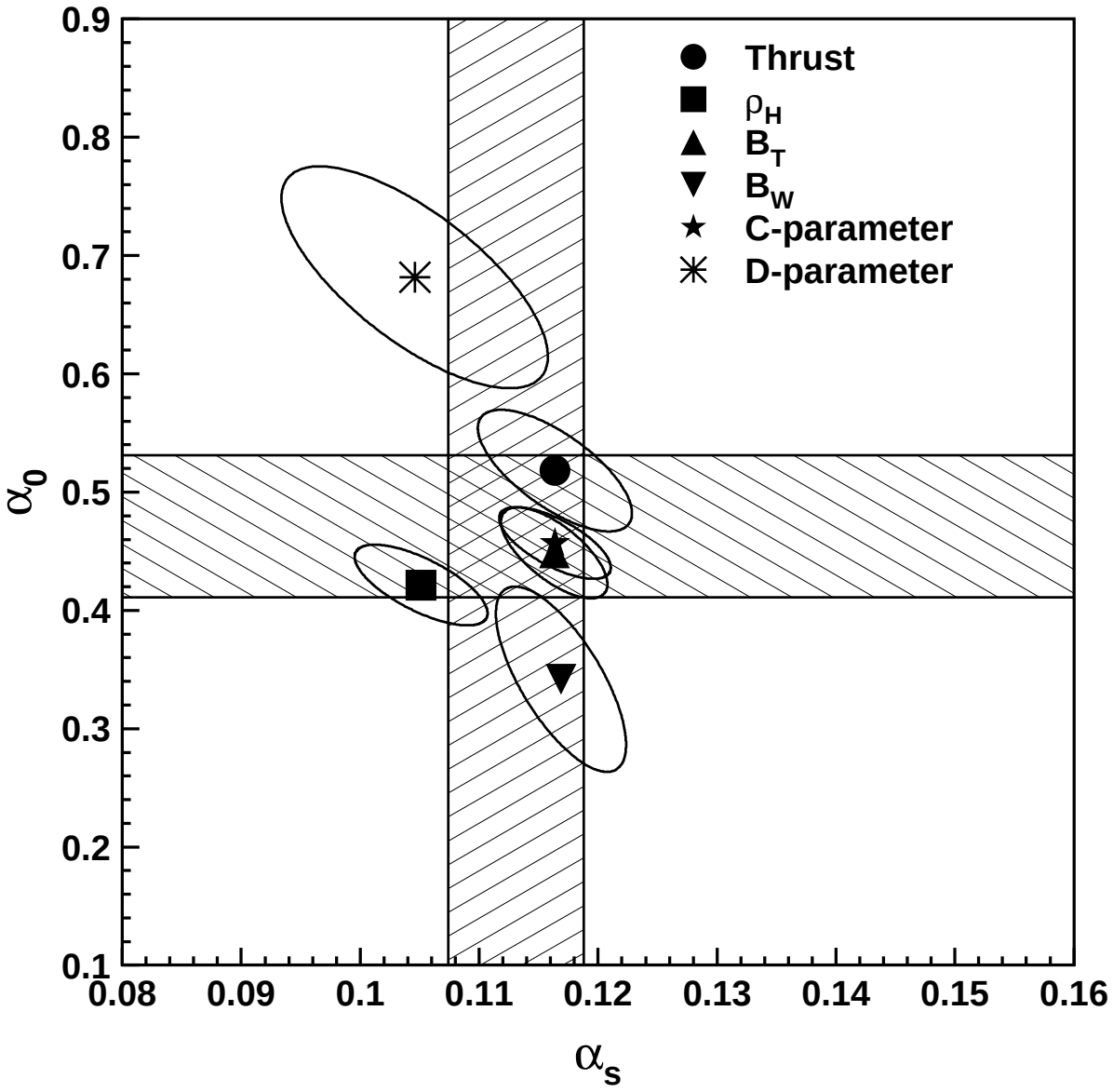

Figure 28: The values of α_s and α_0 from fits of the power correction ansatz to the first moments of the six event-shape variables, $1-T$, ρ_H, B_T, B_W, C and D. The ellipses represent 39% two-dimensional confidence intervals including both statistical and systematic uncertainties. The bands represent unweighted averages of the α_s and α_0 including both statistical and systematic uncertainties.

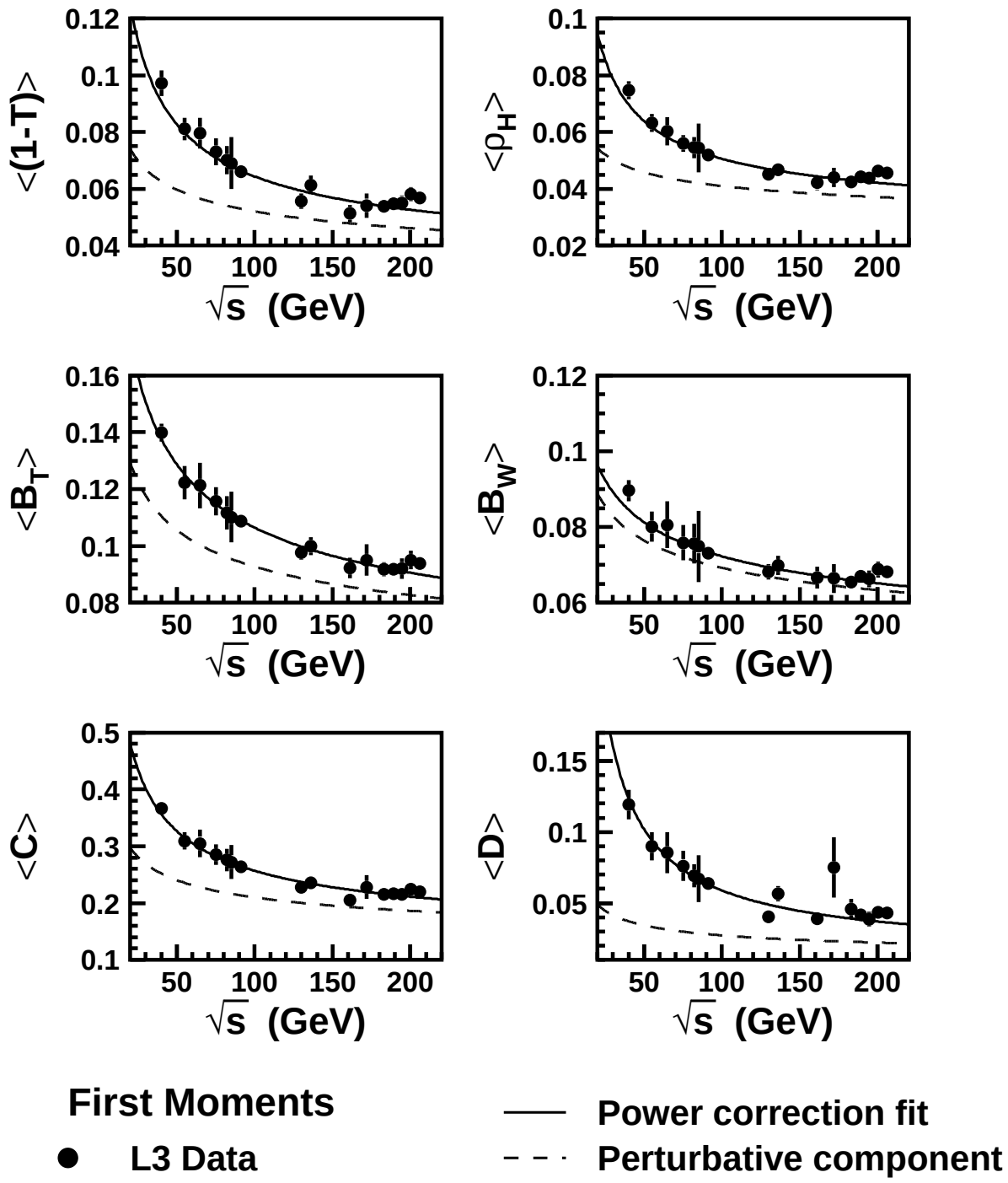

Figure 29: The first moments of the six event-shape variables, $1-T$, ρ_{H}, B_{T}, B_{W}, C and D compared to the results of a fit including perturbative and power law contributions, Equation (34).

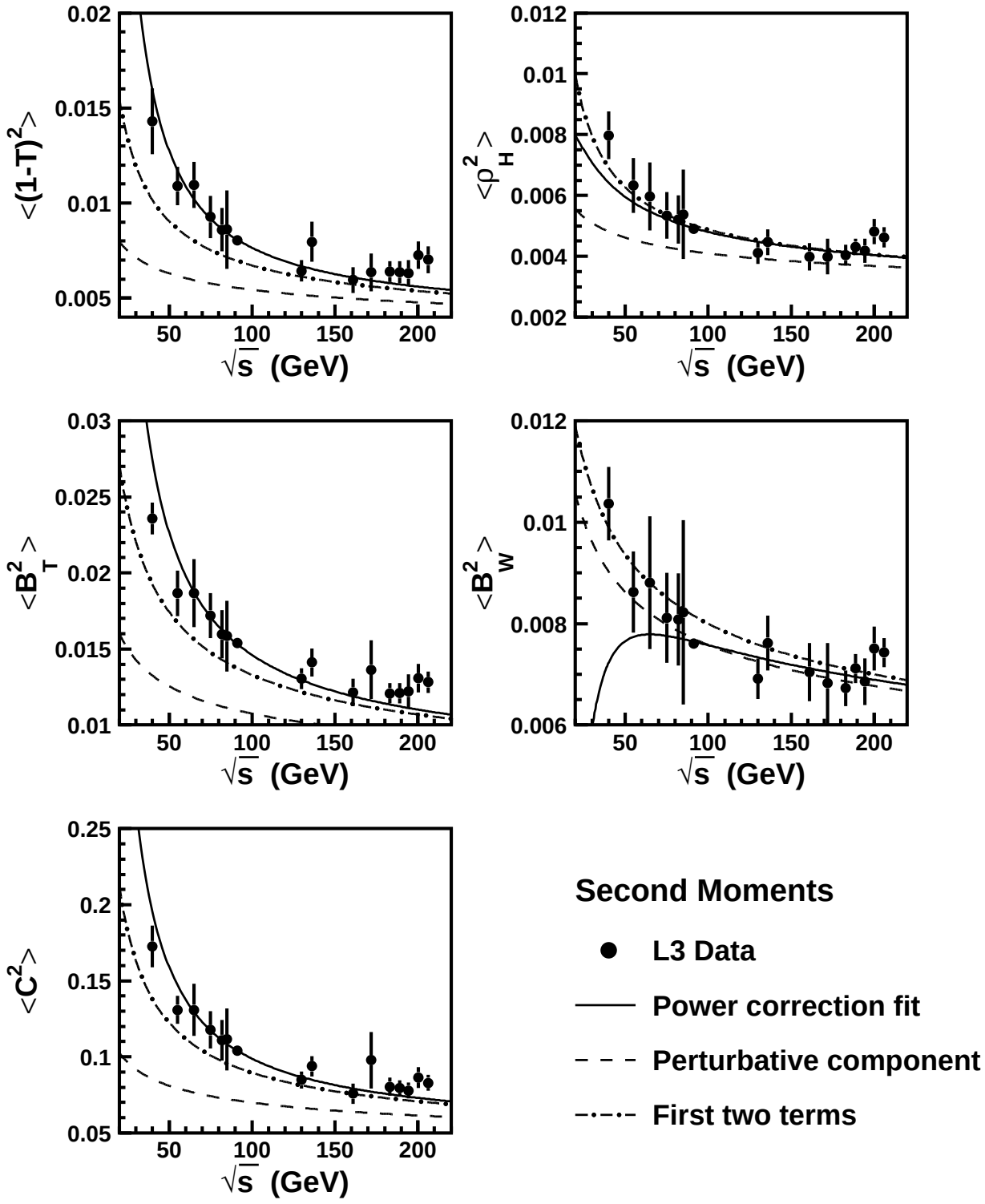

Figure 30: The second moments of the five event-shape variables, $1-T$, ρ_{H}, B_{T}, B_{W} and C compared to the results of a fit including perturbative and power law contributions, Equation (39). The parameters α_0 and α_{s} are fixed to the values obtained by the corresponding fit to the first moment.

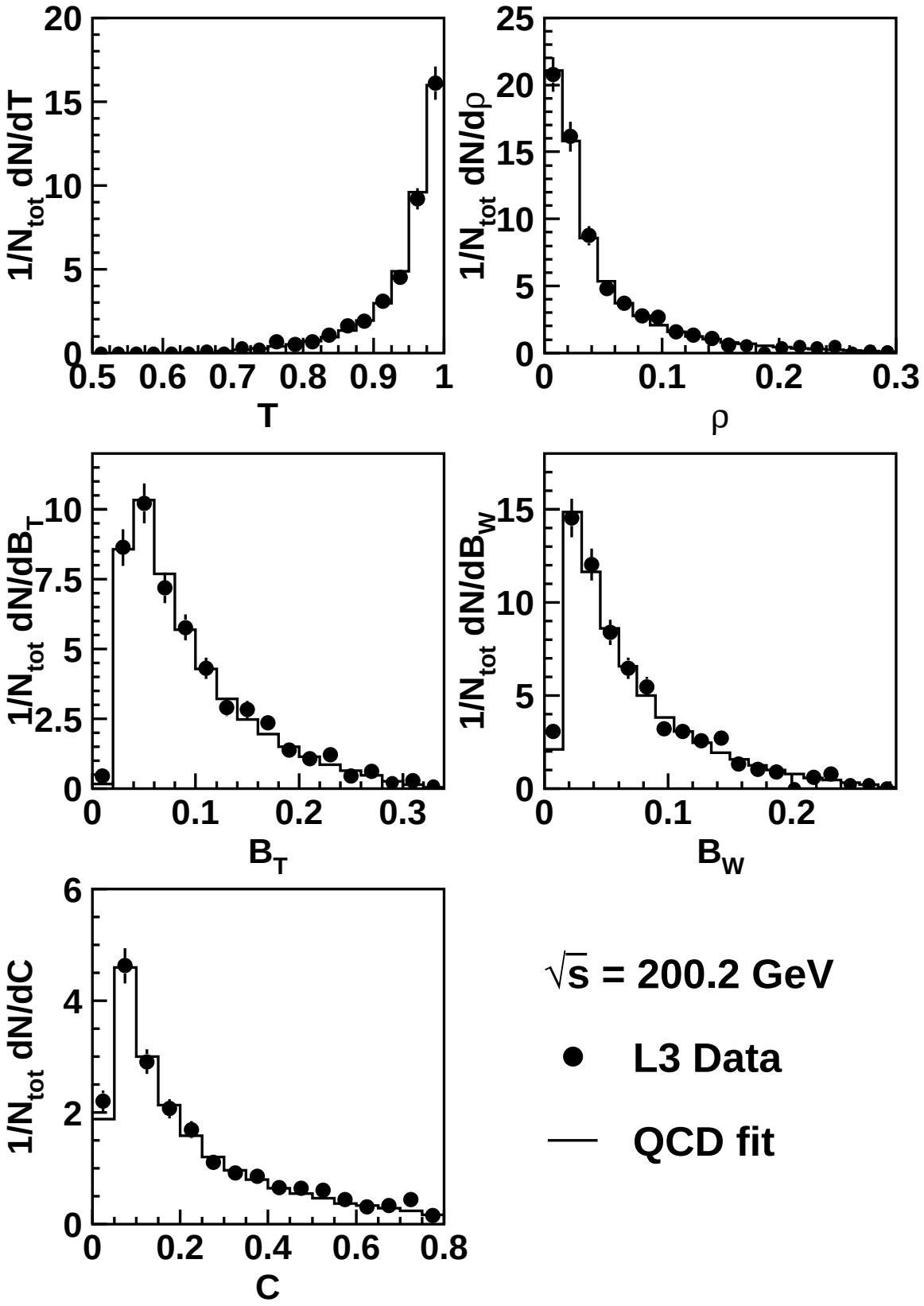

Figure 31: Measured distributions, at $\langle\sqrt{s}\,\rangle = 200.2$ GeV, of thrust, T, scaled heavy jet mass, $\rho_{\rm H}$, total, $B_{\rm T}$, and wide, $B_{\rm W}$, jet broadenings, and C-parameter compared to fitted QCD predictions. The error bars include systematic as well as statistical uncertainties.

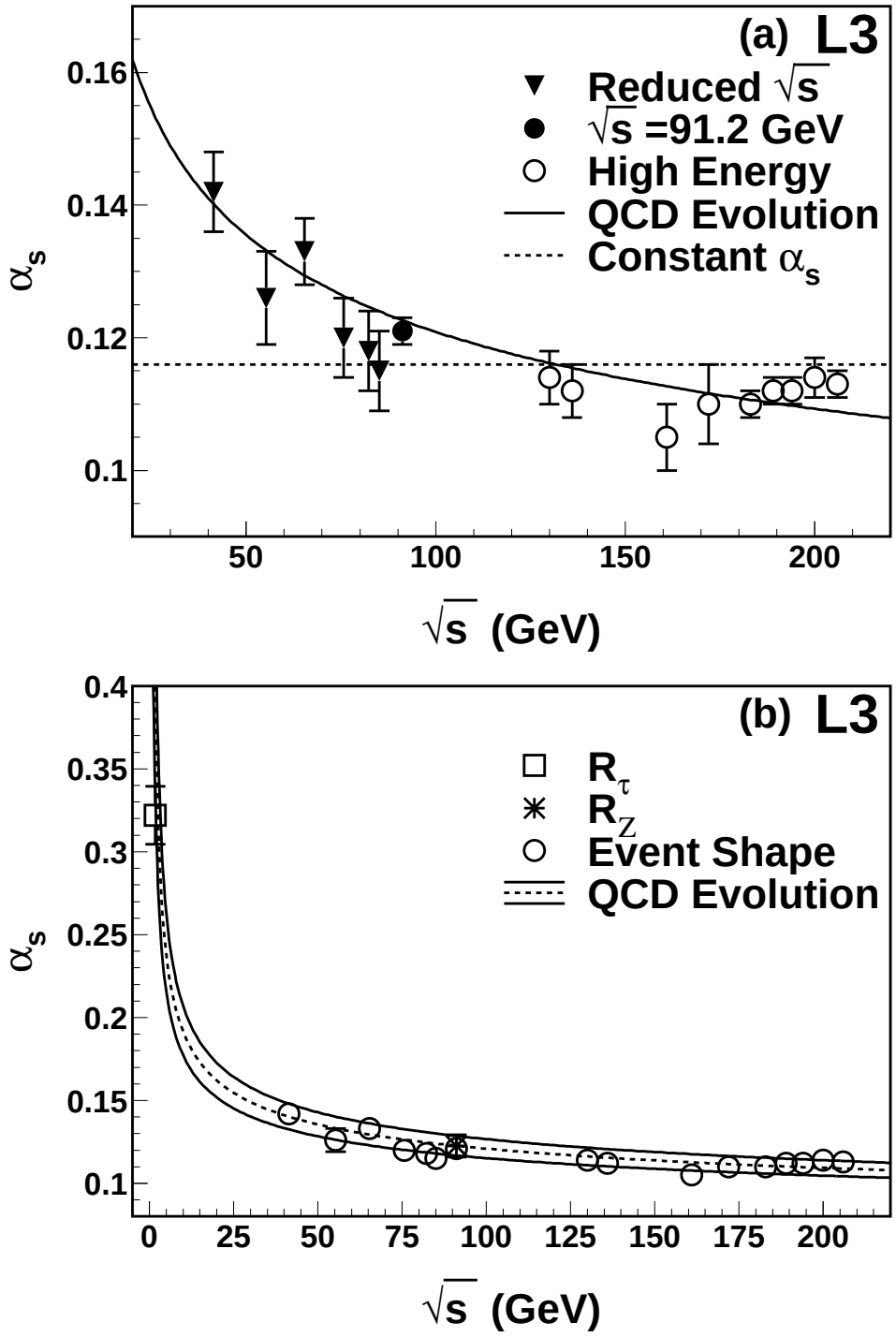

Figure 32: Values of α_s determined as a function of $\sqrt{s}$: a) from event-shape distributions with experimental uncertainties only. The solid and dashed lines are fits with the energy dependence of α_s as expected from QCD and with constant α_s, respectively. b) from the measurement of the τ branching fractions into leptons [174], the Z line shape [175], and event-shape distributions. The dashed line is a fit of the QCD evolution function to the measurements made from event-shape variables. The width of the band corresponds to the evolved uncertainty on $\alpha_s(m_Z)$.

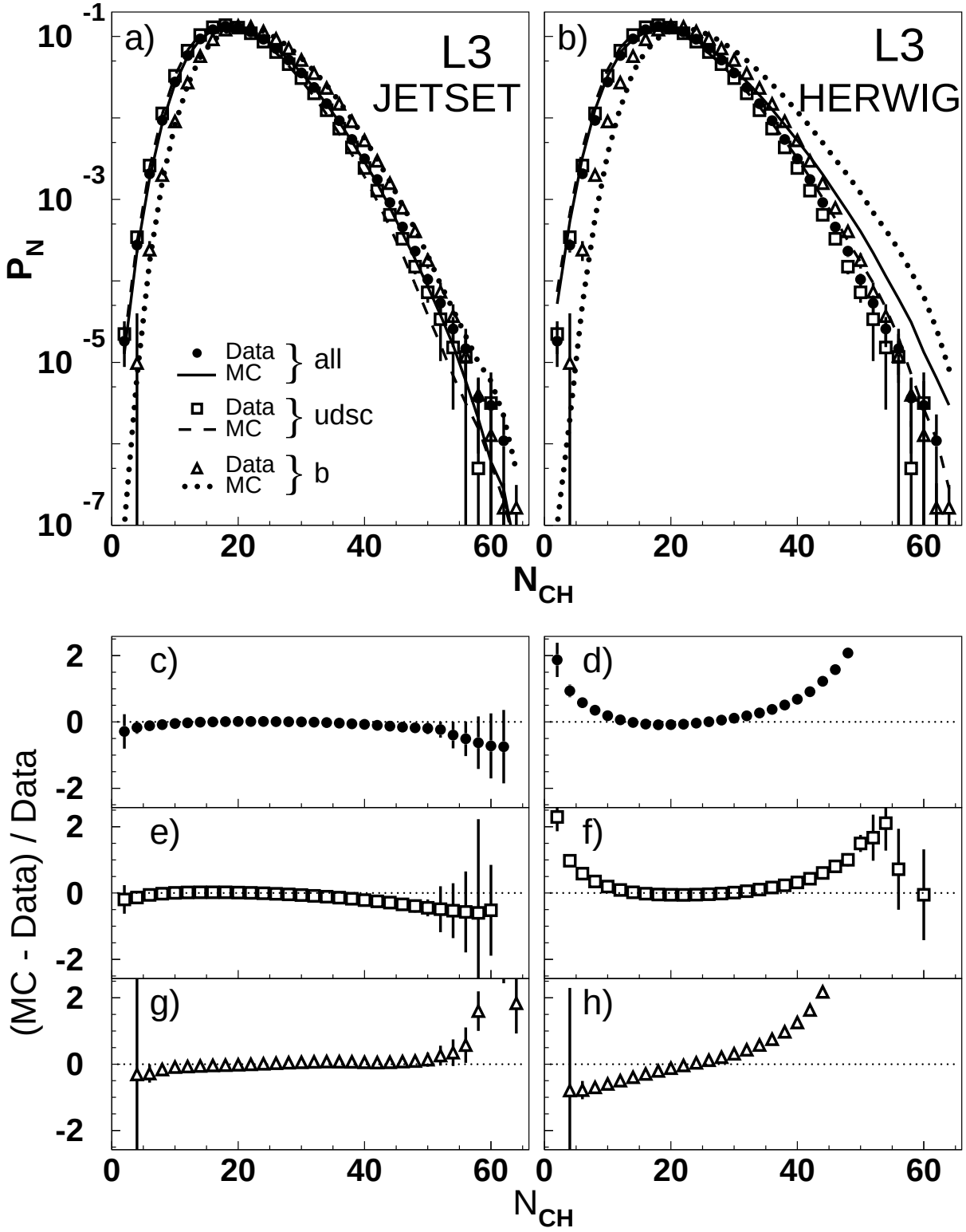

Figure 33: Charged particle multiplicity distributions, normalised to unity, at $\sqrt{s} = 91.2$ GeV compared to (a, c, e, g) JETSET PS and (b, d, f, h) HERWIG.

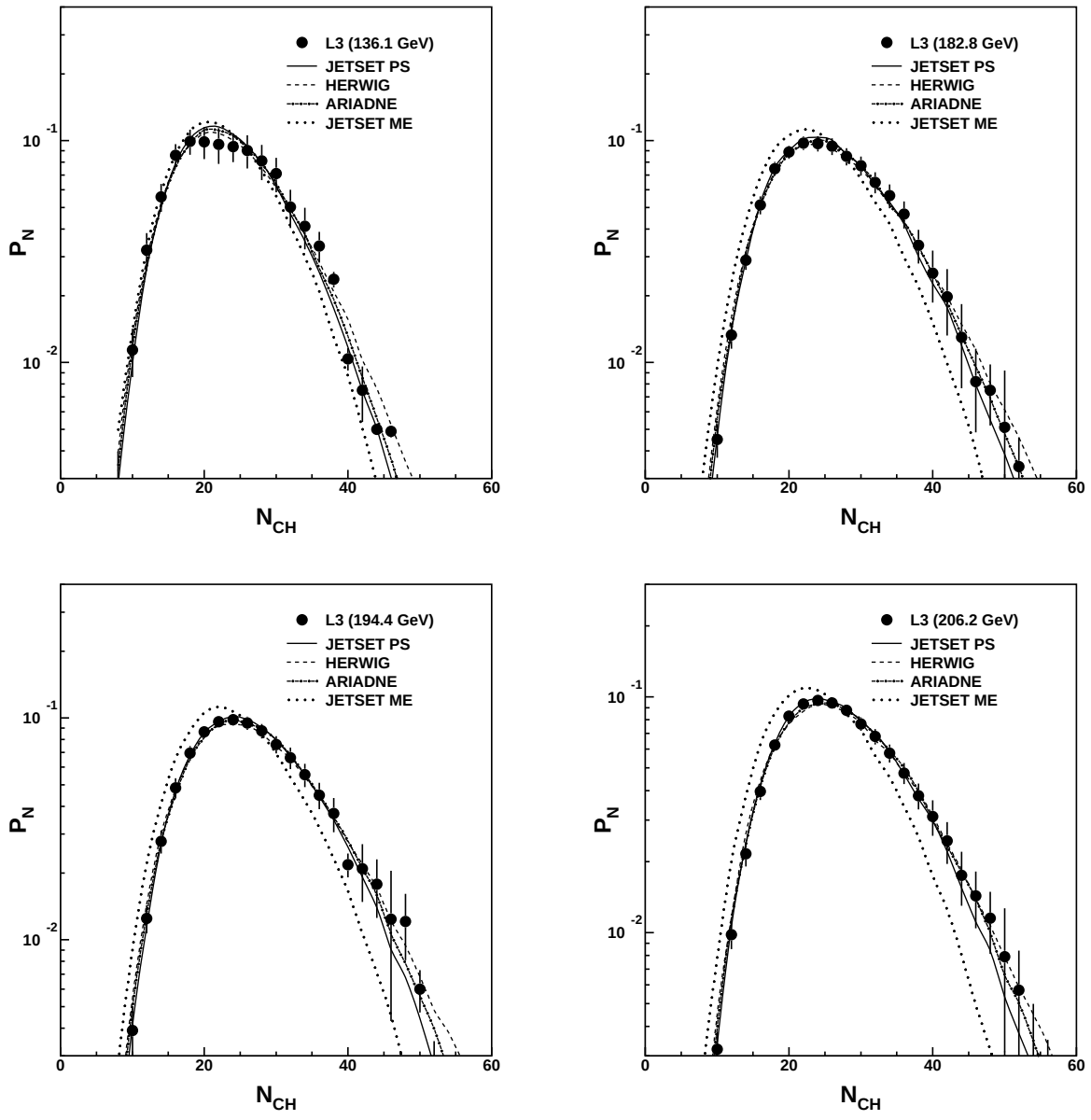

Figure 34: Charged particle multiplicity distributions, normalised to unity, at $\sqrt{s}$ = 136.1, 182.8, 194.4 and 206.2 GeV compared to several QCD models.

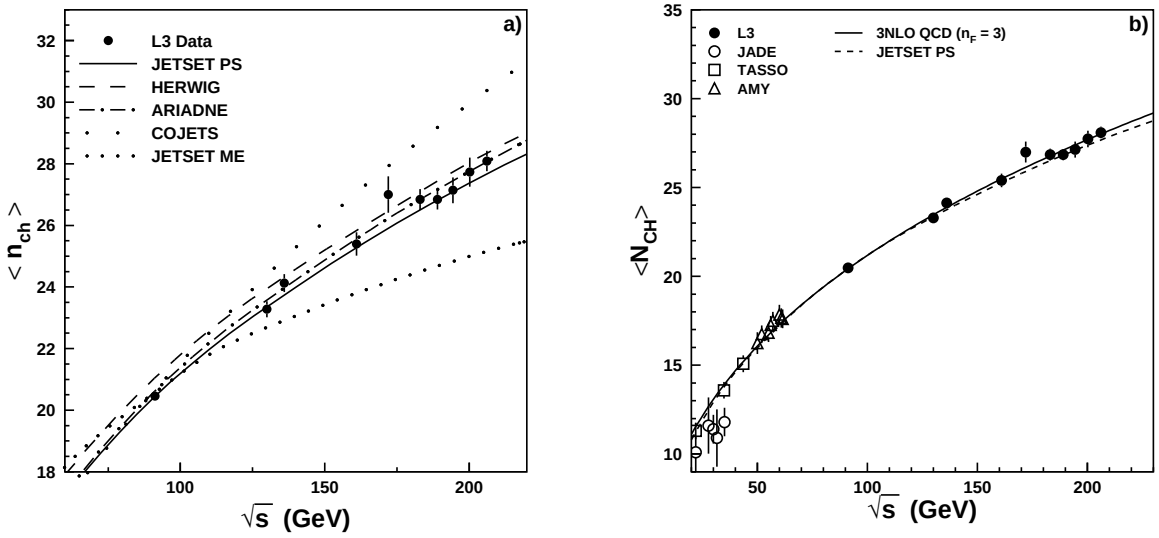

Figure 35: The mean charged particle multiplicity, $\langle N_{\rm ch} \rangle$, as a function of the centre-of-mass energy, (a) compared to several QCD models, (b) fitted to the 3NLO prediction of QCD with local parton hadron duality, assuming 3 active flavours.

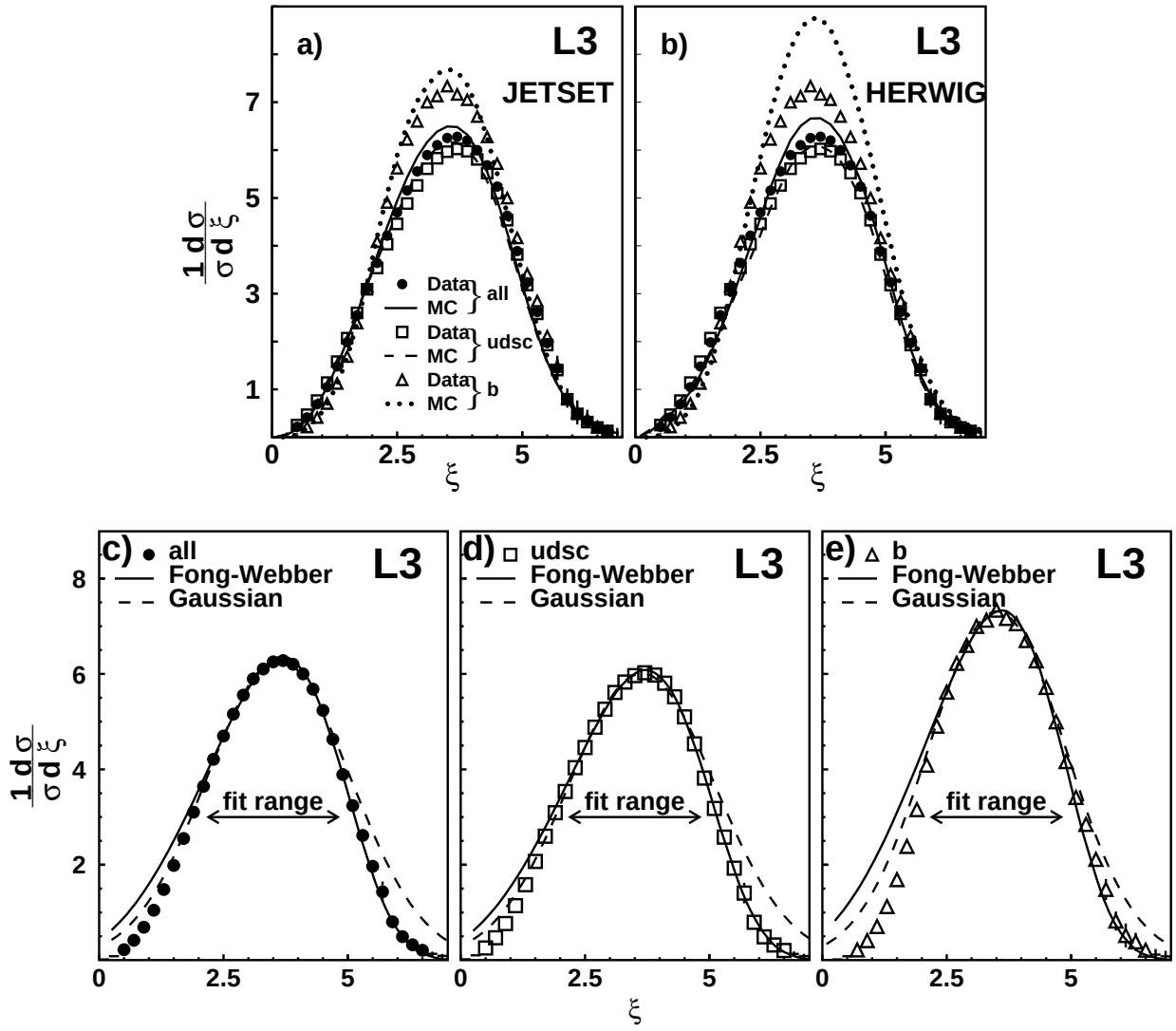

Figure 36: Corrected ξ distributions at $\sqrt{s} = 91.2$ GeV compared to (a) JETSET PS and (b) HERWIG and together with the results of fits to Gaussian and Fong-Webber parametrisations for the (c) all-flavour, (d) udsc- and (e) b-quark samples.

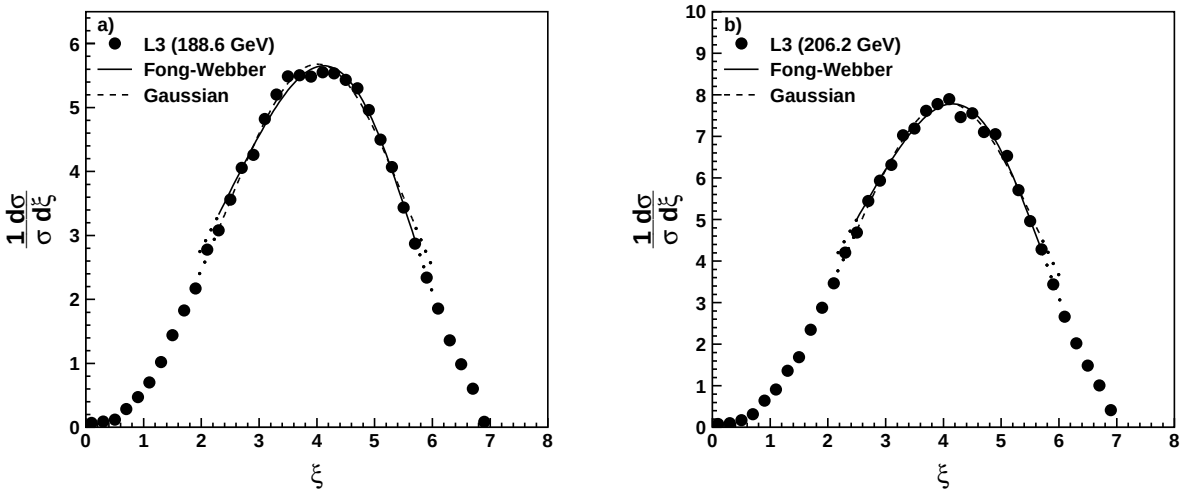

Figure 37: Corrected ξ-spectra at $\sqrt{s} = 188.6$ GeV and $\sqrt{s} = 206.2$ GeV together with the results of fits to Gaussian and Fong-Webber parametrisations.

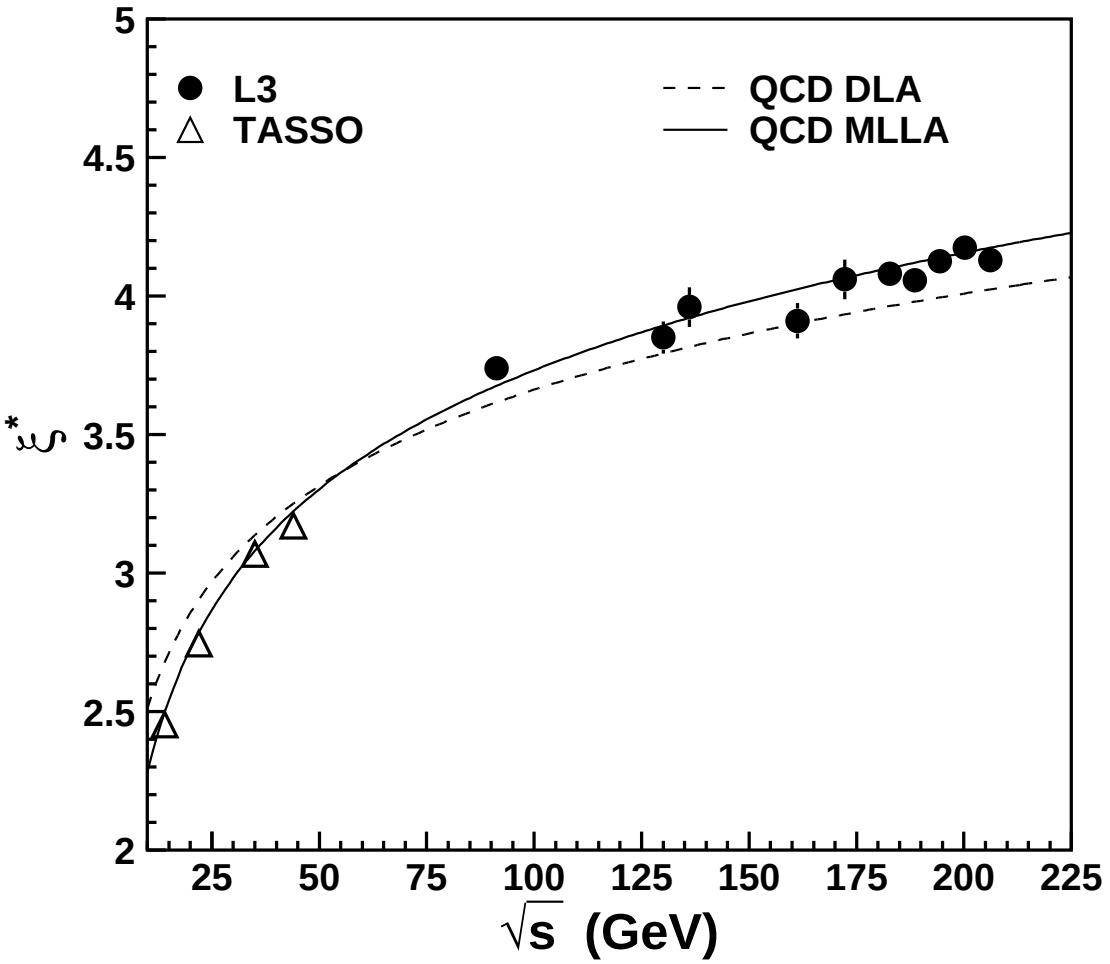

Figure 38: Energy evolution of $\xi^\star$. The solid and dashed lines are fits to the L3 and TASSO data with Modified Leading Log Approximation (MLLA) and Double Log Approximation (DLA) QCD.